

Quantifying the Reactivity of Photolytically Generated Radicals Towards Vinylic Monomers *via* Electrospray Ionization-Mass Spectrometry

Zur Erlangung des akademischen Grades eines
DOKTORS DER NATURWISSENSCHAFTEN
(Dr. rer. nat.)

Fakultät für Chemie und Biowissenschaften
Karlsruher Institut für Technologie (KIT) - Universitätsbereich

genehmigte
DISSERTATION

von

Dipl.-Chem. Dominik Voll

aus

Kirchardt, Deutschland

Dekan: Prof. Dr. Martin Bastmeyer

Referent: Prof. Dr. Christopher Barner-Kowollik

Korreferent: Prof. Dr. Michael A. R. Meier

Tag der mündlichen Prüfung: 19.10.2012

Die vorliegende Arbeit wurde von November 2009 bis September 2012 unter Anleitung von Prof. Dr. Christopher Barner-Kowollik am Karlsruher Institut für Technologie (KIT) – Universitätsbereich angefertigt.

Ich erkläre hiermit, dass ich die vorliegende Doktorarbeit im Rahmen der Betreuung durch Prof. Dr. Christopher Barner-Kowollik, selbständig verfasst und keine anderen als die angegebenen Quellen und Hilfsmittel verwendet habe. Des Weiteren erkläre ich, dass ich mich derzeit in keinem laufenden Promotionsverfahren befinde, und auch keine vorausgegangenen Promotionsversuche unternommen habe.

Dominik Voll

Karlsruhe, den 14.01.2013

Abstract

Exact knowledge of the reactivity of photolytically generated radicals towards initiating free radical polymerization processes is – despite the significant industrial as well as academic importance of photo-initiated free radical polymerization – still scarce. In here, quantitative coupled size-exclusion chromatography (SEC) - electrospray ionization-mass spectrometry (ESI-MS) as well as direct infusion ESI-MS was employed to obtain the propensity of variable photolytically generated radical species to initiate macromolecular growth. Information on the frequency at which a radical species has initiated macromolecular growth is accessible *via* the evaluation of the disproportionation signals of the polymeric materials. SEC/ESI-MS mass spectrometry on polymeric systems has advanced to a point which makes obtaining quantitative species information feasible. The quantitative information on the relative quantities of specific radical endgroups that are incorporated into the polymer can be related to the reactivity of the photolytically generated radical. In addition, femtosecond pump-probe experiments were carried out to provide detailed information about the photoinitiators in terms of their internal energy conversion process and the associated singlet to triplet state transition efficiencies. In a second step and on the basis of the above information, the thesis seeks to interpret the determined order of reactivity in terms of the electronic as well as steric requirements that the individual radical species displays.

Publications Arising from the Thesis

- [6] *The Interplay of Different Relaxation Channels in the Excited State Dynamics of Photoinitiators*
Wolf, T. J. A.; Fischer, J.; **Voll, D.**; Wegener, M.; Barner-Kowollik, C.; Unterreiner, A.-N. *Ultrafast Phenomena XVIII* **2012**, in press.
- [5] *UV-Triggered Endgroup Conversion of Photo-Initiated Poly(Methyl Methacrylate)*
Voll, D.; Neshchadin, D.; Hildebrandt, K.; Gescheidt, G.; Barner-Kowollik, C. *Macromolecules* **2012**, *45*, 5850–5858.
- [4] *A Qualitative and Quantitative Post-Mortem Analysis: Studying Free-Radical Initiation Processes via Soft Ionization Mass Spectrometry*
Voll, D.; Junkers, T.; Barner-Kowollik, C. *J. Polym. Sci., Part A: Polym. Chem.* **2012**, *50*, 2739–2757.
- [3] *Elucidating the Early Steps in Photoinitiated Radical Polymerization via Femtosecond Pump-Probe Experiments and DFT Calculations*
Wolf, T. J. A.; **Voll, D.**; Barner-Kowollik, C.; Unterreiner, A.-N. *Macromolecules* **2012**, *45*, 2257–2266.
- [2] *Quantifying Photoinitiation Efficiencies in a Multi-Photoinitiated Free Radical Polymerization*
Voll, D.; Hufendiek, A.; Junkers, T.; Barner-Kowollik, C. *Macromol. Rapid Commun.* **2012**, *32*, 47–53.
- [1] *Quantitative Comparison of the Mesitoyl vs. the Benzoyl Fragment in Photoinitiation: A Question of Origin*
Voll, D.; Junkers, T.; Barner-Kowollik, C. *Macromolecules* **2011**, *44*, 2542–2551.

Contents

1. Introduction	1
1.1. Qualitative Analysis	3
1.2. Quantitative Analysis	3
1.3. Thermal Initiators	4
1.3.1. Qualitative Investigations of Thermal Initiators	6
1.3.2. Quantitative Investigations of Thermal Initiators	10
1.4. Photoinitiators	12
1.4.1. Qualitative and Quantitative Investigations of Photoinitiators	13
2. Theory of Free Radical Polymerization and Pulsed Laser Polymerization (PLP)	17
2.1. Free Radical Polymerization	17
2.1.1. The Fundamental Steps of Free Radical Polymerization	17
2.2. Pulsed Laser Polymerization (PLP)	21
2.2.1. Excimer Lasers – An Introduction –	22
2.2.2. Pulsed Laser Polymerization-Size-Exclusion Chromatography (PLP-SEC)	23
3. Characterization Techniques	27
3.1. Mass Spectrometry (MS) and Hyphenated SEC/ESI-MS	27
3.1.1. Fundamentals of Mass Spectrometry (MS)	27
3.1.2. ESI Ionization Procedure	28
3.1.3. Interpretation of Mass Spectra	29
3.1.4. Quantitative SEC/ESI-MS of Polymers	30
3.2. Femtosecond Spectroscopy	31
3.2.1. Generation of Ultrashort Femtosecond Pulses	31
3.2.2. Femtosecond Pump-Probe Spectroscopy	32
3.3. Chemically Induced Dynamic Nuclear Polarization-NMR	32
3.3.1. Radical Pairs in a Magnetic Field	33

3.3.2.	The Origin of CIDNP	34
3.3.3.	Kaptein's Rule	35
4.	Quantitative Comparison of the Mesityl vs. the Benzoyl Fragment	37
4.1.	Abstract	37
4.2.	Introduction	38
4.3.	Experimental Part	42
4.3.1.	Synthesis of Mesitylglyoxal	42
4.3.2.	Synthesis of 2-Hydroxy-1-mesityl-2-phenylethanone (2,4,6-Trimethylbenzoin, A)	43
4.3.3.	Pulsed Laser Polymerization (PLP) Procedure	43
4.3.4.	UV/Vis Measurements	45
4.3.5.	NMR Measurements	45
4.3.6.	SEC/ESI-MS Measurements	45
4.4.	Results and Discussion	46
4.4.1.	Reducing the Laser Energy	48
4.4.2.	Initiator Cocktails of Benzoin (B) and 2,4,6-Trimethylbenzoin (A)	49
4.4.3.	Data Analysis and Evaluation of the SEC/ESI-MS Spectra	52
4.5.	Conclusions	58
5.	Elucidating the Early Steps in Photo-Initiated Radical Polymerization	59
5.1.	Abstract	59
5.2.	Introduction	60
5.3.	Experimental Part	63
5.3.1.	UV/Vis Measurements	63
5.3.2.	Femtosecond Pump-Probe Experiments	63
5.3.3.	Theoretical Methods	63
5.3.4.	Photoinitiators	64
5.4.	Results and Discussion	64
5.4.1.	Absorption Spectra	64
5.4.2.	Time-Resolved Spectroscopy	66
5.4.3.	Results from DFT Calculations	70
5.5.	Conclusions	78
6.	Quantifying Photoinitiation Efficiencies in a Multi-Photo-Initiated FRP	81
6.1.	Abstract	81
6.2.	Introduction	82
6.3.	Experimental Part	84
6.3.1.	Synthesis of the Photoinitiators	84
6.3.2.	UV/Vis Measurements	86

6.3.3. NMR Measurements	87
6.3.4. Elemental Analysis	87
6.3.5. Pulsed Laser Polymerization (PLP) Procedure	87
6.3.6. SEC/ESI-MS Measurements	87
6.4. Results and Discussion	92
6.4.1. SEC/ESI-MS of Multi-Photo-Initiated pMMA	94
6.4.2. Quantifying the Initiation Ability in a Multi-Photo-Initiated Polymerization	95
6.4.3. UV-Spectra of the Employed Photoinitiators	97
6.5. Conclusions	100
7. UV-Triggered Endgroup Conversion of Photo-Initiated pMMA	101
7.1. Abstract	101
7.2. Introduction	102
7.3. Experimental Part	103
7.3.1. Hydrogenation of the Post-Irradiated Polymer	103
7.3.2. ¹ H CIDNP	103
7.3.3. ¹ H NMR	104
7.3.4. Polymer Synthesis <i>via</i> PLP and Post-Irradiation of the Polymer	104
7.3.5. SEC/ESI-MS Measurements	104
7.4. Results and Discussion	104
7.4.1. Elucidation of the Mechanism <i>via</i> SEC/ESI-MS	106
7.4.2. Elucidation of the Mechanism <i>via</i> CIDNP	111
7.5. Conclusions	117
8. Concluding Remarks and Outlook	119
9. Materials	123
9.1. Materials Used in Chapter 4	123
9.2. Materials Used in Chapter 5	123
9.3. Materials Used in Chapter 6	124
9.4. Materials Used in Chapter 7	124
10. List of Abbreviations	125
Bibliography	129
A. Appendix	143
Curriculum Vitae	159
Full List of Publications and Conference Contributions	161

Acknowledgment (Danksagung)

165

1

Introduction

Initiation processes are essential for every chain growth polymerization and thus of paramount importance not only for codetermining the rates at which the polymerization process proceeds (by virtue of the rate with which a primary radical reacts with the surrounding monomer units), yet also critically influence the resulting polymer properties. The endgroup chemistry of a polymeric chain is arguably the most powerful tool to gain access to complex macromolecular architectures *via* subsequent – often modular^[1] – transformation reactions. At the same time, the chain termini also present reactive points from which polymer degradation can commence. It is thus self-evident that good control over and (quantitative) knowledge of the endgroups contained in a polymer chain is of high importance. There exists a plethora of avenues to influence the polymer endgroup during free radical polymerization processes, which shall not be the focus of this thesis, including important polymerization protocols featuring living characteristics.^[2–6] Common to all polymerization processes, however, is the need of an initiating species, which commences the macromolecular growth process. In this introduction, the current state-of-the-art (excluding the results from the present thesis) will be discussed for understanding the endgroup chemistry imparted onto polymer chains during conventional thermally and photochemically initiated radical polymerizations. Qualitatively and quantitatively studying the exact nature of the polymer endgroups generated during initiation processes is a daunting task, as their concentration is typically very low, even when only intermediate polymer chain lengths in the range of 20-50 repeating units are investigated. It comes

thus at no surprise that a substantial number of studies have addressed – and continue to address – the fragmentation mechanisms of the used initiators themselves – often *via* highly time resolved pump-probe spectroscopic methodologies – without an ensuing post-mortem investigation of the resulting polymeric materials and a determination of the further fate of the generated radical fragments. Such investigations are undoubtedly of enormous value for the design of new initiators and an understanding of the underpinning decay mechanisms. Yet only in conjunction with a detailed (often monomer-type influenced) post-mortem endgroup analysis can an in-depth performance evaluation of a specific (photo)initiator be provided.

Particular note for the study and design of new photoinitiators should be given to the wide body of work from Fouassier and coworkers,^[7–14] Turro and coworkers,^[15–18] as well as Yagci and coworkers.^[19–21] These authors did not only study the radical formation mechanism associated with the photolytic radical generation in detail, but also suggested a range of new interesting initiation systems. In the realm of studying the molecular mechanics of the photo-induced decay of peroxy-type initiators – which are typically used as thermally decaying units – Buback, Schroeder and coworkers carried out a range of picosecond resolved studies,^[22,23] mapping the primary molecule decomposition pathways.

For several decades, the post-polymerization investigation of polymer endgroups has thus largely remained poorly investigated as techniques such as nuclear magnetic resonance (NMR) spectroscopy feature a poor concentration sensitivity and are not capable to image individual polymer chains, making the exact assignment of polymer endgroups an undertaking that is beset with a high degree of uncertainty. The analytic situation, however, has changed considerably within the last 15 years, when soft ionization-mass spectrometric techniques became sufficiently powerful and high resolving to be applicable toward the study of synthetic macromolecules. Although mass spectrometric techniques cannot heal the caveat that the endgroups of high molecular weight polymers cannot be reliably determined (as high molecular weight material is difficult to ionize and cannot be imaged with high resolution), it nevertheless provides high sensitivity and accuracy for low and intermediate molecular weights, depending on the ionization and detection techniques. The two key soft ionization protocols used for studying synthetic polymers are electrospray ionization (ESI),^[24,25] which is often hyphenated with size-exclusion chromatography (SEC),^[26,27] and matrix-assisted laser desorption ionization (MALDI).^[28–30] Both techniques can be coupled to variable mass analyzers; most often, ESI is coupled to (linear) quadrupole ion traps, Orbitraps or ion cyclotron resonance detectors, whereas MALDI is regularly coupled to time-of-flight (ToF) analyzers. It is not the aim of this thesis to review or reiterate the details of soft ionization mass spectrometry (MS) applied to synthetic polymers; for detailed information on these techniques in the context of macromolecular science, the reader is referred to a recent

book^[31] covering the entire field as well as key reviews.^[32] There is a large body of work on the use of ESI-MS in connection with nitroxide trapping to elucidate initiation pathways by Busfield and Jenkins,^[33,34] however, that work concerns only the first steps in initiation and the assessment of the initiation efficiency of fragments is indirect in that certain initiator derived fragments, which could directly react with nitroxides and thus remain invisible during the analysis. In the context of this introduction, the following key points regarding the analysis of polymers and their endgroups *via* soft ionization MS should be highlighted.

1.1. Qualitative Analysis

The main benefit of soft ionization MS – beside the fact that the polymer chains remain intact during the ionization process and thus molecular ions are imaged – is the unrivaled accuracy of the mass determination. The precision allows the determination of the molecular formula of the imaged polymer chains and thus enables an unambiguous determination of the endgroup. The structural elucidation power is further enhanced when the mass analysis is combined with collision-induced decay (CID) experiments. Thus, the question of which endgroups occur can often quite readily be answered, especially since the molecular structure of the used initiators and monomers are known. A range of studies has focused – for both thermally and photochemically decaying initiators – on the question of the type of endgroups present.

1.2. Quantitative Analysis

Once the question of which radical fragments are featured at the chain termini is clarified, it is of paramount interest to establish how much of each fragment has contributed to the initiation and termination processes and relate this finding to its molecular structure and its short-time molecular decay mechanism. Finally, this can lead to a source database allowing for prediction of the distribution of endgroups within a given polymer. In principle, MS yields the number distribution of the polymeric materials and quantification should thus be readily possible. Unfortunately, chain length dependent ionization biases and distortions can lead to severe misrepresentations of the amounts of individual chains. To overcome the quantification problem, several techniques have been developed^[35] with the most powerful example being a combined SEC/ESI-MS approach (see Chapter 3.1.4).^[27] In the context of this introduction as well as the current thesis, the quantitative evaluation of polymeric materials obtained *via* both thermal and photochemical processes will be discussed.

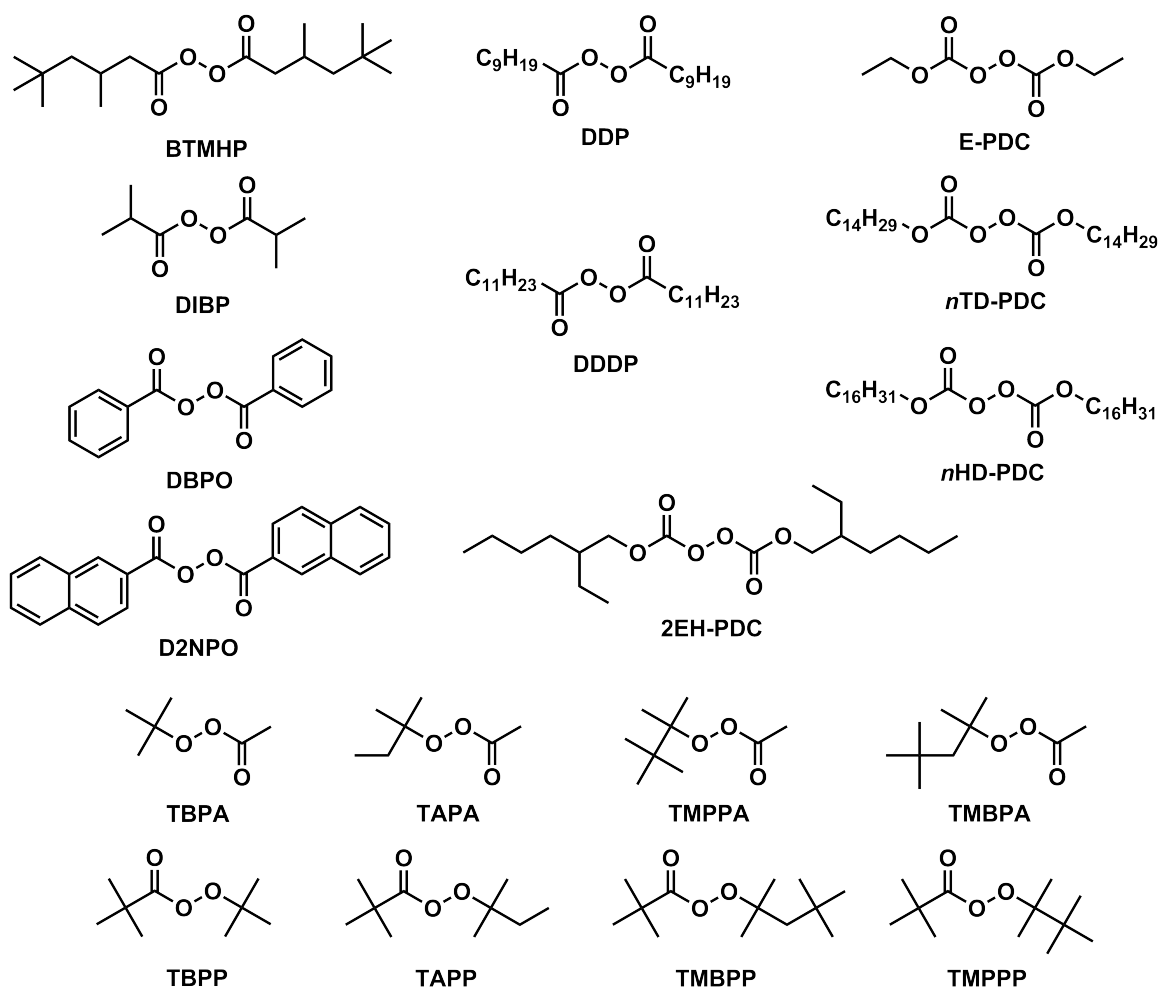
As afore-mentioned, it is critical for a successful mass spectrometric analysis to keep the molecular weights of both thermally as well as photochemically initiated polymers relatively low, typically not exceeding 4000 Da, to achieve sufficiently high isotopic resolution in both

ESI-MS and MALDI-MS. In thermally-initiated processes (where e.g., peroxy-initiators are utilized) the molecular weights can be kept low by using high concentrations of initiator, whereas the limitation of the molecular weight during photochemical initiation is not as straightforward. Although a broadband ultraviolet (UV) lamp could be used to initiate the polymerization process, the ensuing excitation of the photoinitiators would be relatively undefined. For a precise excitation at a specific wavelength, excimer lasers are typically used operating on the XeF line (351 nm, with a pulse width of a few nanoseconds). The advantage of such a laser-induced initiation process is not only the precise excitation at a specific wavelength, but also enables reactions initiated by pulse patterns – so-called pulsed laser polymerization (PLP)^[36–39] – to limit the growth time of the generated macroradicals between two successive laser pulses, thus limiting the molecular weights. It is for this reason that all studies seeking to address endgroup patterns in photolytically generated polymers studied *via* MS use pulsed laser systems (see e.g., refs. 40, 41, and 42). It is additionally interesting to note that the combination of PLP with mass spectrometric analysis can provide calibration free access to propagation rate coefficients in free radical polymerization.^[43–46]

In the following, a concise review on the application of soft ionization MS for the study of thermally initiation processes is provided. At the end of this introduction a transition to photoinitiation processes is given.

1.3. Thermal Initiators

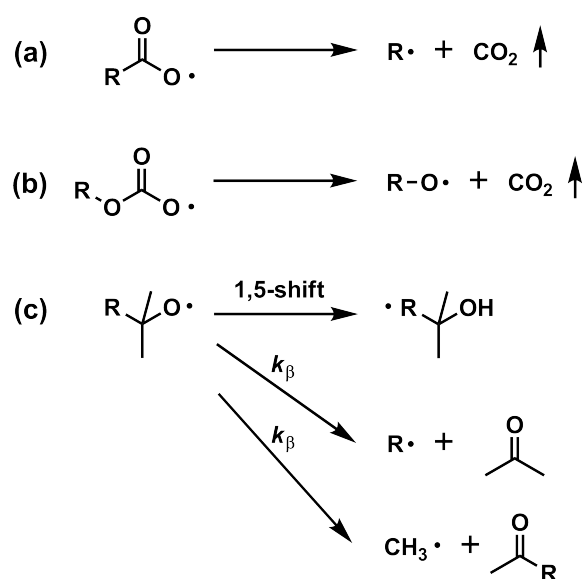
Among the variety of radical initiators that decompose upon thermal stimulus, peroxy compounds are undoubtedly the most important class. Although in laboratory scale (polymer) chemistry azo-initiators may be more used, peroxy compounds are favored in many industrial processes since they give access to a much broader decomposition temperature range due to the wide structural variation that is accessible. Virtually, any decomposition rate/decomposition temperature can be realized with peroxy initiators, while at the same time retaining high initiation efficiencies. Other advantages of peroxy-type thermal initiators are that they often lead to simple, nondegradable endgroups, which improves the performance and durability of the generated polymeric materials. Peroxy initiators are, however, not a uniform class of compounds. Next to classical peroxides, labile peroxy groups are also found in peroxyesters (e.g., peroxy-pivalates or peroxyacetates, see Scheme 1.1), diacyl peroxides or peroxydicarbonates (both see in Scheme 1.1). Each of these compounds is associated with a specific decomposition scheme and may yield various radical fragments. Generally, oxygen-centered radicals are formed in the primary decomposition reaction, resulting in one of the three respective fragments depicted in Scheme 1.2.



Scheme 1.1 Thermal initiators used in methyl methacrylate (MMA) polymerization investigated via ESI-MS techniques. Bis(3,5,5-trimethylhexanoyl) peroxide (BTMHP), di-*iso*-butyryl peroxide (DIBP), di-benzoyl peroxide (DBPO), di-2-naphthoyl peroxide (D2NPO), di-*n*-decanoyl peroxide (DDP), di-*n*-dodecanoyl peroxide (DDDP), ethyl peroxydicarbonate (E-PDC), *n*-tetradecyl peroxydicarbonate (*n*TD-PDC), *n*-hexadecyl peroxydicarbonate (*n*HD-PDC), 2-ethylhexyl peroxydicarbonate (2EH-PDC), *tert*-butyl peroxyacetate (TBPA), *tert*-amyl peroxyacetate (TAPA), 1,1,2,2-tetramethylpropyl peroxyacetate (TMPPA), 1,1,3,3-tetramethylbutyl peroxyacetate (TMBPA), *tert*-butyl peroxy-pivalate (TBPP), *tert*-amyl peroxy-pivalate (TAPP), 1,1,3,3-tetramethylbutyl peroxy-pivalate (TMBPP), and 1,1,2,2-tetramethylpropyl peroxy-pivalate (TMPPP).^[47–50]

As described by Vana and Buback,^[47–50] peroxyesters yield carboxy radicals (Scheme 1.2a), peroxy-carbonates generate carbonic radicals (Scheme 1.2b) and alkoxyradicals (with Scheme 1.2c being a specific *tert*-butoxy-type fragment of this class). All initiators shown in Scheme 1.1 can be derived from these fragments. Regardless, all fragments depicted in Scheme 1.2 may undergo secondary reactions, thus expanding the spectrum of radicals available in further polymerization reactions. Specifically important are decarboxylations of fragments (a) and (b), yielding carbon-centered radicals. Alkoxyradicals are typically less prone to secondary fragmentation, yet in specific cases – such as in the per-pivalate derived fragments (c) – 1,5-shift or β -scission reactions can occur as depicted. Thus, the number

of fragments that can be found as endgroups during the post-mortem analysis of polymers obtained from peroxy initiators can – depending on the reaction conditions – be quite diverse and may only indirectly reflect the primary decomposition products of the initiator. In what follows, each initiator group that has been investigated during the work on thermal initiators to date with mass spectrometric techniques will be described individually.^[47–50] In all cases, decomposition patterns are analyzed on the example of methyl methacrylate (MMA) polymers and thus some of the conclusions drawn from these experiments are only strictly valid for this monomer or monomer family, respectively.



Scheme 1.2 Decomposition pathways of oxygen-centered radicals. Peroxyesters yield carboxy radicals (a), peroxy carbonates generate carbonic radicals (b) and alkoxy radicals (c, being a specific *tert*-butoxy-type fragment of this class).^[47]

1.3.1. Qualitative Investigations of Thermal Initiators

Peroxy pivalates

Peroxy pivalates decompose into pivaloyl radicals and the respective counterpart alkoxy radical. In all cases, the pivaloyl radical decomposes instantly under decarboxylation into CO_2 and a *tert*-butyl fragment, which consequently is identified by endgroup analysis as initiating species in all polymerizations that were studied at 90 °C in benzene as solvent. The alkoxy radicals assessed were *tert*-butoxy radicals (derived from *tert*-butyl peroxy pivalate, TBPP), *tert*-amyloxy radicals (derived from *tert*-amyl peroxy pivalate, TAPP), 1,1,3,3-tetramethylbutoxy radicals (derived from 1,1,3,3-tetramethylbutyl peroxy pivalate, TMBPP), or 1,1,2,2-tetramethylpropyloxy radicals (derived from 1,1,2,2-tetramethylpropyl peroxy pivalate, TMPPP).^[47] Generally, quite diverse mass spectra are observed with different endgroup combinations being present. Chains carrying two initiator-derived endgroups are

products from recombination reactions, that is the reaction of a growing chain with one initiator fragment on the end, with a second chain also carrying an initiator fragment or with an initiator fragment directly. Such combination products exhibit initiator fragments as endgroups on both sides of the polymer chain and thus do not allow to distinguish which fragment initiated the polymerization. Only disproportionation products with one initiator fragment and one unsaturated or saturated chain endgroup allow for the – qualitative or quantitative – evaluation of the individual species in the ESI-MS mass spectra.

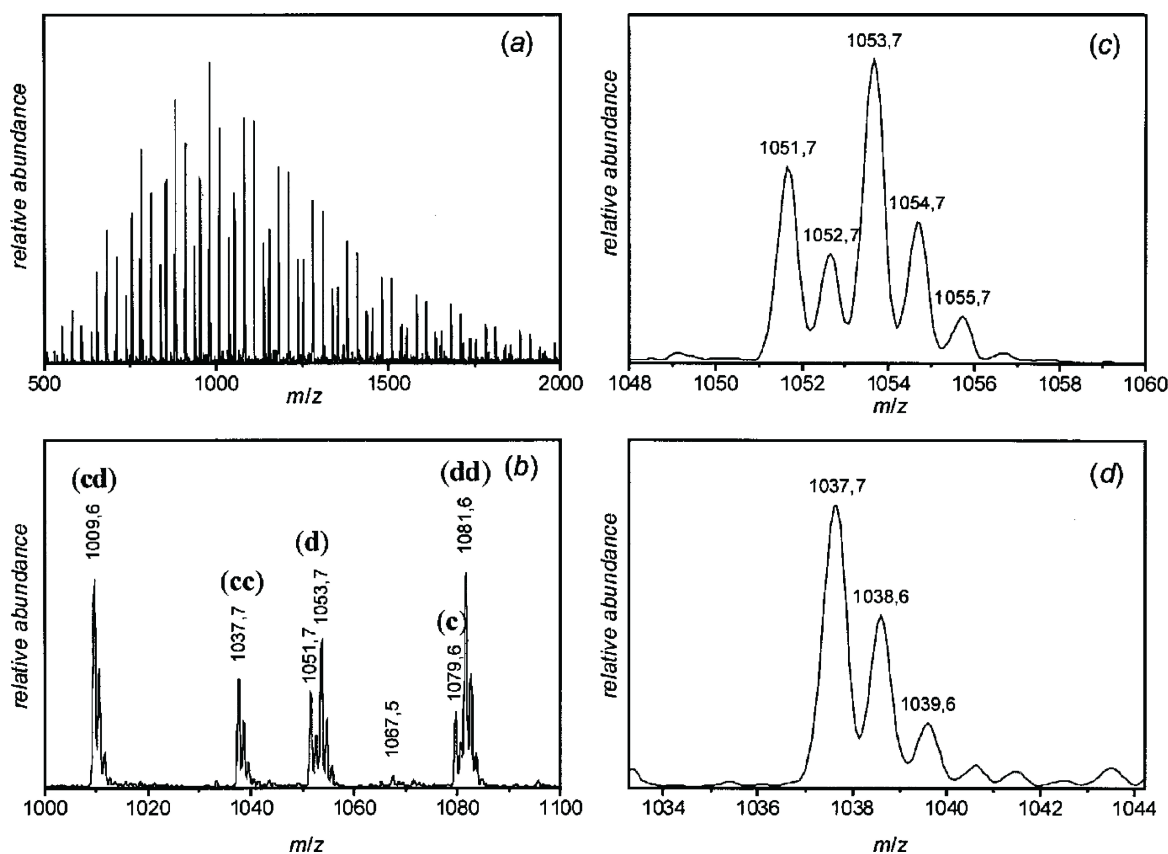


Figure 1.1. ESI-MS spectrum of poly(methyl methacrylate) (pMMA) initiated by *tert*-amyl peroxyvalate (TAPP) in toluene at 90 °C: (a) overview of the spectrum in the range between 500 and 2000 Da, (b) enlarged m/z range covering one monomer repeating unit, (c) enlargement of one selected disproportionation peak, and (d) enlargement of one selected combination peak. Reproduced from ref. 47, with permission from Wiley and Sons.

Figure 1.1 depicts the spectrum of pMMA obtained *via* initiation with TAPP. In the notation of Figure 1.1b, (c) represents the *tert*-butyl fragments and (d) an ethyl radical fragment obtained from β -scission of the primary *tert*-amyl radical. (cc), (dd), and (cd) are the three recombination products resulting from the combination of the present endgroups (c) and (d). As depicted in Figure 1.1, combination and disproportionation species can readily be differentiated by their typical peak pattern. It should be noted that for each species characteristic peak patterns exist due to the isotope effect of the

present atoms. Carbon, which forms the backbone of the analyzed polymers, has a natural ^{12}C occurrence of about 98.9 % and of 1.1 % for ^{13}C . Because of the large number of atoms, chains containing a different amount of ^{13}C and thus multiple peaks with a total mass – each with a difference of 1 Da – are observed. Disproportionation peaks correspond to two species differing exactly by 2 Da (since one hydrogen atom is transferred from one chain to the other). The *tert*-amyl radical completely decomposes into secondary fragments before the initiation of chain growth takes place, indicating that the β -scission reaction is – similar to the decarboxylation a reaction – particularly rapid and occurs before the radicals can escape the solvent cage or very shortly thereafter.^[51–53] Interestingly, only ethyl radicals are observed and no methyl radicals are identified, which would be expected when β -scission would occur to either side. The fate of the methyl radicals remains unresolved, since it cannot be distinguished if these moieties are simply not formed or are consumed in other small-radical reactions prior to chain initiation events.

Much simpler spectra are obtained for the 1,1,2,2-tetramethylpropyloxy radical fragment. Here, scission yields the same fragment as the decarboxylation of the pivaloyl radical. Thus, significantly more simplified spectra can be observed. Again, occurrence of methyl radicals cannot be confirmed, while no alkoxy radical fragments can be found in the product spectra. This situation changes when using TMBPP as initiator. The same analog products are formed as in the case of the previous two initiators, but now also the alkoxy fragments appear in the spectra. Conclusively, it is however assumed that not the oxygen-centered radical initiates chain growth in this case, but rather the product of the 1,5-H-shift is formed (see Scheme 1.2).^[34] Even with TBPP, where an arguably relatively stable *tert*-butoxy radical is generated, β -scission is the dominant reaction pathway and no oxygen centered radical fragments can be identified. Therefore, however, methyl radical fragments (as the only possible reaction product from β -scission) are now observed as initiating and terminating moiety at the chain termini. As an additional product, however, benzyl fragments are seen, which are most likely generated from transfer to solvent reactions either from the longer-lived *tert*-butoxy fragments or by the highly reactive methyl radicals.

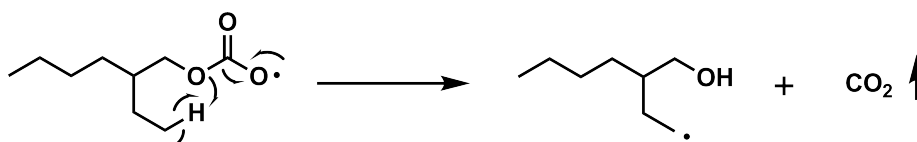
Peroxyacetates

In a following study,^[48] the same alkoxy fragments were assessed against acetoxy radicals, which are derived from peroxyacetates. The peroxyacetates under investigation were *tert*-butyl peroxyacetate (TBPA), *tert*-amyl peroxyacetate (TAPA), 1,1,3,3-tetramethylbutyl peroxyacetate (TMBPA) or 1,1,2,2-tetramethylpropyl peroxyacetate (TMPPA). Decarboxylation of the acetoxy fragment yields methyl fragments at all times, again demonstrating the high rate of the CO_2 scission reaction. Otherwise, the studied product patterns revealed the same trends as in the study involving perpivalates: All alkoxy radical fragments

behaved in a qualitatively identical fashion. β -scission is the dominant pathway and ethyl or *tert*-butyl groups are found as complimentary endgroups. TMBPA again shows a tendency to 1,5-H-shift reactions and TBPA results in methyl fragments from β -scission of the *tert*-butoxy fragment. A higher tendency for transfer reactions was observed with the *tert*-butoxy fragment, which was consequently tested by performing reactions in mesitylene to provide a solvent with more readily abstractable protons. Indeed, formation of a fraction of star polymers by multiple proton abstraction from mesitylene was observed, giving a good example for side reactions that must be considered when certain reaction media are utilized. On the other hand such side reactions can also be used to generate a certain fraction of more complex polymer chains, for example, as *in-situ* formed rheology modifiers.

Diacyl peroxides

A much simpler situation should be found when peroxides are assessed that only fragment into acyclic fragments.^[49] Consequently, a group of symmetrical diacyl peroxides were subjected to ESI-MS analysis. Four peroxides with aliphatic residues (di-*n*-decanoyl peroxide (DDP), di-*n*-dodecanoyl peroxide (DDDP), bis(3,5,5-trimethylhexanoyl) peroxide (BTMHP), and di-*iso*-butyryl peroxide (DIBP)) and two aromatic compounds (di-benzoyl peroxide (DBPO) and di-2-naphtoyl peroxide (D2NPO)) were studied. In case of the aliphatic peroxides, simple mass spectra were obtained and only the corresponding radical fragments after decarboxylation were identified.



Scheme 1.3 Decarboxylation reaction postulated for the primary decomposition fragments derived from 2EH-PDC.

Since only symmetrical initiators were tested, the spectra thus only consisted of one combination and one disproportionation product. Different spectra were obtained in case of the aromatic diacyl peroxides: The aromatic ring adds stability to the acyclic radical, thus giving it a higher propensity to function as an initiating species. When using DBPO, phenyl as well as benzoyloxy endgroups were identified in the product spectra, whereby the decarboxylated phenyl fragment featured a slightly larger presence in the spectra. With the naphthyl analog, both types of endgroups were found, however, the naphthoyloxy fragment appeared in similar quantities as the naphthyl endgroup. The assignment of all peaks (almost isobaric products made the analysis *via* conventional ion-trap analysis difficult) was confirmed with fourier transform-ion cyclotron resonance (FT-ICR) measurements.

Peroxyarbonates

Last but not least, peroxyarbonates were studied by the Buback/Vana group.^[50] Four carbonates, namely ethyl peroxydicarbonate (E-PDC), *n*-tetradecyl peroxydicarbonate (*n*TDPDC), *n*-hexadecyl peroxydicarbonate (*n*HD-PDC), and 2-ethylhexyl peroxydicarbonate (2EH-PDC) were selected and subjected to the same analysis as the other peroxide initiators. The primary fragmentation products of this class of initiators can decarboxylate similarly to the acyclic radicals, with the difference, however, that alkoxy radicals remain as the product. Interestingly, the product spectra revealed that the primary radical fragments are effective initiating moieties, and thus it may be concluded that decarboxylation as shown in Scheme 1.2b is not a very fast reaction compared to monomer addition. Basically, all three *n*-alkyl initiators underwent no significant secondary fragmentation reaction, and only trace amounts of alkoxy fragments were observed. Only 2EH-PDC demonstrated a slight deviation from this rule. Because of the ethyl branch of the substituent, a radical shift can occur and it was postulated that the associated type of fragment undergoes a concerted decarboxylation combined with a radical shift (see Scheme 1.3). When the combination peaks in the spectra were compared, then almost 50 % of all products carried one decarboxylated fragment. For a more detailed summary the reader is referred to Chapter 10 in ref. 31.

1.3.2. Quantitative Investigations of Thermal Initiators

Determination of the Mode of Termination

With regard to the qualitative investigations discussed above, the question arose how far a quantitative analysis may be performed with the data at hand. The clear distinction between combination and disproportionation products leads to the question whether a comparison of their respective peak intensities may be used to derive the exact fraction of chains that undergo disproportionation. Clearly, with MMA, disproportionation is the more dominant mode of termination, although precise values have been scarce in the literature. Nevertheless, Zammit *et al.*^[54] have adopted this idea early on and derived the parameter λ from MALDI-ToF analysis of polymers synthesized *via* free radical polymerization, where λ is described in Eq. 1.1.

$$\lambda = \left(\frac{k_{t,d}}{k_{t,d} + k_{t,c}} \right) = \left(\frac{k_{t,d}}{k_t} \right) \quad (1.1)$$

Where $k_{t,d}$ and $k_{t,c}$ are the rate coefficients for termination by disproportionation and combination, respectively. Zammit *et al.* simply compared peak intensities of the individual

peaks and directly obtained a value for λ . Russell and coworkers^[35] put the above approach on a better theoretical foundation and closely examined the spectra obtained for MMA polymerization with the initiator BTMHP (see Chapter 1.3.1). From the qualitative analysis it was already known that the obtained mass spectrum would be relatively clean and allow at the same time for a clear distinction between the combination and disproportionation product peaks. The derivation of equations to obtain accurate λ is relatively complicated due to the complex accounting of the overall termination levels and the effect of overall radical concentration, which affects the direct ratio of two peaks at any given chain length. However, application of the equations is not difficult and the procedure described can in principle be readily used in forthcoming studies. A general problem with the quantitative analysis of the spectra is that sometimes mass spectrometric methods do not yield spectra corresponding to the true concentrations of a distribution. The measured (apparent) distribution is often subject to mass-bias and thus no overall molecular weights may be derived directly from the spectra.^[31] Comparing species with almost identical overall molecular weight may, however, be allowable under the assumption that both chains consist of an identical backbone and that the ionization bias from the endgroups is negligible. Thus, it is mandatory to establish if the obtained integration result is invariant for all chain lengths, to ensure that a potential mass-bias does not influence the result of the analysis. In fact, no significant deviation of the data depending on the overall chain length (at least in the monitored window of masses below 2000 Da) could be observed and λ was determined to be 0.63 ± 0.10 , which is arguably the most accurate and most reliable value ever determined for the ratio of combination to disproportionation in a free radical polymerization.

Initiator Efficiencies for Diacyl Peroxides

The method of comparing peak intensities can also be used to assess initiation efficiencies of thermal initiators.^[55] The qualitative studies described above allowed a mechanistic understanding of secondary fragmentations and other cage reactions. The effect of these reactions on the performance and overall quality of the individual initiators, was not yet examined. Generally, initiator efficiencies f are given by the ratio of initiator fragments build into the polymer chains compared to the total number of fragments generated by decomposition. f can be deduced in different ways and a common procedure is to compare the efficiency of one initiator to other initiators, whose f is known for a certain reaction condition. Mass spectrometric techniques are – in a similar fashion as for the determination of the mode of termination – advantageous. When initiator cocktails are used in polymerizations, peak intensities of the individual species can be compared and thus directly allow for a quantitative comparison of endgroups. Importantly, mass-bias effects must be accounted for and in this specific case ionization biases stemming from different endgroups must also be considered. Vana and coworkers used

reversible addition-fragmentation chain transfer (RAFT)-made polymers and endgroup modified RAFT polymers to test for the influence of different polarities and could confirm that for oligomeric MMA and methyl acrylate (MA) no significant influences in intensity could be observed stemming from the endgroups in standard ESI-MS analysis.^[55]

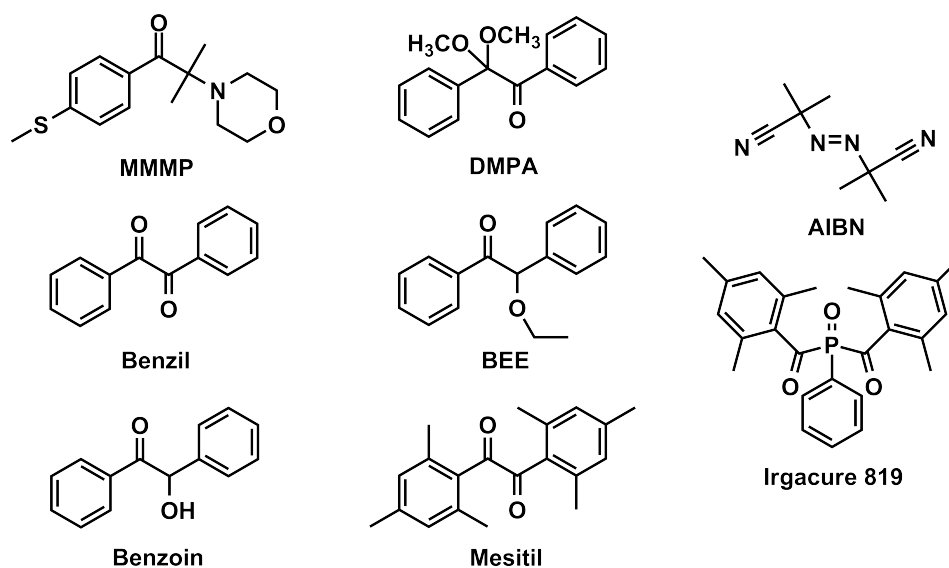
Direct comparison of peak intensities yields f for a given initiator when the polymer was isolated at low reaction times (to allow for a small $k_d \cdot t$) and if f is known for the second initiator. In their study, Vana and coworkers^[55] investigated the diacyl peroxides BTMHP and DBPO against the wellknown initiator azo-bis(isobutyronitrile) (AIBN), which has a efficiency of ~ 0.8 at higher temperatures. Both initiators exhibit increasing apparent efficiencies with increasing chain length. Thus, a long-chain value was approximated by data fitting. For BTMHP, the initiator efficiency was determined to 0.57 ± 0.08 at 80°C and for DBPO an efficiency of 0.89 ± 0.08 was obtained for polymerizations carried out at 100°C . These results are in good agreement with other reported literature values.

1.4. Photoinitiators

Photoinitiators are used for the polymerization of functional monomers or the generation of variable oligomers and polymers.^[56] They are employed in industrial applications including the UV-curing of coatings and inks as well as for more specialized applications,^[57] such as dental restorative materials,^[58,59] biomaterials,^[60,61] and the fabrication of 3-dimensional objects.^[62] Photoinitiation is usually applied to commence a chain growth process where both the initiating species and the growing chain ends are radicals,^[63] cations,^[64] or – in some cases – anions or weak bases.^[65] In particular, substituted thioxanthenes,^[20,21,66,67] Barton esters,^[68,69] disulfides^[11] as well as photoinitiators based on silyl radical chemistry^[9,12] are currently being described. Photoinitiators for radical polymerizations are classified as cleavage (type-I, for example benzoin and derivatives, also employed in the current thesis) and H-abstraction type (type-II, for example thioxanthone and derivatives) initiators.^[70–72] The majority of type-I photoinitiators are aromatic carbonyl compounds with appropriate substitution. Upon absorption of light, benzoin and its derivatives spontaneously undergo α -cleavage and generate free radicals. Benzoin and its derivatives are the most widely used photoinitiators for free radical polymerization due to their high quantum efficiency and reactivity of the generated radical fragments. Photoinitiation processes *via* type-II photoinitiators are based on the reaction of their triplet excited states with a hydrogen donor, thereby producing an initiating radical.^[72]

1.4.1. Qualitative and Quantitative Investigations of Photoinitiators

Preliminary ESI-MS studies with 2-methyl-1-[4-(methylthio)phenyl]-2-morpholinopropan-1-one (MMMP) as photoinitiator (see Scheme 1.4) featured the possibility of determining photoinitiator-derived endgroups in polymers^[73,74] (as seen in the thermal part of this introduction, Section 1.3). In further qualitative studies various photoinitiators (see Scheme 1.4) were investigated in PLP experiments and consecutive ESI-MS analysis of the obtained polymers was carried out (for details see refs. 40, and 41).



Scheme 1.4 Photoinitiators employed to date in qualitative and quantitative studies *via* PLP/ESI-MS; 2-methyl-1-[4-(methylthio)phenyl]-2-morpholinopropan-1-one (MMMP), 1,2-diphenylethane-1,2-dione (benzil), 2-hydroxy-1,2-diphenylethane-1,2-dione (benzoin), 2-ethoxy-1,2-diphenylethane-1,2-dione (BEE), 2,2-dimethoxy-1,2-diphenylethane-1,2-dione (DMPA), azobis(*iso*-butyronitrile) (AIBN), bis(2,4,6-trimethylbenzoyl)-phenylphosphineoxide (Irgacure 819), 1,2-dimesitylethane-1,2-dione (mesitil).

Benzoin vs. Mesitil

In the first quantitative study concerning photoinitiators, Günzler *et al.* determined – in a quantitative fashion *via* ESI-MS – the ratio in which the benzoyl radical (derived from benzoin, see Scheme 1.4) and the mesityl radical (derived from mesitil, see Scheme 1.4) are initiating macromolecular growth toward MMA.^[42] This combination of photoinitiators is inspired by the qualitative study of Szablan *et al.* where Irgacure 819, which also bears the mesityl moiety, was used for qualitative studies providing an indication that the mesityl radical apparently only terminated chain growth but was incapable to initiate new chains.^[41] Figure 1.2a depicts one repeat unit of the ESI-MS spectrum of benzoin/mesitil-initiated pMMA and evidences that the mesityl radical is also able to initiate the macromolecular growth ($D_{3,2,MMA}$ and $D_{3,1,MMA}$, structures see Figure 1.2c) under the employed conditions.

1. Introduction

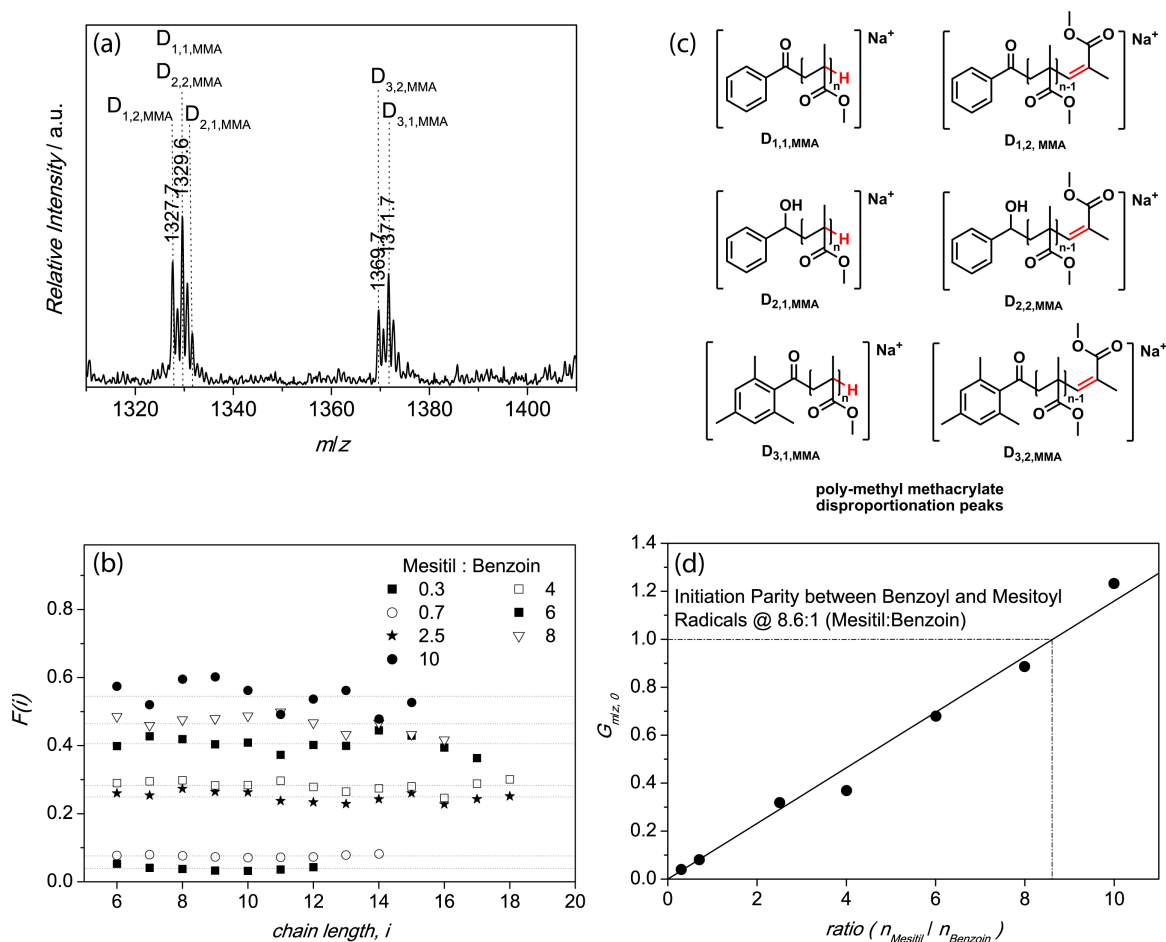


Figure 1.2. (a) ESI-MS spectra of the polymeric material obtained from the benzoin/mesitol-initiated ($c_{PI,0} = 5 \times 10^{-3} \text{ mol L}^{-1}$) PLP of MMA at 5°C at a laser intensity of 5 mJ/pulse and a frequency of 100 Hz . Zoom scan of one monomer repeat unit between 1315 and 1415 m/z . (b) Intensity-derived mole fractions of polymer chains initiated with mesitoyl radicals, $F(i)$, vs. the chain length, i . (c) Expected polymeric disproportionation peaks in the photochemically initiated bulk free radical polymerization of MMA in the presence of a mixture of the benzoin and mesitol photoinitiators. (d) Ratio of the intensities of the disproportionation signals corresponding to polymer chains initiated with a benzoyl and a mesitoyl radical vs. the ratio of both initiators in the reaction mixture (ratio = $n_{mesitol} : n_{benzoin}$). Reproduced from ref. 42, with permission from the American Chemical Society.

Upon inspection of the mole fraction plot (see Figure 1.2b) there is no indication for a chain length dependent mass-bias within all utilized initiator ratios. However, the aforementioned method of mass-bias assessment is nevertheless used to reduce any possible mass distortions.^[35,42,75] Figure 1.2d depicts the initiation parity plot of the benzoyl- and mesitoyl-initiated polymeric material. Initiation parity between both radicals occurs at an initiator ratio of 8.6:1 (mesitol:benzoin). When considering the UV absorbance of the two initiators at the laser wavelength of 351 nm , mesitol should yield by far more primary radicals than benzoin in the initiation of free radical polymerizations, yet this is not the case as 8.6 times more mesitol is necessary to obtain the same amount of chains initiated with the mesitoyl fragment.

The above-mentioned study of benzoin and mesitol is therefore the link between the quantification studies of thermal initiators and photoinitiators. The results presented within the current thesis lead on from these initial findings.

2

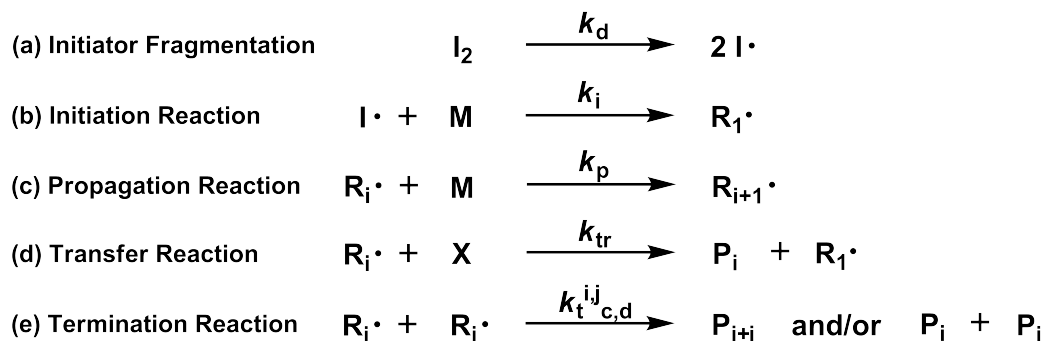
Theory of Free Radical Polymerization and Pulsed Laser Polymerization (PLP)

2.1. Free Radical Polymerization

2.1.1. The Fundamental Steps of Free Radical Polymerization

The overall free radical polymerization process consists of five fundamental reaction steps (see Scheme 2.1) with their corresponding rate coefficients.^[76,77] To describe the complete free radical polymerization process a kinetic rate law expression is required for each individual reaction step. If all rate coefficients for a specific system are known, it is possible to predict the overall polymerization process. The first step is the decomposition of the initiator molecule I_2 (a) into two initiator-derived radical fragments ($I\cdot$) with the rate coefficient of initiator decomposition (k_d) followed by the initiation of the free radical polymerization process (b) with the rate coefficient of initiation (k_i). In a third step the propagation reaction (c) proceeds with the rate coefficient of propagation (k_p) followed by the fourth step, the transfer reaction (d) with the rate coefficient for transfer (k_{tr}). The last step is

the termination reaction (e) which proceeds *via* the combination (P_{i+j} , k with index c) or disproportionation ($P_i + P_j$, k with index d) of two radical species with the rate coefficient of termination ($k_{t\ c,d}^{i,j}$).



Scheme 2.1 Fundamental steps of a free radical polymerization. Given are the rate coefficients for each individual step. I_2 is the initiator, $R_i\cdot$ is a radical of chain length i , M is the Monomer, X is a transfer agent, and P is the polymer.

Initiation of Free Radical Polymerization

The decomposition of the initiator molecules given in Scheme 2.1 is the same for both thermal and photoinitiators and the decrease in initiator concentration ($[I]$) during the polymerization process is

$$-\frac{d[I]}{dt} = k_d \cdot [I] \quad (2.1)$$

The rate of generation of primary radicals is of interest in kinetic studies, therefore the first-order rate law expression for decomposition of the initiator molecules is given by

$$\frac{d[R_1\cdot]}{dt} = 2 \cdot f \cdot k_d \cdot [I] \quad (2.2)$$

The definition of the initiator efficiency (f) was already given in Chapter 1.3.2. Typical values of f are between 0.5 and 0.8. If unsymmetric initiator molecules are used for the initiation process, $I_1\cdot$ and $I_2\cdot$ do not necessarily display the same reactivity toward the monomer unit.^[78–80] Furthermore, this also includes different k_i for the respective radical fragments ($k_{i,1}$ and $k_{i,2}$). The overall rate expression for the diffusion controlled initiation process is given by

$$\frac{d[R_1\cdot]}{dt} = k_i \cdot [M] \cdot [I\cdot] \text{ with } k_i = \frac{k_{i,1} + k_{i,2}}{2} \quad (2.3)$$

There exists a plethora of methods and compounds for the initiation of a free radical polymerization:

- Thermal initiation (see Chapter 1.3)
- Photoinitiation (see Chapter 4 - Chapter 7)
- γ -radiation or electron-induced initiation^[81]
- Plasma-induced initiation^[82]
- Electroinitiation^[83]
- Redox-initiating systems^[84–86]
- Self-initiated polymerization^[87–89]

The values for the rate coefficient of the initiator decomposition step, k_d , can be assessed *via* direct measurement of the initiator concentration as a function of time^[90,91] or the dead-end polymerization method.^[77] Typical values for k_d are in the order of 10^{-1} - 10^{-8} s⁻¹.

Propagation Reaction in Free Radical Polymerization

The addition of a macroradical $R_i\cdot$ to a monomer unit, M, is described by the following rate law expression for the propagation reaction:

$$-\frac{d[M]}{dt} = \sum_i k_p^i \cdot [R_i\cdot] \cdot [M] \quad (2.4)$$

The propagation reaction is a chemically controlled reaction, i.e., it is only to a small extent dependent on the system viscosity and the solvent. For this reason, the propagation rate coefficient is constant up to high monomer conversion. Only at monomer to polymer conversions exceeding 80 % k_p becomes diffusion controlled. The value of k_p is dependent on the reactivity of the propagating radical, $R_i\cdot$ as well as the nature of the monomer unit. Entropic and electronic factors as well as their activation parameters (activation energy (E_a) and pre-exponential factor (A), refer to Chapter 2.2) also influence the value for k_p . Quenched instationary polymerization system (QUIPS),^[92–94] electron spin resonance spectroscopy (ESR) for stationary polymerization^[95,96] and the most common method, pulsed laser polymerization-size-exclusion chromatography (PLP-SEC)^[37] can be utilized for determining the k_p values. In terms of the reproducibility of k_p , PLP-SEC is the preferred method (see Chapter 2.2). At 60 °C MMA shows a k_p of 830 L mol⁻¹ s⁻¹, MA of 24000 L mol⁻¹ s⁻¹, and styrene of 340 L mol⁻¹ s⁻¹.^[97]

Transfer Reaction in Free Radical Polymerization

In a transfer reaction the propagating radical, $R_i\cdot$, is transferred to another species in the reaction mixture. The existence of this – mostly unintended – reaction is also the reason for an often reduced averaged molecular weight in comparison to the predicted one. $R_i\cdot$ has the ability to abstract weakly bonded atoms from the transfer agent (X). The consequence of this reaction is the formation of a dead polymer chain and a new free radical, which possibly might react with monomer units. The rate law expression is given by the following equation:

$$-\frac{d[X]}{dt} = k_{tr} \cdot [R_i\cdot] \cdot [X] \quad (2.5)$$

Chain transfer proceeds *via* transfer to monomer (C_M), transfer to initiators (C_I), transfer to solvents and additives (C_T), and transfer to polymer (C_P , long chain branching *via* intermolecular reactions and short chain branching *via* intramolecular reactions). The transfer rate coefficient, k_{tr} is reported in the literature^[98] in a ratio with k_p , resulting in a so-called transfer constant (C), see Eq. 2.6. Two methods can be utilized to determine values for k_{tr} , the Mayo method^[99] and the chain length distribution (CLD) method^[100,101] which are both theoretically equivalent.^[102]

$$C = \frac{k_{tr}}{k_p} \quad (2.6)$$

Termination Reaction in Free Radical Polymerization

Concerning the complexity of the termination reaction, it is arguably the most complex bimolecular reaction in chemistry. The rate of this reaction, characterized by the rate coefficient of termination, k_t , depends on the monomer conversion, the pressure, the temperature, the chain length of the macroradical which will be terminated as well as the system viscosity. Values for k_t in solution are in the range of 10^6 - 10^8 L mol⁻¹ s⁻¹. The rate of termination is governed by the time radicals take to diffuse to each other, therefore the termination reaction is a diffusion controlled process. Another important consequence of these findings is that the shorter the chains that terminate, the faster their rate of termination, i.e., k_t is chain length dependent.^[103] The rate law expression for the termination reaction is given by Eq. 2.7 where i and j indicate the macroradicals with different chain length ($[R_i\cdot]$ and $[R_j\cdot]$).

$$-\frac{d[R\cdot]}{dt} = \sum_i \sum_j 2 \cdot k_t^{i,j} \cdot [R_i\cdot] \cdot [R_j\cdot] \quad (2.7)$$

In general, there exist two modes of termination: (i) Disproportionation with the rate constant $k_{t,d}$, yielding a saturated and an unsaturated polymer chain and (ii) combination of two macroradicals with the rate constant $k_{t,c}$. Zammit *et al.* reported the favour or disfavour of the modes of termination in thermally-initiated free radical polymerizations *via* MALDI-ToF MS.^[54] For determining k_t various methods are available; CLD methods (see above), stationary polymerization methods (see above), determination of the mode of termination (disproportionation vs. combination),^[104,105] and the single pulse-PLP-near-infrared spectroscopy (SP-PLP-NIR) technique which was pioneered by Buback and coworkers in the late 1980's^[106,107] with further improvements of the technique by utilizing ESR spectroscopy in 2004 (SP-PLP-ESR).^[108] Last but not least, Barner-Kowollik and coworkers developed the reversible addition-fragmentation chain transfer-CLD-termination (RAFT-CLD-T) technique for determining k_t in 2002.^[109,110]

2.2. Pulsed Laser Polymerization (PLP)

PLP is the synthesis method of choice for all studied polymers within the present thesis. The – quantitative – endgroup analysis of photo-initiated polymers *via* (SEC/)ESI-MS requires polymeric material, which has a molecular weight distribution with a considerable amount of low molecular weight polymer (polymer synthesis with a pulsed laser system fulfills this requirement) and is therefore suitable for analysis in the range of 200-2000 m/z . The advantage of such a laser-induced initiation process does not only lie in the precision excitation at a specific wavelength (in this thesis 351 nm), but also opens the option of operating with pulse patterns to limit the growth time of the generated macroradicals between two successive laser pulses, thus limiting the molecular weight.

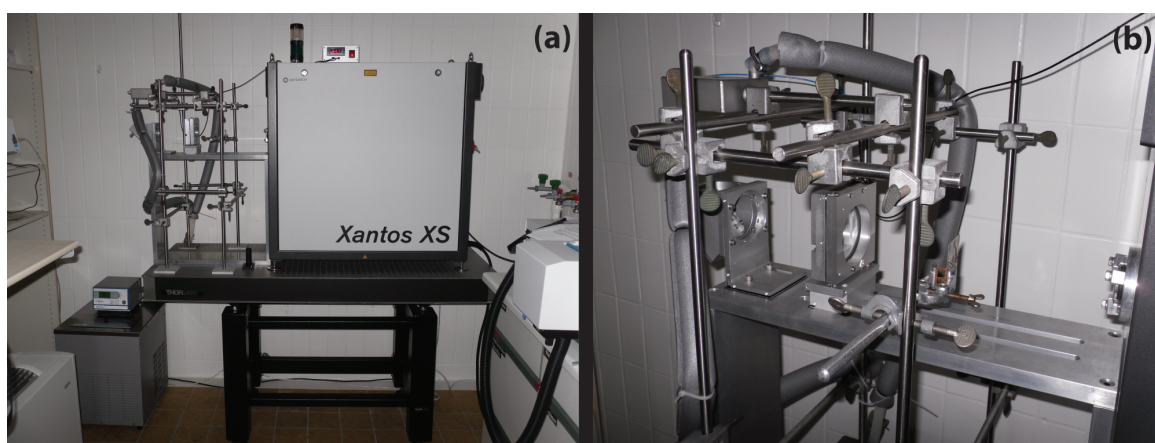


Figure 2.1. (a) PLP setup employed for quantitative endgroup analysis and PLP-SEC. (b) Experimental setup with sample holder and redirection optics for the laser beam.

Furthermore, the control over the reaction conditions is simple to handle and the employed laser system, an excimer laser – Coherent Xantos XS-500, XeF, frequency variable from 1 to 500 Hz – operating at a wavelength of 351 nm allows for the usage of various photoinitiators (for the experimental setup see Figure 2.1).

2.2.1. Excimer Lasers – An Introduction –

First of all it has to be mentioned that the familiar description *LASER* is an abbreviation for Light Amplification by Stimulated Emission of Radiation. Nowadays, the application of laser systems is very popular. The common laser classes and systems are discussed in great detail in ref. 111. As above-mentioned for the PLP experiments carried out in the present thesis an excimer laser system (XeF) was utilized. Molecules which are denoted as excimers^[112] are short-lived dimeric or heterodimeric molecules which only can exist in excited electronic states (*excited dimer*). These are mainly diatomic dimers such as Ar₂^{*}, XeF^{*}, and NaXe^{*} as well as triatomic compounds like Xe₂Cl^{*}. Since excimers only exist in excited electronic states their corresponding ground state is unoccupied. Therefore, excimers are ideal candidates for laser system (population inversion). After a research period of 15 years^[113,114] noble gas-halogen-excimer lasers were introduced in 1975 (an overview for this class of laser is given in Table 2.1). Latest trends in excimer laser technology can be found in ref. 115.

Table 2.1. Emission wavelengths of noble gas-halogen-excimer laser systems. Some commercially available lasers are marked in red.

Laser Substance	$\lambda_{\text{Emission}}$ /nm
XeI [*]	253
XeBr [*]	282
XeCl [*]	308
XeF [*]	351
KrBr [*]	206
KrCl [*]	222
KrF [*]	249
ArCl [*]	175
ArF [*]	193
NeF [*]	108

2.2.2. Pulsed Laser Polymerization-Size-Exclusion Chromatography (PLP-SEC)

With the introduction of pulsed UV lasers an improvement found its way into the field of polymerization kinetics. The PLP technique was first described by Genkin, Sokolov^[116] and Aleksandrov *et al.*^[117] in 1977 and was considerably improved by Olaj and colleagues from 1987 to 1995.^[118-120] PLP coupled with SEC is today the standard technique for the determination of k_p . It has been applied to a large number of monomers^[121] and benchmark values for a number of commonly used monomers have been published by an IUPAC (International Union of Pure and Applied Chemistry) working party.^[37-39,122-124] The success of the PLP-SEC technique relies mostly on the high accuracy of the method as the uncertainty of the resulting coefficients is for most parts only given by the error in the SEC determination of molecular weight distributions. In the PLP-SEC technique, laser pulses (e.g., from a Nd:YAG solid state laser, 355 nm or 532 nm; or XeF excimer laser, 351 nm) are applied at a constant pulse repetition rate to a polymerizable monomer solution consisting of inhibitor-freed monomer and a suitable photoinitiator. With each laser pulse a large population of primary radicals is generated that initiate chain growth while at the same time growing chains that had been started after the preceding laser pulse are terminated. In case laser pulses are applied at a sufficient frequency, most polymer visible in SEC will consist of material terminated by the laser pulsing action and not *via* conventional termination, which forms a background of terminated polymer. Hence, the average chain length of the polymer will reflect the number of propagation steps that have occurred between two consecutive laser pulses. However, firing the laser does not terminate the entire macroradical population and thus few radicals survive for two or even more cycles of primary radical generation forming overtones of the targeted molecular weight distribution. The multimodal molecular weight distributions can be best analyzed by determining the points of inflection (L_i , available *via* differentiating the chain length distribution), where the specific molecular weights are then given by:

$$L_i = k_p \cdot [M] \cdot i \cdot \frac{1}{\nu} \quad \text{with} \quad L_i = \frac{M_i}{M_M} \quad \text{and} \quad i = 1, 2, 3, \dots \quad (2.8)$$

M_M represents the molar mass of one monomer unit, and M_i the molecular weight at the specific inflection points (L_i). $[M]$ is the monomer concentration and ν the laser pulse repetition frequency. It has to be mentioned that due to the validity of Eq. 2.8 the conversion during the PLP experiment should not exceed $\sim 1-3\%$. Figure 2.2 depicts a typical result from a PLP-SEC experiment; clearly recognizable is the well-structured molecular weight distribution (solid line) of poly((hexylcarbamoyloxy)isopropyl acrylate) (polyHCPA) made by PLP at 14.1 °C.^[125]

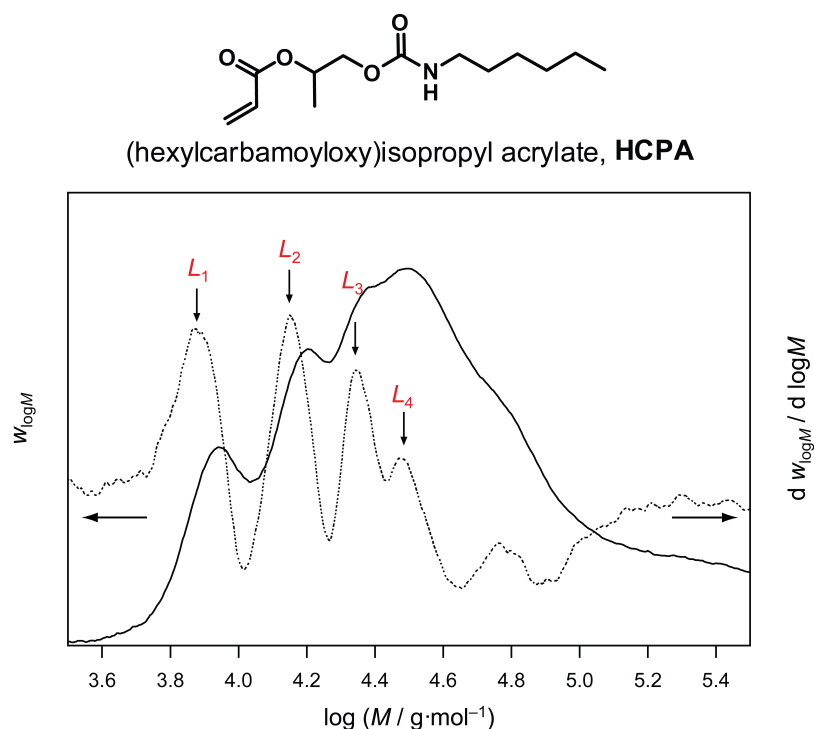


Figure 2.2. Monomer structure of (hexylcarbamoyloxy)isopropyl acrylate (HCPA) as well as the molecular weight distribution as determined *via* SEC and its first derivative of a polyHCPA sample made by PLP at 14.1 °C and a frequency of 500 Hz. The inflection points are marked with L_i . For more details refer to ref. 125.

The first derivative (dotted line) of the molecular weight distribution (solid line) displays four points of inflection (L_1 - L_4). From each point k_p can be obtained individually, which is one of the most important reasons for the high accuracy of the data received from PLP experiments. At 60 °C HCPA has a k_p value of about $43000 \text{ L mol}^{-1} \text{ s}^{-1}$,^[125] which is nearly twice as high as the k_p of MA, being $24000 \text{ L mol}^{-1} \text{ s}^{-1}$ at the same temperature.^[97]

$$k_p = A \cdot e^{-\frac{E_a}{RT}} \quad \text{or} \quad \ln k_p = \ln A - \frac{E_a}{RT} \quad (2.9)$$

After implementation of a series of PLP experiments for a specific monomer at different temperatures, the k_p values for each sample can be plotted in an Arrhenius plot ($\ln k_p$ vs. T^{-1}). Figure 2.3 depicts the Arrhenius plot for polyHCPA made by PLP.^[125] By processing a linear regression with the received k_p values one can obtain the activation energy (E_a) and the frequency factor (pre-exponential factor, A) *via* Eq. 2.9. For polyHCPA (see Figure 2.2 and Figure 2.3) a frequency factor of $6.6 \times 10^6 \text{ L mol}^{-1} \text{ s}^{-1}$ and an activation energy of 14.1 kJ mol^{-1} is deduced.

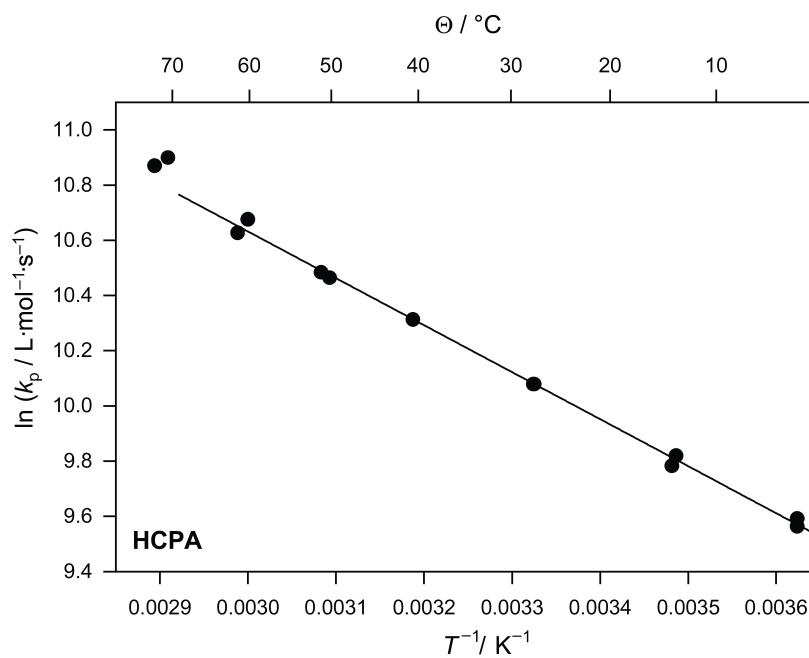


Figure 2.3. Arrhenius plot of the propagation rate coefficient, k_p for HCPA. For more details refer to ref. 125.

3

Characterization Techniques

3.1. Mass Spectrometry (MS) and Hyphenated Size-Exclusion Chromatography-Electrospray Ionization-Mass Spectrometry (SEC/ESI-MS)

3.1.1. Fundamentals of Mass Spectrometry (MS)

In the last two decades MS has been developed into an important method in modern macromolecular analytics and has been increasingly utilized to elucidate the molecular structure of polymers. In addition, advancements in the ionization process employed in MS has made this technique even more useful for characterizing polymeric systems. Macromolecules are high molecular weight – nonvolatile – substances which are difficult to vaporize. Additionally, only soft ionization enables the detection of non-fragmented molecules.^[126] Linear polymer chains always possesses two endgroups which makes MS the analytical method of choice.^[127] These endgroups could possibly be initiator-derived, functional group-derived or could be generated during the termination reaction (see Chapter 2.1.1). However, if the monomer molecular weight is known, the molecular endgroup structures can be assigned.

MS relies on the interaction between gas phase ions and electric or magnetic fields. The influence of these fields on the molecules under investigation depends on the mass and the charge of their respective ions. Separation of the ions is achieved based on their mass-to-charge ratios (m/z -ratios).

A mass spectrometer consists of five key components:

1. Sample injection system for injecting the (dissolved) analyte
2. Ion source for ionizing the sample
3. Analyzer system for separating the respective ions
4. Detector system for quantifying the detected species
5. Computer-aided data analysis

A plethora of ionization methods have been well-established; however, not all methods are suitable for the characterization of all molecules and some methods are better suited for characterizing certain molecular properties than other methods. For macromolecules so-called soft ionization methods are eminently suitable because the molecule is transferred in its entirety – without fragmentation – into the gaseous phase. Examples for soft ionization methods are electrospray ionization (ESI),^[24,128] atmospheric pressure chemical ionization (APCI),^[129] and matrix-assisted laser desorption ionization (MALDI).^[130]

In contrast, so-called hard ionization techniques allow for detection of single fragments thereby revealing valuable information about the chemical structure of a molecule. Thus, these methods are often utilized in organic chemistry for analyzing natural compounds. Typical methods are fast atom bombardment (FAB),^[131] electron ionization (EI),^[132] chemical ionization (CI),^[133] and field ionization (FI).^[134] Separation of ions based on the m/z -ratio can be achieved by a quadrupole mass analyzer, sector field mass analyzer, time-of-flight mass analyzer (ToF), quadrupole ion trap or an ion-cyclotron resonance analyzer (ICR). In the present thesis characterization of the synthesized macromolecules is carried out *via* the ESI ionization method and a quadrupole ion trap between 200-2000 m/z . Additional experimental details can be found in Chapter 4.3.6.

3.1.2. ESI Ionization Procedure

The ESI ionization method dates back to previous studies published by Malcom Dole *et al.* in 1968^[135] and 1970^[136]. John B. Fenn *et al.* developed the technique further^[24,128] and for his work he was awarded the Nobel Prize in Chemistry in 2002. As previously mentioned, ESI represents a soft ionization method, which avoids fragmentation and allows, therefore,

for the analysis of synthetic macromolecules.^[137] By applying a potential, the analyte molecules arrive at the ionization chamber over a heated capillary.^[138] The electrospray ionization technique is mainly applied to the analysis of biopolymers (i.e., peptides, proteins, oligonucleotides), since predominantly multiply charged ions are produced.^[139] This simplifies the analysis of high molecular weight polymers because with multiply charged ions the signals shift to smaller m/z -ratios. The process of ionization can be divided into three fundamental steps:^[140,141]

1. Formation of electrolyte droplets while the dissolved analyte is pumped through a capillary, which possesses a high positive potential.
2. Subsequently, the solvent continuously evaporates and the size of the droplets decreases with an initially constant droplet-charge. By solvent evaporation in an inert gas stream (nitrogen) the droplet diameter additionally decreases. A high field strength and a low droplet radius induces charge-separation with the result that the positive charges are located on the surface.
3. Based on the resulting high charge density, a Coulomb explosion occurs by exceeding the Rayleigh limit through increasing repulsion of charges with the same sign. Consequently, the liquid is sprayed.^[142] The solvent density of the new droplets is then further decreased in the gas stream, leading to an increased charge density, which is followed by new Coulomb explosions. This proceeds several times until finally the (multiple) charged analyte molecule remains. The resulting fine spray is transferred over a so-called transfer capillary into the vacuum chamber of the mass spectrometer.^[143]

Depending on the monomer, highly charged ions are produced, which is ideal for high molecular weight molecules and makes ESI the method of choice for synthetic polymers.

3.1.3. Interpretation of Mass Spectra

Natural compounds and biomolecules display one defined mass m , therefore, for each fragment with the charge z only one signal m/z is detectable. However, polymers are disperse samples and, therefore, molecules with different chain lengths which implies that not a single signal is observed in the spectrum. The chain length of the polymer is determined by the number of monomer units, n . Thus, the repeat unit in a polymer-derived mass spectrum represents the monomer and is, therefore, a characteristic attribute. The structural architecture can be identified by analysis of one repeat unit. The observed signals always represent analyte molecules, which are bound to an ion (e.g., Na^+ , K^+ , H^+ , or NH_4^+). Often, spectra can be recorded without additional doping since sufficient Na^+ ions are present from the laboratory glassware. However, all SEC/ESI-MS samples within the

present thesis were recorded with the addition of sodium iodide (dissolved in methanol) to increase the ionization efficiency and the generation of multiply charged ions.^[27] Evaluation of a mass spectrum proceeds *via* the calculation of the respective m/z -ratios.

$$m/z = \frac{M_r + n \cdot M_a}{n} \quad (3.1)$$

In Eq. 3.1 m/z stands for the mass-to-charge-ratio, M_r is the molecular weight of the unloaded species, M_a is the molecular weight of the ion which is bound to the polymer (e.g., 1.0078 Da for H^+ , 22.9898 Da for Na^+ , 38.9637 Da for K^+), and n is the number of charges per polymer chain. A detailed description for the quantitative evaluation of mass spectra is given in Chapter 4.4.3 as well as Chapter 6.4.2.

3.1.4. Quantitative Size-Exclusion Chromatography-Electrospray Ionization Mass Spectrometry (SEC/ESI-MS) of Polymers

In 1993 and 1995 first attempts were reported by Prokai^[144] and Simonsick^[145] to couple liquid chromatography to ESI-MS. SEC coupled to ESI-MS as well as refractive index (RI) detection is often employed for endgroup determination of polymers. Recently, our team developed a method which allows for obtaining quantitative molar mass distributions.^[27] In order to process the data from the two detectors a computational algorithm based on the maximum entropy principle is employed, yielding quantitative molar mass distributions, corrected for chromatographic band broadening.

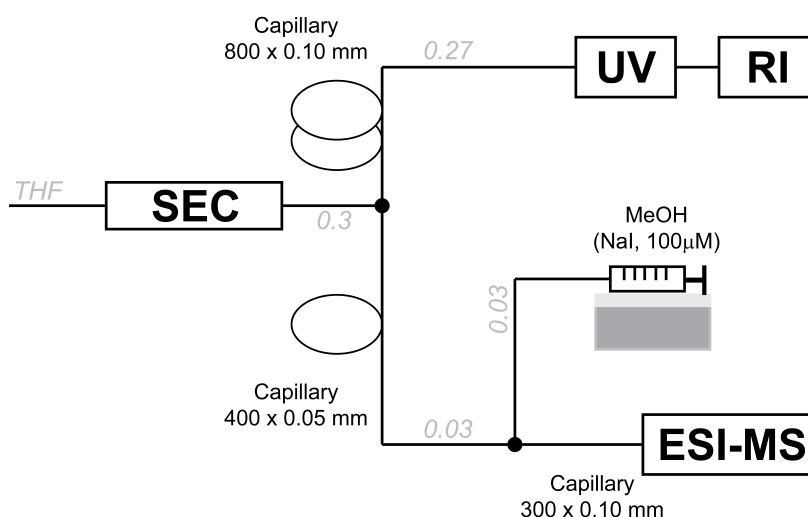


Figure 3.1. Chromatographic setup employed for coupling the ESI-MS and UV/RI-detectors to the chromatographic effluent in parallel. Numbers in gray indicate flow rates in mL min^{-1} . A $100 \mu\text{M}$ solution of sodium iodide in methanol is added post-column to increase the ionization efficiency and multiple charging. The same setup is utilized for the SEC/ESI-MS measurements in the present thesis. Reproduced from ref. 27, with permission of the American Chemical Society.

The procedure can be utilized without an external calibration^[27,146] and employs so-called single oligomer profiles (SOP) and a concomitant SEC distribution deconvolution process to arrive at quantitative concentrations for each single polymer chain present in the sample.^[27] The experimental setup can be found in Figure 3.1 and is utilized in the present thesis for quantifying photoinitiation efficiencies. Since ESI-MS spectra display singly charged, as well as multiply charged ions depending on the nature of the polymer, the molar mass distributions are superimposed onto each other making an evaluation of the mass spectra more difficult. Coupling SEC to ESI-MS allows for separation of the different distributions and facilitates the evaluation of mass spectra.

3.2. Femtosecond Spectroscopy

Ultrashort femtosecond laser pulses ($1 \text{ fs} = 1 \times 10^{-15} \text{ s}$) are, nowadays, utilized for photonics and non-linear optics, as well as for monitoring ultrafast electronic processes within atoms or molecules. In 1999 Ahmed Zewail was awarded the Nobel Prize in Chemistry for his studies concerning transition states of chemical reactions employing femtosecond spectroscopy.^[147]

3.2.1. Generation of Ultrashort Femtosecond Pulses

With the development of the titanium-sapphire laser technique ultrafast spectroscopy was revolutionized. An overview of femtosecond lasers is provided in ref. 148. Usually, for pump-probe spectroscopy laser systems are employed which consist of a mode-locked oscillator and an titanium-sapphire amplifier based on the chirped pulse amplification (CPA)^[149] method.

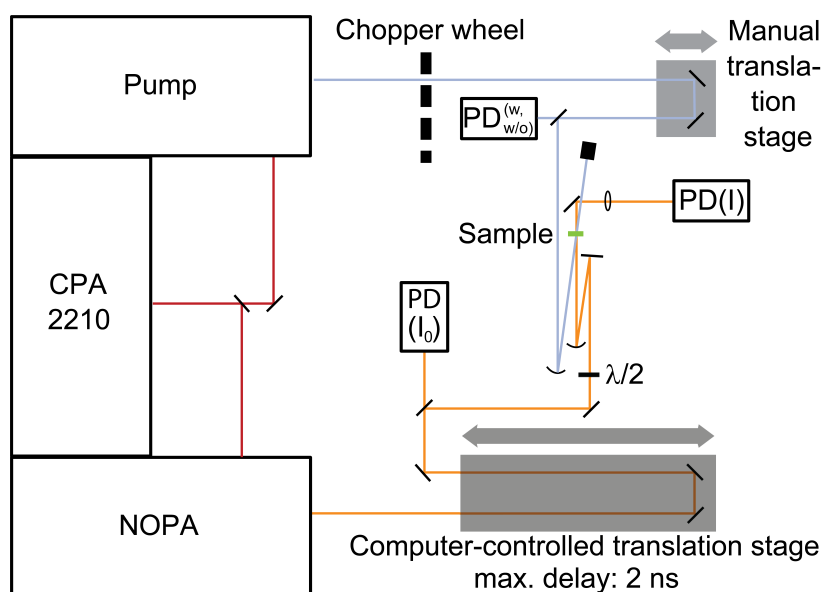


Figure 3.2. A Typical setup for a femtosecond pump-probe experiment (NOPA: noncollinear optical parametric amplifier). Reproduced with permission from Thomas Wolf. For more details the reader is referred to the PhD thesis of Thomas Wolf.^[150]

Non-linear optical phenomena are utilized to receive laser radiation of high spectral tunability. Frequency doubling, sum frequency generation, difference frequency generation, optical parametric amplifiers, and white-light generation are applied to generate pulse laser radiation – based on the central wavelength of the titanium-sapphire laser (775 nm) – from the visible region up to the infrared region of the spectral range.^[151]

3.2.2. Femtosecond Pump-Probe Spectroscopy

Figure 3.2 displays a basic experimental setup for the femtosecond pump-probe experiments that have been carried out by Thomas Wolf in a collaboration with the group of PD Dr. Andreas-Neil Unterreiner (see Chapter 5 for details). In principle the pulse sequence of a femtosecond laser is split into two optical pathways, the first one for the generation of pump – or excitation – pulses (blue line in Figure 3.2) and the second one for the generation of probe pulses (orange line in Figure 3.2). Both pathways are combined to interact with the sample. The result of these experiments are time-dependent changes in optical density ($\Delta OD(\tau)$), which for the purpose of this thesis, have permitted the excited state dynamics of photoinitiator molecules to be observed. For details the reader is referred to Chapter 5 and ref. 150.

3.3. Chemically Induced Dynamic Nuclear Polarization- Nuclear Magnetic Resonance (CIDNP-NMR)

The appearance of unusual NMR or ESR intensity patterns – enhanced absorption or emission – within systems, which have undergone a chemical reaction shortly before spectral recording, can be understood in terms of chemically induced dynamic nuclear polarization (CIDNP) and chemically induced dynamic electron polarization (CIDEP). Hereafter, only CIDNP, which is an NMR based experimental technique, will be discussed. CIDNP was simultaneously discovered by Bargon and Fischer^[152] as well as by Ward and Lawler^[153] in 1967. An explanation for the CIDNP effect was given two years later by Closs,^[154–157] Kaptein and Oosterhoff.^[158,159] They suggested independently of each other that CIDNP occurred through a radical pair mechanism. As a result of a radical pair reaction (i.e., radicals that are spatially separated in two orbitals but are capable of interacting with each other), a non-thermal nuclear polarization of the diamagnetic products is achieved. CIDNP has been exploited during the last 40 years to characterise transient free radicals and their reaction mechanisms. An overview of the technique and possible applications can be found in the literature.^[160–162]

3.3.1. Radical Pairs in a Magnetic Field

A singlet state (S) is characterized by an electron pair with antiparallel spin. With the generation of a radical pair from a molecule that is in a singlet state, due to the principle of preservation of multiplicity, the newly formed radical pair also represents a singlet state resulting in a magnetic moment of zero. Formation of radicals in a magnetic field is only possible if both electron spins are antiparallel with a phase delay of 180° . In a triplet state (T) the magnetic moment is non-zero and by applying a magnetic field there exist three different orientations for the respective radical pair (see Figure 3.3): (i) Both spins are antiparallel without phase delay (T_0) resulting in a magnetic moment in the xy -plane, (ii) both spins are parallel to each other in direction of the magnetic field (T_+), or (iii) both spins are parallel yet opposite to the magnetic field (T_-).

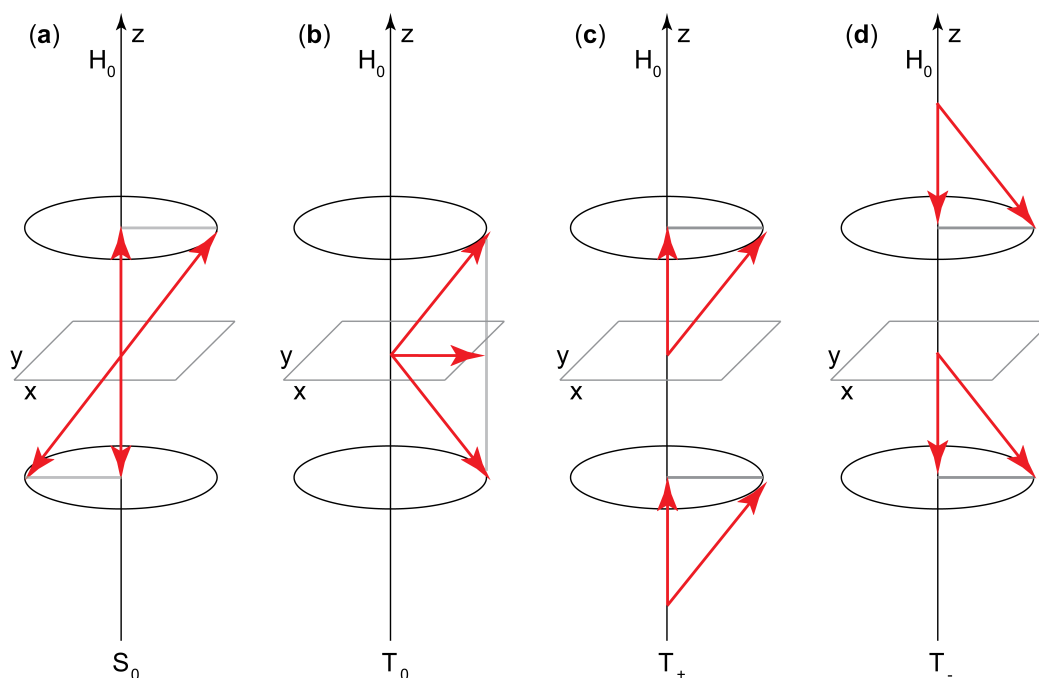


Figure 3.3. Electron spin states of a radical pair in a magnetic field: (a) Singlet state (S_0), (b) triplet state T_0 , (c) triplet state T_+ , and (d) triplet state T_- .

Figure 3.4 displays the potential energy curves of all four states (S_0 , T_0 , T_+ , and T_-), which are depicted as the energy content (E) as a function of the distance (r) between both radicals. At a certain distance, r_m , the energy difference between S_0 and T_0 is minimal, thus transitions from S_0 to T_0 or vice versa can occur. Furthermore, it is assumed that due to the high energy differences between S_0/T_0 and T_+/T_- , the transitions between S_0/T_0 and T_+/T_- are impossible. Since the energy differences are proportional to the applied magnetic field, which is utilized in NMR spectroscopy, the assumption is justified.

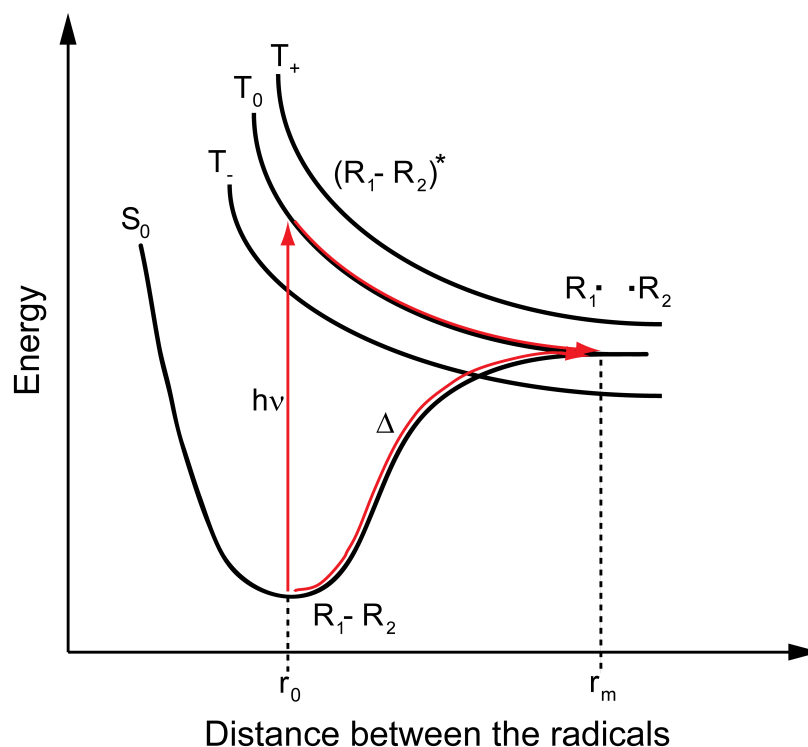


Figure 3.4. The energy dependence of the different spin states of a radical pair in a magnetic field as a function of the distance (r) of the radicals. Within the figure the following abbreviations are given: Bond distance before radical formation (r_0), bond distance at the S_0 - T_0 mixture point (r_m), singlet state (S_0), triplet state T_0 , triplet state T_+ , and triplet state T_- .

3.3.2. The Origin of CIDNP

To understand the cause of CIDNP it is important to reiterate the principle of NMR.^[163] In a magnetic field protons can be located in two different energy levels. According to the Boltzmann distribution more nuclei are located in the lower energy level, the energetically favored level, than in the upper energy level, the energetically unfavored level. Based on these population differences of energy levels is it possible to induce transitions from the lower to the upper energy level by irradiation with radio waves of a suitable frequency, where energy is absorbed. In CIDNP spectroscopy enhanced absorption as well as emission can be observed, which indicates that the nuclear spin levels are occupied according to a non-Boltzmann distribution. More nuclei are located in the upper energy level than in the lower energy level, thus the nuclei can revert from the unfavored upper energy level to the more favored lower energy level and can, thereby, emit their energy under emission of radio waves. The reason for the non-Boltzmann distribution of the nuclear spin levels in radicals is the S_0 - T_0 mixture displayed in Figure 3.4. In radicals the electron spin and the nuclear spin are coupled to each other and the extent of the interconnection is given by the hyperfine coupling constant (a). This coupling is a significant reason for the nuclear spin polarization.

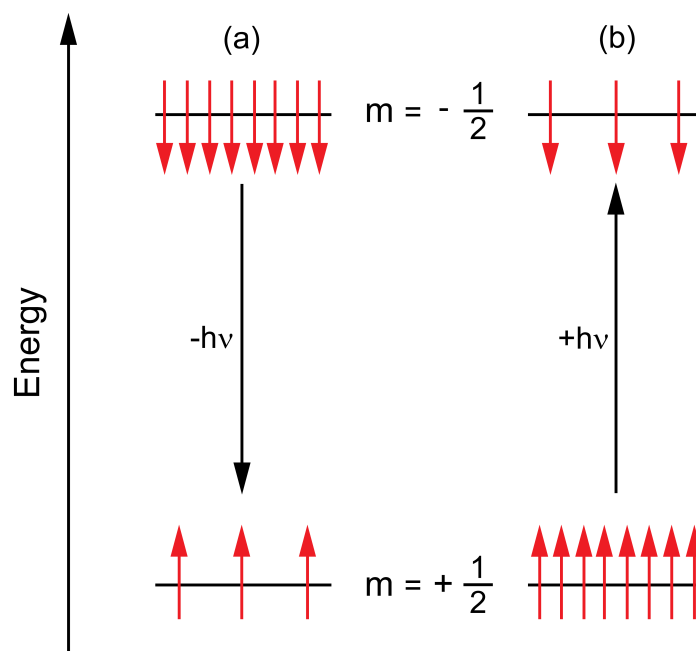


Figure 3.5. The population of the nuclear spin levels during energy polarization. (a) Product derived from recombination which leads to emission of radio waves and (b) product derived from a transfer process which leads to enhanced absorption in the resulting CIDNP-NMR spectrum.

The energy levels of radical-derived recombination and transfer products that are generated during the reaction in a magnetic field are depicted in Figure 3.5. This kind of nuclear spin polarization is also referred to as *energy polarization* because the nuclear spin system either has to absorb or emit energy in the form of radio waves to reach its thermodynamic equilibrium. In recombination products the energetically unfavored level (see Figure 3.5a) is more populated than the energetically favored level and, therefore, the thermodynamic equilibrium will be restored under emission of radio waves. In transfer products (see Figure 3.5b), the energetically favored level is more populated and the equilibrium is reached by the enhanced absorption of radio waves. However, there exist a second type of polarization where emission and enhanced absorption can be found at the same time. This type of polarization is called *entropy polarization* or the *multiplet effect*.^[164]

3.3.3. Kaptein's Rule

For practical applications, the CIDNP-NMR spectrum is primarily recorded (a typical NMR probehead for CIDNP experiments is displayed in Figure 3.6) and based on these results it is possible to draw conclusions from the type of polarization about the mechanism of a radical reaction. The resulting spectrum recorded during the reactions of free radicals consists of NMR lines of both positive and negative intensity from enhanced absorption or emission, respectively.

3. Characterization Techniques

Directions (signs of polarizations, Γ) of CIDNP signals are predicted by Kaptein's rule^[154,159] (Eq. 3.2, Kaptein's rule for energy polarization). The product of the signs associated with each variable either results in a plus (+) sign, indicating absorption, or a minus (-) sign, indicating emission, with regard to energy polarization.

$$\Gamma = a \cdot \Delta g \cdot \mu \cdot \epsilon \quad (3.2)$$

a is the hyperfine coupling constant, Δg is the g -factor difference of radicals within a primary radical pair, μ is the multiplicity of the precursor, and ϵ is the type of the exit channel. For details the reader is referred to refs. 154, 159, and 164.

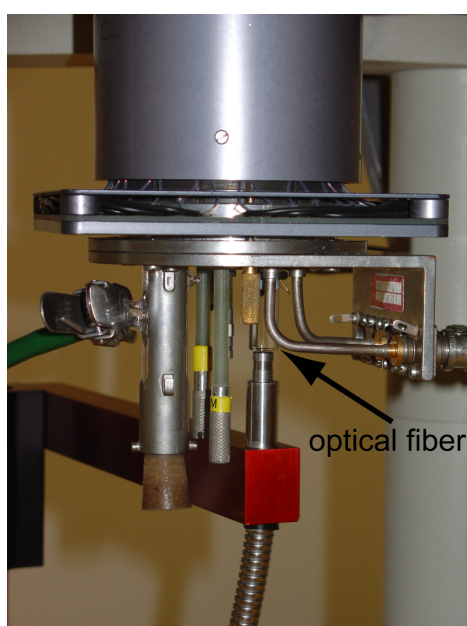


Figure 3.6. A Special NMR probehead for CIDNP experiments. The optical fiber is marked with an arrow. As light sources, laser systems (e.g., Nd:YAG) or UV lamps (e.g., Hamamatsu LC4, as is the case in the present figure) can be employed.

In the present thesis the NMR based CIDNP technique was employed in Chapter 7 to elucidate the UV-induced cleavage mechanism of a polymer-derived endgroup. These investigations were carried out in Graz in collaboration with the group of Prof. Dr. Georg Gescheidt.

4

Quantitative Comparison of the Mesityl *vs.* the Benzoyl Fragment in Photoinitiation: A Question of Origin

4.1. Abstract

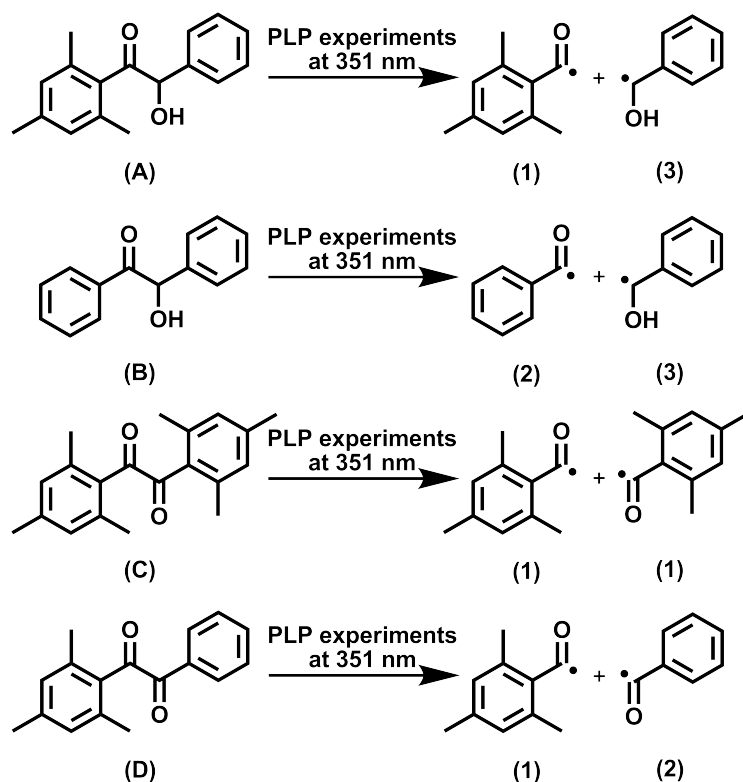
Photolytically generated radicals (at a wavelength of 351 nm) derived from the acetophenone-type photoinitiators benzoin (2-hydroxy-1,2-diphenylethanone, B) and 2,4,6-trimethylbenzoin (2-hydroxy-1-mesityl-2-phenylethanone, A) (specifically the benzoyl (2) and mesityl radical (1)) are quantified in their ability to serve as initiating species in MMA, ethyl methacrylate (EMA), and butyl methacrylate (BMA) bulk free radical polymerizations under optimized conditions. Herein, 2,4,6-trimethylbenzoin (A) is employed for the first time as photoinitiator in PLP utilizing a high-frequency excimer laser, constituting a new source for mesityl radicals (1). The following work presents an improved method for quantifying radical efficiency of photoinitiation processes using coupled online SEC/ESI-MS to analyze the obtained polymers.

Due to the occurrence of side reactions during the benzoin-initiated MMA polymerization, reduced laser energies (~ 0.35 mJ/pulse) as well as low polymerization temperatures (-5 °C) were utilized to avoid side product formation. A plot of the ratio of benzoyl (2) to mesityl (1) (derived from 2,4,6-trimethylbenzoin (A)) endgroups vs. the ratio of both initiators in the reaction mixture indicates that the benzoin-derived benzoyl radical (2) is 3.0 (2.6, 2.4) times more likely to initiate the polymerization process of MMA (EMA, and BMA) than the 2,4,6-trimethylbenzoin-derived mesityl fragment (1). This observation is in sharp contrast to the case when mesityl (C) is employed as a source of mesityl radicals (1) (8.6 times higher likelihood of benzoyl incorporation). These results clearly support the notion that the origin of a radical species significantly determines its propensity to be incorporated at a polymer chain's terminus. The cause of such an origin dependence is tentatively assigned – at least in part – to different triplet lifetimes or intersystem crossing efficiencies (Φ_{ISC}) or both of 2,4,6-trimethylbenzoin (A) and mesityl (C).

4.2. Introduction

Upon absorption of light, benzoin (B) and its derivatives spontaneously undergo α -cleavage and generate free radicals. Benzoin (B) and its derivatives are the most widely used photoinitiators for free radical polymerization due to their high quantum efficiency and reactivity of the generated radical fragments.^[70] In contrast, photoinitiation processes *via* type-II photoinitiators are based on the reaction of their triplet excited states with a hydrogen donor, thereby producing an initiating radical.^[72] Furthermore, photoinitiators are used in academia for PLP. In a refinement of the PLP-technique, a recent study showed that PLP in conjunction with online SEC/ESI-MS can be applied for the determination of highly accurate propagation rate coefficients in free radical polymerization.^[46] The potential of SEC/ESI-MS has been discussed in several publications.^[26,27,146] For the PLP technique, the utilized photoinitiators must be able to initiate the polymerization of a wide range of monomers, and the pathways of initiation are important to know.^[125,165,166] Qualitative studies on photoinitiation processes have been carried out in several publications using ESI-MS.^[40,41,73] While qualitative investigations can reveal some important trends, it is of great importance to quantify the initiation ability of the different initiator fragments toward variable classes of monomers. The initiator fragments are located at the α -endgroups (and if combination modes prevail also the ω -endgroups) of the polymeric chains and should therefore be predestinated for (quantitative) mass spectrometric analysis. In a previous investigation employing ESI-MS to quantitatively study photoinitiation processes, the reaction products of two specific photolytically generated radical fragments during the bulk free radical polymerization of MMA, namely the mesityl (1) and the benzoyl (2) fragments (see Scheme 4.1 for the structures), were mapped in great detail.^[42] A large disparity in *net-initiation efficiency* between both fragments with respect to their ability

to start chain growth was found. The initiator fragments in the previous chapter were generated from the photoinitiators benzoin (B) and mesityl (C). The observed difference in initiation efficiency can be assigned to three effects, i.e., the actual initiation rate and/or the overall quantum yield and/or the ability of the molecule to absorb light. All three effects result in the above-noted *net-initiation efficiency* that can be compared between different photoinitiator systems.



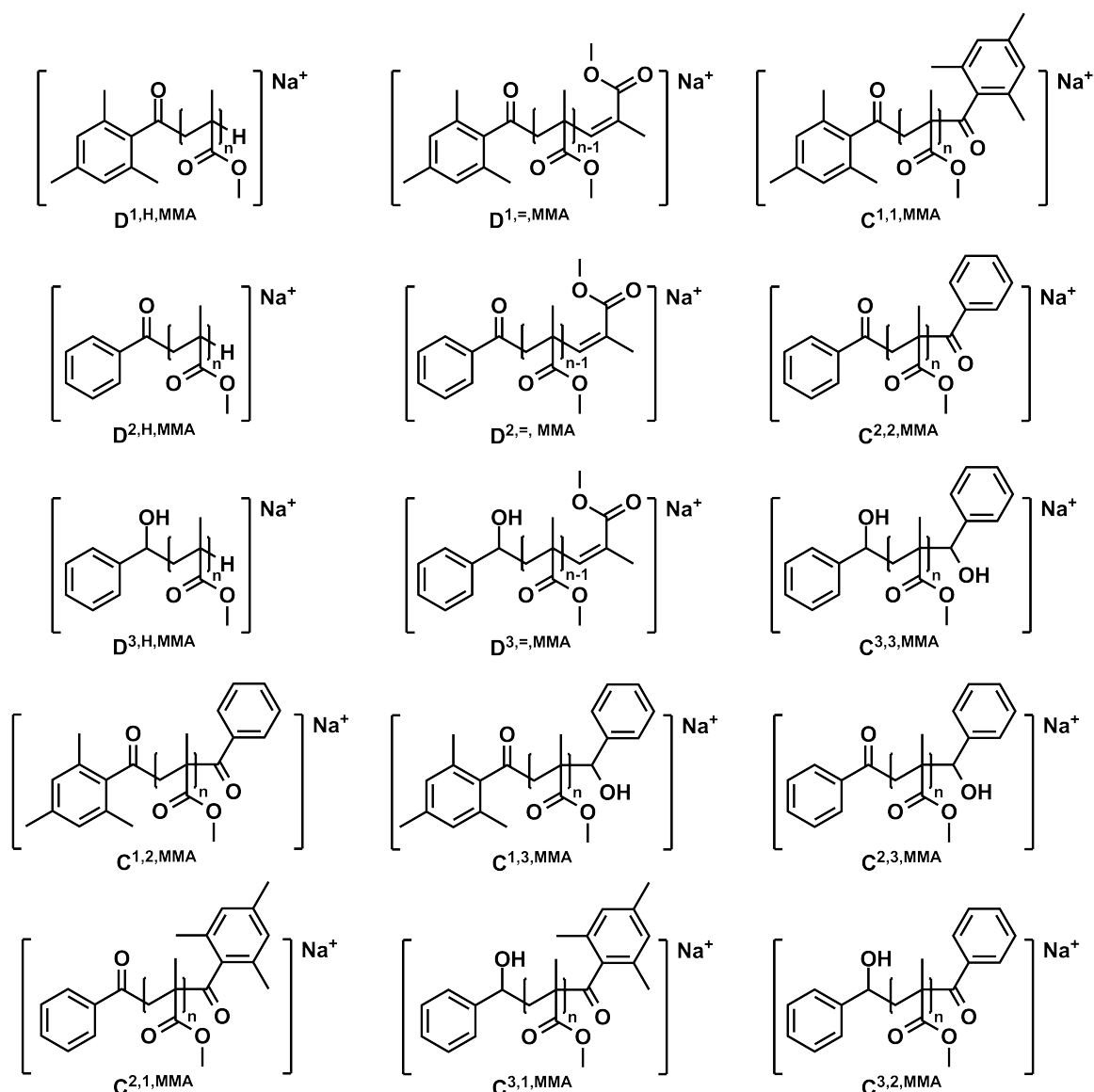
Scheme 4.1 Photolytic decomposition pattern of 2,4,6-trimethylbenzoin (A), benzoin (B), mesityl (C), and 2,4,6-trimethylphenylbenzil (D). The photoinitiators A and B are used in the current study for quantifying the initiation efficiency of the radical fragments (1, and 2). To compare the latest results with a former study between benzoin (B) and mesityl (C), the decomposition pattern of mesityl (C) is also depicted. Note that the combination of compound (C) with (B) was the subject of a previous study.^[42]

Thus, even though the rate of initiation of a certain radical fragment toward the same monomer should be universal, one may anticipate an origin dependence of the net-initiation efficiency, and it is therefore mandatory to study different sources of such fragments with respect to their abundance in the polymeric product. In the current chapter, the above-mentioned PLP/SEC/ESI-MS method is utilized to quantitatively study the reaction behavior of a related couple of initiators, bearing the same initiator fragments as in a previous investigation (i.e., mesityl (1) and benzoyl (2)),^[42] yet originating from different source molecules. PLPs were performed at low laser energy on a homologous series of alkyl methacrylates, differing in chain lengths of the ester sidegroup, i.e., methyl methacrylate

(MMA), ethyl methacrylate (EMA), and butyl methacrylate (BMA). Methacrylates are purposefully chosen as they predominantly terminate *via* disproportionation, providing certainty that the terminal group in the chain has truly initiated the chain growth process.

The reason for employing online SEC/ESI-MS for quantifying photolytically generated radicals in their ability to serve as initiating species in the free radical bulk polymerization of variable methacrylates is due to the fact that ESI-MS spectra, which are measured *via* direct infusion of the polymer samples can – under certain circumstances – be less accurate (for details see Chapter 4.4). Compared to the previous study,^[42] the laser energy as well the temperature has been reduced to minimize side product formation during the free radical polymerization using the PLP-technique and benzoin (B) as initiator. The below-described observation of unassigned signals in the ESI-MS spectra of macromolecules initiated by benzoin (B) presented herein, may be associated with the improvement in the employed ESI-MS system in the current study (for details see 4.3), which is up to 10 times more sensitive compared to the ESI-MS system used previously.^[42] For a quantitative evaluation of the SEC/ESI-MS spectra it is of primary importance to assign or – better eliminate – all of the side products, as long as their formation process remains unresolved (for more details see Chapter 7). In the present study, two benzoin-type photoinitiators, i.e., benzoin (B) and 2,4,6-trimethylbenzoin (A), were employed to study the (net) efficiency of the benzoyl fragment (2) to initiate the free radical bulk polymerization of MMA, EMA, and BMA, which is quantitatively compared to the initiation efficiency of the mesityl fragment (1). Scheme 4.1 depicts the chemical structure as well as the UV-light-induced radical decomposition products of all (in the quantitative studies) applied photoinitiators, which have been used to initiate macromolecular chain growth *via* PLP. Note that the disproportionation product having radical fragment (3) as an endgroup is not the subject of the present study (for details see below). The choice for studying the comparative efficiency of benzoyl (2) vs. mesityl (1) is driven by previous quantitative findings that the mesityl fragment (1) – when derived from mesityl (C) – has an 8.6 times reduced propensity to be found as a polymer endgroup in poly(methyl methacrylate) (pMMA) than that of the benzoyl fragment (2) (derived from benzoin (B)).^[42] In the current study 2,4,6-trimethylbenzoin (A) was used for the first time in photoinitiation processes of free radical bulk polymerizations of methacrylates. The reason for employing 2,4,6-trimethylbenzoin (A) instead of mesityl (C) is twofold: First – and most importantly – this initiator has the same general structure as benzoin (B) (benzoin-type photoinitiator), thus potentially featuring a similar triplet lifetime and intersystem crossing (ISC) behavior, therefore allowing a differentiation of the origin of the sluggish incorporation of mesityl radicals (1) when they are derived from mesityl (C).^[42]

The term *net-initiation efficiency* is employed to denote the propensity of a radical to commence macromolecular growth from the point of the laser pulse hitting the source molecule. It thus summarizes a true initiator efficiency (*net-efficiency*), including all effects from the ability of the initiator to absorb light to the reactivity of the radical towards the monomer units.



Scheme 4.2 Expected polymeric disproportionation and combination products in the photochemically initiated bulk free radical polymerization of MMA in the presence of a cocktail of the benzoin (B) and 2,4,6-trimethylbenzoins (A) photoinitiators depicted in Scheme 4.1. Note that the position of the double bond in the unsaturated disproportionation product may also be at the site of the former α -methyl group. See Table 4.1 for a collation of the m/z -ratios of the individual radical fragments. Furthermore, the combination products are not of interest but are mentioned because of completeness of assignment ($C^{1,2,MMA}$, $C^{2,1,MMA}$, $C^{1,3,MMA}$, $C^{3,1,MMA}$ and $C^{2,3,MMA}$, $C^{3,2,MMA}$ cannot be distinguished in the mass spectra). A detailed description of the nomenclature is given in Chapter 4.4.

Note that the hypothesis of similar triplet lifetimes and ISC behavior for the two initiators may not be tenable under all circumstances, as the additional methyl groups on the phenyl ring in 2,4,6-trimethylbenzoin (A) may alter the geometry of the molecule (out-of-plane twisted configurations may be preferred), leading to an altered behavior.^[167] Secondly, the initiator comprises only one mesityl fragment. Therefore, the ratio of both radical fragments (coming from 2,4,6-trimethylbenzoin (A) and benzoin (B), respectively) as they are generated is 1:1. The primary aim of the current study is thus to quantify the *net-efficiency* difference (i.e., their respective propensity to be found as the initiating group at the chain end) between the benzoyl (2) and the mesityl fragments (1), derived from benzoin (B) and 2,4,6-trimethylbenzoin (A), to establish whether the propensity of the mesityl fragment to be found as an initiating species is a function of its origin.

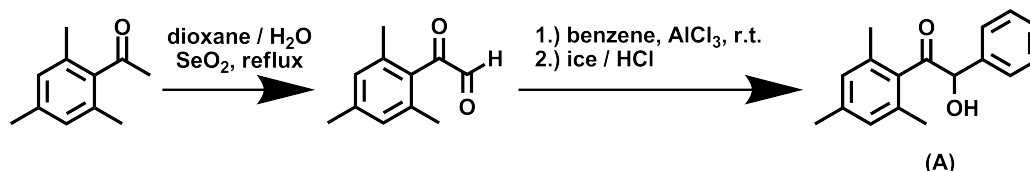
The following experimental strategy is employed: Mixtures of benzoin (B) and 2,4,6-trimethylbenzoin (A) (ranging from equimolar composition to a large excess of A) are prepared and subjected to PLP as described in the Experimental Part 4.3. The generated polymer is isolated and subjected to online SEC/ESI-MS. From the mass spectral evaluation procedure, the ratio of benzoyl (2) and mesityl radicals (1) that have initiated macromolecular growth is plotted as a function of the ratio of both initiators in the reaction mixture. The evaluation procedure for such a plot, as well as the mass spectral evaluation, is described elsewhere.^[35,75] Scheme 4.2 depicts the expected disproportionation and combination products, which are formed in the presence of MMA as monomer (for the schemes of EMA and BMA as monomer see Scheme A.1 and Scheme A.2 in the Appendix). Table 4.1 contains the corresponding experimentally observed as well as the theoretically expected *m/z*-ratios for the identified disproportionation and combination products in one repeat unit (for tables of EMA and BMA as monomer see Table A.1 and Table A.2 in the Appendix).

4.3. Experimental Part

4.3.1. Synthesis of Mesityl glyoxal

The following preparation procedure of mesityl glyoxal is adapted from the literature.^[168–170] A solution of 6.48 g selenium dioxide (58.4 mmol, 1.00 eq), 5 mL of water and 9.56 g 2,4,6-trimethylacetophenone (9.80 mL, 58.9 mmol, 1.00 eq) in 65 mL of dioxane was refluxed for 5 h at 105 °C under vigorous stirring. During the heating of the solution a gradual precipitation of selenium takes place and the colour changes from colourless to yellow. The solution was decanted from the selenium and the dioxane was evaporated. The crude yellow product was purified *via* vacuum distillation. The product was collected at $T = 62\text{ °C}$ and $p = 4.1 \times 10^{-1}\text{ bar}$ as a clear yellow oil which afterwards crystallized upon cooling. (Yield: 2.95 g, 16.7 mmol, 28 %). ESI-MS: $[M+Na]_{\text{exp.}} = 199.1\text{ Da}$ and $[M+Na]_{\text{calc.}} = 199.07\text{ Da}$.

^1H NMR (400 MHz, CDCl_3); [δ , ppm]: 9.53 (s, 1H, $-\text{CHO}$), 6.89 (s, 2H, $-\text{H}_{\text{arom.}}$), 2.31 (s, 3H, $-\text{CH}_3$), 2.18 (s, 6H, $2 \times -\text{CH}_3$). ^{13}C NMR (100 MHz, CDCl_3); [δ , ppm]: 196.79 (C_1), 188.30 (C_2), 141.37 (C_3), 136.47 (C_4), 131.18 (C_5), 129.09 (C_6), 21.28 (C_7), 20.16 (C_8). For more details see Figure 4.1a, Figure A.1a (in the Appendix), and Chapter 9.1.



Scheme 4.3 Synthesis of 2,4,6-trimethylbenzoin (A); 2,4,6-trimethylacetophenone, mesitylgyoxal.

4.3.2. Synthesis of 2-Hydroxy-1-mesityl-2-phenylethanone (2,4,6-Trimethylbenzoin, A)

To a suspension of 1.53 g anhydrous aluminium chloride (11.5 mmol, 2.01 eq) in 5.8 mL benzene at 10 °C, 1.01 g mesitylgyoxal (5.74 mmol, 1.00 eq) dissolved in 5.8 mL of benzene was added. The reaction mixture was vigorously stirred over a period of 2 h at 10 °C (cooled with ice). Stirring was continued over night at ambient temperature. The reaction mixture was subsequently poured onto ice and concentrated hydrochloric acid. The organic layer was removed and the aqueous layer was extracted twice with a minimal amount of benzene. The combined organic layers were dried over MgSO_4 and benzene was evaporated under reduced pressure. The crude, pale, yellowish solid was recrystallized from ethanol to give 2,4,6-trimethylbenzoin (A) as a white powder. (Yield: 0.58 g, 2.28 mmol, 40 %). ESI-MS: $[\text{M}+\text{Na}]_{\text{exp.}} = 277.2$ Da and $[\text{M}+\text{Na}]_{\text{calc.}} = 277.12$ Da. ^1H NMR (400 MHz, CDCl_3); [δ , ppm]: 7.25–7.19 (m, 3H, $-\text{H}_{\text{ph.}}$), 7.15–7.08 (m, 2H, $-\text{H}_{\text{ph.}}$), 6.74 (s, 2H, $-\text{H}_{\text{arom.}}$), 5.59 (d, $^3J = 5.2$ Hz, 1H, $-\text{H}_{\text{tert.}}$), 4.50 (d, $^3J = 5.5$ Hz, 1H, $-\text{OH}$), 2.26 (s, 3H, $-\text{CH}_3$), 1.82 (s, 6H, $2 \times -\text{CH}_3$). ^{13}C NMR (100 MHz, CDCl_3); [δ , ppm]: 208.21 (C_1), 139.55 (C_2), 136.58 (C_3), 134.59 (C_4), 134.12 (C_5), 128.37 (C_6), 128.31 (C_7), 126.77 (C_8), 80.54 (C_9), 21.11 (C_{10}), 18.90 (C_{11}). For more details see Figure 4.1b, Figure A.1b (in the Appendix), and Chapter 9.1.

4.3.3. Pulsed Laser Polymerization (PLP) Procedure

All MMA, EMA and BMA samples consisted of monomer (sample volume ~ 0.5 mL) with a mixture of both photoinitiators with an overall concentration of $c_{\text{PI},0} = 5 \times 10^{-3}$ mol L^{-1} . The samples were carefully freed of oxygen prior to laser irradiation by purging the reaction mixture with high-purity nitrogen for 2 min. The sample vial was subsequently placed into a sample holder which was held at a constant temperature of -5 °C by a thermostat (Model: 1196D, VWR, Darmstadt, Germany). The temperature was independently measured at the

4. Quantitative Comparison of the Mesityl vs. the Benzoyl Fragment

sample holder. The sample temperature was allowed to equilibrate for 5 min before starting the polymerization. Photoinitiation was achieved by an excimer laser system (Coherent Xantos XS-500, XeF, frequency variable from 1 to 500 Hz, operating at a wavelength of 351 nm (pulse width ~ 20 ns) and an laser energy of 2-6 mJ/pulse) at 100 Hz for an overall polymerization time of 90000 laser pulses (15 min).

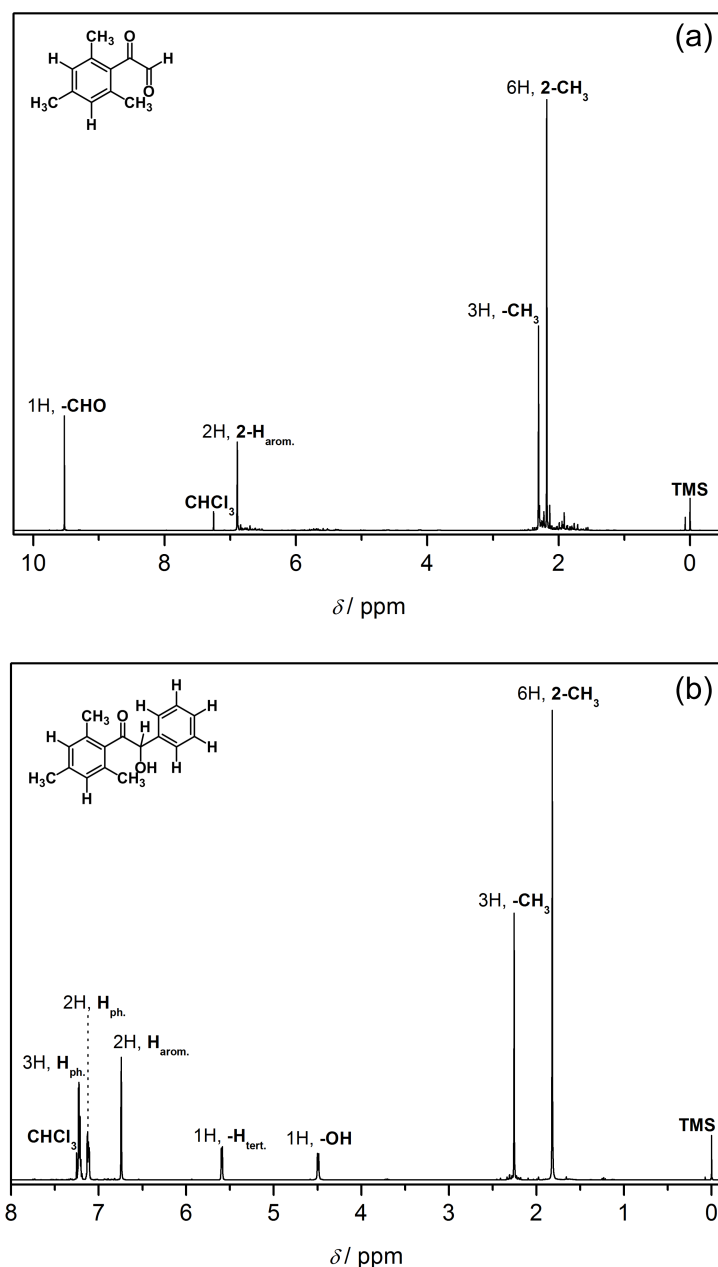


Figure 4.1. (a) 400 MHz ^1H NMR spectrum of mesityl glyoxal, (b) 400 MHz ^1H NMR spectrum of 2,4,6-trimethylbenzoin (A).

A self-made metal filter (fine-mesh metal grid) was implemented next to the radiation exit window to obtain a reduced laser energy of ~ 0.35 mJ/pulse. The laser beam, which was adjusted to an energy of close to 0.35 mJ/pulse hitting the sample, was redirected to illuminate the vial from the bottom. For more details see Chapter 9.1.

4.3.4. UV/Vis Measurements

UV/Vis spectra were recorded in methanol at ambient temperature using a Varian Cary 300 Bio photospectrometer. For more details see Chapter 9.1.

4.3.5. NMR Measurements

The structures of the synthesized photoinitiator were confirmed by ^1H NMR spectroscopy on a Bruker AM 400 spectrometer at 400 MHz for hydrogen nuclei and 100 MHz for carbon nuclei. All samples were dissolved in CDCl_3 . For more details see Chapter 9.1.

4.3.6. SEC/ESI-MS Measurements

Spectra were recorded on a LXQ mass spectrometer (ThermoFisher Scientific, San Jose, CA, USA) equipped with an atmospheric pressure ionization source operating in the nebulizer assisted electrospray mode. The instrument was calibrated in the m/z range 195–1822 Da using a standard containing caffeine, Met-Arg-Phe-Ala acetate (MRFA) and a mixture of fluorinated phosphazenes (Ultramark 1621) (all from Aldrich). A constant spray voltage of 4.5 kV was used and nitrogen at a dimensionless sweep gas flowrate of 2 (~ 3 L min^{-1}) as well as a dimensionless sheath gas flowrate of 12 (~ 1 L min^{-1}) were applied. The capillary voltage, the tube lens offset voltage and the capillary temperature were set to 60 V, 110 V and 275 °C, respectively. The LXQ was coupled to a Series 1200 HPLC-system (Agilent, Santa Clara, CA, USA) consisting of a solvent degasser (G1322A), a binary pump (G1312A), a high-performance autosampler (G1367B), followed by a thermostatted column compartment (G1316A). Separation was performed on two mixed bed size-exclusion chromatography columns (Polymer Laboratories, Mesopore 250 \times 4.6 mm, particle diameter 3 μm) with precolumn (Mesopore 50 \times 4.6 mm) operating at 30 °C. THF at a flow rate of 0.30 mL min^{-1} was used as eluent. The mass spectrometer was coupled to the column in parallel to an RI-detector (G1362A with SS420x A/D) in a setup described earlier.^[27] An aliquot of 0.27 mL min^{-1} of the eluent was directed through the refractive index (RI)-detector and 30 μL min^{-1} infused into the electrospray source after post-column addition of a 100 μM solution of sodium iodide in methanol at 20 μL min^{-1} by a micro-flow HPLC syringe pump (Teledyne ISCO, Model 100DM). Flow-rates, instrument settings and salt concentrations were optimized to yield maximum ionization efficiency while keeping salt cluster formation to a minimum.^[171] 50 μL of a polymer solution with a concentration of 5.5 mg mL^{-1} were injected onto the HPLC system. For more details see Chapter 9.1.

4.4. Results and Discussion

The overall point of the current chapter is to establish whether the origin of a specific photolytically generated radical (i.e., mesityl (1) derived from mesityl (C) vs. mesityl (1) derived from 2,4,6-trimethylbenzoin (A)) has an influence on its ability to serve as an initiating species in free radical polymerizations. In the previous study,^[42] the effectiveness of mesityl (1) (derived from mesityl (C)) vs. benzoyl (2) (derived from benzoin (B)) radicals for initiating MMA polymerization was established. The study concluded that it is unlikely that a potential (relative) net-efficiency difference of up to a factor of 8.6 (or potentially up to 86 when additionally considering the very different (factor of ~ 10) UV absorptivities of mesityl (C) and benzoin (B) at 351 nm; see below) is solely caused by a difference in the ISC ability of mesityl (C) or its triplet lifetime (or a combination of both) (for details see Chapter 1.4.1).^[42] Employing an alternative photoinitiator to mesityl (C), which also bears the mesityl fragment (1), should aid in solving the question of origin dependence. Such an initiator is 2,4,6-trimethylbenzoin (A), bearing a mesityl fragment (1) and a hydroxyl fragment (3) (see Scheme 4.1). 2,4,6-trimethylbenzoin (A) is a completely different type of initiator compared to mesityl (C) (i.e., 2,4,6-trimethylbenzoin (A) being of the benzoin-type) and should thus be ideally suited for a comparison with mesityl (C). Concomitantly, the present thesis is interested in quantifying the net-initiation efficiency of the benzoyl fragment (2) (derived from benzoin(B)) and the mesityl fragment (1) (derived from 2,4,6-trimethylbenzoin (A)) in photochemically induced PLP experiments with MMA, EMA, and BMA as monomer to assess a potential change in relative reactivity with a change in monomer. 2,4,6-trimethylbenzoin (A) was synthesized according to a literature procedure (see Scheme 4.3) and is used for the first time as a photoinitiator in PLP experiments with the above-mentioned monomers. To ensure that 2,4,6-trimethylbenzoin (A) absorbs UV-light at 351 nm, a UV/Vis spectrum was recorded (see below Figure 4.6). Within the current study all assigned signals obtained in ESI mass spectra were labeled according to the following nomenclature: Disproportionation peaks occur in pairs removed by 2 Da from each other. Thus, each peak is labeled with $D^{v,=,x}$ or v,H,x , where v denotes the radical fragment that has initiated the polymerization ((1), (2) or (3), see Scheme 4.1) and x denotes the monomer (MMA, EMA, or BMA). Combination products are mentioned for the sake of completeness of the assignments, yet they are of limited use in the present study as it is not possible to differentiate whether they have been generated by initiation or termination of macromolecular growth. All combination peaks are labeled with $C^{v,w,x}$ where v and w denotes the radical fragment as endgroup (see Scheme 4.1) and x denotes the monomer (MMA, EMA, or BMA).

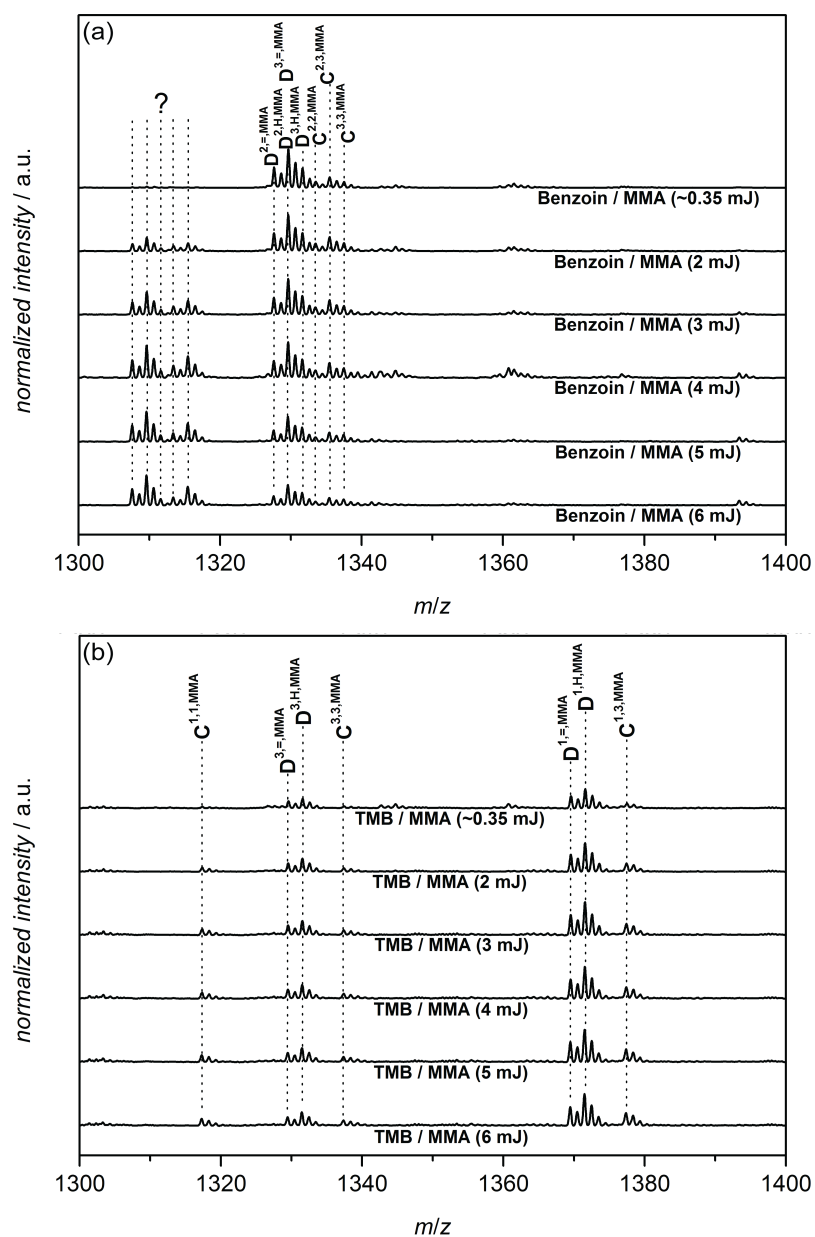


Figure 4.2. (a) ESI-MS spectra (one repeat unit) of benzoin-initiated pMMA obtained at variable laser pulse energies (~ 0.35 to 6 mJ/pulse; measured in DCM/MeOH (3:1) *via* direct infusion) synthesized *via* PLP at 100 Hz, -5°C , and $c_{\text{PI}} = 5 \times 10^{-3} \text{ mol L}^{-1}$. (b) ESI-MS spectra (one repeat unit) of 2,4,6-trimethylbenzoin-initiated pMMA obtained at variable laser pulse energies (~ 0.35 to 6 mJ/pulse; measured in DCM/MeOH (3:1) *via* direct infusion) synthesized *via* PLP at 100 Hz, -5°C , and $c_{\text{PI}} = 5 \times 10^{-3} \text{ mol L}^{-1}$. The nomenclature employed to identify the individual disproportionation and combination products is provided in Scheme 4.2.

4.4.1. Reducing the Laser Energy

During the work with freshly recrystallized benzoin (B) as photoinitiator in photochemically-initiated free radical bulk polymerizations of MMA, EMA, and BMA using the PLP method a surprising and unexpected observation was made. The polymeric material, synthesized *via* the PLP method up to 3 % conversion, was analyzed with high sensitivity ESI-MS where each repeat unit of the polymer should only show four disproportionation products (in case of MMA as monomer: $D^{2,H,MMA}$, $D^{2,=,MMA}$, $D^{3,H,MMA}$, $D^{3,=,MMA}$; see Scheme 4.2) as well as six combination products (in case of MMA as monomer: $C^{1,1,MMA}$, $C^{2,2,MMA}$, $C^{3,3,MMA}$, $C^{1,2,MMA}$, $C^{1,3,MMA}$, and $C^{2,3,MMA}$; see Scheme 4.2). Optimization of the reaction temperature (-5 °C) leads to a minimization of the combination products, thus, mainly disproportionation products were obtained in the ESI-MS spectra. However, the ESI-MS spectra in the present work show a new set of signals, which cannot be assigned to any known disproportionation or combination product (see Figure 4.2a, peak series denoted with a question mark). Neither can new radical fragments derived from benzoin (B) nor salt adducts be assigned to the unexpected signals (denoted with a question mark in Figure 4.2a, the reader is referred to Chapter 7). The only successful option to eliminate the side products from the polymer was to minimize the laser energy. The employed laser system provides stable laser energies down to 2 mJ/pulse. Figure 4.2a depicts the ESI-MS spectra of benzoin-initiated pMMA synthesized at different laser energies *via* the PLP method. The energy series indicates that the side products are energy dependent (less laser energy leads to less side products). However, at the lowest stable laser energy of 2 mJ/pulse the ESI-MS spectra are not yet free of side products as evident from Figure 4.2a (see peak ensemble at 1307.6 m/z). Only through the subsequent installation of a fine-mesh metal grid as beam attenuator next to the beam output window it was possible to reduce the laser energy to ~ 0.35 mJ/pulse. With a significant reduction in laser energy the ideally expected scenario was achieved, i.e., the disappearance of the unassigned species. Clearly, a large energy input into benzoin (B) opens primary or secondary reaction channels that lead to unexpected products. This alone is a significant observation since such fragments can have disturbing effects on PLP or any other technique relying on photoinitiation and 2 mJ/pulse is usually considered a moderate (or even low) energy input for a PLP experiment. Regardless, it has thus become feasible to obtain side product free benzoin-initiated pMMA, pEMA, and pBMA samples *via* a reduction of the laser energy. A photoinitiator concentration or temperature dependence of the side product formation was not detected.

To establish the behavior of the new initiator during PLP, a second set of polymerizations under variation of the incident energy was carried out for 2,4,6-trimethylbenzoin-initiated MMA polymerization. The corresponding mass spectra are depicted in Figure 4.2b. Pleasingly, no effect of the laser energy on the product distribution can be observed; only

Table 4.1. Collation of the polymeric product signals observed during SEC/ESI-MS of pMMA samples generated during the pulsed laser-initiated bulk free radical polymerization of MMA at 100 Hz and -5 °C. The table provides experimentally observed as well as theoretically expected m/z -ratios for the found disproportionation (D) and combination (C) products (consisting of 8, 9 or 10 monomer units, n is the number of repeat units). The structures corresponding to the individual peaks are depicted in Scheme 4.2. The tabulated values correspond to the peaks displayed in Figure 4.3.

Species	Ionization	$(m/z)_{\text{theo.}}$ / Da	$(m/z)_{\text{exp.}}$ / Da	$\Delta(m/z)$ / Da
D ^{1,H,MMA}	Na ⁺	1171.6 ($n = 10$)	1171.7	0.1
D ^{1,=,MMA}	Na ⁺	1169.6 ($n = 10$)	1169.7	0.1
D ^{2,H,MMA}	Na ⁺	1129.6 ($n = 10$)	1129.7	0.1
D ^{2,=,MMA}	Na ⁺	1127.5 ($n = 10$)	1127.6	0.1
D ^{3,H,MMA}	Na ⁺	1131.6 ($n = 10$)	1131.7	0.1
D ^{3,=,MMA}	Na ⁺	1129.6 ($n = 10$)	1129.7	0.1
C ^{1,1,MMA}	Na ⁺	1117.6 ($n = 8$)	1117.4	0.2
C ^{2,2,MMA}	Na ⁺	1133.5 ($n = 9$)	1133.7	0.2
C ^{3,3,MMA}	Na ⁺	1137.6 ($n = 9$)	1137.5	0.1
C ^{1,2,MMA}	Na ⁺	1175.6 ($n = 9$)	1175.6	0.0
C ^{1,3,MMA}	Na ⁺	1177.6 ($n = 9$)	1177.5	0.1
C ^{2,3,MMA}	Na ⁺	1135.5 ($n = 9$)	1135.4	0.1

the four expected disproportionation products (in case of MMA as monomer: D^{1,H,MMA}, D^{1,=,MMA}, D^{3,H,MMA}, D^{3,=,MMA}; see Scheme 4.2) and six combination products (in case of MMA as monomer: C^{1,1,MMA}, C^{2,2,MMA}, C^{3,3,MMA}, C^{1,2,MMA}, C^{1,3,MMA}, and C^{2,3,MMA}; see Scheme 4.2) are identified in the ESI-MS spectra. A collation of the polymeric product signals observed during ESI-MS *via* direct infusion of benzoin as well as 2,4,6-trimethylbenzoin-initiated pMMA samples is shown in Table 4.1. For further quantification studies of these two photoinitiators the following PLP conditions were used: $\nu = 100$ Hz, $E \sim 0.35$ mJ/pulse, $T = -5$ °C and an overall concentration of the photoinitiators of $c_{\text{PI}} = 5 \times 10^{-3}$ mol L⁻¹.

4.4.2. Initiator Cocktails of Benzoin (B) and 2,4,6-Trimethylbenzoin (A)

Figure 4.3a provides a depiction of all SEC/ESI mass spectra recorded of pMMA, generated *via* PLP of MMA in the presence of different mixtures of benzoin (B) and 2,4,6-trimethylbenzoin (A) (1:1, 1:3, 1:6, 1:9, 1:18). Furthermore, Figure 4.3b shows a representative repeat unit of the above mass spectra, with every peak labeled according to the

4. Quantitative Comparison of the Mesitoyl vs. the Benzoyl Fragment

above-noted nomenclature. The expected and found m/z -ratios for the depicted repeat unit are collated in Table 4.1. The additionally – to a much less part – occurring combination products are of no interest for deducing initiation efficiencies as explained above.

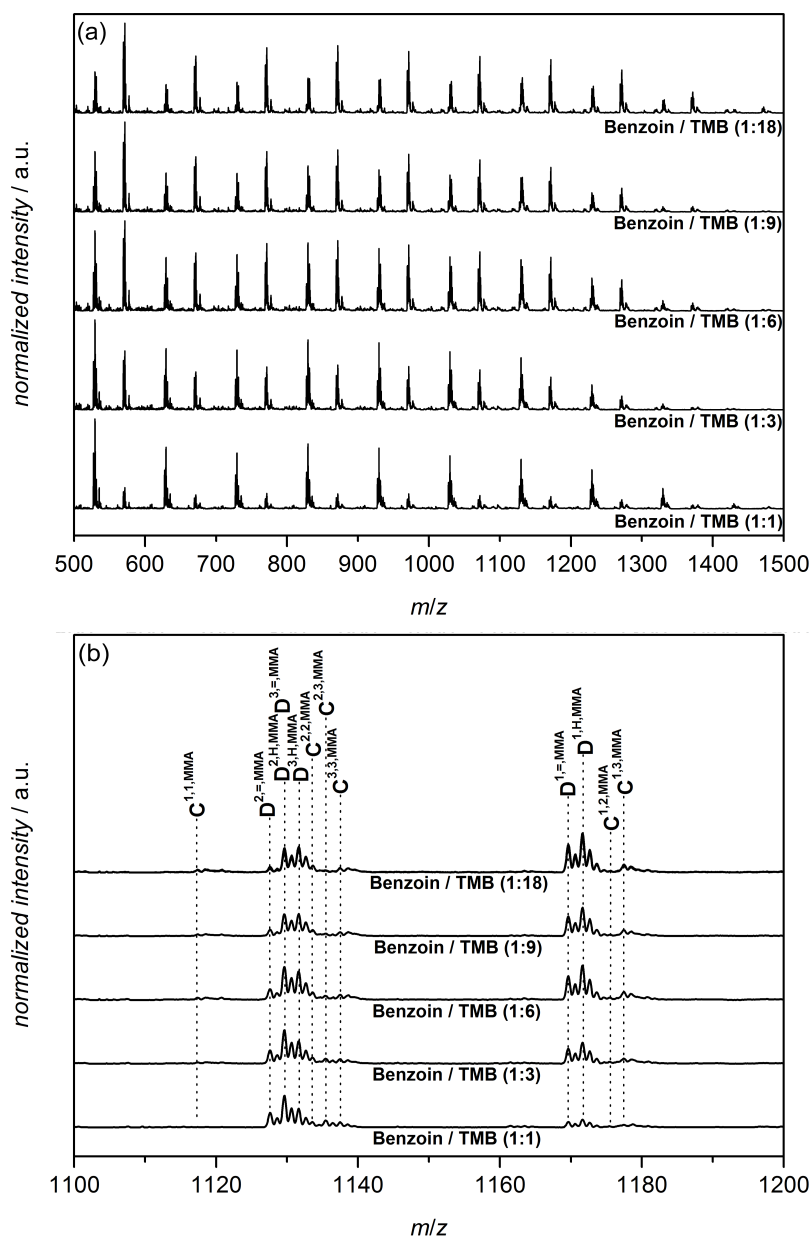


Figure 4.3. (a) SEC/ESI-MS overview spectra of polymeric material obtained from five different ratios of benzoil/2,4,6-trimethylbenzoil-initiated ($c_{PI} = 5 \times 10^{-3} \text{ mol L}^{-1}$, 1:1, 1:3, 1:6, 1:9, 1:18) PLP of MMA_{bulk} at $\sim 0.35 \text{ mJ/pulse}$ laser energy, 100 Hz, $-5 \text{ }^\circ\text{C}$. The figure depicts the single charged products ionized with sodium iodide at a retention time between 16.86 and 19.93 min. (b) Zoom into one repeat unit of the SEC/ESI-MS overview spectra of polymeric material obtained from five different ratios of benzoil/2,4,6-trimethylbenzoil-initiated ($c_{PI} = 5 \times 10^{-3} \text{ mol L}^{-1}$, 1:1, 1:3, 1:6, 1:9, 1:18) PLP of MMA_{bulk} at $\sim 0.35 \text{ mJ/pulse}$ laser energy, 100 Hz, $-5 \text{ }^\circ\text{C}$. For the m/z -ratios of the assigned products see Table 4.1. The nomenclature employed to identify the individual disproportionation and combination products is provided in Scheme 4.2.

Inspection of Table 4.1 indicates that the theoretically and experimentally expected m/z -ratios agree well within the accuracy of the mass spectrometric analysis (~ 0.3 Da). Such an agreement is found in every repeat unit and is representative for any initiator mixture composition employed within the current chapter (data for pEMA, pBMA and tables for the expected m/z -ratios can be found in Figure A.2 as well as Table A.1 (for pEMA); Figure A.3 as well as Table A.2 (for pBMA) in the Appendix). Before proceeding to a quantitative analysis of the individual disproportionation peaks, it is worthwhile to briefly provide a qualitative description of how the SEC/ESI-MS mass spectra changes with increasing amounts of 2,4,6-trimethylbenzoin (A) in the initiation cocktail. For this purpose a reconsideration of Figure 4.3b is necessary. Inspection of this figure demonstrates that with increasing amounts of 2,4,6-trimethylbenzoin (A) in the reaction mixture the number of chains carrying a mesitoyl endgroup increases ($D^{1,=,MMA}$) and the number of chains carrying a benzoyl group decreases ($D^{2,=,MMA}$). Qualitatively, one can also note that a relatively low amount of 2,4,6-trimethylbenzoin (A) in the initiation cocktail is needed to achieve a significant signal of $D^{1,=,MMA}$. Compared to the previous study employing benzoin (B)/mesitol (C) mixtures,^[42] a smaller amount of the mesitoyl bearing photoinitiator is necessary to achieve a significant signal. To place this qualitative observation onto a quantitative basis, the disproportionation peaks corresponding to the chains initiated with mesitoyl radicals (1) depicted in Figure 4.3b and Figure 4.4 are placed into relation to the peaks associated with chains initiated by benzoyl radicals (2). The signals which are directly and quantitatively compared to each other need to be free of isobaric overlap with any other peaks. The disproportionation peak ensemble of all occurring radicals (1, 2, and 3) is depicted in Figure 4.4. The enlarged disproportionation peak ensemble shown in Figure 4.4 demonstrates that only the peaks labeled with $D^{2,=,MMA}$ and $D^{1,=,MMA}$ are free of any isobaric interference. The isotopic pattern of the disproportionation products associated with $D^{1,=,MMA}$ and $D^{1,H,MMA}$ overlap with each other; for this reason, it is only possible to use $D^{1,=,MMA}$ for quantitative evaluations.

In the case of the isotopic pattern associated with $D^{2,=,MMA}$, $D^{2,H,MMA}$, $D^{3,=,MMA}$, and $D^{3,H,MMA}$ the situation is more complex. Radical fragment (2) and (3) differ in molecular weight by 2 Da, leading to an unavoidable overlap of both disproportionation signals. The signals for $D^{2,H,MMA}$ and $D^{3,=,MMA}$ appear at $m/z = 1129.6$, making their quantitative evaluation nonfeasible. In addition, the isobaric overlap does not allow to obtain quantitative information about the initiation ability of (3). It is also important to compare disproportionation products that carry an identical endgroup (unsaturated vs. unsaturated or saturated vs. saturated). Thus, the only choice for quantitatively evaluating the SEC/ESI-MS mass spectra is to compare $D^{2,=,MMA}$ with $D^{1,=,MMA}$. For the other investigated polymers, (pEMA and pBMA) the same considerations apply ($D^{2,=,EMA}$ vs. $D^{1,=,EMA}$ and $D^{2,=,BMA}$ vs. $D^{1,=,BMA}$ (for further information see Figure A.2 and Scheme A.1 (for pEMA);

Figure A.3 and Scheme A.2 (for pBMA) in the Appendix). Figure 4.4 additionally indicates how the heights $\Delta h^{D^{2,=,MMA}}$ and $\Delta h^{D^{1,=,MMA}}$ are defined, which are employed for the mass spectrometric evaluation procedure.

4.4.3. Data Analysis and Evaluation of the SEC/ESI-MS Spectra

First of all, it should be mentioned why online SEC/ESI-MS is used instead of direct infusion ESI-MS for the determination of the disproportionation signals. Direct infusion ESI-MS mass spectra in the range of 200-2000 m/z show a slightly rising baseline, caused by the presence of multiply charged ions from higher mass ranges. Such multiply charged ions appear in the lower m/z range (up to 2000 m/z) and lead to a mild, yet constant, baseline shift. For the evaluation method of the mass spectra an accurate measure of the height of the disproportionation products (as mentioned above) is required. Therefore, it is of importance to have a constant baseline as otherwise the derived initiation efficiency of the different radicals is beset with an error. The advantage of online SEC/ESI-MS is the possibility of choosing only the singly charged ion region (defined range in the RI trace) of an entire mass spectrum. By employing SEC/ESI-MS for determining $D^{1,=,MMA}$ and $D^{2,=,MMA}$, it is, however, only possible to evaluate 8 or 9 repeat units within one mass spectrum (with ESI-MS direct infusion it is possible to evaluate in the range of up to 15 repeat units). Yet, it makes practically no difference for the final initiation ratios when 7 repeat units less are used for the evaluation of the mass spectra. In the most simple and straightforward approach for evaluating the mass data in the current work, the height of the only two peaks that do not show isobaric overlap ($D^{1,=,MMA}$ and $D^{2,=,MMA}$), $\Delta h^{D^{v,=x}}$ is evaluated in each repeat unit. Figure 4.4 depicts a graphical representation on how $\Delta h^{D^{v,=x}}$ is determined. Furthermore, the height of the individual peaks can be employed to arrive at the mole fraction of the disproportionation product $D^{1,=,MMA}$, $F(i)$ (see Eq. 4.1). Nevertheless, it is important to establish if there exists any potential chain length dependent mass-bias. For this purpose a modified method from Günzler *et al.* was established in previous quantitative mass spectrometric evaluations.^[35,75] The modified approach taken in here is equivalent to that employed in the previous study on the mesitil (C)/benzoin (B) pairing.^[42] The basic equations for this approach are shown in Eq. 4.2 – Eq. 4.4 where $G(i)$ is the ratio of the peak heights of $D^{1,=,MMA}$ and $D^{2,=,MMA} \forall i$ (where i is the present repeat unit, $(i - 1)$ one repeat unit lower and $(i + 1)$ one repeat unit higher). After averaging, one receives $\langle G \rangle$, $\langle G' \rangle$, and $\langle G'' \rangle$, which can be plotted as $\langle G \rangle_{\Delta m/z,0}$ against the used initiator ratios, yielding a mass-bias free ratio of the two disproportionation products in the polymer sample (the same procedure is used for the evaluation of the pEMA and pBMA samples). The maximum deviation of the averaged $G(i)$ in each polymer sample ($\langle G \rangle$, $\langle G' \rangle$, and $\langle G'' \rangle$) from the averaged mass-bias corrected ratio, $\langle G \rangle_{m/z,0}$ is defined as an error bar in Figure 4.5b. It is important to note that this error represents an upper bound of the statistical yet, but was

chosen to also acknowledge errors stemming from the peak height determination during ESI-MS measurement.

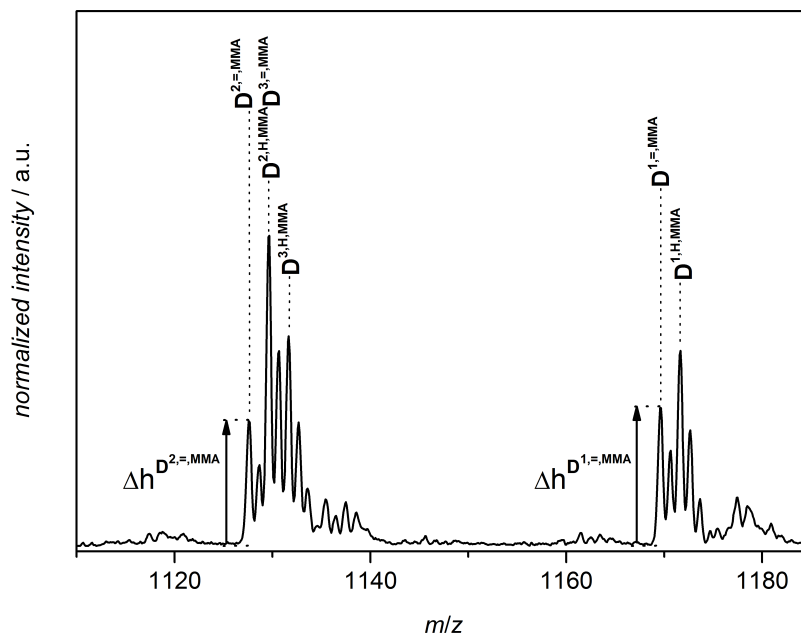


Figure 4.4. Enlarged section of the two disproportionation peak ensembles associated with polymer chains (pMMA) initiated by radical fragments (1), (2), and (3) (initiator ratio (B):(A) = 1:3). The first signal employed for evaluation purposes is $D^{2=,MMA}$ as it is the only isotopically non-overlapping signal derived from benzoin (B). The second signal employed for quantitative evaluation purposes is $D^{1=,MMA}$ derived from 2,4,6-trimethylbenzoin (A). The height of both signals in every repeat unit is employed to calculate the quantitative ratio between these two initiator fragments at the polymer chain terminus.

For the mole fraction diagrams as a function of i see Figure 4.5a (for pMMA), Figure A.4a (for pEMA, see in the Appendix), and Figure A.4b (for pBMA, see in the Appendix). As mentioned above, they depict the mesityl radicals (1) that have initiated the bulk free radical polymerization process towards the different monomers as a function of the analyzed chain length, i . Note that equal initiation ability is observed at $F(i) = 0.5$. Two important observations can be made: (i) $F(i) = F$; i.e., there is no dependence of F on the mass range that has been analyzed, implying that mass-bias effects are not pronounced. (ii) Nearly 3 times excess of 2,4,6-trimethylbenzoin (A) over benzoin (B) is required (in the case of MMA) to achieve an identical number of chains initiated with mesityl (1) and benzoin (2) radical fragments. In the case of EMA and BMA the situation is similar (see below).

The mass-bias corrected plot of $G(i)$, $\langle G \rangle_{\Delta m/z, 0}$, is used to obtain the direct ratio of chains initiated with mesityl fragments (1) over those initiated with benzoyl radicals (2). This allows direct and quantitative comparison of the initiation efficiency of benzoin (B) and 2,4,6-trimethylbenzoin (A) with respect to the benzoyl (2) and mesityl radicals (1).

Inspection of Figure 4.5b shows a linear correlation between the ratio of benzoin (B) to 2,4,6-trimethylbenzoin (A) in the reaction mixture and $\langle G \rangle_{\Delta m/z,0}$ of the benzoyl (2) and mesityl radicals (1) that have initiated the polymerization process. Parity in the initiation between 2,4,6-trimethylbenzoin (A) and benzoin (B) derived fragments ($\langle G \rangle_{\Delta m/z,0} = 1$) occurs at an initiator mixture composition of 3.0 (MMA), 2.6 (EMA), and 2.4 (BMA). Considering the error bars given in Figure 4.5b, one can note that there is a clear difference in the initiation parity between MMA and EMA/BMA, while the difference between pEMA and pBMA is not as pronounced.

$$F(i) = \frac{\Delta h^{D^{1,=,MMA}}(i)}{\Delta h^{D^{1,=,MMA}}(i) + \Delta h^{D^{2,=,MMA}}(i)} \quad (4.1)$$

$$G(i) = \frac{\Delta h^{D^{1,=,MMA}}(i)}{\Delta h^{D^{2,=,MMA}}(i)} \quad (4.2)$$

$$G'(i,i-1) = \frac{\Delta h^{D^{1,=,MMA}}(i)}{\Delta h^{D^{2,=,MMA}}(i-1)} \quad (4.3)$$

$$G''(i,i+1) = \frac{\Delta h^{D^{1,=,MMA}}(i)}{\Delta h^{D^{2,=,MMA}}(i+1)} \quad (4.4)$$

The reason for the slight disparity between the three monomers may be caused by their different densities and viscosities as well as the mobility of the ester side chains. All these factors can have an impact on the polymerization behavior and especially on the solvent cage around the fragmenting photoinitiator, thus changing its net-efficiency. *Via* inspection of Figure 4.5b, one can come to the conclusion that benzoyl radicals (2) are a factor 3.0 (2.6, 2.4) more efficient in reacting with MMA (EMA, BMA) in the initiation of bulk free radical polymerizations than mesityl radicals (1) derived from 2,4,6-trimethylbenzoin (A). This is a surprising quantitative experimental finding because the former study with mesitol (C) as source for mesityl radicals (1) demonstrated that benzoyl radicals (2) are a factor 8.6 more likely in being found as a pMMA chain terminus.^[42] These results support the hypothesis that not only the reactivity of specific radicals in relation to each other is an important parameter, but furthermore the origin of a specific radical plays a key role in determining its availability to initiate macromolecular growth. As noted above, upon inspection of Figure 4.5b, small differences between pMMA, pEMA and pBMA can be observed. However, the difference is small at low ratios of (B):(A) and significant at higher ratios of (B):(A).

To establish whether the observed difference in the propensity of the mesityl (1) vs. the benzoyl fragment (2) to initiate the polymerization is potentially caused by a difference in the UV absorptivity, it is mandatory to establish whether the two initiators

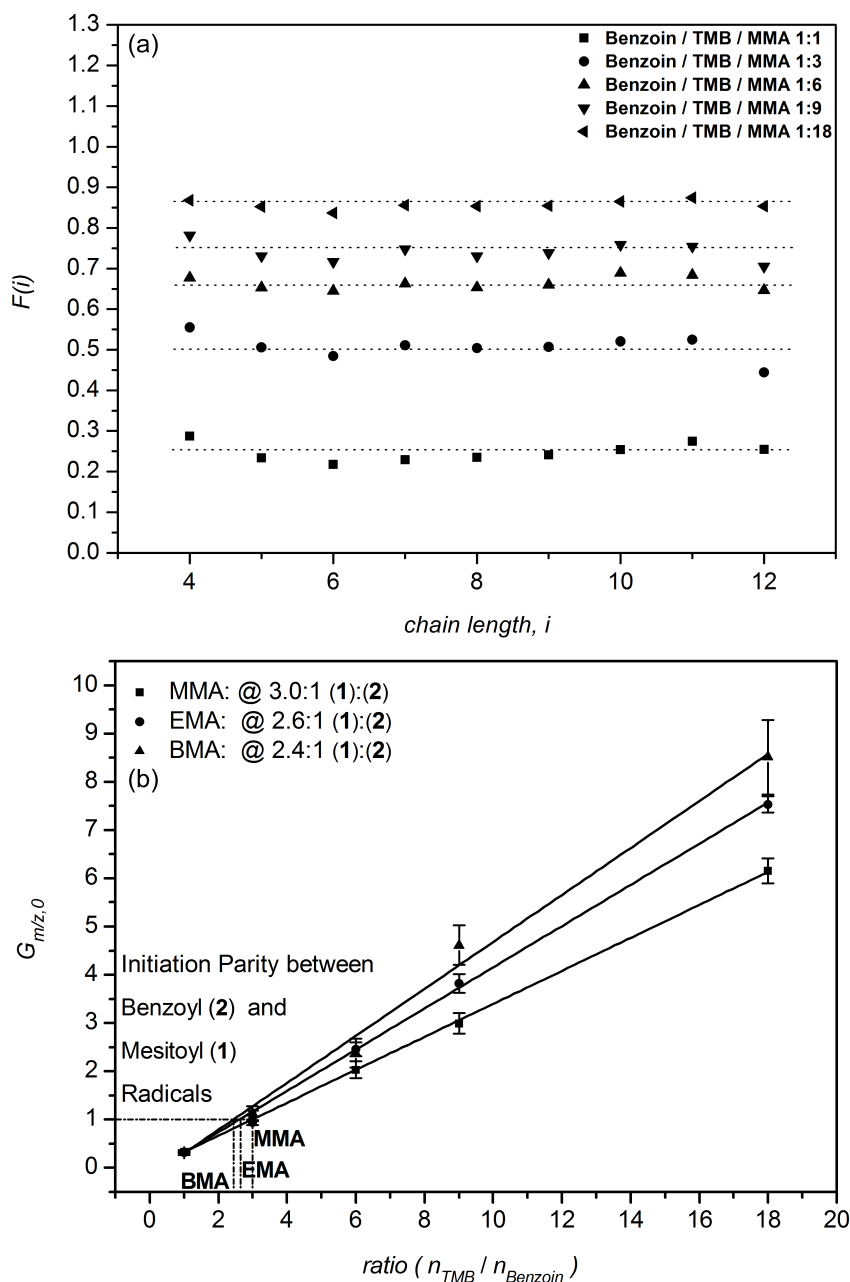


Figure 4.5. (a) Intensity-derived mole fractions of polymer chains initiated with mesityl radicals (1). $F(i)$, vs. their chain length, i . The dotted lines give the average of the mole fraction over the entire chain length range of pMMA at different photoinitiator ratios. (b) Plotted is the ratio of the intensities of the disproportionation products corresponding to polymer chains (pMMA, pEMA, and pBMA) initiated with a benzoyl radical (2) (derived from benzoil (B)) and a mesityl radical (1) (derived from 2,4,6-trimethylbenzoil (A)) vs. the ratio of both initiators in the reaction mixture (ratio = $n_{2,4,6\text{-trimethylbenzoil}}:n_{benzoil}$). An evaluation procedure has been adopted, which allows for the minimization of mass-bias and yields the mass-bias free intensity ratio $\langle G \rangle_{\Delta m/z,0}$. The figure also presents the initiation parity between the benzoyl (2) and the mesityl radical (1) at $\langle G \rangle_{\Delta m/z,0} = 1$ from pMMA, pEMA, and pBMA.

absorb UV-light of 351 nm equally well. Figure 4.6 depicts a comparative set of UV spectra (mesitol (C), benzoin (B), and 2,4,6-trimethylbenzoin (A)). At a concentration of $c_{PI} = 1 \times 10^{-3} \text{ mol L}^{-1}$ (in methanol) and an optical path length of 10 mm, mesitol (C), benzoin (B), and 2,4,6-trimethylbenzoin (A) have an absorption of 1.10 (set to 100 %), 0.07 (6.9 %), and 0.02 (2.0 %), respectively. It is important to note that mesitol (C) features the highest absorbance, yet in PLP experiments with MMA at low laser energy (conditions: $\nu = 100 \text{ Hz}$, $T = -5 \text{ }^\circ\text{C}$, $E \sim 0.35 \text{ mJ/pulse}$, $c_{PI} = 5 \times 10^{-3} \text{ mol L}^{-1}$) it was not possible to obtain polymer. The cause for this observation may be twofold: First, it implies that a certain (relatively high) amount of energy (of photons featuring a 351 nm wavelength) is required – in the case of mesitol (C) – to cause a significant decay of the photoinitiator (the generation of radicals occurs out of T_1 via ISC). The above experimental finding supports the quantitative results that the mesityl radical (1) – when derived from mesitol (C) – is found 8.6 times less as endgroup with respect to the benzoyl radical (2) in pMMA. Second, in addition to the efficiency of intersystem crossing (Φ_{ISC}) the question of the lifetime of the triplet state needs to be considered. The longer the triplet lifetime, the higher the chances that deactivation processes can reduce the quantum yield for the forming radical (Φ_R). In the current system (benzoin (B)/2,4,6-trimethylbenzoin (A), $\sim 0.35 \text{ mJ/pulse}$) the UV absorbance of 2,4,6-trimethylbenzoin (A) is more than 3.5 times less with respect to benzoin (B). The experimental quantitative finding that the mesityl radical (1) can be found ~ 3 times less as initiating group than the benzoyl radical (2) in bulk free radical polymerizations of MMA, EMA, and BMA appears to directly reflect the reduced ability of 2,4,6-trimethylbenzoin (A) to absorb the laser UV-light, thus potentially being the cause for the provision of less mesityl radicals (1) per single laser pulse. If this notion is accepted, the conclusion may be drawn that both initiators 2,4,6-trimethylbenzoin (A) and benzoin (B) – although having different UV absorbivities at 351 nm – feature similar Φ_{ISC} as well as triplet lifetimes. Considering their structural similarities, such a hypothesis may not be entirely untenable. However, it must be noted that the differences in UV absorbance (at 351 nm) which correspond to the difference in the net-initiation efficiencies may be purely coincidental. Nevertheless, these observations may imply that the previously observed 8.6 times difference^[42] (which rises up to a factor of 86 when considering that mesitol (C) absorbs ~ 10 times more energy at 351 nm than benzoin (B) and the assumption is made that the difference in UV absorbance is directly translated into a reduced ability to provide radicals) in the net-initiation efficiency between mesityl (1) and benzoyl radicals (2) derived from mesitol (C) and benzoin (B) is potentially caused by a significantly increased triplet lifetime of mesitol (C) (leading to more deactivation processes), a strongly reduced Φ_{ISC} (leading to a smaller population of T_1), or a combination of both.

Irrespective of the individual contributions of the factors governing the net-efficiency, the present data unambiguously evidence a strong origin dependence of the propensity

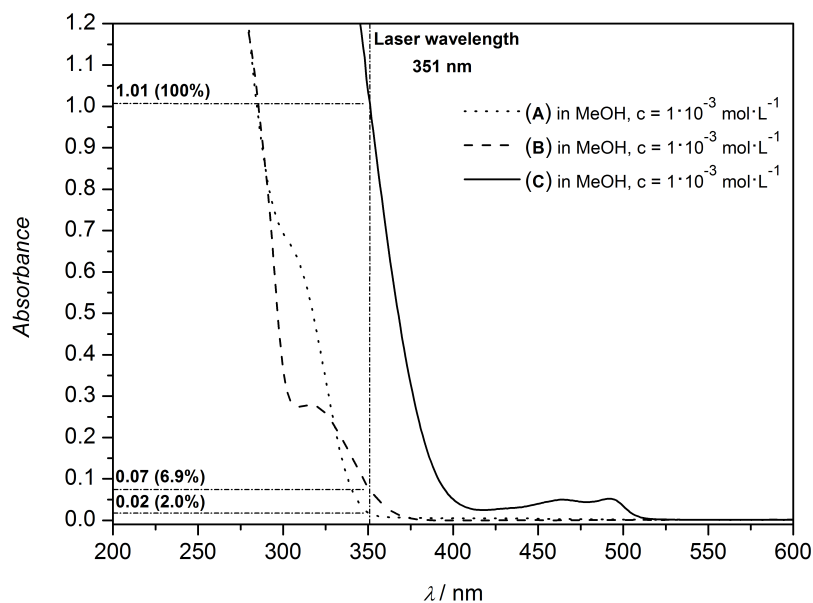


Figure 4.6. UV spectra of the employed photoinitiators, dissolved in MeOH at a concentration of $c_{\text{PI}} = 1 \times 10^{-3} \text{ mol L}^{-1}$ to compare the absorbance at the laser wavelength of 351 nm with mesitol (C) (set to 100 %).

of photolytically generated radical fragments for initiating polymerizations. In principle, a direct comparison of the mesitoyl (1) and the benzoyl fragment (2) could be made if an initiator is employed that produces both fragments at the same time. From such an initiator, i.e., 2,4,6-trimethylphenylbenzil (1-mesityl-2-phenylethane-1,2-dione, D; see Scheme 4.1), interferences from energy transitions or cage effects on the initiation process can be excluded. Thus, such an initiator was consequently synthesized^[172] and subjected to PLP as well as the above product evaluation procedure. Unfortunately, when initiated with low-energy laser pulses ($\sim 0.35 \text{ mJ/pulse}$), no polymer was produced as was already observed with mesitol (C) (see the discussion above). At higher incident laser energies (6 mJ/pulse), significant side products were observed making a reliable evaluation of the disproportionation products impossible.

Absolute rate coefficients for the addition of benzoyl (2) and mesitoyl (1) radicals to *n*-butyl acrylate have been previously reported using laser flash photolysis and fast time-resolved infrared spectroscopy (TR-IR).^[173] Although the current study investigates methacrylates, a comparison with the data reported in the above study may nevertheless be instructive. The rate coefficients for the addition to *n*-butyl acrylate read $k = 2.7 \times 10^5 \text{ M}^{-1} \text{ s}^{-1}$ for the benzoyl radical (2) (derived from 1-hydroxycyclohexyl phenyl ketone) and $k = 1.8 \times 10^5 \text{ M}^{-1} \text{ s}^{-1}$ for the mesitoyl radical (1) (derived from (2,4,6-trimethylbenzoyl)diphenylphosphine oxide). The rate coefficient for the addition of the benzoyl radical (2) to *n*-butyl acrylate is thus 1.5 times higher than that of the mesitoyl radical (1), thus indeed suggesting a somewhat decreased reactivity of the mesitoyl radical (1). If one entertains the possibility

that a similarly (small) difference in reactivity holds for the two radicals toward addition to methacrylate monomers, the conclusion can be drawn that the difference in net-initiation efficiency found between mesityl (1) and benzoyl (2) (a factor of 8.6 when the mesityl radical (1) is derived from mesitol (C)^[42] and a factor of close to 3.0 when the mesityl radical (1) is derived from 2,4,6-trimethylbenzoin (A)) is not, however, primarily due to a difference in their reactivity toward the monomer, but rather caused by variable triplet lifetimes and ISC efficiencies (as well as potential cage effects). However, at this stage no definite conclusion is possible, as this would require detailed knowledge of the above parameters (for more details see Chapter 5). Regarding the question of the generally increased relative termination ability of the mesityl radical (1) (compared to the benzoyl radical (2)) as suggested earlier from qualitative data based on both radicals being derived from benzoin (B) and bis(2,4,6-trimethylbenzoyl)phenylphosphine oxide,^[41] caution needs to be exercised: Origin effects may also play a significant role in governing the relative propensity of primary radicals to undergo termination and initiation reactions.

4.5. Conclusions

Within the current chapter an improved method is presented for determining initiator efficiencies in the system of benzoin (B) and 2,4,6-trimethylbenzoin (A) toward MMA, EMA, and BMA, *via* online SEC/ESI-MS, which enables collection of baseline-shift free mass spectra for the precision evaluation of photolytically generated endgroups in macromolecules. In addition, reducing the temperature to -5 °C to further reduce combination products and reducing the laser energy by employing a beam attenuator leads to the formation of side product free polymers that only carry the characteristic benzoin-type fragments as endgroups. In addition, 2,4,6-trimethylbenzoin (A) was employed for the first time as a photoinitiator in the bulk free radical polymerization using the PLP method. The key finding of the current chapter is that the benzoyl radical (2) (derived from benzoin (B)) is 3.0 times more likely to initiate the polymerization process of MMA than the mesityl radical (1) (derived from 2,4,6-trimethylbenzoin (A)) (2.6 (EMA) and 2.4 (BMA)). These data – in comparison with previously recorded initiation efficiency data of mesityl (1) and benzoyl fragments (2) derived from mesitol (C) and benzoin (B) – provide strong evidence that a significant origin dependence of the initiators' net-efficiency to commence macromolecular growth. Further studies within the present thesis will focus on directly measuring the triplet lifetimes of mesitol (C) and 2,4,6-trimethylbenzoin (A) as well as establishing whether radical cage effects can contribute to differences in initiation ability (for details see Chapter 5).

5

Elucidating the Early Steps in Photo-Initiated Radical Polymerization *via* Femtosecond Pump-Probe Experiments and DFT Calculations

5.1. Abstract

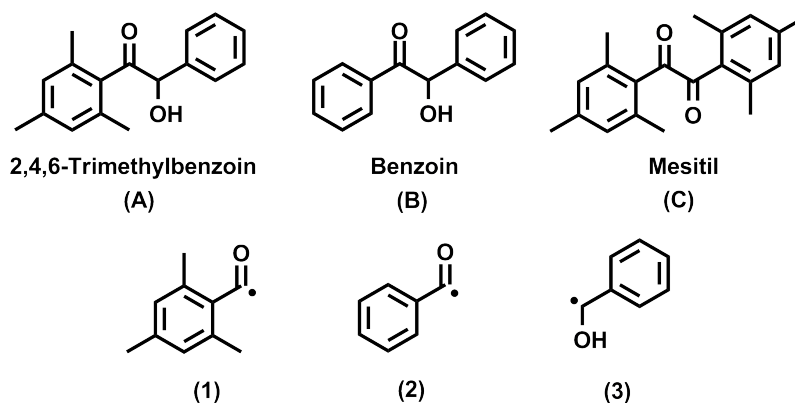
The excited states and dynamics of the three triplet radical photoinitiators 2,4,6-trimethylbenzoin (2-hydroxy-1-mesityl-2-phenylethanone, A), benzoin (2-hydroxy-1,2-diphenylethanone, B) and mesitol (1,2-bis(2,4,6-trimethylphenyl)-1,2-ethanedione, C) – employed in previous studies for quantifying *net-initiation efficiencies* in PLP with

methacrylate monomers^[174] (see Chapter 4) – are investigated *via* both femtosecond transient absorption (TA) spectroscopy and density functional theory (DFT) methods to elucidate the underlying mechanisms causing different initiation efficiencies when excited at 351 nm. Benzoin (B) and 2,4,6-trimethylbenzoin (A) are found to have very similar properties in the calculated excited states as well as in the experimentally observed dynamics. After excitation into the first excited singlet state (S_1) benzoin (B) and 2,4,6-trimethylbenzoin (A) undergo rapid ISC. The ISC can compete with ultrafast internal conversion (IC) processes, because an excited triplet state (T_n) of nearly the same energy is present in both cases. ISC is therefore the dominating depopulation channel of S_1 and subsequent α -cleavage to produce radicals takes place on the picosecond time scale. In contrast, mesitol (C) is excited into the second excited singlet state (S_2). In this case no isoenergetic triplet state is available, which inhibits ISC from competing with ultrafast deactivation processes. ISC is therefore assigned to be a minor deactivation channel in mesitol (C). Employing these findings, quantitative photoinitiation efficiency relations of benzoin (B), 2,4,6-trimethylbenzoin (A) and mesitol (C) obtained by PLP can be directly correlated with the relative TA intensities found in the femtosecond experiments. The ISC efficiency is thus a critical parameter for evaluating the overall photoinitiation efficiency and demonstrates that the employment of the herein presented method represents a powerful tool for attaining a quantitative picture on the suitability of a photoinitiator.

The results described in Chapter 5 stem from a collaboration with the group of PD Dr. Andreas-Neil Unterreiner from the Institute of Physical Chemistry – Molecular Physical Chemistry Group – at the Karlsruhe Institute of Technology, KIT. The femtosecond experiments and the DFT calculations were carried out by Thomas Wolf.

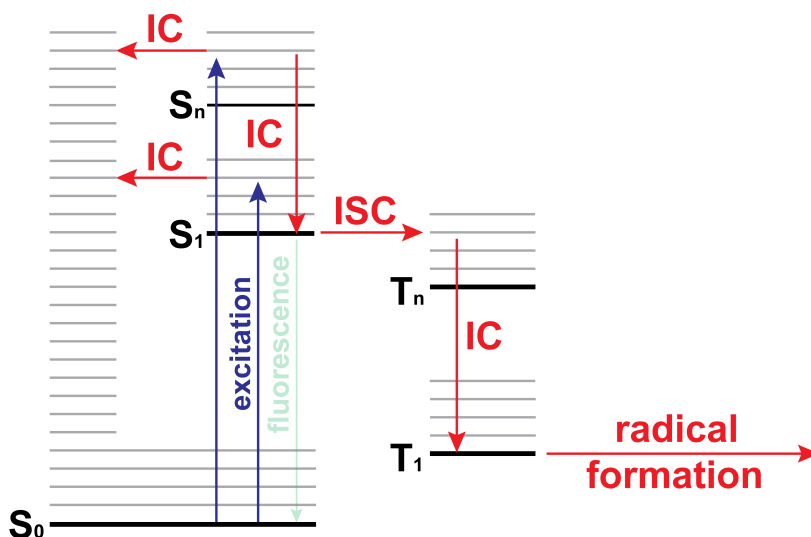
5.2. Introduction

In Chapter 4 a comparison of the net-initiation efficiencies of benzoyl (2) and mesitoyl (1) radicals for the monomers MMA, EMA, and BMA was given.^[174] As photoinitiators benzoin (B), 2,4,6-trimethylbenzoin (A), and mesitol (C) (see Scheme 5.1) were employed. It was found that not only the type of radical (benzoyl (2) vs. mesitoyl (1), i.e., the kinetics of addition to double bonds) is important for the initiation efficiency but also its origin (2,4,6-trimethylbenzoin (A) vs. mesitol (C) for mesitoyl radicals (1), i.e., excited state dynamics leading to radical formation).



Scheme 5.1 Photoinitiators employed in the present study (2,4,6-trimethylbenzoin (A), benzoin (B), and mesitil (C)) as well as their resulting radicals after irradiation with UV-light at a wavelength of 351 nm during PLP experiments (mesitoyl radical (1), benzoyl radical (2), and benzyl alcohol radical (3)).

The benzoin-derived benzoyl radical (2) is between 2.4 and 3.0 times more likely to initiate polymerization than the 2,4,6-trimethylbenzoin-derived mesitoyl fragment (1), depending on the monomer. Interestingly, the benzoin-derived benzoyl radical (2) is 8.6 times more likely to initiate the bulk free radical polymerization than mesitoyl radicals (1) derived from mesitil (C).^[42]



Scheme 5.2 Jablonski-type diagram of the possible processes following excitation of a photoinitiator into the first (S_1) or higher (S_n) excited states. These include IC into S_1 or S_0 and ISC into excited triplet states (T_n), followed by IC into T_1 . From T_1 radical formation can be achieved.

This observation is especially surprising as mesitil (C) has a considerably higher absorbance than 2,4,6-trimethylbenzoin (A) at 351 nm, the excitation wavelength of the experiments. Furthermore, it is not possible to employ mesitil (C) for PLP experiments

at low laser energies (~ 0.35 mJ/pulse).^[174] These experimental findings can only be explained by significant differences in the intrinsic excited state properties of benzoin (B), 2,4,6-trimethylbenzoin (A), and mesitol (C). Possible relaxation and reaction processes in the excited states of these molecules after photoexcitation are summarized in a Jabłoński-type diagram in Scheme 5.2.

Typically, the excitation from the ground state (S_0) leads to population of the first (S_1) or higher excited singlet states (S_n). Subsequent rapid radiationless deactivation of these excited singlet states by IC into S_0 is an unwanted process, yet cannot be ruled out in most cases, especially after excitation into higher excited states. From S_n IC can take place into S_1 . S_1 can be depopulated by ISC into an excited triplet state (T_n), which is considered to be the dominant process for excited photoinitiators. Thus, IC and fluorescence into S_0 have to be weak depopulation channels of S_1 . The fluorescence intensity is dependent both on the electronic transition dipole moment and on the Franck-Condon overlap. As the very low oscillator strengths of the $S_1 \leftarrow S_0$ transitions in the absorption spectra of many photoinitiators suggest,^[21,175,176] the low value of the electronic dipole moment is the relevant effect in most cases. Thus, the lack of fluorescence is an intrinsic property of the electronic wave function of S_1 . Furthermore, the T_n energy levels should be as close in energy as possible to the S_n states because the ISC transition probability is crucially sensitive to this energy gap.^[177] Having arrived in the triplet manifold the molecule rapidly relaxes to T_1 . T_1 has to be sufficiently longlived in order for radical formation to compete with other depopulation processes such as phosphorescence. Benzoin (B) has been subjected to several theoretical^[178] and experimental^[179–181] studies. It is known that after photoexcitation benzoin (B) performs rapid ISC.^[179,180] The triplet state is depopulated on the picosecond time scale by α -cleavage leading to a benzoyl radical (2) and a benzyl alcohol radical (3) which both can induce polymerization reactions.^[179,180] However, the exact mechanism and time scale of the ISC in benzoin (B) could so far not be investigated due to poor time resolution.^[179,180] The excited state properties of 2,4,6-trimethylbenzoin (A) and mesitol (C) are hitherto investigated neither experimentally nor theoretically. The aim of the present investigation is to elucidate the mechanistic aspects leading the molecules to the T_1 state. By exploring excited state structure, applying theoretical methods and elucidating excited state dynamics by femtosecond time-resolved spectroscopy, a better understanding is to be developed, which not only explains the previous findings^[42,174] in initiation disparity of benzoin (B), 2,4,6-trimethylbenzoin (A), and mesitol (C) – observed by mass spectrometric analysis of photo-initiated polymer synthesized *via* PLP – yet also serves as a classification tool for the efficiency of triplet radical photoinitiators.

5.3. Experimental Part

5.3.1. UV/Vis Measurements

The UV/Vis steady-state absorption spectra in methanol solution were recorded with a Varian Cary 500 spectrometer in fused silica cuvettes with an optical path length of 1 mm. For more details see Chapter 9.2.

5.3.2. Femtosecond Pump-Probe Experiments

In the femtosecond pump-probe experiments, a Clark 2210 laser system was employed with a repetition rate of 1 kHz, a central wavelength of 775 nm, a typical pulse duration of 150 fs, and an energy of 1.6 mJ/pulse. A small portion was used to pump a noncollinear optical parametric amplifier,^[151] which produces tunable pulses in the visible region. These pulses were up-converted with another portion of the fundamental laser output to produce pump pulses at excitation wavelengths (λ_{pump}) between 300 and 370 nm by a sum frequency mixing process in a barium borate (BBO) crystal. The pulse length of the desired excitation (pump) wavelength (351 nm) was dispersion optimized by a prism compressor and weakly focused into the sample. A further portion of the laser output was employed to pump another noncollinear optical parametric amplifier, which produced probe pulses with wavelengths (λ_{probe}) tunable between 470 and 750 nm. The probe pulses were also dispersion optimized by a second prism compressor and delayed *via* a translation stage with respect to the pump pulses; their polarization was rotated with a wave plate to magic angle relative to the pump-pulse polarization, and the pulses were temporally and spatially overlapped with the pump-pulses in the sample. The time resolution was measured by cross-correlation in the dye stilbene 3 to be below 200 fs. The pump intensity was kept below $4 \times 10^8 \text{ W/cm}^2$ to ensure that only small changes in optical density (OD) occur. The repetition rate of the pump pulses was reduced by a chopper wheel to allow the recording of the change in optical density with and without pump-pulse, ΔOD . The samples were prepared as methanol solutions in 1 mm fused silica cuvettes with an OD of 0.5 at the excitation wavelength resulting in concentrations of $7.8 \times 10^{-2} \text{ mol L}^{-1}$ (benzoin (B)), 1.9 mol L^{-1} (2,4,6-trimethylbenzoin (A)), and $4.9 \times 10^{-3} \text{ mol L}^{-1}$ (mesitol (C)). All samples were excited at a central wavelength $\lambda_{\text{pump}} = 351 \text{ nm}$, in agreement with earlier experiments,^[174] and probed at wavelengths of $\lambda_{\text{probe}} = 470, 500, \text{ and } 600 \text{ nm}$. The maximum delay between pump and probe pulses was 1.6 ns. For the experimental setup the reader is referred to Figure 3.2 in Chapter 3.2.

5.3.3. Theoretical Methods

Quantum chemical calculations were carried out with the TURBOMOLE V-6.3 program package.^[182] Ground state minimum geometries were optimized with DFT/BP86/def2-SV(P).^[183–188] Ground state energies at the optimized geometries were calcu-

lated with DFT/B3LYP/aug-cc-pVDZ,^[183–187,189] singlet and triplet excitations with TDDFT/B3LYP/aug-cc-pVDZ.^[189–192] For Cartesian coordinates of the optimized structures, see Table A.3, Table A.4, and Table A.5 in the Appendix.

5.3.4. Photoinitiators

The preparation procedures for 2,4,6-trimethylbenzoin (A)^[168–170,174] and mesitol (C)^[42,193,194] are adapted from the literature. For benzoin (B) see Chapter 9.2.

5.4. Results and Discussion

5.4.1. Absorption Spectra

The wavelength-dependent extinction coefficients of benzoin (B), 2,4,6-trimethylbenzoin (A), and mesitol (C) in methanol solution are shown in Figure 5.1. Both the excitation wavelength and the probe wavelength range of the TA experiment are indicated within the graph. Benzoin (B, red) exhibits a very weak absorption band centered at 320 nm and a strong absorption band at 247 nm (not shown in Figure 5.1, see Figure A.5, Figure A.6, and Figure A.7 in the Appendix for the overview UV spectra of benzoin (B), 2,4,6-trimethylbenzoin (A), and mesitol (C)).

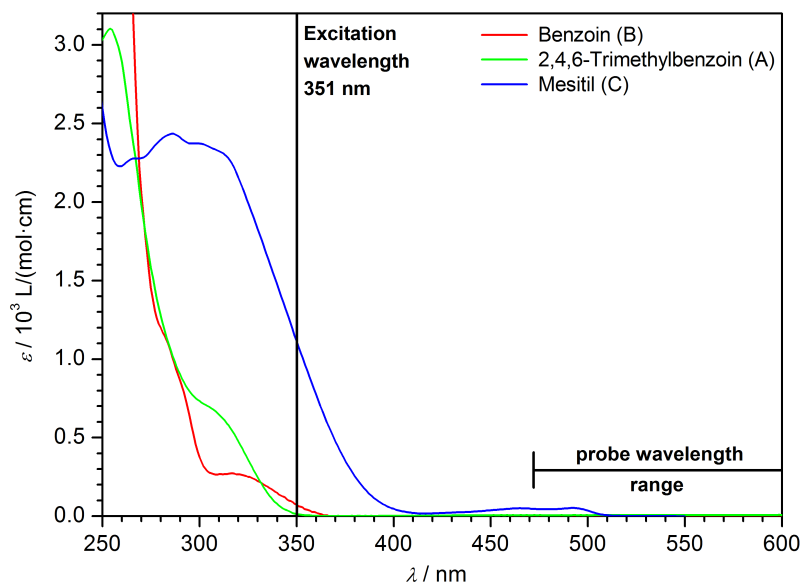


Figure 5.1. Wavelength-dependent absolute extinction coefficients of the three photoinitiators benzoin (B) (red), 2,4,6-trimethylbenzoin (A) (green), and mesitol (C) (blue). The excitation wavelength of 351 nm and the probe wavelength range of the TA experiment are marked. Note the different extinction coefficients of the photoinitiators at 351 nm.

This band has two weak shoulders at ~ 289 and 282 nm. The first absorption band of 2,4,6-trimethylbenzoin (A) is blue-shifted with respect to benzoin (B) and appears as a shoulder centered at ~ 304 nm of a stronger absorption band centered at 254 nm. Interestingly, the difference of the 2,4,6-trimethylbenzoin (A) spectrum compared to the benzoin (B) spectrum is a blue shift of the first absorption band and a red shift of the higher absorption band. The shoulders observed in the UV spectrum of benzoin (B) cannot be resolved in 2,4,6-trimethylbenzoin (A). Mesityl (C), in contrast, features a spectrum that is distinctively red-shifted with respect to the other two spectra. Its first very weak absorption band exhibits two maxima at 493 and 467 nm. The second strong absorption band is also structured and centered at 285 nm. The absolute extinction coefficients at the excitation wavelength of both the earlier PLP^[174] (see Chapter 4) and the TA experiment (at 351 nm) differ considerably for the three photoinitiators. 2,4,6-Trimethylbenzoin (A) has a low extinction coefficient ($\epsilon = 12 \text{ L mol}^{-1} \text{ cm}^{-1}$), with benzoin (B) ($\epsilon = 64 \text{ L mol}^{-1} \text{ cm}^{-1}$) the extinction coefficient is considerably higher, while mesityl (C) displays by far the highest extinction coefficient ($\epsilon = 1075 \text{ L mol}^{-1} \text{ cm}^{-1}$). Assuming the same excited state properties of all three species and that the excitation promotes the molecules into comparable higher states, mesityl (C) would be expected to be by far the most efficient polymerization initiator as also initially assumed in Chapter 4. However, as the analysis of the spectra reveals, the excited state into which the molecules are promoted into is not the same. Benzoin (B) and 2,4,6-trimethylbenzoin (A) are excited almost nonresonantly at the red wing of the first, very weak absorption band, while mesityl (C) is excited much more likely into a higher lying excited state.

It can already be concluded here that the extinction coefficient at the excitation wavelength is no suitable tool to estimate the efficiency of a photoinitiator, particularly when employing different systems as photoinitiators – benzoin (B) and 2,4,6-trimethylbenzoin (A) as benzoin-type initiators and mesityl (C) as a benzil-type initiator. For the following considerations the efficiency relationships observed in the earlier PLP/ESI-MS experiments (see Chapter 4),^[42,174] which are normalized to the concentration of the photoinitiators, thus have to be made independent of the excitation probability by normalizing them with the extinction coefficients at 351 nm (dividing both sides of the efficiency relation by the respective extinction coefficient). Such normalization leads to the prediction that an excited 2,4,6-trimethylbenzoin (A) molecule is between 1.8 and 2.2 times more likely to induce polymerization than an excited benzoin (B) molecule and that an excited benzoin (B) molecule is 144 times more likely to induce polymerization than an excited mesityl (C) molecule. It is thus evident that especially the relation between benzoin (B) and mesityl (C) with regard to their relative absorptivities is drastically altered compared with a direct comparison of the extinction coefficients.

5.4.2. Time-Resolved Spectroscopy

To obtain deeper insight into the nature and order of the time scale of the processes included in the excited states dynamics of the three photoinitiators benzoin (B), 2,4,6-trimethylbenzoin (A), and mesitol (C), TA traces were measured in methanol solution (for the concentration of the photoinitiators in methanol please refer to the Experimental Part 5.3). Thereby, the sample under investigation is excited by a femtosecond excitation pulse to a specific electronic state. The evolution of the excited state's population is investigated by projecting it through a femtosecond probe pulse, which has a variable time delay with respect to the excitation pulse, onto either a set of higher excited states or the ground state. In the first case, the sample is further excited into a region of the molecules energy diagram with a high density of electronic states in the vicinity but still well below the ionization threshold for absorption leading to positive TA values. The knowledge of the exact electronic state, which is populated by absorption of the probe photon, is thereby not mandatory. In fact, due to the high density of electronic states with their respective vibrational substructure and consequently overlapping bands, an assignment to particular states is problematic in most cases. In the second case, the emission of photons is stimulated by the probe pulse, leading to negative TA values. The TA traces thus represent the spectral properties of the excited states of the investigated molecule, convoluted with their time-dependent population. It has to be noted that the central wavelength of the femtosecond excitation pulse was 351 nm, as in the earlier PLP experiments (see Chapter 4.3) followed by mass spectrometric analysis.^[42,174] However, the spectral bandwidth of the femtosecond excitation pulse was considerably larger (with a full width at half-maximum of 490 cm^{-1} , assuming a Gaussian profile), caused by time-bandwidth limitations.^[148] Nevertheless, the steady state absorption spectra give no hint about excited state features, which could be additionally excited by the broader pulse spectrum. On the other hand, the number of vibrational states in the electronically excited state prepared by the femtosecond pulse is substantially larger than in the earlier PLP experiments.^[42,174] The same considerations apply to the probe pulses with central wavelengths of 470, 500, and 600 nm (see Figure 5.2). These wavelengths were chosen to be outside of the spectral regions where the samples have considerable absorption to avoid the influence of ground state bleaching on the TA traces. Mesitol (C) shows low absorption both at 470 and 500 nm, yet with the extinction coefficients at these wavelengths being lower by at least a factor of 22 than at the excitation wavelength, this contribution can be neglected. The TA traces of benzoin (B), 2,4,6-trimethylbenzoin (A), and mesitol (C) in methanol solution at pump-probe delays τ from -2 to 80 ps are shown in parts a, b, and c of Figure 5.2, respectively, together with global fit functions of the type

$$\Delta OD(\tau) = \left(1 + \operatorname{erf}\left(\sqrt{4\ln(2)}\frac{\tau}{\tau_0}\right)\right) \sum_{i=1}^3 A_i \cdot e^{-\frac{\tau}{\tau_i}} \quad (5.1)$$

representing the sum of three exponential decay functions with time constants τ_i and amplitudes A_i as parameters, convoluted with an error function with τ_0 as parameter. The latter models the onset of the TA within the temporal overlap of excitation and probe pulses. The fit parameters are listed in Table 5.1 and Table 5.2. A comparison of the TA traces of benzoin (B) and 2,4,6-trimethylbenzoin (A) at a probe wavelength of 500 nm and pump-probe delays from -4 ps to 1.6 ns is shown in Figure 5.3a. A comparison of the TA traces of benzoin (B), 2,4,6-trimethylbenzoin (A), and mesitol (C) at a probe wavelength of 500 nm is shown in Figure 5.3b.

Table 5.1. Time constants (refer to Eq. 5.1) derived from global multiexponential fits for the three studied photoinitiators benzoin (B), 2,4,6-trimethylbenzoin (A), and mesitol (C).

Photoinitiator	τ_1 /ps	τ_2 / ps	τ_3 / ns
B	1.2 ± 0.2	14.3 ± 0.9	> 1.6
A	0.7 ± 0.2	15.9 ± 0.4	> 1.6
C	0.2 ± 0.2	25 ± 2	> 1.6

Table 5.2. Relative amplitudes (refer to Eq. 5.1) of the TA probed at 470 nm, 500 nm, and 600 nm derived from global multiexponential fits for the three studied photoinitiators benzoin (B), 2,4,6-trimethylbenzoin (A), and mesitol (C). For mesitol (C) no TA could be found at 600 nm.

Probed wavelength	Photoinitiator	$A_{1,rel}$	$A_{2,rel}$	$A_{3,rel}$
470 nm	B	0.39 ± 0.06	0.52 ± 0.03	0.08 ± 0.01
	A	0.08 ± 0.05	0.66 ± 0.01	0.27 ± 0.01
	C	0.66 ± 0.07	0.29 ± 0.01	0.05 ± 0.01
500 nm	B	0.60 ± 0.03	0.32 ± 0.02	0.07 ± 0.01
	A	0.33 ± 0.03	0.40 ± 0.01	0.28 ± 0.01
	C	0.85 ± 0.04	0.12 ± 0.01	0.03 ± 0.01
600 nm	B	0.76 ± 0.01	0.17 ± 0.01	0.07 ± 0.01
	A	0.50 ± 0.03	0.30 ± 0.02	0.20 ± 0.01

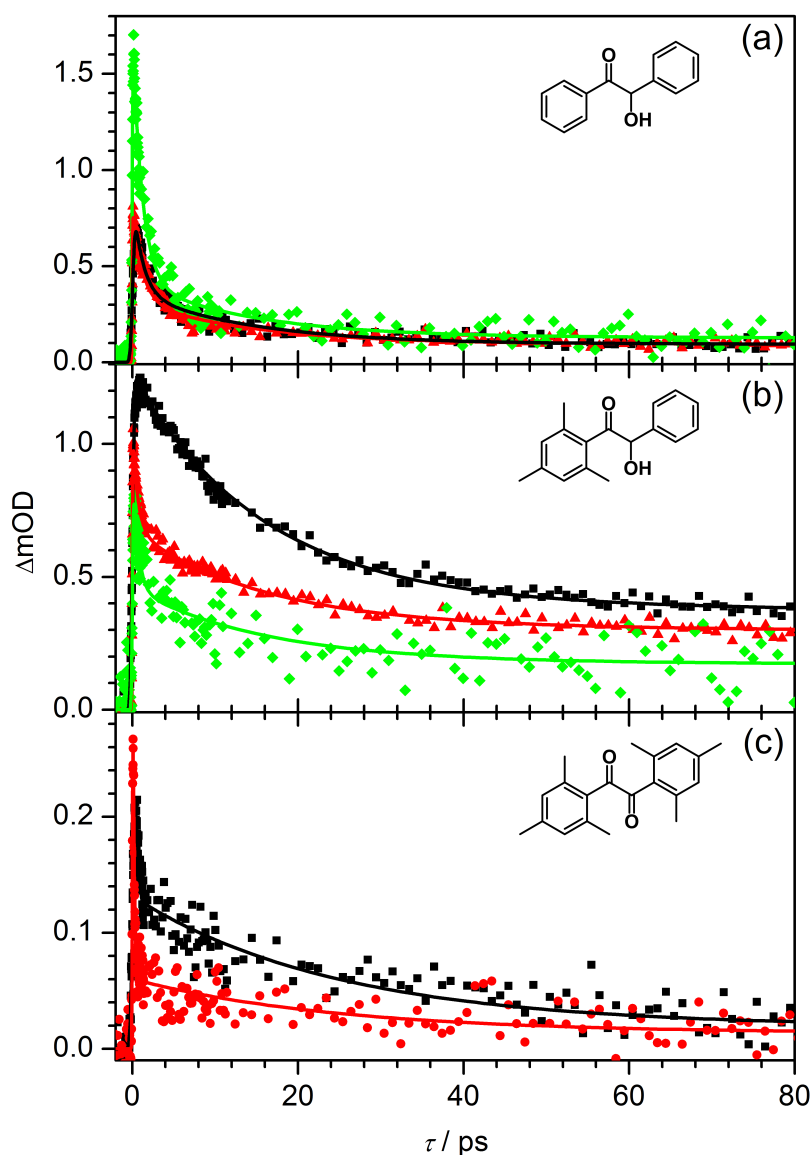


Figure 5.2. TA of (a) benzoin (B), (b) 2,4,6-trimethylbenzoin (A), and (c) mesitol (C) in methanol solution pumped at 351 nm and probed at 470 nm (black), 500 nm (red), and 600 nm (green), respectively, together with fit functions (according to Eq.5.1 and the fit parameters collated in Table 5.1 and Table 5.2).

The TAs of all three samples have two features in common (see Figure 5.2 and Figure 5.3): They show an initial biexponential decay on the picosecond time scale and a residual TA stable throughout the whole investigated time window (1.6 ns). In the case of mesitol (C), this residual TA is too low to be detected on the nanoseconds time scale. The two time constants for the biexponential decay found in the fits of benzoin (B) and 2,4,6-trimethylbenzoin (A) are similar ($\tau_1 = 1.2$ ps and $\tau_2 = 14.3$ ps for benzoin (B) vs. $\tau_1 = 0.7$ ps and $\tau_2 = 15.9$ ps for 2,4,6-trimethylbenzoin (A)), while the fits of mesitol (C) display considerably different values ($\tau_1 = 0.2$ ps and $\tau_2 = 25$ ps). The value of the first time constant of mesitol (C) is approaching the experimental time resolution. Thus, the underlying dynamical process is

most likely faster than the value suggests. The second time constant of mesitol (C) is by a factor of ~ 1.7 higher than in benzoin (B) and 2,4,6-trimethylbenzoin (A). The respective third time constants of all three samples are considerably higher than the experimentally accessible time window and therefore undefined. Inspection of Figure 5.2 and Figure 5.3 reveals that the absolute initial TA values at $\tau = 0$ are comparable in the cases of benzoin (B) and 2,4,6-trimethylbenzoin (A). For mesitol (C) the values are lower by a factor of 4 with respect to the other two samples.

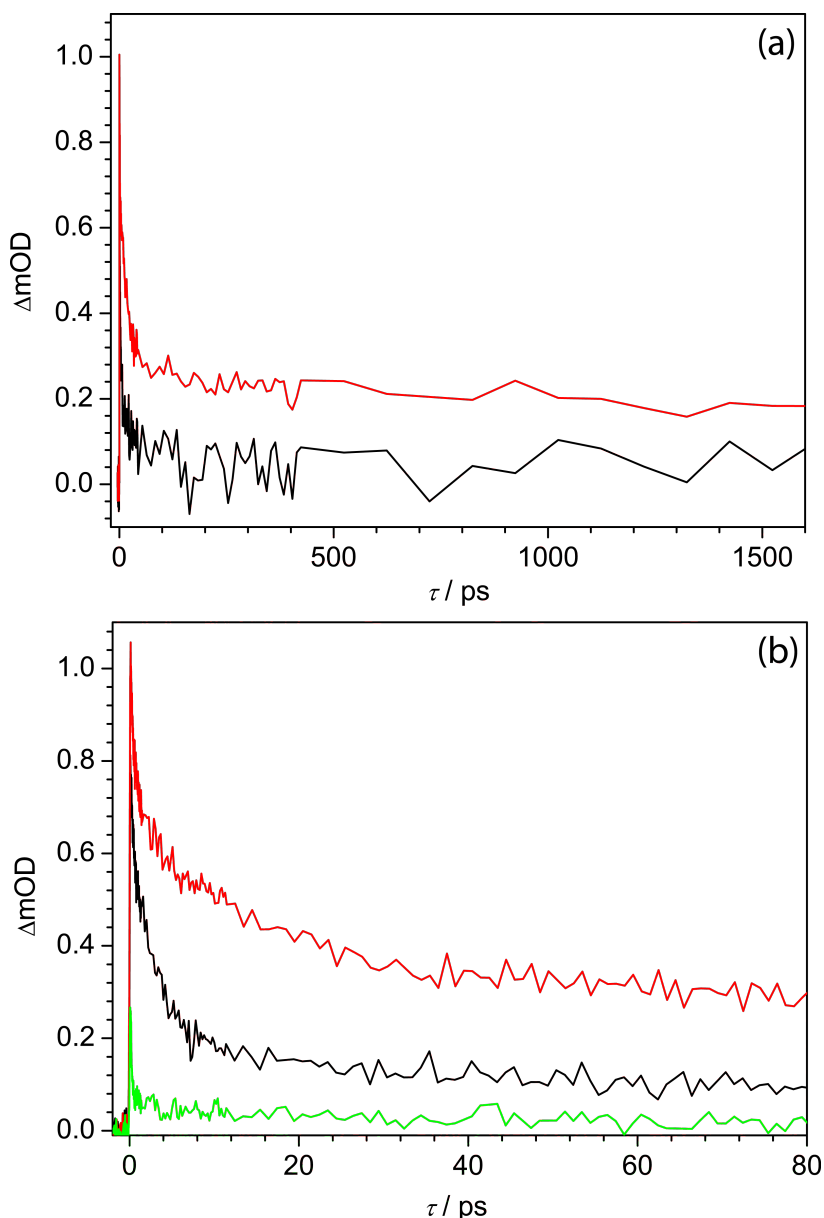


Figure 5.3. (a) TA of benzoin (B) (black) and 2,4,6-trimethylbenzoin (A) (red) pumped at 351 nm and probed at 500 nm and (b) TA of benzoin (B) (black), 2,4,6-trimethylbenzoin (A) (red), and mesitol (C) (green) in methanol solution pumped at 351 nm and probed at 500 nm.

The residual TA is the highest with 2,4,6-trimethylbenzoin (A) (see for example Figure 5.3), the values of benzoin (B) are lower by a factor of 3. Mesityl (C) shows a very low residual TA. A large wavelength dependence of TA can only be found for 2,4,6-trimethylbenzoin (A). For comparison, the relative amplitudes from the fits at a probe wavelength of 500 nm are collated in Table 5.2. For benzoin (B) the first component has the highest contribution to the TA. The second and third components have smaller contributions by factors of close to 2 and 10, respectively. In 2,4,6-trimethylbenzoin (A) all three components contribute nearly equally to the TA. In mesityl (C) the first component has the by far highest contribution. The second component is lower by a factor of 7 and the third by a factor of 30.

5.4.3. Results from DFT Calculations

To obtain insights into the electronic structure properties of the three experimentally investigated photoinitiators, minimum energy geometries were optimized with DFT/BP86/def2-SV(P).^[183–188] In good agreement with the literature,^[178] two low energy minimum geometries of benzoin (B) could be found: one with an intramolecular hydrogen bond between the carbonyl group and the OH group (geometry 1) and one geometry without this hydrogen bond (geometry 2).

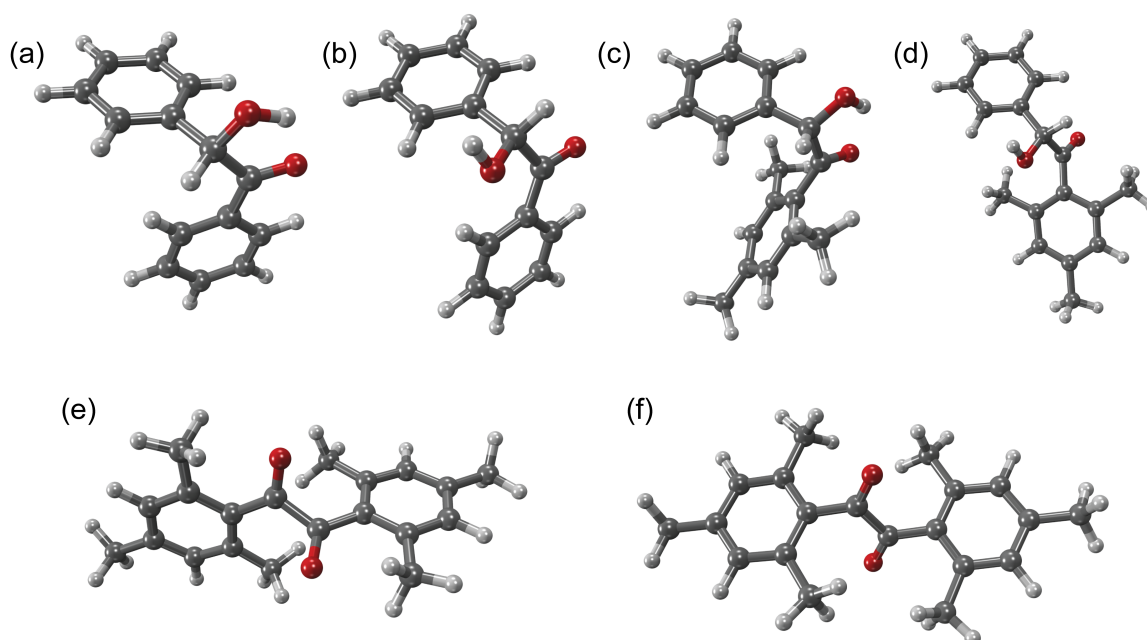


Figure 5.4. Optimized geometries of benzoin (B) with an intramolecular hydrogen bond (a) and without a hydrogen bond (b), 2,4,6-trimethylbenzoin (A) with an intramolecular hydrogen bond (c) and without a hydrogen bond (d) and mesityl (C) with aromatic ring planes perpendicular (e) and parallel (f) to each other. Optimization: DFT/BP86/def2-SV(P).^[183–188]

These two minimum geometries are shown in Figure 5.4a and Figure 5.4b, respectively. Corresponding geometries could also be found for 2,4,6-trimethylbenzoin (A). They are depicted in Figure 5.4c and Figure 5.4d. At the minimum geometries, single-point calculations with DFT/B3LYP/aug-cc-pVDZ^[183–187,189] were performed. The resulting energies are depicted in Table 5.3.

Table 5.3. Energies at optimized geometries of the three investigated photoinitiator molecules benzoin (B), 2,4,6-trimethylbenzoin (A), and mesitol (C) obtained *via* DFT/B3LYP/aug-cc-pVDZ^[183–187,189]. ZPC is an abbreviation for zero point correction and E for energy.

	B		A		C	
	geometry 1	geometry 2	geometry 1	geometry 2	geometry 1	geometry 2
E [hartree]	-690.8328	-690.8230	-808.6958	-808.6864	-925.3540	-925.3513
E + ZPC [hartree]	-690.6104	-690.6024	-808.3939	-808.3845	-924.9923	-924.9905
ΔE [kJ mol ⁻¹]		21.8		24.7		4.7

Table 5.4. Energies of selected excited singlet and triplet states relative to the singlet ground state of benzoin (B), 2,4,6-trimethylbenzoin (A), and mesitol (C), respectively, calculated at the TDDFT/B3LYP/aug-ccpVDZ level of theory.^[189–192]

Photoinitiator	Singlet State	$E_{\text{rel.}}$	Triplet State	$E_{\text{rel.}}$
		/ eV		/ eV
B	S ₁	3.59	T ₁	3.13
	S ₂	4.37	T ₂	3.17
	S ₃	4.43	T ₃	3.58
	S ₄	4.51	T ₄	3.74
A	S ₁	3.93	T ₁	3.27
	S ₂	4.25	T ₂	3.46
	S ₃	4.33	T ₃	3.62
	S ₄	4.85	T ₄	3.96
C	S ₁	2.85	T ₁	2.36
	S ₂	3.68	T ₂	3.01
	S ₃	3.84	T ₃	3.02
	S ₄	3.85	T ₄	3.28
	S ₅	4.04	T ₅	3.41
	S ₆	4.05	T ₆	3.43
	S ₇	4.55	T ₇	3.98

The energy differences between the two geometries are 21.8 kJ mol⁻¹ for benzoin (B) and 24.7 kJ mol⁻¹ for 2,4,6-trimethylbenzoin (A) and can predominantly be attributed to the intramolecular hydrogen bond. Their values are in the range of typical energies of intermolecular hydrogen bonds between methanol molecules.^[195] Thus, geometry 2 is very likely to compensate its disfavor in energy by developing intermolecular hydrogen bonds with solvent molecules. Additionally, clear experimental evidence was reported in ref. 180 for geometry 2 of benzoin (B) being the most stable and active structure for α -cleavage from the triplet state in methanol solution. Therefore geometry 2 was assigned to be the active geometry in both benzoin (B) and 2,4,6-trimethylbenzoin (A). As can be seen in Figure 5.4a-d, the common feature of all benzoin (B) and 2,4,6-trimethylbenzoin (A) geometries is the hydroxyl-substituted sp³-carbon effectively isolating the two phenyl and benzoyl (mesityl) π -systems from each other, resulting in overall nonplanar geometries. In agreement with crystal structures and calculations of mesitol (C) and its analogue without methyl substituents at the aromatic rings, benzil,^[196–198] two low energy geometries could also be found for mesitol (C) (geometry 1 and geometry 2). They are depicted in Figure 5.4e and Figure 5.4f. The energies of the two geometries are listed in Table 5.3. Geometry 1 is calculated to be 4.7 kJ mol⁻¹ lower in energy than geometry 2, which cannot be attributed to a solvent-dependent stabilization effect as the intramolecular hydrogen bond in benzoin (B) and 2,4,6-trimethylbenzoin (A). Therefore, geometry 1 is assigned to be the active geometry for further considerations. In mesitol (C) an isolating sp³-carbon between the two mesityl π -systems is missing. However, because of steric effects induced by the methyl groups, the two mesityl ring planes are perpendicular in geometry. From that one can assume a considerable disturbance of the resonance between the two rings. For the active geometries singlet and triplet excitations are calculated at the TDDFT/B3LYP/aug-cc-pVDZ^[189–192] level of theory. A comparison between experimental and calculated spectra is shown in Figure 5.6 and Figure 5.7. Selected transition energies are summarized in Table 5.4.

The agreement between experimental spectrum and calculations is very reasonable, if one takes into account that no solvent effect is included in the calculations. It can be clearly seen that irradiation of the sample at 351 nm leads exclusively to excitation of the first singlet transition of benzoin (B) and 2,4,6-trimethylbenzoin (A) as well as the second singlet transition of mesitol (C) (the calculated first singlet transition of 2,4,6-trimethylbenzoin (A) is – in agreement with the experimental spectrum – centered at a shorter wavelength with respect to the excitation wavelength of 351 nm). By molecular orbital (MO) analysis this transition can be assigned to an excitation from the highest occupied MO (HOMO) to the lowest unoccupied MO (LUMO) in the case of benzoin (B). These MOs are visualized in Figure 5.5a and Figure 5.5b, respectively. It can be seen that the HOMO has both the character of a π -MO on the side of the phenyl π -system and the character of a lone pair at the carbonyl oxygen. The LUMO has mainly the character of a π -MO in

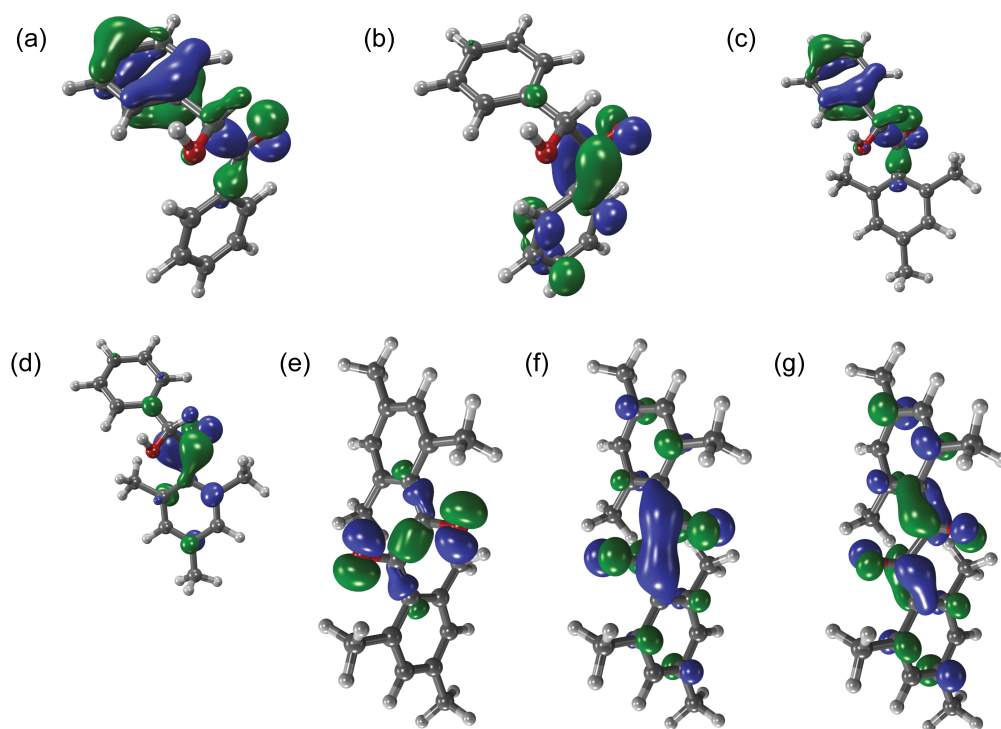


Figure 5.5. Visualization of the HOMO (a) and LUMO (b) of benzoin (B), of the HOMO-2 (c) and LUMO (d) of 2,4,6-trimethylbenzoin (A), and of the HOMO (e), LUMO (f), and LUMO+1 (g) of mesitil (C), calculated at the DFT/B3LYP/aug-cc-pVDZ level of theory.^[183–186,189]

the benzoyl part of the molecule. The LUMO \leftarrow HOMO transition can therefore be described as a charge-transfer excitation into a $n\pi^*$ state. Such states are known to easily undergo ISC into $\pi\pi^*$ states, as predicted by the well-known El-Sayed selection rule.^[199] In the case of 2,4,6-trimethylbenzoin (A), the first singlet transition is governed by a LUMO \leftarrow HOMO-2 excitation. The corresponding MOs can be seen in Figure 5.5c and Figure 5.5d, respectively. They match quite precisely the ones of benzoin (B). The first singlet transition of mesitil (C) is governed by a LUMO \leftarrow HOMO excitation. A visualization of the involved molecular orbitals is depicted in Figure 5.5e and Figure 5.5f. The striking observation is that despite the considerations discussed above based on the rectangular position of the two phenyl rings relative to each other, the two mesitil (C) π -systems are far from being isolated from each other. The HOMO is predominantly of oxygen lone-pair character and the LUMO of carbonyl- π^* character. Thus, again it is a $n\pi^*$ transition, but in contrast to benzoin (B) and 2,4,6-trimethylbenzoin (A) not a charge-transfer transition. The second singlet transition which was actually excited in the experiments is a LUMO+1 \leftarrow HOMO transition (see Figure 5.5e and Figure 5.5g). The LUMO+1 has also strong π^* -character, but is of different symmetry compared to the LUMO, which accounts for the stronger absorption probability of the second singlet transition.

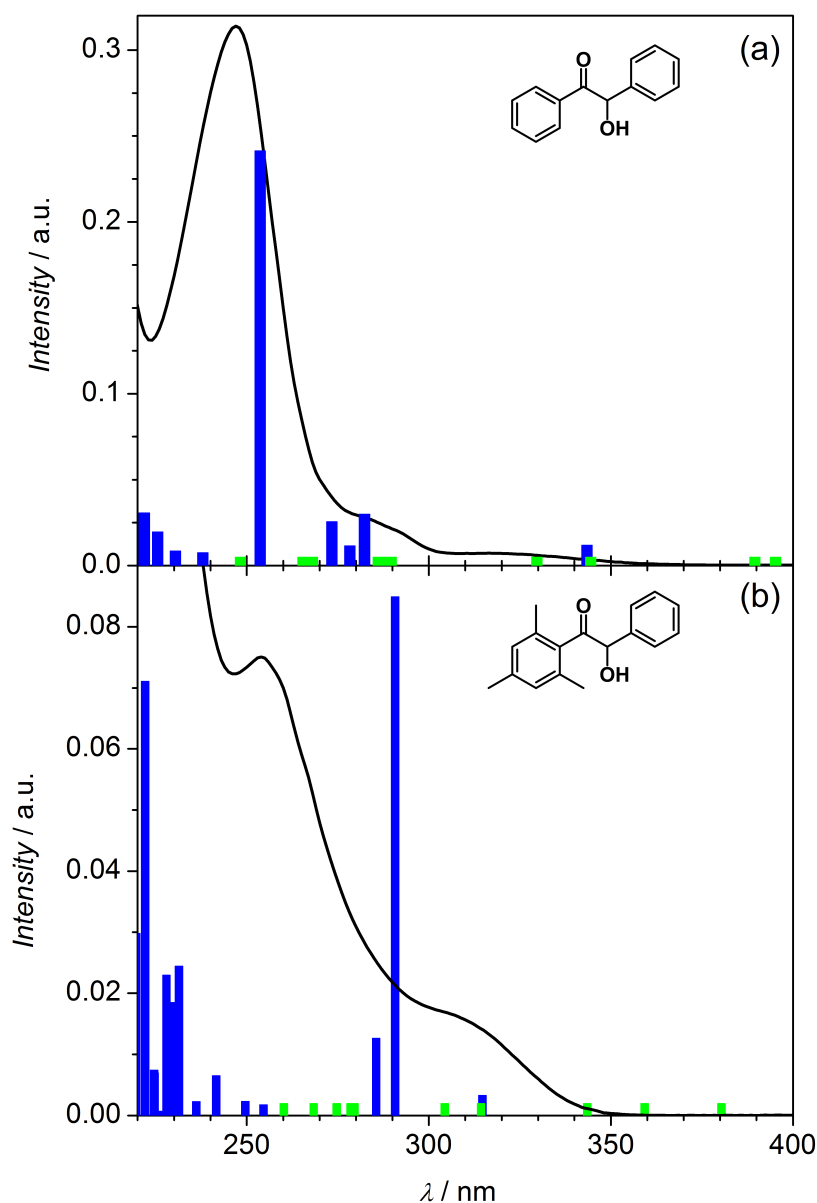


Figure 5.6. Experimental absorption spectrum of benzoin (B) (a), and 2,4,6-trimethylbenzoin (A) (b) in methanol solution (black) and calculated singlet (blue) and triplet (green) excitations, calculated at the TDDFT/B3LYP/aug-cc-pVDZ level of theory.^[189–192]

Reviewing the presented experimental and theoretical results, benzoin (B) and 2,4,6-trimethylbenzoin (A) seem to behave relatively similar. TA experiments show relaxation in a comparable manner on near-identical time scales. Theoretical calculations relate the excitation wavelength employed in the experiments to corresponding transitions into the first excited singlet state. Thus, in the following, the two systems are jointly discussed. Considering Scheme 5.2, the first question to address is whether the overall process from photoexcitation to depopulation of T_1 by α -cleavage can be observed within the time window of 1.6 ns investigated by the experiments. Earlier studies of benzoin (B)^[179,180] found values of 830 and 20 ps for the triplet lifetime, whereas only the

second value was derived by time-resolved experiments.^[180] An ISC time constant could only be estimated due to 20 ps time resolution.^[180] Other studies of similar systems also found time constants for the α -cleavage reaction in the order of picoseconds.^[200–202] This suggests that the depopulation of T_1 by α -cleavage should be observable in the present TA traces. Thus, the residual TA observed in benzoin (B) and 2,4,6-trimethylbenzoin (A) samples is associated with the time constant τ_3 and can be attributed to absorption of the reaction products of α -cleavage. Hence, the process connected with the time constant τ_2 has to be assigned to the depopulation of T_1 . The observed values of 14.3 and 15.9 ps for benzoin (B) and 2,4,6-trimethylbenzoin (A), respectively, reveal a surprisingly fast α -cleavage reaction, yet are in good agreement with earlier findings.^[180] Furthermore, the process associated with the time constant τ_1 is at least in part attributable to ISC. Although even sub-100 fs ISC has been reported for aromatic systems,^[203] such values could be connected to special substituent features which are not present in benzoin (B) and 2,4,6-trimethylbenzoin (A). Typical ISC time constants are on the time scale of several picoseconds to microseconds.^[204] ISC time constants of 2.3 ps have already been observed in similar photoinitiators undergoing α -cleavage,^[205] but the values of 0.7 and 1.2 ps observed here seem to be surprisingly fast. They can only be explained by the assumption of convolution of an additional ultrafast IC deactivation channel competing with ISC in depopulation of S_1 . The observed time constant is in this case related to the ISC and IC time constant by $\tau_1 = (\tau_{IC}\tau_{ISC})/(\tau_{IC} + \tau_{ISC})$ and can therefore be only regarded as a lower limit for τ_{ISC} . Nevertheless, ISC has to take place within a few picoseconds in both benzoin (B) and 2,4,6-trimethylbenzoin (A). The most probable reason for this behavior is apparent when comparing the calculated energies of S_1 and T_3 (T_4) in benzoin (B) (2,4,6-trimethylbenzoin (A)) as collated in Table 5.4. As pointed out earlier, ISC efficiency is crucially dependent on the singlet-triplet energy gap.^[177] According to the calculations in both benzoin (B) (0.01 eV) and 2,4,6-trimethylbenzoin (A) (0.03 eV) this energy gap is negligible. A very efficient and therewith fast ISC can thus be suggested. Its time scale is even competitive to IC processes.

Analysis of the TA of mesitol (C) reveals the same number of components as for benzoin (B) and 2,4,6-trimethylbenzoin (A), but the values of the associated time constants and particularly their relative amplitudes differ by a substantial amount. The excited states dynamics of benzil – the same system as mesitol (C), but without methyl substituents at the aromatic rings – were studied earlier.^[206] In this system the dynamics take place on comparable time scales and were assigned to conformational rearrangements on the S_1 potential energy surface. Taking the present experimental results into account, the assignment to configurational rearrangements seems questionable, because substitution at the carbon rings of benzil – as it is the case in mesitol (C) – should hinder such rearrangements. However, a substantial shift in time constants between benzil and

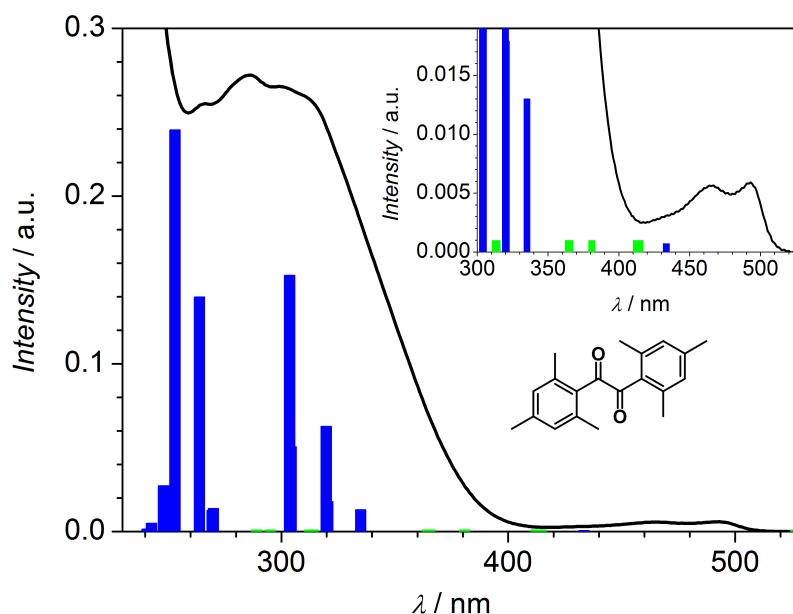


Figure 5.7. Experimental absorption spectrum of mesitil (C) in methanol solution (black) and calculated singlet (blue) and triplet (green) excitations, calculated at the TDDFT/B3LYP/aug-cc-pVDZ level of theory.^[189–192] The inset represents a more detailed plot of the region between 300 and 530 nm.

mesitil (C) cannot be observed. Furthermore, an additional channel into triplet states leading to photoinitiation, as evidenced for benzil^[207] was not discussed. Thus, the question is if the observed differences in photoinitiation efficiency^[174] (see Chapter 4) can be explained by employing the same reaction model as it was utilized for benzoin (B) and 2,4,6-trimethylbenzoin (A). In this case, the process connected with τ_1 would be assigned to depopulation of the excited S_2 , τ_2 would be assigned to α -cleavage and the residual absorption with a decay time τ_3 to the produced radicals. The value of τ_1 is substantially lower than in benzoin (B) and 2,4,6-trimethylbenzoin (A) and within the experimental time resolution. Applying the same considerations as before, the value would point to a convolution of the ISC with an ultrafast IC channel. In opposite to benzoin (B) and 2,4,6-trimethylbenzoin (A) this IC channel is the by far dominating channel in mesitil (C). The assignment is also supported by the relative amplitude ratios of mesitil (C). There are several reasons for the prevalence of IC processes. First, the molecule is excited to a higher singlet state (S_2), where the density of states and therewith the probability for IC is strongly increased. At least one ultrafast depopulation channel leading to S_1 is predicted by Kasha's rule.^[208] Additionally, as already observed, the MOs involved in the transition are much more delocalized over the whole system increasing the probability of conical intersections between singlet states, which allows for very efficient IC. Moreover, as can be seen from Table 5.4, mesitil (C) does not provide excited triplet states with an energy gap to either S_2 or S_1 , which is nearly as low as in the case of benzoin (B) and 2,4,6-trimethylbenzoin (A). Thus, whether ISC starts from S_2 or S_1 in

mesitol (C) cannot be discerned. The α -cleavage reaction takes place with a time constant τ_2 of 25 ps, which is substantially slower than in 2,4,6-trimethylbenzoin (A) (15.9 ps). This finding can be explained again by the different structure of the mesitoyl radical (1) producing molecules 2,4,6-trimethylbenzoin (A) and mesitol (C). The residual TA of mesitol (C) then partly consists of the same absorbing species like 2,4,6-trimethylbenzoin (A).

The earlier observations in Chapter 4 of different photoinitiation efficiencies^[42,174] are thus in the framework of the mechanism proposed here ascribed mainly to a competition between IC and ISC processes in the photoinitiator molecules, while the efficiency of ISC can be estimated sufficiently by time-dependent density functional theory (TDDFT) calculations. The process of radical formation, i.e., the triplet lifetime and kinetics of radical addition to double bonds, seems to play a much less important role. It has to be stressed that the crucial condition, which causes the high efficiency of benzoin (B) and 2,4,6-trimethylbenzoin (A), is the excitation of S_1 , which shows low oscillator strength to S_0 , only minor IC deactivation channels and a quasi-isoenergetic triplet state. It is very likely that excitation into S_n states of both benzoin (B) and 2,4,6-trimethylbenzoin (A) leads to a breakdown of the ISC efficiency for the same reasons mentioned in the case of mesitol (C). In the following considerations an attempt has been made to quantitatively describe the earlier observed efficiency ratios obtained from the hyphenated PLP/ESI-MS experiments.^[42,174] As pointed out during the examination of the steady state spectra of benzoin (B), 2,4,6-trimethylbenzoin (A), and mesitol (C), the relation of initiation efficiency between excited benzoin (B) and excited 2,4,6-trimethylbenzoin (A) is 1:1.8 to 1:2.2 and between excited benzoin (B) and excited mesitol (C) 144:1. As the presented results clearly reveal, the properties of benzoin (B) and 2,4,6-trimethylbenzoin (A) are very similar. The efficiency ratio between the excited benzoin (B) and 2,4,6-trimethylbenzoin (A) photoinitiators is therefore predominantly assigned to different initiation efficiencies of the benzoyl radicals (2) and mesitoyl radicals (1), formed from the photoinitiators in their triplet state. Because benzoin (B) and 2,4,6-trimethylbenzoin (A) only differ by the radicals they produce (benzoyl (2) vs. mesitoyl (1)), an efficiency relation between 2,4,6-trimethylbenzoin (A) and mesitol (C) can be achieved by multiplying the ratio retrieved for excited benzoin (B) and mesitol (C) (144:1) with the relation between excited benzoin (B) and 2,4,6-trimethylbenzoin (A), i.e., approximately a factor of 0.5. The relation between excited 2,4,6-trimethylbenzoin (A) and mesitol (C) is therefore 72:1. This relation is now only dependent on the excited state properties of the respective photoinitiators and not on the nature of the radicals and their reaction kinetics. Assuming comparable TA values of the initially excited state and the produced radicals of 2,4,6-trimethylbenzoin (A) and mesitol (C), this relation should be revealed by ISC quantum yields, estimated from the relative amplitudes A_1 and A_3 of the fit functions collected in Table 5.2, which originate from the fits of the TA probed at 500 nm. It is thereby assumed that the quantum yield of radical formation from molecules

in their triplet state is $\Phi_R = 1$. As mentioned above, there are differences in TA depending on the probe wavelength. These differences can be ascribed to features in the excited state absorption spectra. However, in the cases of 2,4,6-trimethylbenzoin (A) and mesitil (C) these probe wavelength dependent differences are small compared to the differences between TA of 2,4,6-trimethylbenzoin (A) and mesitil (C). Because of the difference in initial TA values by a factor of 4, a convolution of the initial relaxation process of mesitil (C) with the time resolution of the experiment is assumed. This is justified by the value of the time constant as discussed above. Therefore, A_1 of mesitil (C) is multiplied by a factor of 4. The considerations result in A_3 having a relative value of 85 % with respect to A_1 in the case of 2,4,6-trimethylbenzoin (A), resulting in a quantum yield $\Phi_{ISC} = 0.85$. The same considerations result in quantum yields of $\Phi_{ISC} = 0.01$ for mesitil (C) and $\Phi_{ISC} = 0.12$ for benzoin (B). This leads to an approximated relation of 2,4,6-trimethylbenzoin (A) being more efficient than mesitil (C) by a factor of 82 or benzoin (B) being more efficient than mesitil (C) by a factor of 164. The values are in reasonably good agreement with the factor of 72 (144), derived from the steady state spectra presented herein as well as the normalized extinction coefficients discussed in the context of the PLP/ESI-MS experiments.^[42,174] It should be mentioned that due to the low TA intensities observed for mesitil (C), the neglect of any radical addition kinetics to monomers and the convolution of ISC dynamics with both the experimental time resolution and additional IC channels, the considerations made above only allow for an estimation of quantum yields and efficiency ratios with relatively large error bars (at least a factor of 2). The same holds for estimated quantum yields where additional uncertainties due to the lack of reproducible pump-probe overlaps in the experiments have to be taken into account.

5.5. Conclusions

In summary, it can be stated that the crucial steps for efficient photo-induced polymerization initiation take place in the investigated photoinitiator molecules benzoin (B), 2,4,6-trimethylbenzoin (A), and mesitil (C) within the first tens of picoseconds after excitation. The absence of dominating ultrafast radiationless deactivation channels is thereby a critical property of a molecule suitable for triplet photoinitiation. The efficiency of photoinitiation is predominantly governed by the efficiency of ISC. Care should be taken with the choice of the state to be excited, e.g., primarily the excitation wavelength, as the initiation efficiency is likely to significantly decrease if the molecule is excited into unsuitable states. Importantly, the irradiation at the highest absorption band does not correlate with the most efficient excitation and thus initiation pathway.

TA experiments with the concomitant electronic structure theory calculation prove to be a highly useful tool not only for the clarification of the underlying mechanism but in particular

for attaining a quantitative picture on the suitability of a particular photoinitiating system. The performance of the studied systems can be estimated by combining femtosecond TA spectroscopy with DFT calculations *via* a comparison of the derived efficiency relation between benzoin (B) and mesitol (C) of 164:1 with a value of 144:1 obtained by PLP/ESI-MS experiments (see Chapter 4).^[42,174] Thereby, determinations of excited singlet and triplet energies at the respective ground state minimum geometry by TDDFT, which are computationally inexpensive, prove to give sufficient information about excited state structure for estimation of ISC efficiencies preventing computationally intensive excited state surface scans. Because of large differences in extinction coefficients ($64 \text{ L mol}^{-1} \text{ cm}^{-1}$ (benzoin, B) vs. $12 \text{ L mol}^{-1} \text{ cm}^{-1}$ (2,4,6-trimethylbenzoin, A) vs. $1075 \text{ L mol}^{-1} \text{ cm}^{-1}$ (mesitol, C)) and TA intensities at the detection limit in the case of mesitol (C), the comparison of the three photoinitiators presented here can be regarded as a test case for the capability of the employed combined experimental and theoretical approach.

6

Quantifying Photoinitiation Efficiencies in a Multi-Photo-Initiated Free Radical Polymerization

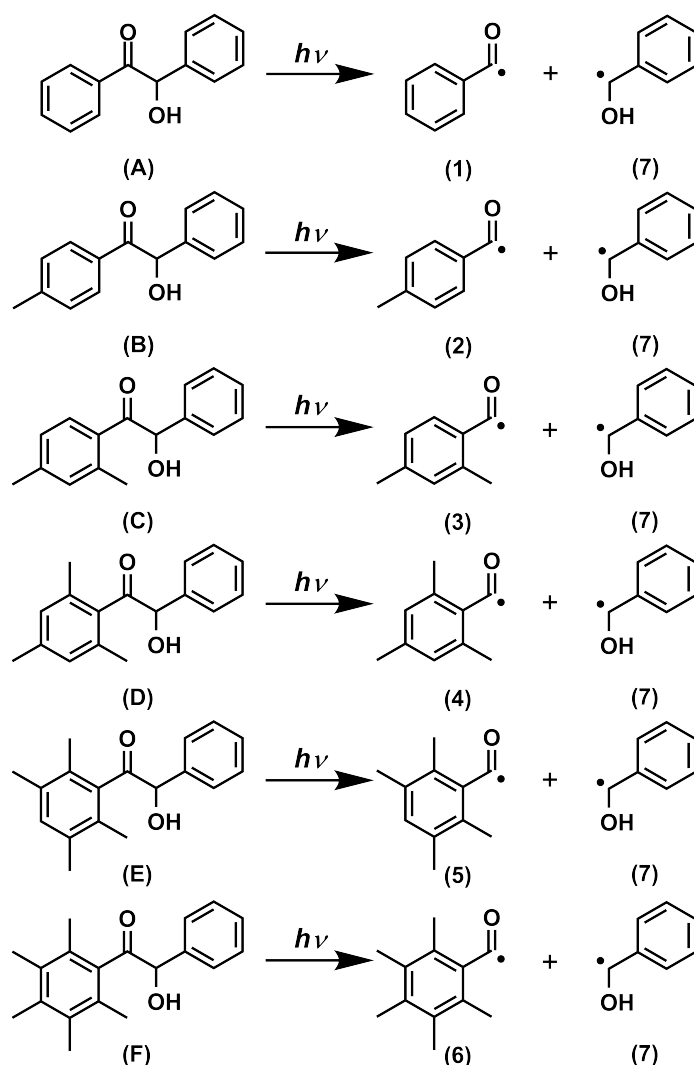
6.1. Abstract

Throughout the present thesis, online SEC/ESI-MS is employed for quantifying the overall initiation efficiencies of photolytically generated radical fragments. In a unique experiment, the current chapter presents the first quantitative and systematic study of methyl-substituted acetophenone-type photoinitiators being employed in a single cocktail to initiate the free radical polymerization of MMA in bulk. The photoinitiators are constituted of a set of two known and four new molecules, which represent an increasing number of methyl substituents on their benzoyl fragment, that is, benzoin (A), 4-methylbenzoin (B), 2,4-dimethylbenzoin (C), 2,4,6-trimethylbenzoin (D), 2,3,5,6-tetramethylbenzoin (E), and 2,3,4,5,6-pentamethylbenzoin (F). The absolute quantitative evaluation of the mass spectra shows a clear difference in the

initiation ability of the differently substituted benzoyl-type radical fragments: Increasing the number of methyl substituents leads to a decrease in incorporation of the radical fragments.

6.2. Introduction

Typically, a photo-initiated polymer consists of two components, that is, the initiating radical fragments and the monomer repeat units. Considerable information can be obtained from investigating the quantity and nature of the incorporated endgroups *via* techniques that can image these.



Scheme 6.1 Photolytic decomposition pattern of benzoin (A), 4-methylbenzoin (B), 2,4-dimethylbenzoin (C), 2,4,6-trimethylbenzoin (D), 2,3,5,6-tetramethylbenzoin (E), and 2,3,4,5,6-pentamethylbenzoin (F).

As shown in qualitative^[40,41,73] and quantitative studies (see Chapter 4)^[42,174] based upon the ability of radical fragments to initiate the free radical polymerization in bulk of various monomers, coupled online SEC/ESI-MS is the method of choice making a direct and quantitative comparison between the propensity of different radical fragments to contribute to the initiation processes.^[27,171,174] In Chapter 4, a quantitative comparison of the incorporation propensity of the benzoyl fragment (1) to the mesitoyl fragment (4) (derived from the photoinitiator molecules benzoin (A), 2,4,6-trimethylbenzoin (D), and mesitol, respectively) was given,^[42,174] always employing a cocktail of two initiators in one experiment. Encouraged by these results, the possibility of employing a cocktail of six photoinitiators in one single experiment to establish a systematic understanding of the initiation ability of the derived radicals was explored. To enable such a single cocktail experiment, the photoinitiators have to be carefully designed so that the associated mass spectrometric peaks of the derived endgroups do not overlap and allow for a quantitative evaluation of the data. The systematic substitution of the benzoyl fragment (1) in acetophenone-type initiators is an ideal platform for such experiments. As noted above, in earlier studies (see Chapter 4), the incorporation propensity of the benzoyl (1) vs. the mesitoyl fragment (4) as a function of their origin was compared.^[174] In here, the benzoyl fragment (1) is systematically substituted with an increasing number of methyl units, thus rendering mass spectra with non-overlapping signals separated by 14 Da (methyl group minus one proton of the aromatic ring). The outcome of such a single six-membered cocktail experiment is a quantitative order of the incorporation ability of the six individual benzoyl-type fragments ((1)-(6)). The experiments carried out thus describe the first systematic study of six acetophenone-type photoinitiators, that is, benzoin (2-hydroxy-1,2-diphenylethanone, A), 4-methylbenzoin (2-hydroxy-2-phenyl-1-*p*-tolylethanone, B), 2,4-dimethylbenzoin (1-(2,4-dimethylphenyl)-2-hydroxy-2-phenylethanone, C), 2,4,6-trimethylbenzoin (2-hydroxy-1-mesityl-2-phenylethanone, D), 2,3,5,6-tetramethylbenzoin (2-hydroxy-2-phenyl-1-(2,3,5,6-tetramethylphenyl)ethanone, E), and 2,3,4,5,6-pentamethylbenzoin (2-hydroxy-1-(2,3,4,5,6-pentamethylphenyl)-2-phenylethanone, F) depicted in Scheme 6.1. Five of these photoinitiators are successively substituted with methyl groups; compounds (B), (C), (E), and (F) were especially synthesized for the current study. Scheme 6.1 depicts the employed photoinitiators as well as their photolytic decomposition pattern.

6.3. Experimental Part

6.3.1. Synthesis of the Photoinitiators

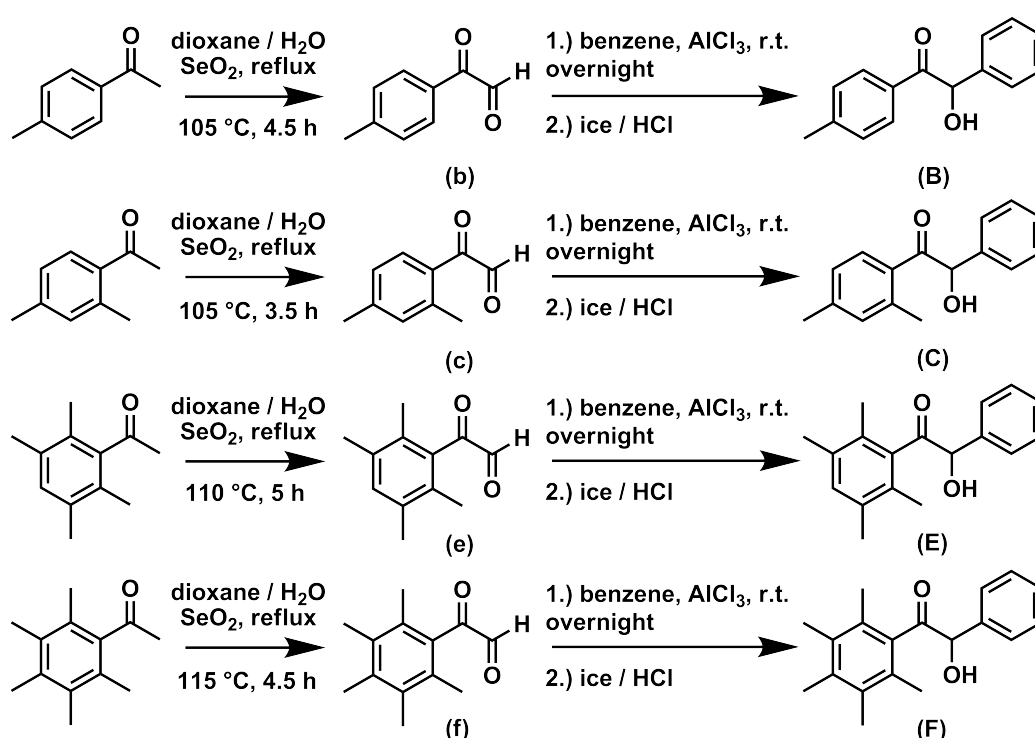
**Synthesis of the Glyoxals 2-Oxo-2-*p*-tolylacetaldehyde (b),
2-(2,4-Dimethylphenyl)-2-oxoacet-aldehyde (c),
2-Oxo-2-(2,3,5,6-tetramethylphenyl)acetaldehyde (e), and
2-Oxo-2-(2,3,4,5,6-pentamethylphenyl)acetaldehyde (f)**

The following preparation procedure of the glyoxals is adapted from the literature.^[170] The order in which the data is presented refers to the different products b, c, e, and f. A solution of 3.53 g/ 3.74 g/ 2.96 g/ 2.92 g selenium dioxide (31.8 mmol, 1.00 eq/ 33.7 mmol, 1.00 eq/ 26.7 mmol, 1.00 eq/ 26.3 mmol, 1.00 eq), 1 mL/ 1.1 mL/ 1.2 mL/ 1.2 mL of water and 4.27 g 4-methylacetophenone/ 5.00 g 2,4-dimethylacetophenone/ 4.70 g 2,3,5,6-tetramethylacetophenone/ 5.00 g 2,3,4,5,6-pentamethylacetophenone (4.20 mL, 31.8 mmol, 1.00 eq/ 5.05 mL, 33.7 mmol, 1.00 eq/ 26.7 mmol, 1.00 eq/ 26.3 mmol, 1.00 eq) in 32 mL/ 35 mL/ 33 mL/ 33 mL of dioxane was refluxed for 4.5 h at 105 °C/ 3.5 h at 105 °C/ 5 h at 110 °C/ 4.5 h at 115 °C under vigorous stirring. During the heating of the solution a gradual precipitation of selenium occurs and the colour changes from colourless to yellow. The solution was decanted from the free selenium and the dioxane was evaporated under reduced pressure. The crude yellow products were purified *via* vacuum distillation. The products were collected as clear yellow oils, which crystallized upon cooling. (Yield: 3.04 g, 20.5 mmol, 71 %/ 3.10 g, 19.1 mmol, 62 %/ 3.26 g, 17.1 mmol, 69 %/ 1.75 g, 8.57 mmol, 35 %). For more details see Scheme 6.2 and Chapter 9.3.

**Synthesis of 2-Hydroxy-2-phenyl-1-*p*-tolylethanone (4-methylbenzoin, B),
1-(2,4-Dimethylphenyl)-2-hydroxy-2-phenylethanone (2,4-dimethylbenzoin, C),
2-Hydroxy-2-phenyl-1-(2,3,5,6-tetramethylphenyl)ethanone
(2,3,5,6-tetramethylbenzoin, E), and
2-Hydroxy-1-(2,3,4,5,6-pentamethylphenyl)-2-phenylethanone
(2,3,4,5,6-pentamethylbenzoin, F)**

The following preparation procedure of the substituted benzoin is adapted from the literature.^[168,169] The order in which the data is presented refers to the different products B, C, E, F (structures shown in Scheme 6.1). To a suspension of 5.47 g/ 5.09 g/ 4.32 g/ 2.04 g anhydrous aluminium chloride (41.0 mmol, 2.00 eq/ 38.2 mmol, 2.00 eq/ 32.4 mmol, 2.00 eq/ 15.4 mmol, 2.00 eq) in 15 mL/ 7.5 mL/ 15 mL/ 7 mL dry benzene at 10 °C, 3.04 g 2-oxo-2-*p*-tolylacetaldehyde (b)/ 3.10 g 2-(2,4-dimethylphenyl)-2-oxoacetaldehyde (c)/ 3.08 g 2-oxo-2-(2,3,5,6-tetramethyl-phenyl)acetaldehyde (e)/ 1.57 g 2-oxo-2-(2,3,4,5,6-pentamethylphenyl)-acetaldehyde (f) (20.5 mmol, 1.00 eq/ 19.1 mmol, 1.00 eq/ 16.2 mmol, 1.00 eq/ 7.69 mmol, 1.00 eq) dissolved in 15 mL/ 7.5 mL/ 15 mL/ 7 mL of dry benzene

were added. The reaction was then vigorously stirred over a period of 2 h at 10 °C (cooled with ice). Stirring was continued over night at ambient temperature. The reaction mixture was subsequently poured onto ice and concentrated hydrochloric acid. The organic layer was removed and the aqueous layer was extracted twice with a minimal amount of benzene. The combined organic layers were dried over MgSO_4 and benzene was evaporated under reduced pressure. The crude, pale, yellowish solid was recrystallized from ethanol to give 4-methylbenzoin (B)/ 2,4-dimethylbenzoin (C)/ 2,3,5,6-tetramethylbenzoin (E)/ 2,3,4,5,6-pentamethylbenzoin (F) as a white powder. Yield: 1.92 g, 8.49 mmol, 63 %/ 0.34 g, 1.43 mmol, 11 %/ 2.39 g, 8.91 mmol, 78 %/ 0.93 g, 3.31 mmol, 59 %. For more details see Scheme 6.2 and Chapter 9.3.



Scheme 6.2 Synthesis of 4-methylbenzoin (B), 2,4-dimethylbenzoin (C), 2,3,5,6-tetramethylbenzoin (E), and 2,3,4,5,6-pentamethylbenzoin (F).

Analytical Data for 4-Methylbenzoin (B)

^1H NMR (400 MHz, CDCl_3); [δ , ppm]: 7.81 (d, $^3J = 8.3$ Hz, 2H, $-\text{H}_{\text{arom},2}$), 7.35-7.22 (m, 5H, $-\text{H}_{\text{ph}}$), 7.18 (d, $^3J = 8.0$ Hz, 2H, $\text{H}_{\text{arom},1}$), 5.92 (s, 1H, H_{tert}), 4.61 (bs, 1H, $-\text{OH}$), 2.34 (s, 3H, $-\text{CH}_3$). ^{13}C NMR (100 MHz, CDCl_3); [δ , ppm]: 198.48 (C_1), 145.02 (C_2), 139.33 (C_3), 130.93 (C_4), 129.41 (C_5), 129.30 (C_6), 129.09 (C_7), 128.50 (C_8), 127.77 (C_9), 76.05 (C_{10}), 21.73 (C_{11}). ESI-MS: $[\text{M}+\text{Na}]_{\text{exp.}} = 249.08$ Da and $[\text{M}+\text{Na}]_{\text{calc.}} = 249.09$ Da. Anal. calcd. for $\text{C}_{15}\text{H}_{14}\text{O}_2$: C 79.62, H 6.24, O 14.14; found: C 80.00, H 6.38, O 14.41. For more details see Figure 6.1.

Analytical Data for 2,4-Dimethylbenzoin (C)

^1H NMR (400 MHz, CDCl_3); [δ , ppm]: 7.51 (d, $^3J = 7.7$ Hz, 1H, $-\text{H}_{\text{arom.2}}$), 7.34-7.16 (m, 5H, $-\text{H}_{\text{ph.}}$), 7.06-6.95 (m, 2H, $-\text{H}_{\text{arom.1}}$), 5.89 (d, $^3J = 5.9$ Hz, 1H, $-\text{H}_{\text{tert.}}$), 4.65 (d, $^3J = 5.9$ Hz, 1H, $-\text{OH}$), 2.32 (s, 3H, $-\text{CH}_3$), 2.29 (s, 3H, $-\text{CH}_3$). ^{13}C NMR (100 MHz, CDCl_3); [δ , ppm]: 201.50 (C_1), 142.81 (C_2), 139.57 (C_3), 138.62 (C_4), 132.83 (C_5), 131.48 (C_6), 129.11 (C_7), 128.79 (C_8), 128.21 (C_9), 127.34 (C_{10}), 126.20 (C_{11}), 77.04 (C_{12}), 21.43 (C_{13}), 20.94 (C_{14}). ESI-MS: $[\text{M}+\text{Na}]_{\text{exp.}} = 263.08$ Da and $[\text{M}+\text{Na}]_{\text{calc.}} = 263.10$ Da. Anal. calcd. for $\text{C}_{16}\text{H}_{16}\text{O}_2$: C 79.97, H 6.71, O 13.32; found: C 79.02, H 6.85, O 13.77. For more details see Figure 6.2.

Synthesis Procedure and Analytical Data for 2,4,6-Trimethylbenzoin (D)

The following preparation procedure of 2,4,6-trimethylbenzoin (D) is adapted from the literature.^[169,170,174] Anal. calcd. for $\text{C}_{17}\text{H}_{18}\text{O}_2$: C 80.28, H 7.13, O 12.58; found: C 80.39, H 7.29, O 12.72. For more details see Chapter 4.3.2.

Analytical Data for 2,3,5,6-Tetramethylbenzoin (E)

^1H NMR (400 MHz, CDCl_3); [δ , ppm]: 7.24-7.17 (m, 3H, $-\text{H}_{\text{ph.2}}$), 7.12-7.03 (m, 2H, $-\text{H}_{\text{ph.1}}$), 6.96 (s, 1H, $-\text{H}_{\text{arom.}}$), 5.52 (s, 1H, $-\text{H}_{\text{tert.}}$), 4.51 (bs, 1H, $-\text{OH}$), 2.48-0.59 (m, 12H, $4 \times -\text{CH}_3$). ^{13}C NMR (100 MHz, CDCl_3); [δ , ppm]: 209.29 (C_1), 137.57 (C_2), 136.47 (C_3), 134.16 (C_4), 132.69 (C_5), 129.69 (C_6), 128.18 (C_7), 128.15 (C_8), 126.87 (C_9), 81.05 (C_{10}), 19.38 (C_{11}), 15.98 (C_{12}). ESI-MS: $[\text{M}+\text{Na}]_{\text{exp.}} = 291.08$ Da and $[\text{M}+\text{Na}]_{\text{calc.}} = 291.14$ Da. Anal. calcd. for $\text{C}_{18}\text{H}_{20}\text{O}_2$: C 80.56, H 7.51, O 11.92; found: C 80.48, H 7.66, O 12.23. For more details see Figure 6.3.

Analytical Data for 2,3,4,5,6-Pentamethylbenzoin (F)

^1H NMR (400 MHz, CDCl_3); [δ , ppm]: 7.17-7.09 (m, 3H, $-\text{H}_{\text{ph.2}}$), 7.04-6.98 (m, 2H, $-\text{H}_{\text{ph.1}}$), 5.43 (s, 1H, $-\text{H}_{\text{tert.}}$), 4.45 (bs, 1H, $-\text{OH}$), 2.31-0.63 (m, 15H, $5 \times -\text{CH}_3$). ^{13}C NMR (100 MHz, CDCl_3); [δ , ppm]: 209.65 (C_1), 136.61 (C_2), 135.39 (C_3), 132.86 (C_4), 128.85 (C_5), 126.90 (C_6 , C_9), 128.17 (C_7), 128.07 (C_8), 81.20 (C_{10}), 17.20 (C_{11}), 16.81 (C_{12}), 15.88 (C_{13}). ESI-MS: $[\text{M}+\text{Na}]_{\text{exp.}} = 305.17$ Da and $[\text{M}+\text{Na}]_{\text{calc.}} = 305.15$ Da. Anal. calcd. for $\text{C}_{19}\text{H}_{22}\text{O}_2$: C 80.82, H 7.85, O 11.33; found: C 80.35, H 8.02, O 11.59. For more details see Figure 6.4.

6.3.2. UV/Vis Measurements

For details see Chapter 4.3.4 and Chapter 9.3.

6.3.3. NMR Measurements

For details see Chapter 4.3.5 and Chapter 9.3.

6.3.4. Elemental Analysis

The elemental composition of the photoinitiators (B, C, D, E, F) was analyzed using an automatic elemental analyzer Flash EA 1112 from Thermo Scientific, which was equipped with a MAS 200R auto sampler. The calibration standards methionine, and 2,5-bis-5-*tert*-butyl-2-benzoxazolylthiophene (BBOT), and vanadium pentoxide, tin capsules, and silver containers were purchased from IVA Analysentechnik e. K., Germany. Helium 5.0 for the GC-TCD analysis was purchased from Linde, Germany.

6.3.5. Pulsed Laser Polymerization (PLP) Procedure

All samples consisted of MMA (sample volume ~ 0.5 mL) with the respective photoinitiator or a mixture of the six photoinitiators (all in a 1:1 molar ratio to each other) with an overall concentration of $c_{PI,0} = 5 \times 10^{-3}$ mol L⁻¹. For more details see Chapter 4.3.3 and Chapter 9.3.

6.3.6. SEC/ESI-MS Measurements

The samples were measured at a capillary temperature of 300 °C, for more details see Chapter 4.3.6 and Chapter 9.3.

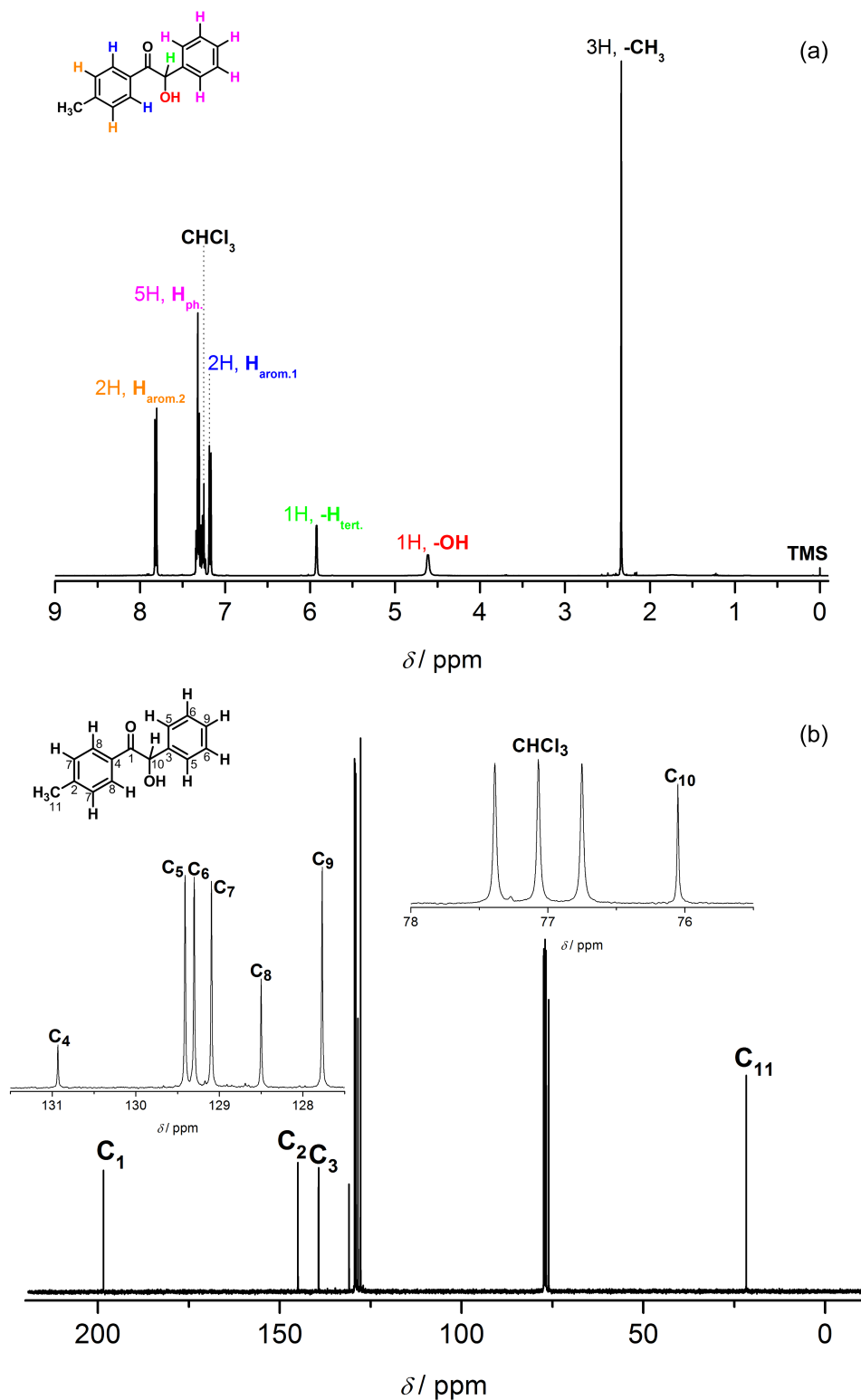


Figure 6.1. (a) 400 MHz ^1H NMR spectrum of 4-methylbenzoic acid (B), (b) 100 MHz ^{13}C NMR spectrum of 4-methylbenzoic acid (B). For more details see Chapter 6.3.1.

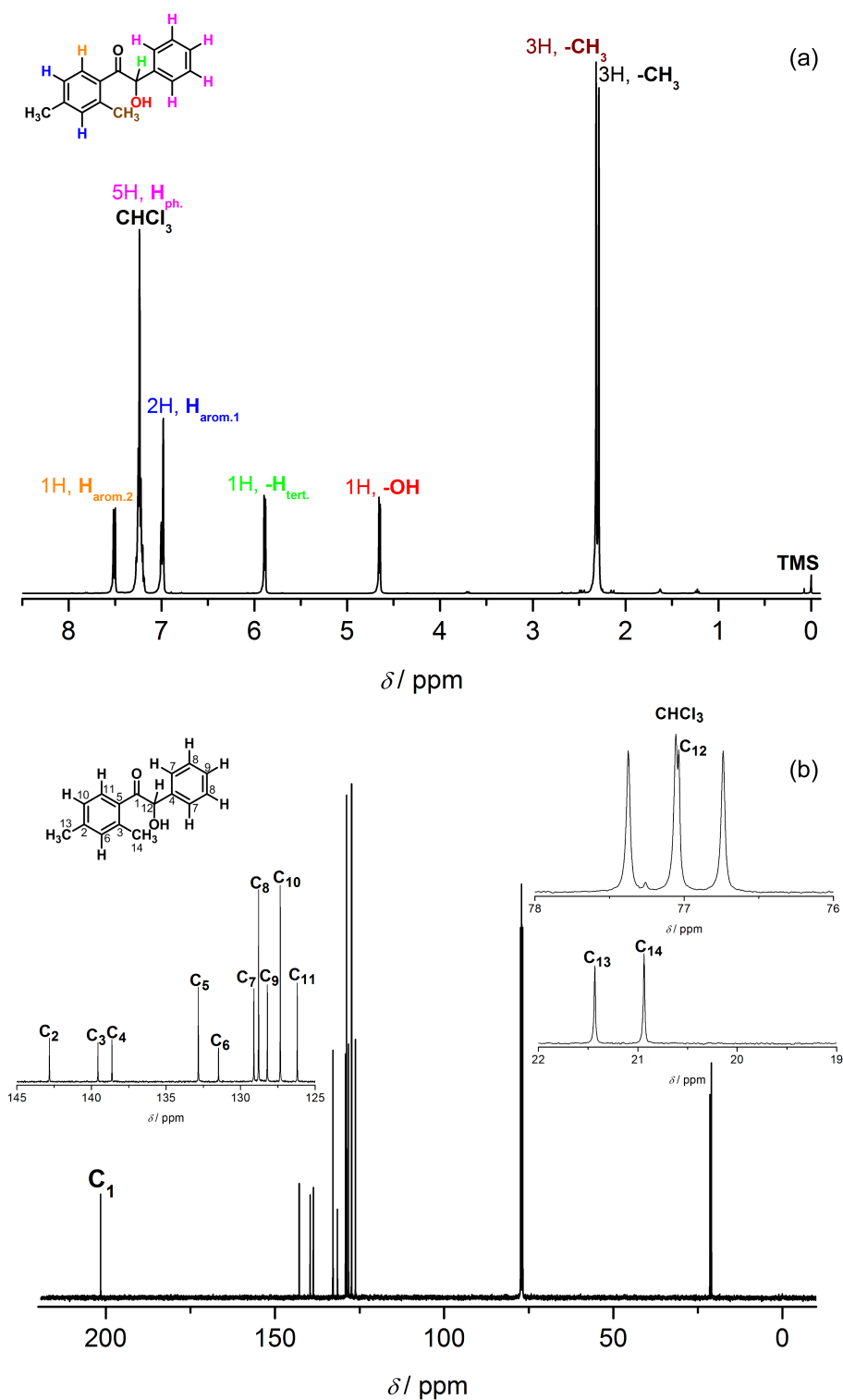


Figure 6.2. (a) 400 MHz ¹H NMR spectrum of 2,4-dimethylbenzoic acid (C), (b) 100 MHz ¹³C NMR spectrum of 2,4-dimethylbenzoic acid (C). For more details see Chapter 6.3.1.

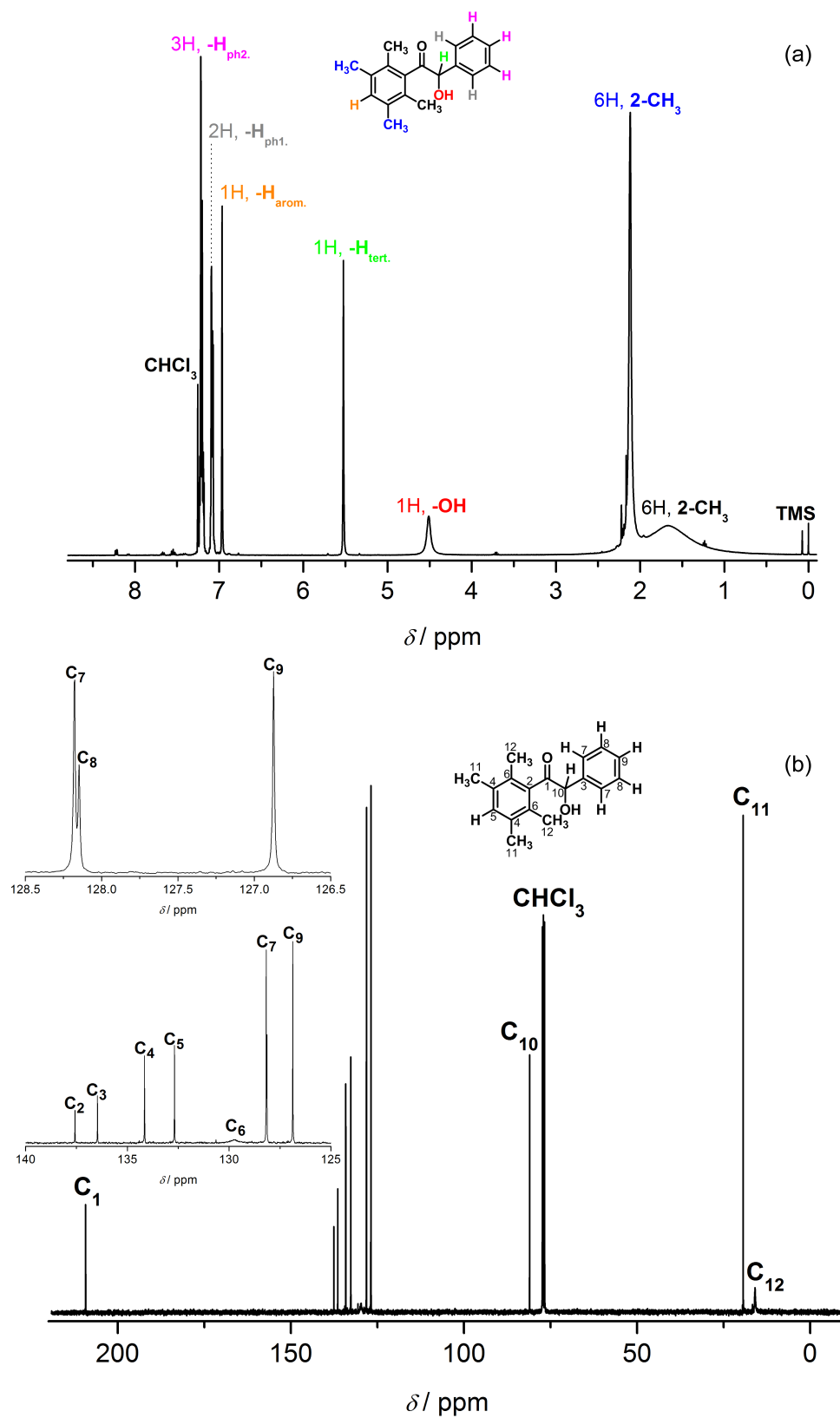


Figure 6.3. (a) 400 MHz ^1H NMR spectrum of 2,3,5,6-tetramethylbenzoic acid (E), (b) 100 MHz ^{13}C NMR spectrum of 2,3,5,6-tetramethylbenzoic acid (E). For more details see Chapter 6.3.1.

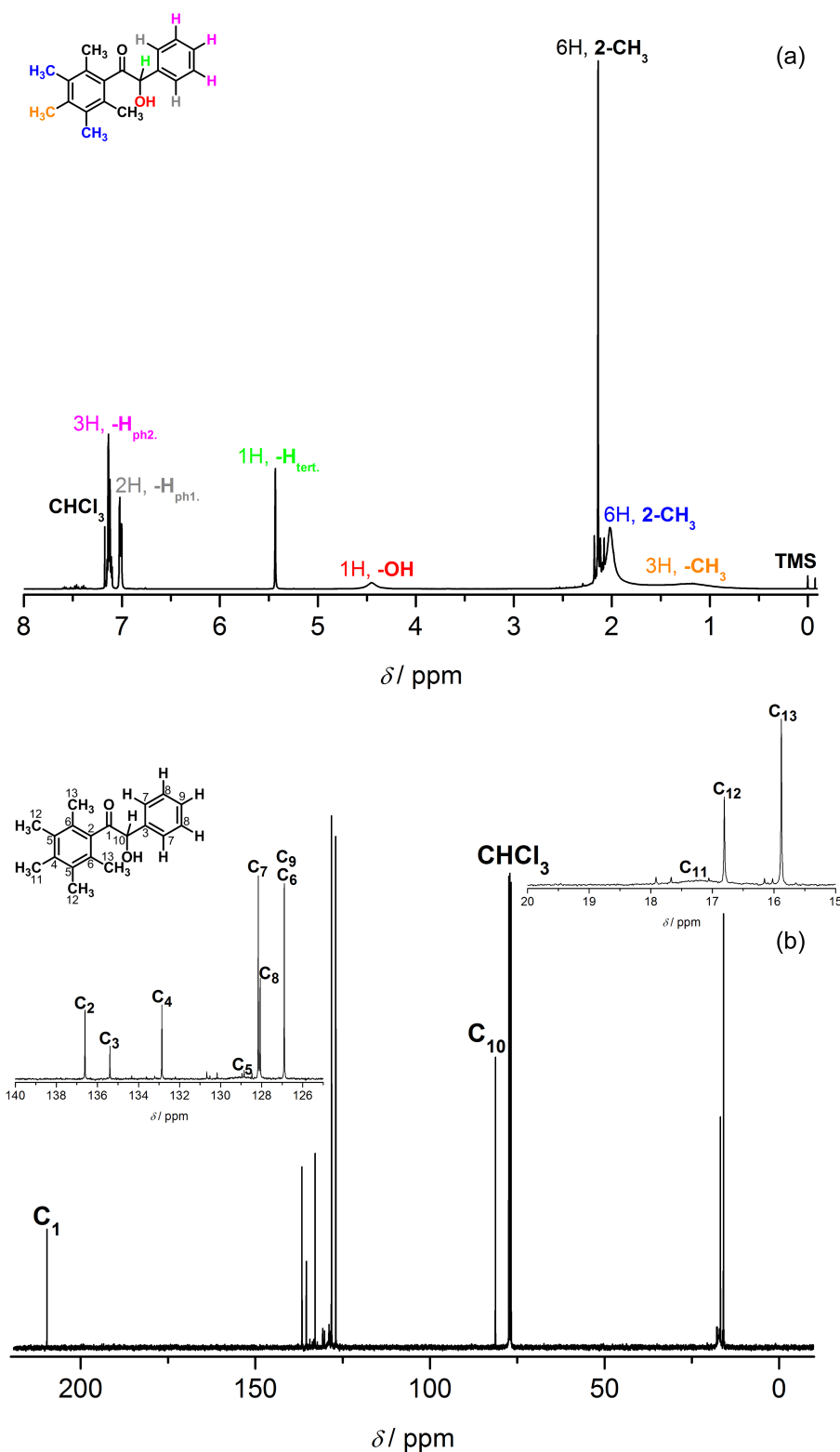
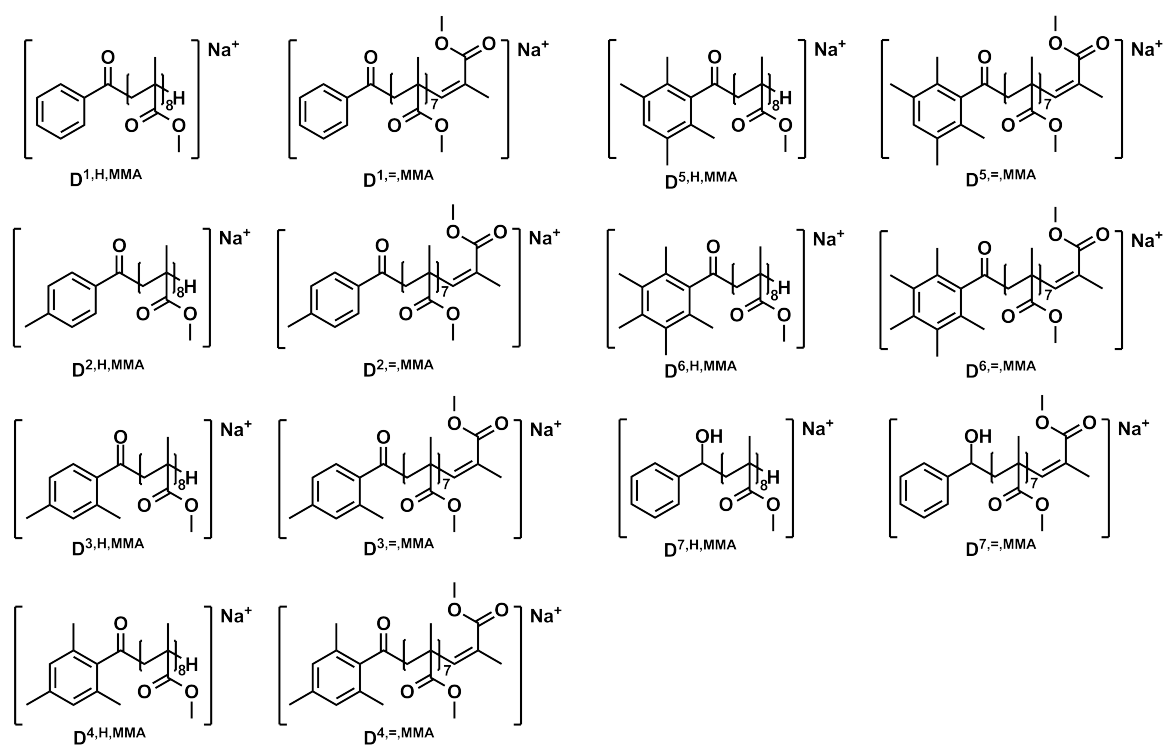


Figure 6.4. (a) 400 MHz ^1H NMR spectrum of 2,3,4,5,6-pentamethylbenzoic acid (F), (b) 100 MHz ^{13}C NMR spectrum of 2,3,4,5,6-pentamethylbenzoic acid (F). For more details see Chapter 6.3.1.

6.4. Results and Discussion

As described in Chapter 4, benzoin (A) and 2,4,6-trimethylbenzoin (D) have shown a different overall initiation ability of the respective benzoyl (1) and mesityl radical (4).^[174] For a systematic study of methyl-substituted benzoin (A, B, C, D, E, F, see Scheme 6.1) it is necessary to design novel photoinitiators containing a variable number of methyl groups. Details of the synthetic procedures can be found in the Experimental Part 6.3.^[168–170] By employing six photoinitiators with a variable non-identical number of methyl substituents in a free radical PLP of MMA in bulk, the resulting pMMA features in each repeat unit six disproportionation patterns, with the difference in mass between each disproportionation pattern being 14 Da.



Scheme 6.3 Expected ionized disproportionation products of degree of polymerization 8 in the photochemically-initiated free radical polymerization of MMA in bulk in the presence of an equimolar cocktail of all six photoinitiators depicted in Scheme 6.1. Note that the position of the double bond in the unsaturated disproportionation product may also be at the site of the former α -methyl group. See Table 6.1 for a collation of the m/z -ratios of the individual radical fragments. Furthermore, the combination products are not of interest, but are mentioned because of completeness of assignment in Figure 6.7.

Within the current study, all assigned signals obtained in ESI-MS mass spectra were labeled according to the following nomenclature: Disproportionation peaks occur in pairs separated by 2 Da from each other. Thus, each peak is labeled with $D^{v,=,MMA}$ or $D^{v,H,MMA}$ where v denotes the radical fragment that has initiated the polymerization ((1), (2), (3),

(4), (5), (6) or (7), see Scheme 6.1). Combination products (labeled with $C^{v,w,MMA}$, where v and w denote the radical fragment as endgroup (see Scheme 6.1)) are mentioned for the sake of completeness of the assignments and can be found in (Figure 6.7 and Scheme A.3 - Scheme A.6 in the Appendix), yet they are of limited use in the present study as it is not possible to differentiate whether they have been generated by initiation or termination of the macromolecular growth. Scheme 6.3 depicts all expected ionized disproportionation products of degree of polymerization 8 originating from the employed photoinitiators. It has to be noted that it is not possible to evaluate $D^{7,=,MMA}$ quantitatively, because of the isobaric overlap with $D^{1,H,MMA}$.

Table 6.1. Collation of the polymeric disproportionation product signals observed during SEC/ESI-MS of pMMA samples generated during the multi-photo-initiated free radical PLP of MMA in bulk at 100 Hz, $-5\text{ }^{\circ}\text{C}$ and a laser energy of $\sim 0.35\text{ mJ/pulse}$ with a mixture of all photoinitiators mentioned in Scheme 6.1. The table provides the experimentally observed as well as the theoretically expected m/z -ratios for the found disproportionation (D) products (consisting of 8 monomer units). The structures corresponding to the individual products are depicted in Scheme 6.3. The tabulated values correspond to the peaks displayed in Figure 6.5 and Figure 6.6.

Species	Ionization	$(m/z)_{\text{theo.}}$ / Da	$(m/z)_{\text{exp.}}$ / Da	$\Delta(m/z)$ / Da
D ^{1,H,MMA}	Na ⁺	929.4	929.7	0.3
D ^{1,=,MMA}	Na ⁺	927.4	927.6	0.2
D ^{2,H,MMA}	Na ⁺	943.5	943.7	0.2
D ^{2,=,MMA}	Na ⁺	941.4	941.7	0.3
D ^{3,H,MMA}	Na ⁺	957.5	957.7	0.2
D ^{3,=,MMA}	Na ⁺	955.5	955.7	0.2
D ^{4,H,MMA}	Na ⁺	971.5	971.7	0.2
D ^{4,=,MMA}	Na ⁺	969.5	969.7	0.2
D ^{5,H,MMA}	Na ⁺	985.5	985.7	0.2
D ^{5,=,MMA}	Na ⁺	983.5	983.7	0.2
D ^{6,H,MMA}	Na ⁺	999.5	999.7	0.2
D ^{6,=,MMA}	Na ⁺	997.5	997.7	0.2
D ^{7,H,MMA}	Na ⁺	931.5	931.7	0.2
D ^{7,=,MMA}	Na ⁺	929.4	929.7	0.3

6.4.1. SEC/ESI-MS of Multi-Photo-Initiated pMMA

After successfully synthesizing the four novel photoinitiators ((B), (C), (E), and (F)), it had to be – prior to the single cocktail experiment – established whether they are on their own able to initiate the free radical PLP of MMA in bulk.

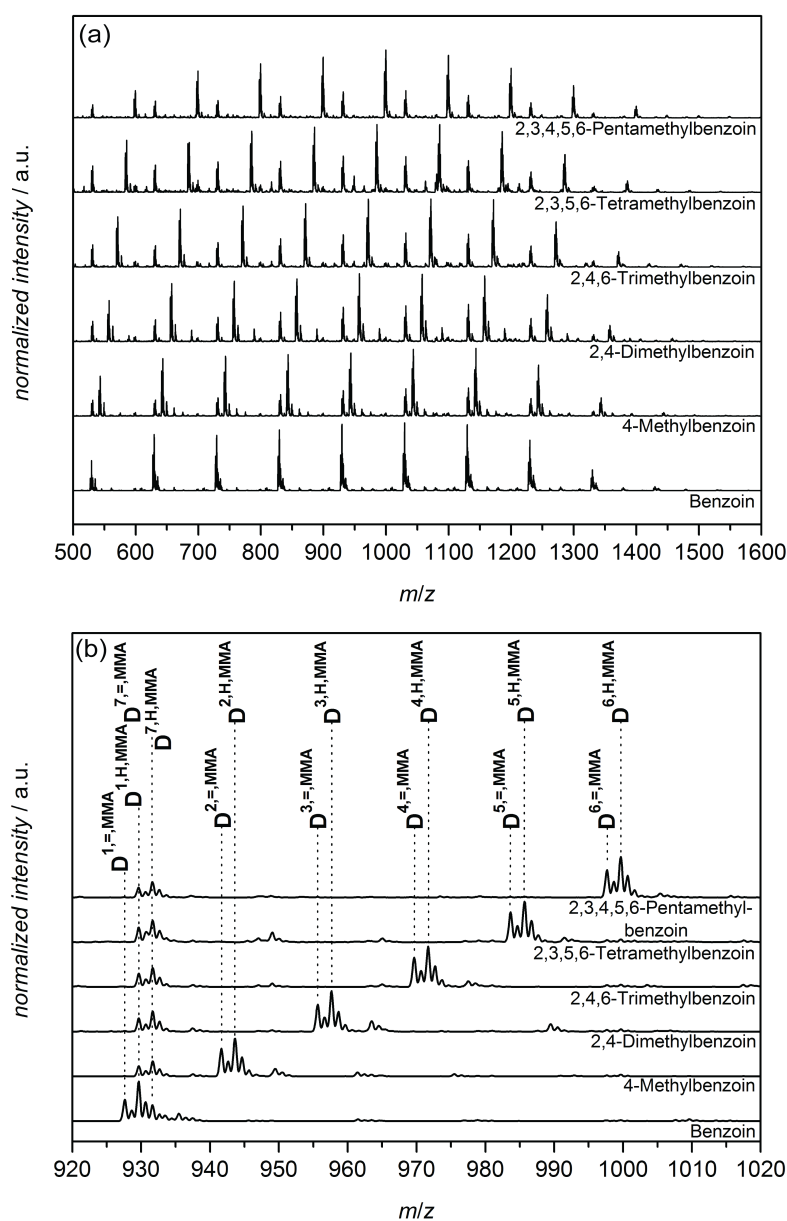


Figure 6.5. (a) SEC/ESI-MS overview spectra of polymeric material obtained from (A)-, (B)-, (C)-, (D)-, (E)-, (F)- initiated pMMA synthesized *via* PLP of MMA_{bulk} at ~ 0.35 mJ/pulse laser energy, 100 Hz, -5 °C and $c_{PI,0} = 5 \times 10^{-3}$ mol L⁻¹. The figure depicts the singly charged products ionized with sodium iodide at a retention time between 16.84-18.36 min. (b) Zoom of one repeat unit of the SEC/ESI-MS overview spectra of polymeric material obtained from (A)-, (B)-, (C)-, (D)-, (E)-, (F)- initiated pMMA synthesized *via* PLP of MMA_{bulk} at ~ 0.35 mJ/pulse laser energy, 100 Hz, -5 °C and $c_{PI,0} = 5 \times 10^{-3}$ mol L⁻¹. For the m/z -ratios of the assigned products see Table 6.1.

For this purpose, each photoinitiator was tested separately in preliminary polymerizations. Figure 6.5a depicts the singly charged region of the overview spectra of each polymeric material polymerized with the above-mentioned photoinitiators. An inspection of the respective repeat units in Figure 6.5b indicates that all photoinitiators initiate the polymerization very well. Furthermore, it shows that – as expected – mainly disproportionation products are formed ($D^{1,=,MMA}$, $D^{1,H,MMA}$ to $D^{7,=,MMA}$, $D^{7,H,MMA}$; see Scheme 6.3) at the employed conditions ($c_{PI} = 5 \times 10^{-3} \text{ mol L}^{-1}$, $\nu = 100 \text{ Hz}$, $T = -5 \text{ }^\circ\text{C}$, laser energy of $\sim 0.35 \text{ mJ/pulse}$).^[174] In addition, clean and by-product free mass spectra of each polymeric material synthesized with the new initiators (B), (C), (E), and (F) are obtained. As mentioned above, the difference in mass of each disproportionation pattern is 14 Da, which is the key characteristic for quantifying the initiation ability of the radical fragments (1), (2), (3), (4), (5), and (6) (Scheme 6.1), as only one polymerization is necessary to achieve quantitative initiation results of all employed initiators. A free radical polymerization of MMA in bulk in the presence of a mixture of all six photoinitiators ((A)-(F), see Scheme 6.1) – all in a 1:1 ratio to each other – leads to a multi-photo-initiated pMMA sample. Figure 6.6a shows the singly charged overview mass spectrum of the multi-photo-initiated pMMA and Figure 6.6b depicts one repeat unit of the same polymeric material. Clearly, an inspection of the repeat unit in Figure 6.6b demonstrates that the peak intensities of the disproportionation products ($D^{1,=,MMA}$ to $D^{6,=,MMA}$) are not equal: A qualitative inspection suggests that an increasing number of methyl groups leads to a decrease in initiation ability of the different radical fragments toward MMA (whereby the analysis assumes that there is no ionization bias according to the different endgroups; see ref. 174). Figure 6.5 and Figure 6.6 only display the assignment of the disproportionation products, the assignment of the combination signals as well as their respective structures can be found in Figure 6.7, Table 6.2, and Scheme A.3 - Scheme A.6 in the Appendix.

6.4.2. Quantifying the Initiation Ability in a Multi-Photo-Initiated Polymerization

For quantifying the initiation ability, the unsaturated disproportionation products were evaluated in each singly charged repeat unit. Table 6.1 contains the corresponding experimentally observed as well as theoretically expected m/z -ratios of the identified disproportionation products in one repeat unit. The total ratio of the intensity of each disproportionation signal itself ($D^{v,=,MMA}$) in all singly charged repeat units of the SEC/ESI-MS overview spectrum (9 repeat units in sum) of the multi-photo-initiated pMMA sample (Figure 6.6) in comparison to all disproportionation signals ($D^{1,=,MMA}$ to $D^{6,=,MMA}$) was calculated and multiplied by 100 % (Eq. 6.1) to achieve the absolute initiation ability percentage of the substituted benzoyl-type fragments ((1) - (6)). For a detailed description of the procedure

for arriving at quantitative peak integration values *via* SEC/ESI-MS, the reader is referred to Chapter 4.4.3. [174]

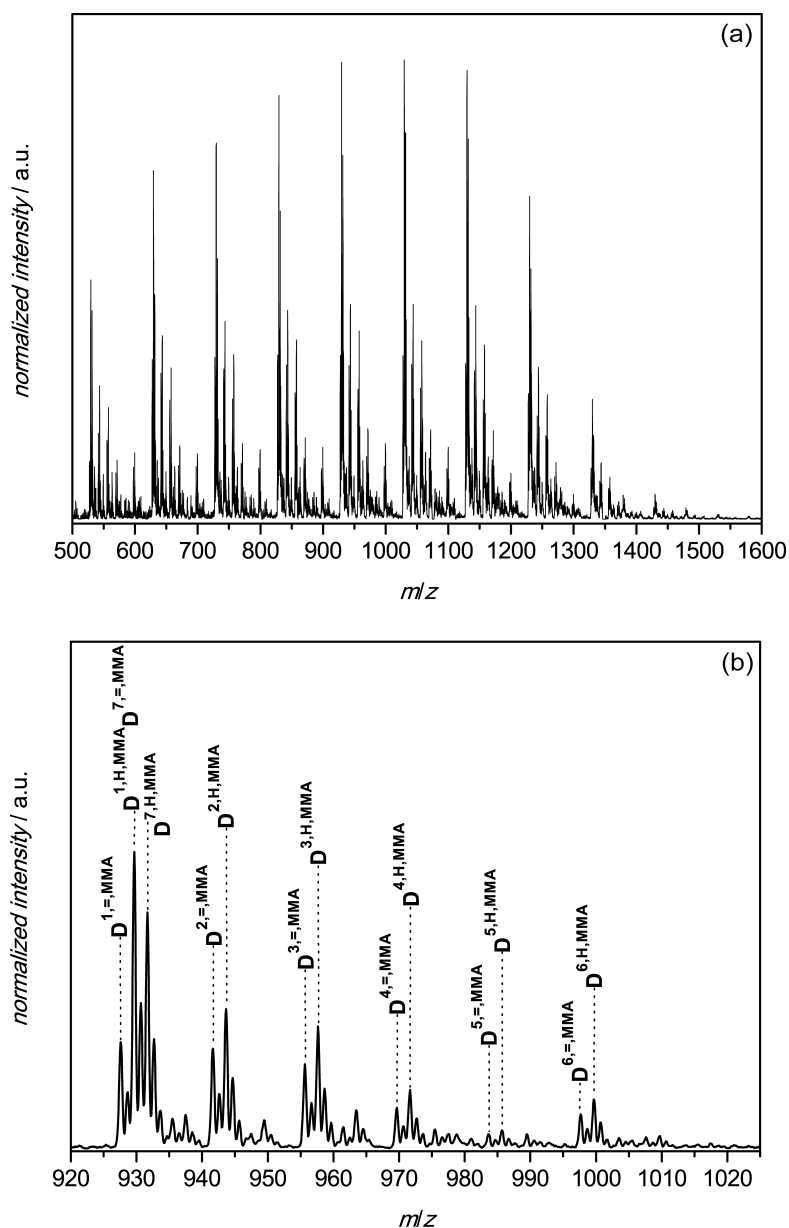


Figure 6.6. (a) SEC/ESI-MS overview spectra of pMMA obtained from an initiator cocktail mixture of all six photoinitiators depicted in Scheme 6.1 ($c_{PI,0} = 5 \times 10^{-3} \text{ mol L}^{-1}$, ratio 1:1:1:1:1:1) synthesized *via* a multi-photo-initiated PLP of MMA_{bulk} at $\sim 0.35 \text{ mJ/pulse}$ laser energy, 100 Hz and -5°C . The figure depicts the singly charged products ionized with sodium iodide at a retention time between 16.84–18.36 min. (b) Zoom of one repeat unit of the SEC/ESI-MS overview spectra of pMMA obtained from an initiator cocktail mixture of all six photoinitiators depicted in Scheme 6.1 ($c_{PI,0} = 5 \times 10^{-3} \text{ mol L}^{-1}$, ratio 1:1:1:1:1:1) synthesized *via* a multi-photo-initiated PLP of MMA_{bulk} at $\sim 0.35 \text{ mJ/pulse}$ laser energy, 100 Hz and -5°C . For the m/z -ratios of the assigned products see Table 6.1.

$$D^{v,=,MMA}_{\text{abs.}} = \left(\frac{D^{v,=,MMA}}{\sum_{n=1}^6 D^{v,=,MMA}} \right) \cdot 100 \% \quad (6.1)$$

The final values for the absolute incorporation propensities (or net/overall initiation abilities) of the individual radical fragments toward MMA are 28.2 % for (1), 26.6 % for (2), 22.0 % for (3), 10.7 % for (4), 3.9 % for (5), and 8.6 % for (6). This implies that 28.2 % of all unsaturated disproportionation products were initiated with fragment (1), 26.6 % with fragment (2), 22.0 % with fragment (3), 10.7 % with fragment (4), 3.9 % with fragment (5), and 8.6 % with fragment (6). These results support the earlier hypothesis that the number of methyl substituents has a marked influence on the initiation ability of the benzoyl-type radical fragments toward MMA.^[174] The unsubstituted benzoyl radical fragment (1) – and therefore benzoin (A) – leads to the highest incorporation ability. Somewhat surprising, fragment (5) featuring four methyl groups appears to have a less efficient overall initiation ability than fragment (6) with five methyl groups.

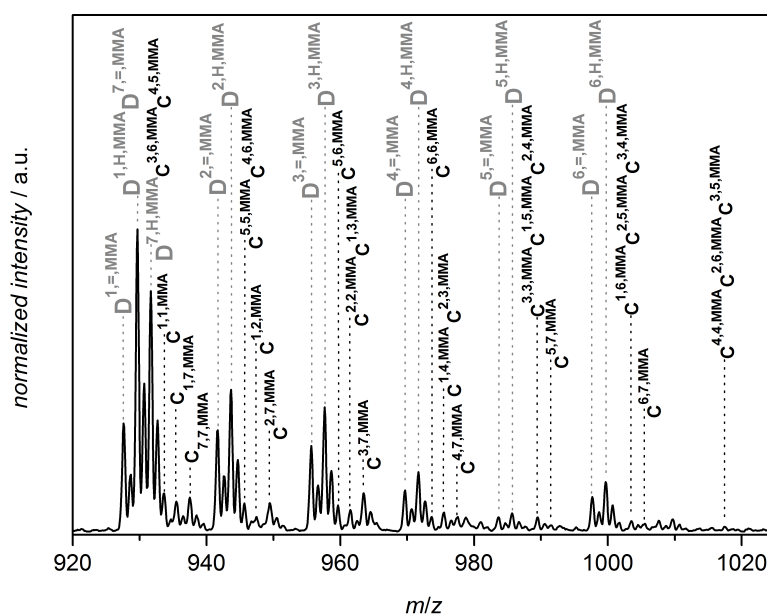


Figure 6.7. Expected polymeric disproportionation (D) and combination (C) products in the photochemically-initiated free radical polymerization of MMA performed in bulk in the presence of a cocktail of all six photoinitiators depicted in Scheme 6.1. For the m/z -ratios of the assigned products see Table 6.2. The structures for all combination products are shown in Scheme A.3 - Scheme A.6 in the Appendix.

6.4.3. UV-Spectra of the Employed Photoinitiators

In Chapter 4,^[174] the term *net-initiation efficiency* was defined, which is employed to denote the propensity of a radical to commence macromolecular growth from the point of

the laser pulse hitting the source molecule. It thus summarizes a true initiator efficiency (*net-efficiency*), including all effects from the ability of the initiator to absorb light to the reactivity of the radical toward the monomer units.

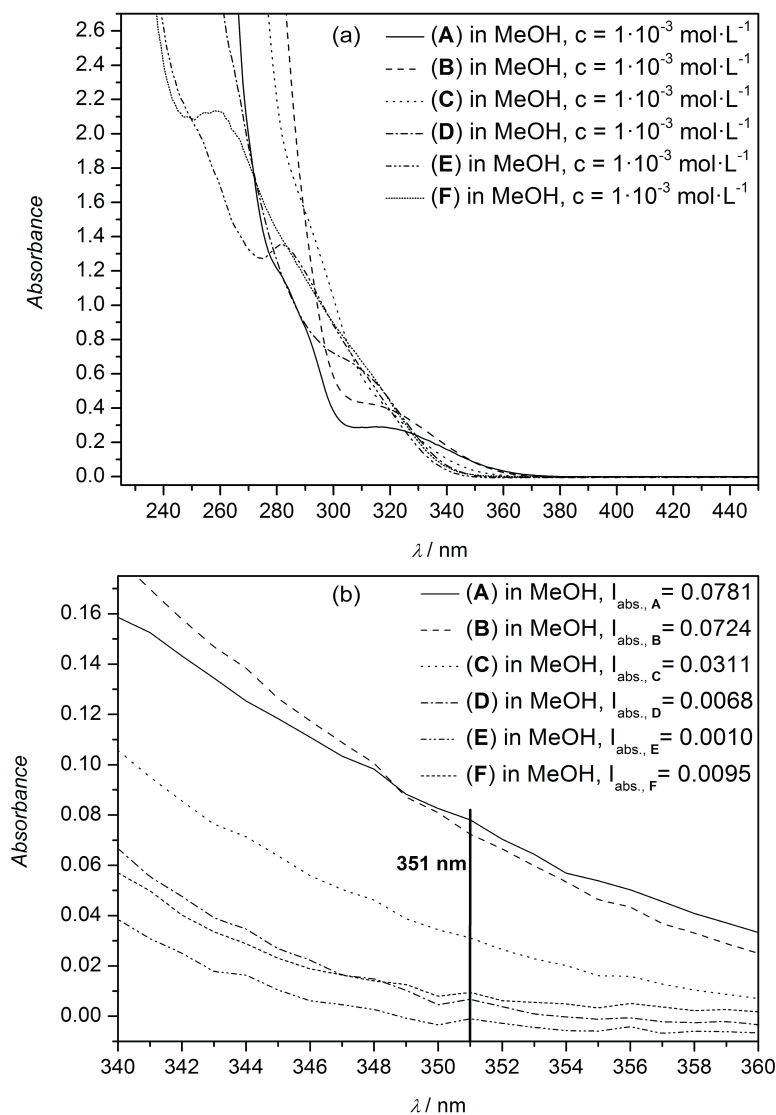


Figure 6.8. (a) Overview UV-spectra of the employed photoinitiators (A-F, see Scheme 6.1), dissolved in MeOH at a concentration of $c_{PI} = 1 \times 10^{-3} \text{ mol L}^{-1}$ from 225 nm to 450 nm. (b) Zoom UV-spectra of the employed photoinitiators (A-F) in the range of 20 nm to compare the absorbance to each other at the laser wavelength of 351 nm as well as the absorbance values $I_{\text{abs., A}} - I_{\text{abs., F}}$ at 351 nm.

To establish whether the UV absorbance of the six photoinitiators also decreases with an increase of methyl substituents, UV-spectra of all initiators were recorded. Figure 6.8 depicts a comparative set of UV-spectra (benzoin (A), 4-methylbenzoin (B), 2,4-dimethylbenzoin (C), 2,4,6-trimethylbenzoin (D), 2,3,5,6-tetramethylbenzoin (E), and 2,3,4,5,6-pentamethylbenzoin (F)).

Table 6.2. Collation of the polymeric combination product signals observed during SEC/ESI-MS of pMMA samples generated during the multi-photo-initiated free radical PLP of MMA performed in bulk at 100 Hz and -5 °C with a mixture of benzoin (A), 4-methylbenzoin (B), 2,4-dimethylbenzoin (C), 2,4,6-trimethylbenzoin (D), 2,3,5,6-tetramethylbenzoin (E), and 2,3,4,5,6-pentamethylbenzoin (F) as photoinitiators (see Scheme 6.1). All assigned combination (C) products are depicted in Figure 6.7, the structures for the corresponding products can be found in Scheme A.3–Scheme A.6 in the Appendix.

Species	Ionization	$(m/z)_{\text{theo.}}$ / Da	$(m/z)_{\text{exp.}}$ / Da	$\Delta(m/z)$ / Da
C _{1,1} ,MMA	Na ⁺	933.4	933.7	0.3
C _{2,2} ,MMA	Na ⁺	961.5	961.5	0
C _{3,3} ,MMA	Na ⁺	989.5	989.5	0
C _{4,4} ,MMA	Na ⁺	1017.5	1017.4	0.1
C _{5,5} ,MMA	Na ⁺	945.5	945.7	0.2
C _{6,6} ,MMA	Na ⁺	973.5	937.7	0.2
C _{7,7} ,MMA	Na ⁺	937.5	937.5	0
C _{1,7} ,MMA , C _{7,1} ,MMA	Na ⁺	935.4	935.5	0.1
C _{2,7} ,MMA , C _{7,2} ,MMA	Na ⁺	949.5	949.4	0.1
C _{3,7} ,MMA , C _{7,3} ,MMA	Na ⁺	963.5	963.5	0
C _{4,7} ,MMA , C _{7,4} ,MMA	Na ⁺	977.5	977.6	0.1
C _{5,7} ,MMA , C _{7,5} ,MMA	Na ⁺	991.5	991.4	0.1
C _{6,7} ,MMA , C _{7,6} ,MMA	Na ⁺	1005.5	1005.5	0
C _{1,2} ,MMA , C _{2,1} ,MMA	Na ⁺	947.4	947.4	0
C _{1,3} ,MMA , C _{3,1} ,MMA	Na ⁺	961.5	961.5	0
C _{1,4} ,MMA , C _{4,1} ,MMA	Na ⁺	975.5	975.5	0
C _{1,5} ,MMA , C _{5,1} ,MMA	Na ⁺	989.5	989.5	0
C _{1,6} ,MMA , C _{6,1} ,MMA	Na ⁺	1003.5	1003.5	0
C _{2,3} ,MMA , C _{3,2} ,MMA	Na ⁺	975.5	975.5	0
C _{2,4} ,MMA , C _{4,2} ,MMA	Na ⁺	989.5	989.5	0
C _{2,5} ,MMA , C _{5,2} ,MMA	Na ⁺	1003.5	1003.5	0
C _{2,6} ,MMA , C _{6,2} ,MMA	Na ⁺	1017.5	1017.4	0.1
C _{3,4} ,MMA , C _{4,3} ,MMA	Na ⁺	1003.5	1003.5	0
C _{3,5} ,MMA , C _{5,3} ,MMA	Na ⁺	1017.5	1017.4	0.1
C _{3,6} ,MMA , C _{6,3} ,MMA	Na ⁺	931.5	931.7	0.2
C _{4,5} ,MMA , C _{5,4} ,MMA	Na ⁺	931.5	931.7	0.2
C _{4,6} ,MMA , C _{6,4} ,MMA	Na ⁺	945.5	945.7	0.2
C _{5,6} ,MMA , C _{6,5} ,MMA	Na ⁺	959.5	959.7	0.2

At a concentration of $c_{PI} = 1 \times 10^{-3} \text{ mol L}^{-1}$ (in methanol) and an optical path length of 10 mm, the initiators have a decreasing absorbivity with an increase of methyl substituents at UV-light of 351 nm. Furthermore, the absorbivities of (D) and (F) are nearly identical, with (E) displaying the lowest absorbivity of all employed photoinitiators. These experimental findings support the quantitative results derived from the evaluation of the SEC/ESI-MS spectra. Initiator (E) (from which radical (5) is derived) has the lowest UV absorbivity at 351 nm and with 3.9 % of all disproportionation products radical (5) has also the lowest initiation efficiency toward MMA. These data suggest that there exists a clear correlation between the initiation efficiency of the employed photoinitiators with respect to the substituted benzoyl fragment and their UV absorbivity at the laser wavelength. However, earlier studies have demonstrated that such a correlation does not generally hold as a strong origin dependence can apply: Mesitoyl radicals (4) derived from mesitol show a much poorer incorporation propensity than benzoyl radicals (1) derived from benzoin (A) (see Chapter 4), although mesitol features a 10 times stronger absorbance than benzoin (A) at 351 nm.^[42,174] The origin of such different behavior lies in the molecular structure of the employed photoinitiators: UV absorbivity and initiation ability only correlate well for molecules of the same general type (here benzoin-type), yet do not correlate when molecules with different ISC abilities are employed,^[209] for details see Chapter 5.

6.5. Conclusions

Within the current chapter, four novel photoinitiators were presented, that is, 4-methylbenzoin (B), 2,4-dimethylbenzoin (C), 2,3,5,6-tetramethylbenzoin (E), and 2,3,4,5,6-pentamethylbenzoin (F). Furthermore, their use in free radical PLP with MMA in bulk was shown. In combination with two known photoinitiators (benzoin (A) and 2,4,6-trimethylbenzoin (D)), they were employed in a multi-photo-initiated free radical PLP in bulk for quantifying the radical fragments (1), (2), (3), (4), (5), and (6) in their initiation efficiency toward MMA employing SEC/ESI-MS as analytical quantification method. 28.2 % of all disproportionation products are initiated with fragment (1), 26.6 % with (2), 22.0 % with (3), 10.7 % with (4), 3.9 % with (5), and 8.6 % with (6). The experimental results support the hypothesis that the number of methyl substituents on the benzoyl fragment decreases the initiation ability, correlated with a decreasing UV absorbivity at 351 nm with increasing substitution due to the overall identical photoinitiator molecular type, which ensures similar ISC behavior.

7

UV-Triggered Endgroup Conversion of Photo-Initiated Poly(Methyl Methacrylate)

7.1. Abstract

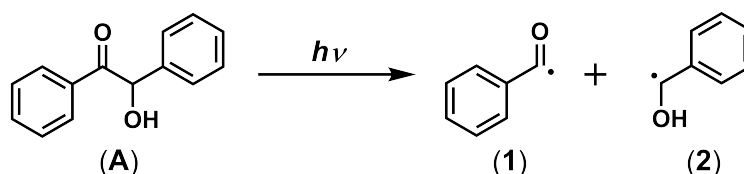
The analysis of photo-initiated pMMA *via* ESI-MS (synthesized by PLP (at $\lambda = 351$ nm) of MMA and benzoin (A) as photoinitiator at 6 mJ/pulse laser energy) evidences the presence of unidentified species as discussed in Chapter 4. The determination of the origin of these species requires a detailed investigation *via* SEC/ESI-MS and chemically induced dynamic nuclear polarization-nuclear magnetic resonance spectroscopy (CIDNP-NMR). It was found that post-irradiation of benzoin-initiated pMMA leads to α -cleavage of the benzoyl fragment leading to a sequence of cascade reactions, including the formation of an additional double bond within the polymer chain as evidenced *via* ESI-MS. Furthermore, the reaction products of the benzoyl radical post α -cleavage (e.g., benzaldehyde, acetophenone,

methyl formate or methane) as well as the formed macroradical can be followed by CIDNP-NMR, which allows establishing a reaction mechanism for the UV-induced cleavage process. The study thus evidences that – if the integrity of UV-initiated polymers is to be kept intact during their synthesis – very low irradiation energies need to be employed.

The results described in Chapter 7 stem from a collaboration with the group of Prof. Dr. Georg Gescheidt from the Institute of Physical and Theoretical Chemistry at the Graz Institute of Technology. The CIDNP experiments were carried out by Dr. Dmytro Neshchadin and myself.

7.2. Introduction

During the qualitative and quantitative studies (determining the incorporation propensity of photolytically generated radical species as polymer chain termini) employing benzoin (A) (see Scheme 7.1) – a type-I photoinitiator, which produces two primary radicals ((1) and (2)) via α -cleavage – unexpected species, whose intensity depends on the energy of the incident laser pulse could be identified in the ESI-MS spectra (see Figure 4.2a in Chapter 4).^[40–42,174] In the previous study, low single pulse energies were employed (~ 0.35 mJ/pulse) to avoid the formation of these undesired by-products, whose formation is clearly associated with elevated incident irradiation intensities.



Scheme 7.1 Photolytic decomposition pattern of benzoin (A) into a benzoyl radical (1) and a benzyl alcohol radical fragment (2).

The origin of these energy dependent yet unassigned species remained unresolved, as neither ionization problems during the electrospray process nor different types of ionization (e.g., H^+ , Na^+ , K^+ , NH_4^+) are the cause for these unusual signals. There are three remaining possibilities for the origin of these signals: (i) The species are photoinitiator-derived (i.e., an unknown photoinitiator dissociation pathway leading to yet unidentified primary radicals), (ii) polymer-derived (i.e., the polymer backbone suffers from degradation at higher single pulse energies), or (iii) endgroup-derived (i.e., higher laser energies lead to a cleavage of the chain termini) or a combination of these factors. For material research it is highly important to establish how the endgroup of a polymer is constituted and whether it can be altered by UV-irradiation as further reactions could take place under (exterior) environmental conditions (e.g., during solar irradiation). Thus, the decisive question is if

the polymer itself as well as the photoinitiator-derived endgroups are stable under such (potentially harsh) conditions. The current chapter seeks to solve the UV-triggered endgroup conversion question by examining a photo-initiated pMMA, which is initiated by benzoin (A) (benzoin-pMMA) at high laser intensities (6 mJ/pulse at $\lambda = 351$ nm). A combination of two techniques was employed to resolve the structure of the unknown species in benzoin-pMMA synthesized at these high laser energies: SEC/ESI-MS was employed for the quantitative determination of the variable endgroups and CIDNP experiments for resolving the radical cleavage mechanism and the resulting products including small molecules. The aim of the present endeavors is to establish the complete endgroup transformation mechanism at the typical laser wavelength of the PLP experiments ($\lambda = 351$ nm) and CIDNP ($\lambda = 355$ nm).

7.3. Experimental Part

7.3.1. Hydrogenation of the Post-Irradiated Polymer

The hydrogenation experiment of the post-irradiated (at 6 mJ/pulse) benzoin-initiated polymer was carried out in a Berghof high pressure reaction vessel (170 mL, maximal pressure of 200 bar) at ambient temperature and a hydrogen pressure of ~ 45 bar for 4.5 h. Because of the small amount of solvent the reaction was performed in an additional small glass vial which was placed into the high pressure reaction vessel. The glass vial was equipped with a magnetic stirrer and consisted of 30 mg of post-irradiated (at 6 mJ/pulse) benzoin-initiated pMMA, 4 mL of a mixture of ethyl acetate/ethanol (1:1) as solvent and 10 mg Pd on activated carbon (5 % Pd) as catalyst for the hydrogenation reaction. After the hydrogenation reaction the solution was filtered with a syringe filter (VWR) to remove the catalyst; subsequently, the solvent was removed by evaporation. For more details see Chapter 9.4.

7.3.2. ^1H CIDNP

For the photo-induced CIDNP experiments, ^1H NMR and ^1H CIDNP spectra were recorded on a 200 MHz Bruker AVANCE DPX spectrometer (for the experiments in Graz). Irradiation was carried out by using a frequency-tripled Quantel Nd:YAG Brilliant B laser (355 nm, ca. 120 mJ/pulse, 20 Hz, pulse duration 8 ns). The following pulse sequence was used: presaturation – laser flash – RF detection pulse (2 μs) – free induction decay. Dummy CIDNP spectra without the application of a laser pulse were always recorded to ensure an effective suppression of the parent NMR spectra. For more details see Chapter 9.4.

7.3.3. ^1H NMR

The NMR spectra in Karlsruhe were recorded on a Bruker AM 400 spectrometer operating at 400 MHz. Each sample contains 50 mg of precipitated benzoin-pMMA (generated at ~ 0.35 mJ/pulse or 6 mJ/pulse laser energy) and was dissolved in 0.5 mL of chloroform- d_1 . For more details see Chapter 9.4.

7.3.4. Polymer Synthesis *via* PLP and Post-Irradiation of the Polymer

All MMA samples consisted of monomer (sample volume ~ 0.5 mL) and benzoin (A) with a concentration of $c_{\text{benzoin}} = 5 \times 10^{-3}$ mol L $^{-1}$. All post-irradiation samples consisted of benzoin-pMMA (8-10 mg) and methyl isobutyrate (MIB) (sample volume ~ 0.4 mL). Before performing the post-irradiation, the benzoin-pMMA was precipitated twice from hexane to remove the residual amount of photoinitiator (benzoin (A)). The polymerization and post-irradiation experiments were carried out at ~ 0.35 mJ/pulse and 6 mJ/pulse, respectively. Irradiation time of 5 s to 60 min (see Figure 7.4) for the time series and 15 min for the synthesis of benzoin-pMMA at low (~ 0.35 mJ/pulse) and high (6 mJ/pulse) laser energies (see Figure 7.3). For more details see Chapter 4.3.3 and Chapter 9.4.

7.3.5. SEC/ESI-MS Measurements

The samples were measured at a capillary temperature of 300 °C, for more details see Chapter 4.3.6 and Chapter 9.4.

7.4. Results and Discussion

As noted above, the unexpected appearance of laser energy dependent signals, which can be observed during benzoin-initiated (and also with e.g., benzoin ethyl ether and benzil) PLP of MMA at higher laser intensities ($\lambda = 351$ nm, laser energy > 0.35 mJ/pulse), was discussed in previous publications (see Chapter 4.4.1).^[40,41,174] The laser energy dependence of the unknown signals has now been systematically studied. Inspection of Figure 7.1 depicts all observed disproportionation (marked with D) and combination (marked with C) products (structures for the observed signals in the ESI-MS spectra are shown in Scheme 7.2) as a function of the incident laser energy. Within the current study, all assigned signals observed in the ESI-MS spectra were labeled according to the following nomenclature: Disproportionation peaks occur in pairs removed by 2 Da from each other. Thus, each peak is labeled with $D^{v,=,x}$ or $D^{v,H,x}$ where v denotes the radical fragment that has initiated the polymerization ((1, 2 or 3, 4, and 5) derived from post-irradiation and hydrogenation experiments; see Scheme 7.1 and Scheme 7.2) and x denotes the monomer type (MMA in the present case). Combination products are included for the sake of completeness of the assignments, yet they are of limited use in the present study as it is not possible to

differentiate whether they have been generated by initiation or termination of macromolecular growth. All combination peaks are labeled with $C^{v,w,x}$ where v and w denote the radical fragment as endgroup (or the formed endgroup after post-irradiation of the polymer, see Scheme 7.1 and Scheme 7.2) and x denotes the monomer (MMA in the present case). Inspection of Figure 7.1 evidences that the intensity of the unassigned species (marked with a red question mark) shows a strong laser energy dependency. Reducing the laser energy (from 6 mJ/pulse to ~ 0.35 mJ/pulse under otherwise identical polymerization conditions) leads to a decrease and disappearance of the unexpected species (see Chapter 4.4.1). Therefore, the laser energy was reduced to a minimum amount in previous initiation efficiency studies to avoid misinterpretation through additional – unassigned – species in the ESI-MS spectra (see Chapter 4.4.1 and Chapter 6).^[174,210]

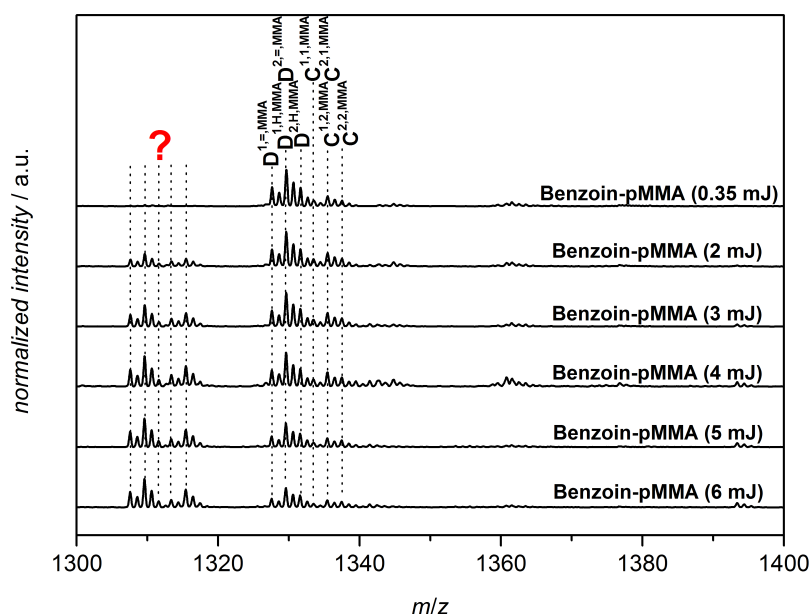


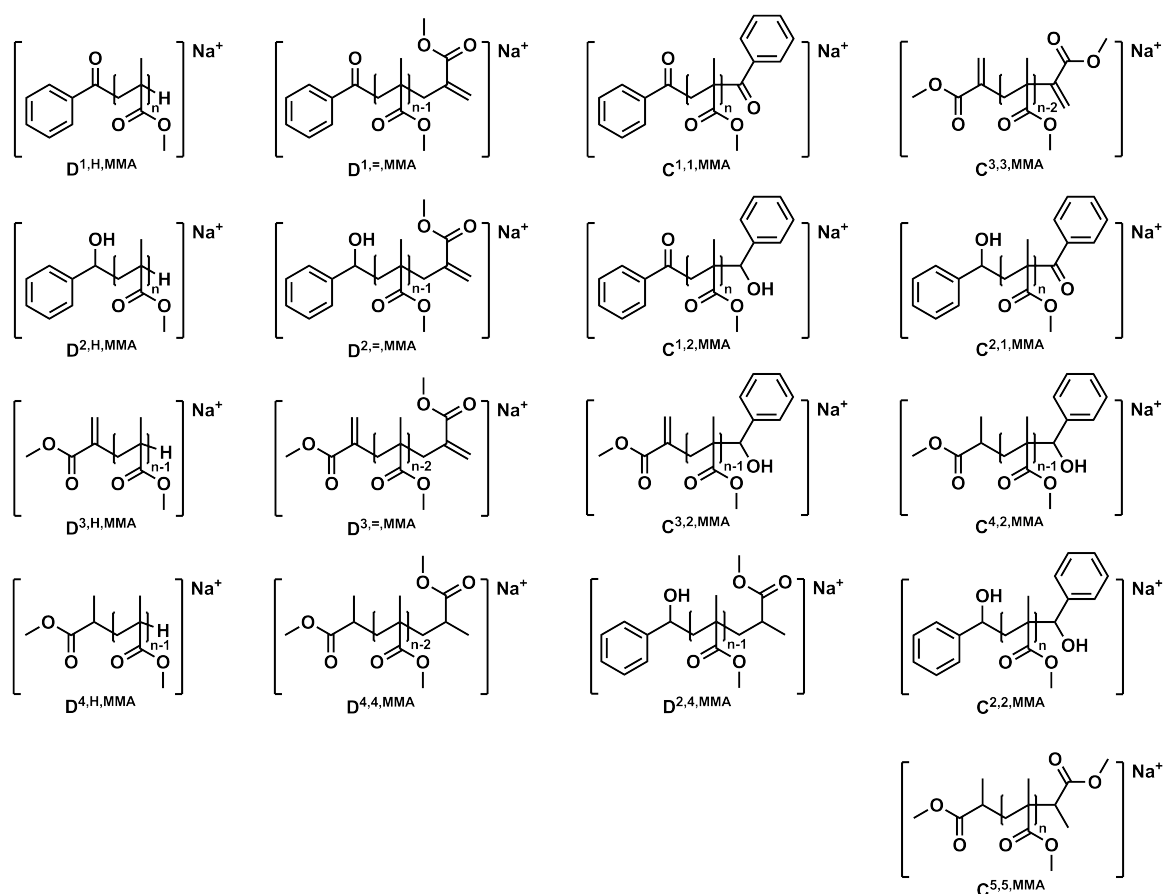
Figure 7.1. ESI-MS spectra (one repeat unit) of benzoin-initiated pMMA obtained at variable laser pulse energies (~ 0.35 to 6 mJ/pulse; measured in DCM/MeOH (3:1) *via* direct infusion) synthesized *via* PLP at 100 Hz, -5 °C, $c_{\text{benzoin}} = 5 \times 10^{-3}$ mol L $^{-1}$ and 15 min polymerization time in bulk. The nomenclature employed to identify the individual disproportionation and combination products is provided in Scheme 7.2.

To date, chemical structures for the energy dependent products could not be identified. However, post-irradiation of isolated and by-product free benzoin-pMMA (synthesized at ~ 0.35 mJ/pulse laser energy and precipitated from hexane to remove the residual amount of photoinitiator) at high laser energy (6 mJ) in a non-polymerizable solvent with similar physicochemical parameters as MMA, i.e., methyl isobutyrate (MIB), shows the same unassigned species (see below Figure 7.3b, red spectra) during analysis of the ESI-MS spectra. Because of the absence of any impurities after precipitation of the polymer and reconfirmation of the appearance of unassigned species, it is an incontrovertible fact that

the formation of these unexpected products proceeds *via* a UV-triggered endgroup-derived (*iii*) or polymer backbone-derived (*ii*) conversion from material produced at low energies (~ 0.35 mJ/pulse) not carrying the unexpected moieties. Thus, it can be ruled out that the additional species are generated during the primary photolytic dissociation process associated with benzoin (A) (*i*), see above). For the following experiments – where uncontaminated, i.e., by-product free polymer is required – material generated at ~ 0.35 mJ/pulse is employed, which contains polymer chains initiated by photoinitiator fragment (1) or (2) and terminated *via* disproportionation.

7.4.1. Elucidation of the Mechanism *via* SEC/ESI-MS

To establish the origin and chemical nature of the unexpected species, a two-pronged strategy was adopted:



Scheme 7.2 Expected polymeric disproportionation and combination products in the photochemically-initiated bulk free radical polymerization of MMA in the presence of benzoin (A) (depicted in Scheme 7.1) as well as polymeric disproportionation and combination products after post-irradiation and hydrogenation experiments. See Table 7.1 for a collation of the m/z -ratios of the individual radical fragments. Furthermore, the combination products are not of interest, but are mentioned because of completeness of assignment ($C^{1,2,MMA}$ and $C^{2,1,MMA}$ cannot be distinguished in the mass spectra).

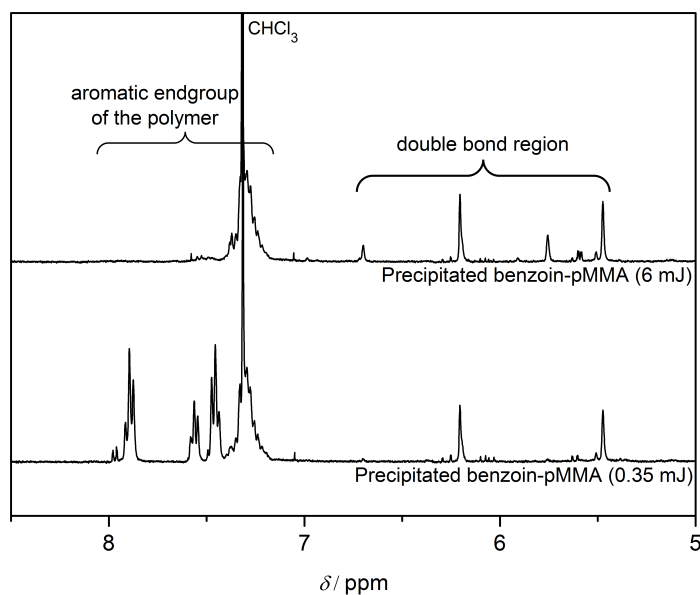


Figure 7.2. Zoom into the 400 MHz NMR spectra (from 5 ppm to 8.5 ppm) of precipitated benzoin-initiated pMMA generated at ~ 0.35 mJ/pulse laser energy (lower spectrum) and precipitated post-irradiated (at 6 mJ/pulse laser energy) benzoin-initiated pMMA (upper spectrum).

Initially, hydrogenation of the post-irradiated material is carried out to assess – *via* MS – if the newly formed species contains additional double bonds. On the basis of these experiments, a possible structure of the newly formed species is proposed, whose formation mechanism is subsequently probed *via in-situ* CIDNP experiments. A comparison of ^1H NMR spectra from precipitated benzoin-pMMA synthesized at low laser energies (~ 0.35 mJ/pulse) with a post-irradiated sample synthesized at high laser energies (6 mJ/pulse) in Figure 7.2 indicates a decrease in signal intensity in the aromatic region of the NMR spectra. During the photo-initiated polymerization process with benzoin (A) – bearing two aromatic rings – two radical fragments are incorporated as endgroups into the polymer chain (see Scheme 7.1 ((1) and (2))). On the basis of the decreasing signal intensity in the aromatic region during observation of the post-irradiated (at 6 mJ/pulse laser energy) NMR sample an endgroup conversion appears likely. Figure 7.3a depicts the SEC/ESI-MS overview spectra of benzoin-pMMA synthesized at ~ 0.35 mJ/pulse laser energy (black spectrum), post-irradiated benzoin-pMMA synthesized at 6 mJ/pulse laser energy (red spectrum) and hydrogenated post-irradiated material at 6 mJ/pulse laser energy (blue spectrum). One repeat unit of all three SEC/ESI-MS spectra is displayed in Figure 7.3b. Clearly, the starting polymer (Figure 7.3b, black spectra) – synthesized at low laser energy (~ 0.35 mJ/pulse) – only depicts the expected disproportionation products ($\text{D}^{1,=,\text{MMA}}$, $\text{D}^{1,\text{H},\text{MMA}}$, $\text{D}^{2,=,\text{MMA}}$, and $\text{D}^{2,\text{H},\text{MMA}}$, structures see in Scheme 7.2) as well as the combination products ($\text{C}^{1,1,\text{MMA}}$, $\text{C}^{1,2,\text{MMA}}$, $\text{C}^{2,1,\text{MMA}}$, and $\text{C}^{2,2,\text{MMA}}$, structures see in Scheme 7.2). The mass spectrum is free from any unexpected side products (all values for the disproportionation and combination products within one repeat unit are collated in Table 7.1). The SEC/ESI-MS spectrum

of one repeat unit of post-irradiated benzoin-pMMA at 6 mJ/pulse (Figure 7.3b, red spectra), however, displays the appearance of unidentified species (signals at 807.4, 809.4, and 815.4 Da, see Table 7.1). The difference in mass within one repeat unit between the expected species (827.7 Da) and the unexpected one (807.7 Da) is 20.0 Da.

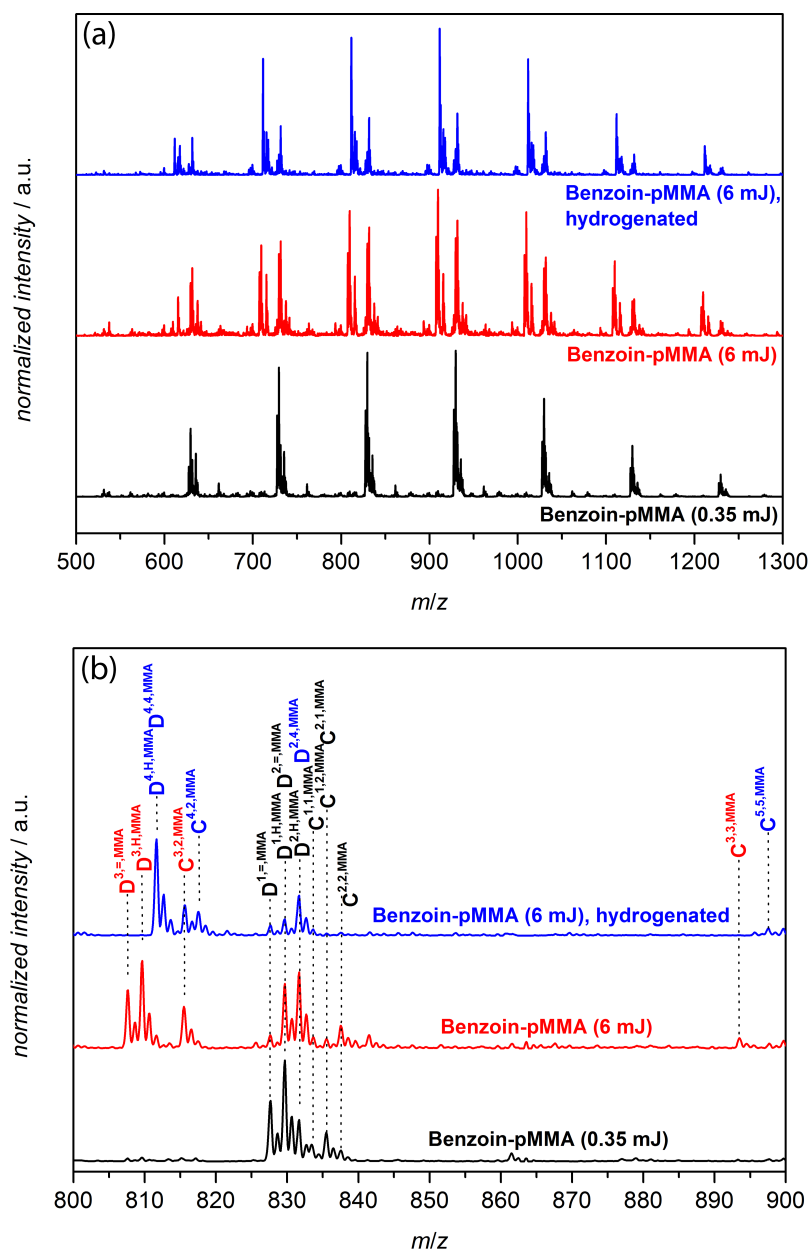


Figure 7.3. (a) SEC/ESI-MS overview spectra of benzoin-initiated pMMA obtained at ~ 0.35 mJ/pulse (black spectra), post-irradiated benzoin-initiated pMMA at 6 mJ/pulse (red spectra) and hydrogenated, post-irradiated (at 6 mJ/pulse) benzoin-initiated pMMA synthesized *via* PLP at 100 Hz, -5 $^{\circ}\text{C}$, and 15 min reaction time (for the black and red spectra). The figure depicts the singly charged products ionized with sodium iodide at a retention time between 17.00 and 18.21 min. (b) Zoom into one repeat unit of the SEC/ESI-MS overview spectra. The nomenclature employed to identify the individual disproportionation and combination products is provided in Scheme 7.2.

Table 7.1. Collation of the polymeric product signals observed during ESI-MS and SEC/ESI-MS of benzoin-initiated pMMA samples generated during the bulk free radical PLP of MMA with benzoin (A) at 100 Hz and -5 °C. The table provides experimentally observed as well as theoretically expected m/z -ratios for the found disproportionation (D) and combination (C) products (consisting of 6 or 7 monomer units). The structures corresponding to the individual peaks are depicted in Scheme 7.2. The tabulated values correspond to the peaks displayed in Figure 7.3.

Species	Ionization	$(m/z)_{\text{theo.}}$ / Da	$(m/z)_{\text{exp.}}$ / Da	$\Delta(m/z)$ / Da
D ^{1,H} ,MMA	Na ⁺	829.4	829.7	0.3
D ^{1,=} ,MMA	Na ⁺	827.4	827.7	0.3
D ^{2,H} ,MMA, D ^{2,4} ,MMA	Na ⁺	831.4	831.7	0.3
D ^{2,=} ,MMA	Na ⁺	829.4	829.7	0.3
D ^{3,H} ,MMA	Na ⁺	809.4	809.7	0.3
D ^{3,=} ,MMA	Na ⁺	807.4	807.7	0.3
D ^{4,H} ,MMA, D ^{4,4} ,MMA	Na ⁺	811.4	811.7	0.3
C ^{1,1} ,MMA	Na ⁺	833.4	833.5	0.1
C ^{3,3} ,MMA	Na ⁺	893.4	893.5	0.1
C ^{1,2} ,MMA, C ^{2,1} ,MMA	Na ⁺	835.4	835.5	0.1
C ^{3,2} ,MMA	Na ⁺	815.4	815.5	0.1
C ^{4,2} ,MMA	Na ⁺	817.4	817.6	0.2
C ^{2,2} ,MMA	Na ⁺	837.4	837.6	0.2
C ^{5,5} ,MMA	Na ⁺	897.5	897.6	0.1

However, this mass difference cannot be achieved by a single cleavage process and therefore α -cleavage of the aromatic endgroup was proposed ($\Delta m/z = 105.0$ Da), indicating that the cleavage process starts at $n + 1$ (one repeat unit higher, 927.7 Da) and ends up at n (one repeat unit less, 807.7 Da). Furthermore, a secondary cleavage reaction has to take place to reach the mass difference of 120 Da. The mass spectrum of the post-irradiated sample (red spectra) illustrates that due to the decreasing signal intensity of species D^{1,=},MMA, D^{1,H},MMA, and C^{1,2},MMA/C^{2,1},MMA the newly formed products originate from these three species. To establish whether the newly formed endgroups contain vinyl bonds, a hydrogenation experiment was carried out. Post-irradiated benzoin-pMMA (at 6 mJ/pulse) was hydrogenated (at a hydrogen pressure of 45 bar, for details see the Experimental Part in Chapter 7.3) in a high pressure reactor with a solvent mixture of ethanol/ethyl acetate (1:1). The SEC/ESI-MS spectrum of the hydrogenated sample (Figure 7.3b, blue spectrum) depicts a shift in mass in several signals. A species carrying one double bond from the termination reaction *via* disproportionation – e.g., D^{2,=},MMA – is shifted by 2 Da after the hydrogenation reaction. The most important new insight for a structural assignment

7. UV-Triggered Endgroup Conversion of Photo-Initiated pMMA

of the unexpected products is given by the shift in mass from 807.4 to 811.4 Da (shift of 4 Da), 809.4 to 811.4 Da (shift of 2 Da), and 815.4 to 817.4 Da (shift of 2 Da). As explained above, a shift of 2 Da results from the double bond formed *via* disproportionation (termination reaction). A difference in mass of 4 Da as displayed between the unexpected species 807.4 Da in the post-irradiated sample (Figure 7.3b, red spectrum) and 811.4 Da in the hydrogenated sample (Figure 7.3b, blue spectrum) indicates the formation of a new, additional double bond.

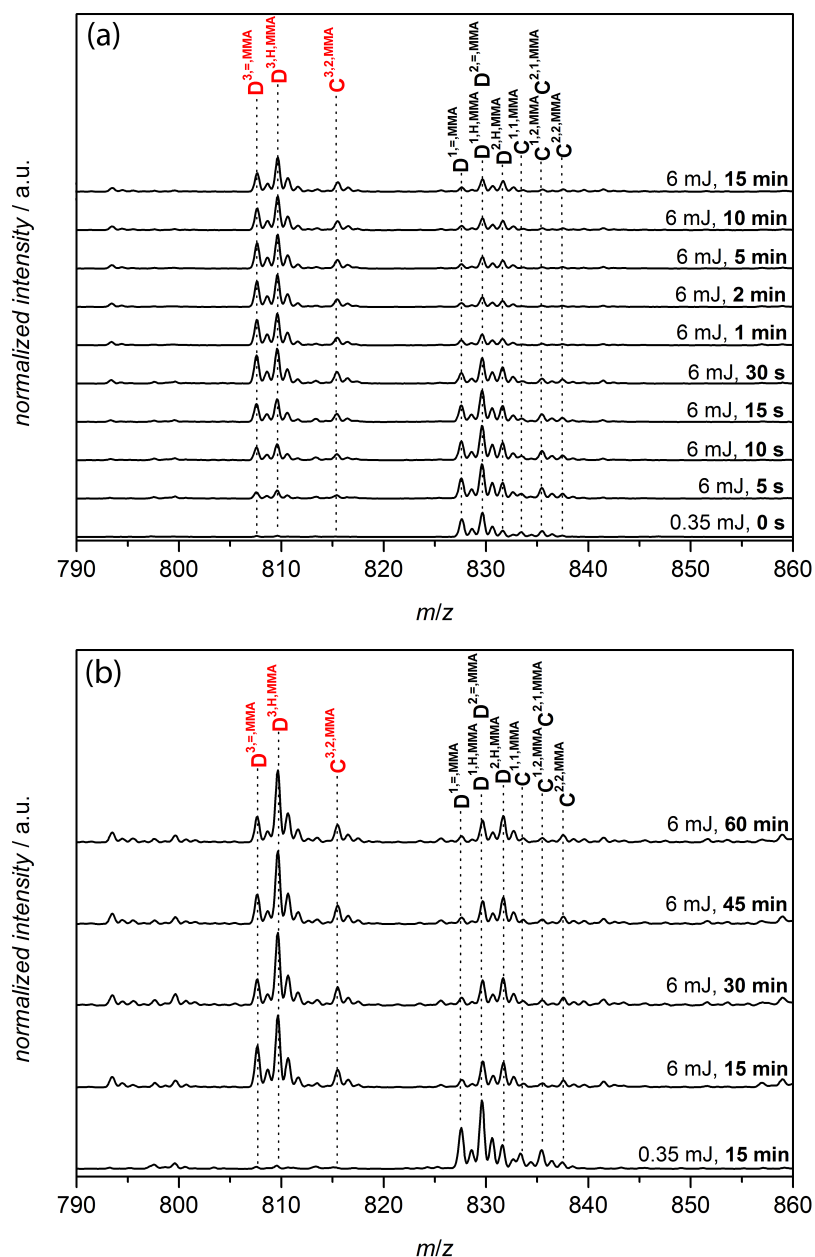


Figure 7.4. (a) Zoom into one repeat unit of the SEC/ESI-MS spectra of a time series of post-irradiated benzoin-initiated pMMA (6 mJ/pulse, reaction time from 5 s to 15 min) at 100 Hz and -5°C . (b) Zoom into one repeat unit of the SEC/ESI-MS spectra of a time series of post-irradiated benzoin-initiated pMMA (6 mJ/pulse, reaction time from 15 to 60 min) at 100 Hz, and -5°C .

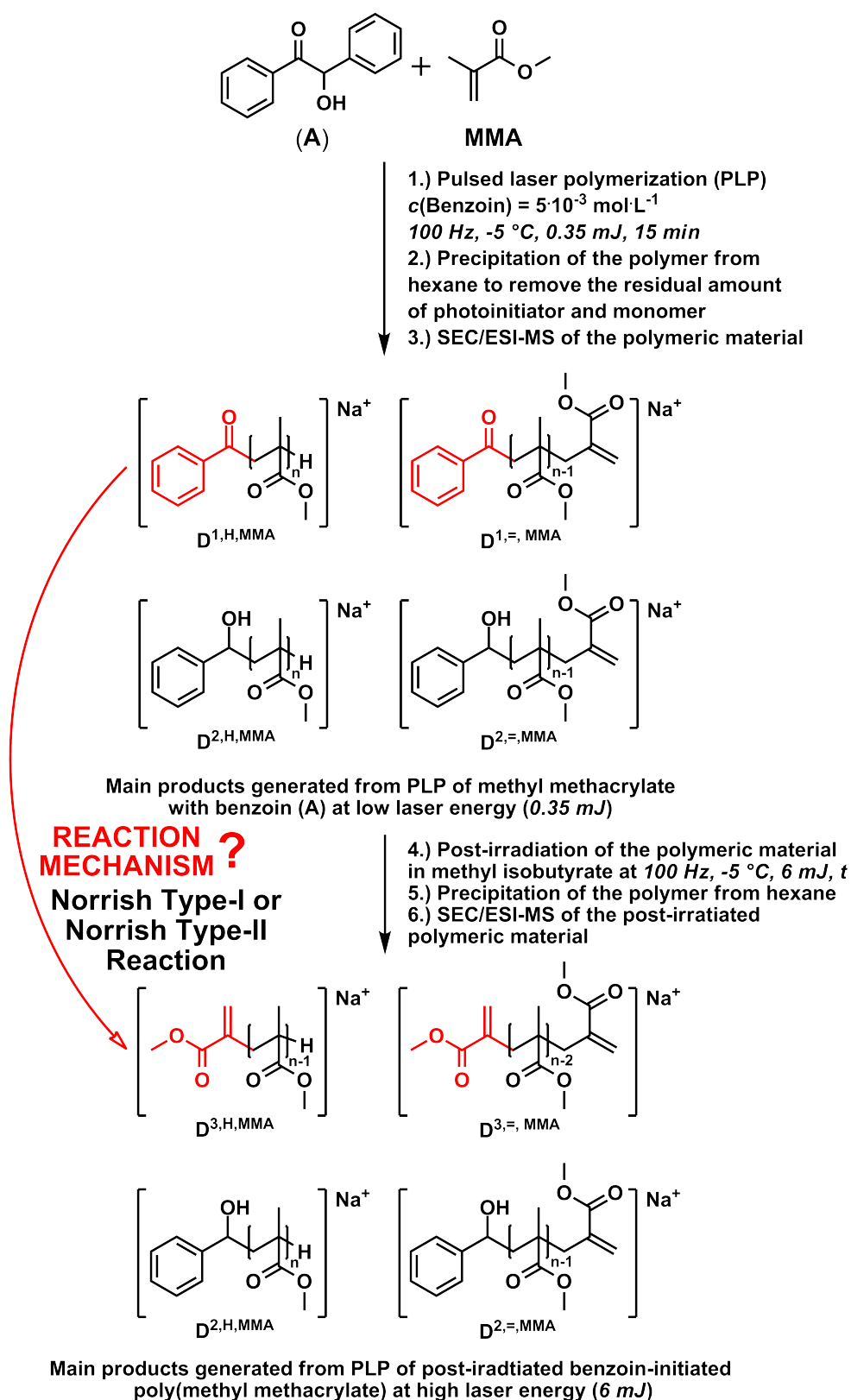
An explanation for the generation of the new double bond could be as follows: During the polymerization and also the post-irradiation process, the polymer chain bearing radical fragment (1) (see Scheme 7.1) – the benzoyl fragment – can absorb UV-light ($D^{1,=,MMA}$, $D^{1,H,MMA}$, $C^{1,1,MMA}$ and $C^{1,2,MMA}/C^{2,1,MMA}$, structures see in Scheme 7.2) which leads to a consecutive cleavage of the endgroup (the same process can also occur with combination products). The unexpected products observed in Figure 7.1 (labeled with a question mark) can thus be assigned to polymer chains bearing a new endgroup with a second double bond ($D^{3,=,MMA}$, $D^{3,H,MMA}$, $C^{3,2,MMA}$, and $C^{3,3,MMA}$). The hydrogenation experiment (Figure 7.3b, blue spectrum) leads – as explained above – to the formation of $D^{4,H,MMA}$, $D^{4,4,MMA}$, $D^{2,4,MMA}$, $C^{4,2,MMA}$, and $C^{5,5,MMA}$ (see Scheme 7.3 below) and is therefore evidence for the existence of a new endgroup bearing a second double bond at the polymer terminus. An important question to resolve is how fast the UV-triggered conversion into the new endgroup proceeds. Figure 7.4a depicts a time series of post-irradiated (at 6 mJ/pulse) benzoin-pMMA (generated at ~ 0.35 mJ/pulse laser energy) from 5 s to 15 min reaction time and Figure 7.4b from 15 to 60 min reaction time. As evidenced by Figure 7.4a, the conversion of $D^{1,=,MMA}$, $D^{1,H,MMA}$, $C^{1,1,MMA}$, and $C^{1,2,MMA}/C^{2,1,MMA}$ (for structures, see Scheme 7.2) into $D^{3,=,MMA}$, $D^{3,H,MMA}$, $C^{3,2,MMA}$, and $C^{3,3,MMA}$ is finished within 2 min.

The mechanism of the discovered endgroup conversion is thus most likely associated with the loss of the benzoyl group (1) as well as a methyl group at the former monomer repeat unit (see Scheme 7.3). However, SEC/ESI-MS is not the method of choice for finally resolving the mechanism as cleavage products – e.g., small molecules which are highly important for confirming the structures $D^{3,=,MMA}$, $D^{3,H,MMA}$, $C^{3,2,MMA}$, and $C^{3,3,MMA}$ – cannot be detected. Valuable insight is provided by chemically induced dynamic nuclear polarization (CIDNP), which is well-established to detect primary species formed *via* radical pairs at very short time scales and is thus ideally suited for elucidating the reaction mechanism of an *in-situ* radical-based cleavage of endgroups from a polymer chain. Furthermore, the method allows a detailed observation of all cleavage products including small molecules.

7.4.2. Elucidation of the Mechanism *via* CIDNP

To further clarify the mechanism of the conversion of benzoin-pMMA, synthesized *via* PLP at low laser energies (~ 0.35 mJ/pulse) bearing a benzoyl moiety (1, Scheme 7.1), CIDNP was employed. CIDNP is an NMR based experimental technique, which is ideally suited for following reactions involving homolytic bond cleavage since it allows establishing reaction pathways proceeding *via* radical pairs. NMR spectra taken at a short delay (μ s-ms) after the generation of a radical pair indicate unusual line intensities. This originates in magnetic-field effects depending on the initial multiplicity of the (spin correlated) radical pair (singlet or triplet) and magnetic parameters (g -factors and the isotropic hyperfine coupling constants

7. UV-Triggered Endgroup Conversion of Photo-Initiated pMMA



Scheme 7.3 Synthesis of by-product free benzoin-initiated pMMA at low laser energies (~ 0.35 mJ/pulse) and post-irradiation at high laser energies (6 mJ/pulse). Depicted are the structures of the species formed during both processes.

of the two radicals).^[159,162] Accordingly, CIDNP spectra provide information regarding the character of the reaction products formed exclusively in radical reactions by the chemical shifts of the NMR resonances whereas the unusual signal intensities contain information regarding the spin distribution in the intermediate radicals.^[211] For a detailed discussion of the working principles of CIDNP experiments, the reader is referred to ref. 162.

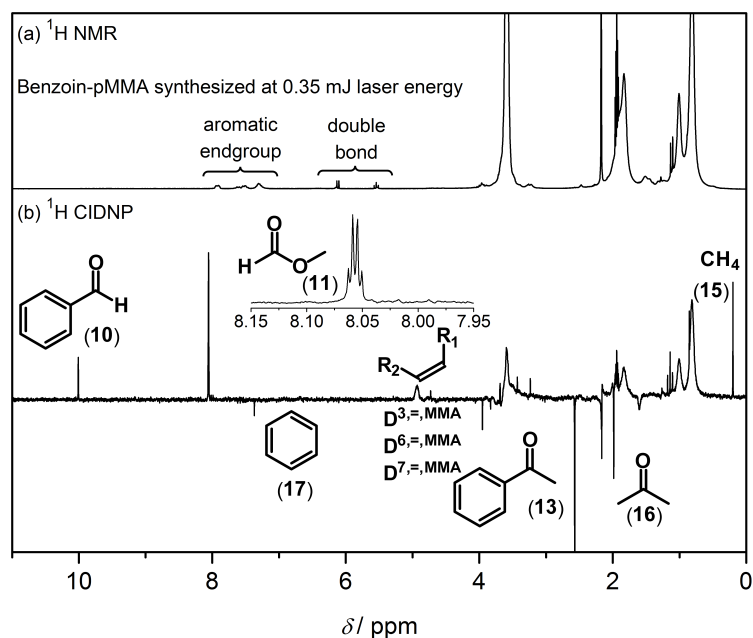


Figure 7.5. (a) ^1H NMR (200 MHz) of benzoin-initiated pMMA synthesized at ~ 0.35 mJ/pulse laser energy and (b) ^1H CIDNP spectrum of benzoin-initiated pMMA (synthesized at ~ 0.35 mJ/pulse laser energy), recorded 1 μs after (time to the center of the RF pulse) the laser flash ($\lambda = 355$ nm) in acetonitrile- D_3 at close to 120 mJ/pulse, together with the assignments of the most important products of the free radical reactions. The associated reaction mechanism is depicted in Scheme 7.4.

^1H NMR and ^1H CIDNP spectra of benzoin-pMMA (synthesized at ~ 0.35 mJ/pulse laser energy) are depicted in Figure 7.5. Polarized NMR lines in the ^1H CIDNP spectrum, recorded 1 μs after (time between the laser pulse and the center of the observing radio frequency (RF) pulse) the laser flash clearly shows that the photo-induced transformation of benzoin-pMMA proceeds *via* free radical pathways. The singlet at 10.0 ppm in enhanced absorption (Figure 7.5b) can be unambiguously assigned to the single proton at the carbonyl group of benzaldehyde (10). This implies an α -cleavage of the benzoyl (1) group of benzoin-pMMA (Norrish type-I reaction) and formation of benzoyl radicals (1) and macroradicals (8) with subsequent hydrogen transfer from (8) to the benzoyl radical (1) (see Scheme 7.4). It is important to point out that in order to exhibit CIDNP polarization, the single proton in benzaldehyde (10) has to stem from a position of (8) revealing a hyperfine coupling constant between electron and nuclear spin of a substantial size. The quartet (enhanced absorption, $^4J = 0.8$ Hz) at 8.06 ppm is – according to the literature data^[212,213] – attributed to

the single proton of methyl formate (11). Its precursor has to be radical (12) originating from direct cleavage of ester groups in benzoin-pMMA as observed earlier by Fischer and coworkers.^[214] However, in that case, photolysis was performed at approximately 260 nm (since aliphatic acyl groups absorb UV-light at these wavelengths). In the CIDNP experiments, a wavelength of 355 nm was employed, therefore a directly induced ester cleavage is not straightforward under the current reaction conditions. It is noteworthy that tertiary alkyl radicals such as (9) absorb between 300 and 400 nm,^[215] i.e., these radicals can be excited in the implemented experiment. Accordingly, (12) can be formed *via* excitation of (9). An alternative pathway toward (12) is the disproportionation of the macroradical (8).^[216] A similar disproportionation of (8) leads to methyl radicals (14), indicated by the polarized signal of methane (15) at 0.2 ppm. A competitive reaction to the α -cleavage of $D^{1,=,MMA}$ (Norrish type-I reaction) is a Norrish type-II reaction involving a six-membered transition state leading to a 1,4-biradical (18) followed by the generation of an enol (19). In addition, a new product containing a second double bond was generated, which is evidenced by the hydrogenation experiment ($D^{3,=,MMA}$, see Figure 7.3 above). Both subsequent reactions of the macroradical (8) (Norrish type-I pathway) as well as the Norrish type-II pathway lead to the formation of diamagnetic macromolecules containing double bonds in their endgroups ($D^{6,=,MMA}$ and $D^{3,=,MMA}$; see Scheme 7.4). However, inspection of Figure 7.6a, a zoom into the SEC/ESI-MS spectra of post-irradiated benzoin-pMMA synthesized at 6 mJ/pulse (red spectrum) and benzoin-pMMA (synthesized at ~ 0.35 mJ/pulse) after the 1H CIDNP experiment (brown spectrum), indicates both direct cleavage of the ester group over species (9) to $D^{7,=,MMA}$ and disproportionation of the macroradical (8) into $D^{6,=,MMA}$ (structures for the observed signals in the mass spectra as well as their theoretical and experimental m/z -ratios can be found in Figure 7.6b). In addition, an alternative possibility for the formation of $D^{7,=,MMA}$ has to be considered, i.e., the ester photo-cleavage *via* sensitization of the benzoyl moiety of benzoin-pMMA.^[217] A probable reason for the weak signal intensities of $D^{6,=,MMA}$ and $D^{7,=,MMA}$ in the mass spectrum (Figure 7.6a) in comparison to the signal intensity of methyl formate in the 1H CIDNP (11, Figure 7.5b) is the loss of ester groups during the formation of $D^{6,=,MMA}$ and $D^{7,=,MMA}$. The ionization ability of the polymeric material in the ESI source will decrease drastically with a decreasing fraction of well ionizable ester groups which are responsible for the polymers ionization ability. The formation of new double bonds is reflected by the weak positive polarizations at 4.5-5.0 ppm. Acetophenone (13) is the result of the coupling of primary benzoyl (1) and methyl radicals (14) (*via* the Norrish type-I pathway) or the keto-enol tautomerism of the enol form (19) of acetophenone (*via* the Norrish type-II pathway); the NMR transition of the methyl group of (13) is found in the 1H CIDNP spectrum at 2.6 ppm. Because of the similar signal intensity of (13) and (15) in the 1H CIDNP spectrum one cannot infer that the Norrish type-I is more favored than the Norrish type-II pathway.

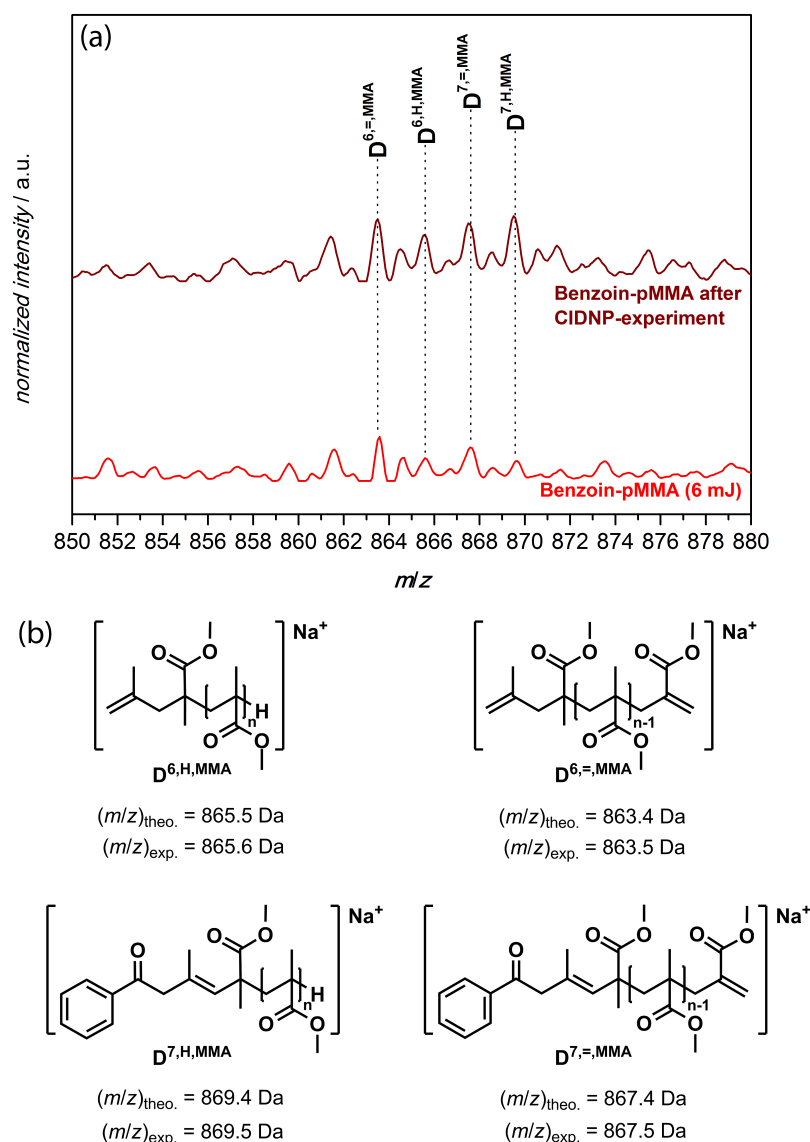
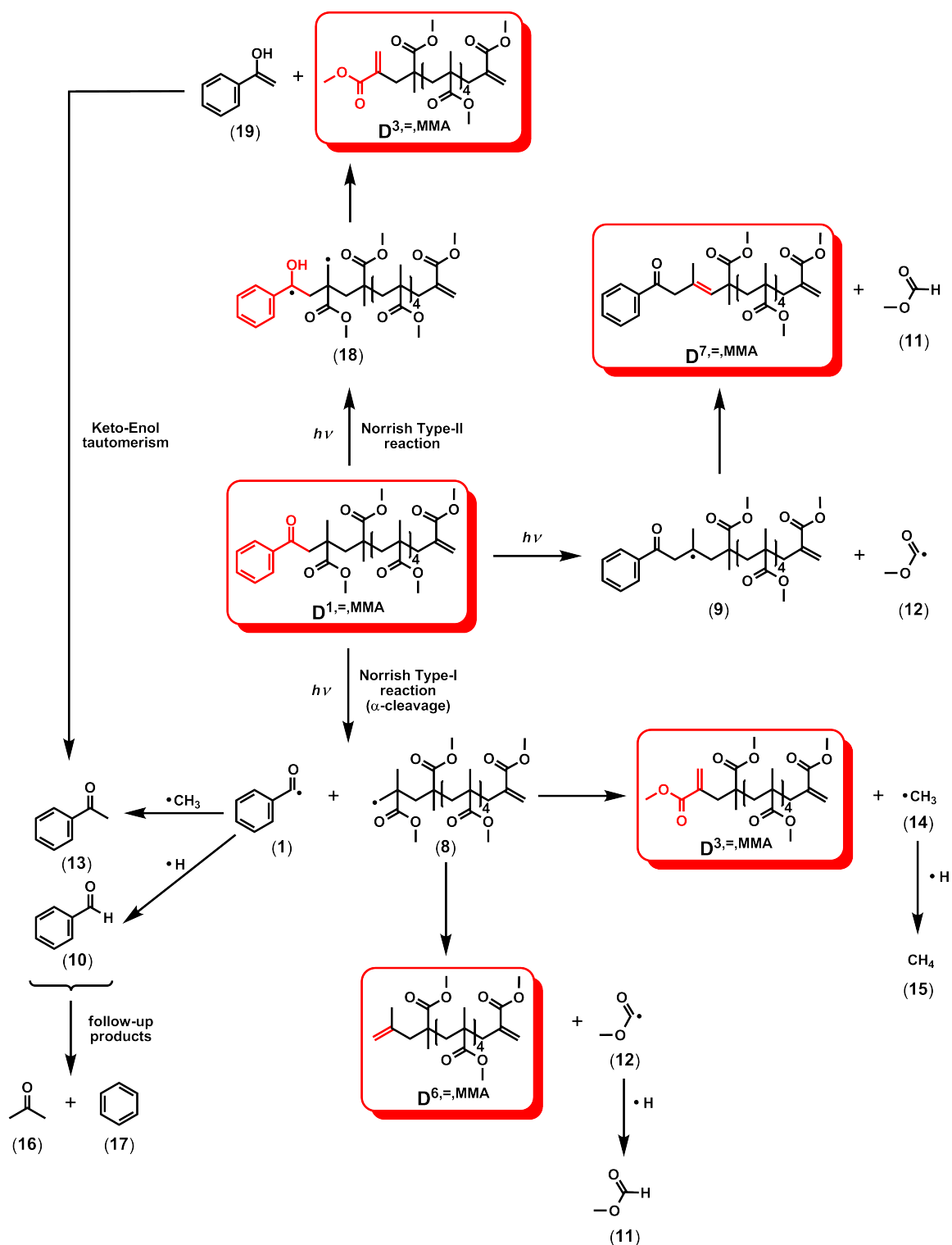


Figure 7.6. (a) Zoom into the SEC/ESI-MS overview spectra of post-irradiated benzoin-initiated pMMA at 6 mJ/pulse synthesized *via* PLP at 100 Hz, -5°C and 15 min reaction time (red spectrum) and benzoin-initiated pMMA (synthesized at ~ 0.35 mJ/pulse) after the CIDNP-experiment at close to 120 mJ/pulse (brown spectrum). (b) Proposed structures for the observed species as well as theoretical and experimental m/z -ratios in the given zoom of the SEC/ESI-MS spectra.

The complete reaction pathway of UV-light irradiated benzoin-pMMA (synthesized at ~ 0.35 mJ/pulse laser energy) as determined by ^1H CIDNP and SEC/ESI-MS is depicted in Scheme 7.4. Acetone (16) and benzene (17), which appear polarized at 2.0 and 7.4 ppm, respectively, are subsequent products of acetophenone (13) and benzaldehyde (10). Those polarizations appear only after a sustained irradiation of the benzoin-pMMA solution. It has to be mentioned that the reaction pathways given in Scheme 7.4 are the same for the other species bearing a benzoyl fragment (1) as endgroup, including disproportionation as well as combination products (see Scheme 7.2 above).



Scheme 7.4 UV-induced reaction pathways of benzoin-initiated pMMA (synthesized at ~ 0.35 mJ/pulse laser energy) as determined by ¹H CIDNP and SEC/ESI-MS.

Polymeric species bearing the benzyl alcohol radical fragment (2) (Scheme 7.1 above) are – due to their low propensity to absorb UV-light – of no interest in the context of UV-induced endgroup transformations.

7.5. Conclusions

A combination of SEC/ESI-MS and CIDNP-NMR spectroscopy – in conjunction with hydrogenation experiments – has been employed to identify the endgroup transformations occurring during the UV-irradiation ($\lambda = 351$ nm) of pMMA generated *via* benzoin-initiated free radical polymerization. The observed – and previously unidentified – species (see Chapter 4) in the ESI-MS spectrum of benzoin-initiated pMMA synthesized at elevated laser energies (6 mJ/pulse, $\lambda = 351$ nm) originate from the α -cleavage (Norrish type-I reaction) or a Norrish type-II reaction of the benzoyl fragment (1). The endgroup constitution was analyzed *via* hydrogenation of the polymer, which evidences the generation of a new double bond ($D^{3,=,MMA}$ and $D^{3,H,MMA}$) during post-irradiation of benzoin-pMMA at high laser energies (6 mJ/pulse). A time series of SEC/ESI-MS experiments examining samples irradiated for variable time intervals indicates the near complete conversion of $D^{1,=,MMA}$ into $D^{3,=,MMA}$ within 2 min. Furthermore, *in-situ* 1H CIDNP-NMR spectroscopy was employed (irradiation of the polymeric material at $\lambda = 355$ nm) to investigate the reaction pathways of the radical-based cleavage mechanism of by-product free benzoin-pMMA (synthesized at low laser energies of ~ 0.35 mJ/pulse). Small molecules such as benzaldehyde (10), acetophenone (13), and methane (15) can be observed in the 1H CIDNP spectrum, which are associated with the formation of $D^{3,=,MMA}$ and $D^{3,H,MMA}$. In addition, the formation of methyl formate (11) can be identified in the 1H CIDNP experiment as a cleavage product, a product originating from ester side group cleavage. Typically, such cleavage reaction occur at shorter irradiation wavelength, yet it appears that 351/355 nm laser irradiation can also lead to a certain amount of cleavage. Such a notion is underpinned by the SEC/ESI-MS spectrum of a CIDNP sample (see Figure 7.6a), depicting weak signals for $D^{6,=,MMA}$ and $D^{7,=,MMA}$. Further studies should focus on the kinetics and photophysics of the processes associated with UV-induced endgroup transformations.

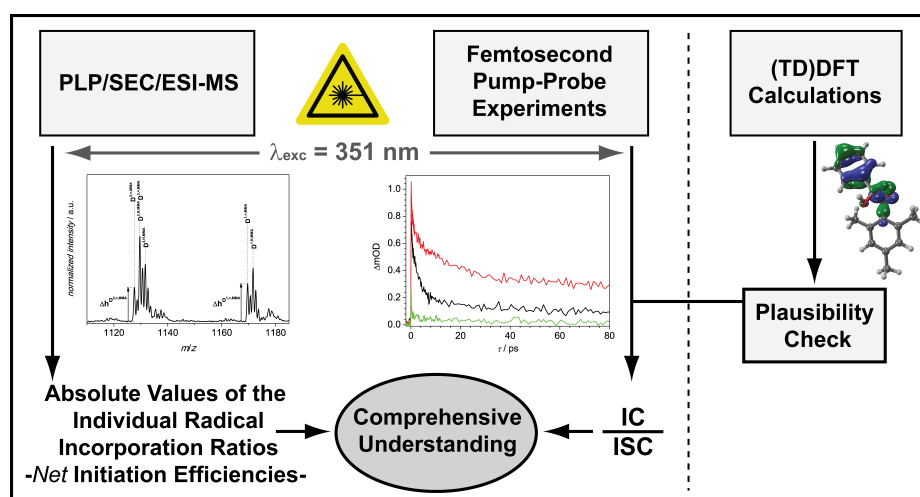
8

Concluding Remarks and Outlook

In the current thesis, an in-depth quantitative assessment of photoinitiation processes *via* the provision of relative *net-initiation* ratios associated with individual radical fragments originating from various photoinitiators was demonstrated. Furthermore, the application of coupled online SEC/ESI-MS to analyze the obtained polymers led to an improvement of the evaluation method (see Chapter 4 and Chapter 6). The origin dependence of the incorporation propensity of different types of photoinitiators was studied in detail (refer to Chapter 4 and Chapter 5) and in the course of the research it was found that femtosecond spectroscopy in combination with PLP/SEC/ESI-MS experiments yields not only insights into the relative *net-efficiency* of a radical fragment, yet also allows to correlate the observed *net-efficiencies* with the internal energy distribution within the excited molecule, i.e., the efficiency of the singlet to triplet ISC after laser excitation. The introduced experimental approach highlights the power of the combined techniques to – for the first time – generate quantitative knowledge about *net-efficiencies* of photoinitiators with their internal energy dissipation channels. Last but not least, the elucidated UV-induced endgroup transformation mechanism described in Chapter 7 needs to be considered during the light-triggered generation process of polymers.

8. Concluding Remarks and Outlook

Within an accepted extension project for the current thesis-topic from the German Research Council (DFG), the combined experimental set-up – femtosecond pump-probe spectroscopy in conjunction with DFT calculations and PLP/SEC/ESI-MS – should be exploited in a collaborative project between the KIT Polymer and Physical Chemistry institutes (an overview is given in Scheme 8.1). The key aim is the quantitative determination of the relative *net-initiation efficiency* via the now established PLP/SEC/ESI-MS technique for a wide range of radical fragments coupled with the quantitative understanding of the ISC behavior of the constituting initiator molecules, to arrive at a map of origin dependent radical fragment initiation efficiencies. A unique opportunity exists to – for the first time – provide a full and comprehensive understanding of final polymer endgroup distribution of photolytically generated radical fragments with the structure dependent internal energy conversion within the photoinitiators.



Scheme 8.1 Schematic representation of the research strategy applied in the accepted grant extension.

The main tasks of the extension project from the polymer chemistry point of view are:

- Providing single cation ionization in SEC/ESI-MS for macromolecules featuring nitrogen containing endgroups
- Synthesis of libraries of benzoin-derivative photoinitiators
- PLP/SEC/ESI-MS experiments on the benzoin-derivative as well as specialty photoinitiators such as 2-methyl-4'-(methylthio)-2-morpholinopropiophenone (MMMP) and phenylbis(2,4,6-trimethylbenzoyl)phosphine oxide (Irgacure 819)
- Assessment of the influence of the monomer structure on the incorporation propensity of the individual radical fragments

The main tasks of the extension project from the physical chemistry point of view are:

- Testing and calibrating the transient absorption spectrometer
- Femtosecond spectrometric and DFT assessment of the photoinitiators of the benzoin-type and the existing benzoyl fragment variation in benzoin depicted in Scheme 6.1
- Influence of the solvent environment on the outcome of the femtosecond experiments
- Femtosecond spectrometric and DFT assessment of the specialty photoinitiators MMMP and Irgacure 819
- Assessing the feasibility of femtosecond experiments in polymerizing systems

9

Materials

9.1. Materials Used in Chapter 4

Methyl methacrylate (MMA, Sigma-Aldrich, 99 %, stabilized), ethyl methacrylate (EMA, Acros, 99 %, stabilized), and butyl methacrylate (BMA, Acros, 99 %, stabilized) were freed from inhibitor by passing through a column of activated basic alumina (Merck). Benzoin (Sigma-Aldrich, 98 %) was recrystallized twice in ethanol prior to use. Benzene (Sigma-Aldrich, puriss. p.a.) was dried over molecular sieves (4 Å) for 4 h. Dioxane (Acros), selenium dioxide (Acros, 99.8 %), aluminum chloride (ABCR, anhydrous), and 2,4,6-trimethylacetophenone (Sigma-Aldrich, purum) were used as received. For SEC/ESI-MS measurements sodium iodide (Fluka, puriss. p.a.), tetrahydrofuran (THF, Scharlau, multisolvent GPC grade, 250 ppmBHT) and methanol (VWR, chromanorm) were also employed as received. For UV/Vis measurements methanol (VWR, chromanorm) was used. CDCl_3 was purchased from euriso-top.

9.2. Materials Used in Chapter 5

Methanol (Carl Roth, HPLC grade) was used as received. Benzoin (purchased from Sigma-Aldrich, 98 %) was recrystallized twice in ethanol prior to use.

9.3. Materials Used in Chapter 6

Methyl methacrylate (MMA, Sigma Aldrich, 99 %, stabilized) was freed from inhibitor by passing through a column of activated basic alumina (VWR). Benzoin (Sigma Aldrich, 98 %) was recrystallized twice in ethanol prior to use. Benzene (Sigma Aldrich, puriss. p.a.) was dried over molecular sieves (4 Å) for one day. Dioxane (Acros), selenium dioxide (Acros, 99.8 %), aluminium chloride (ABCR, anhydrous), 4-methylacetophenone (Alfa Aesar, 96 %), 2,4-dimethylacetophenone (Alfa Aesar, 97 %), 2,3,5,6-tetramethylacetophenone (Alfa Aesar, 98+ %) and 2,3,4,5,6-pentamethylacetophenone (Alfa Aesar, 98+ %) were used as received. For SEC/ESI-MS measurements sodium iodide (Fluka, puriss. p.a.), tetrahydrofuran (THF, Scharlau, multisolvent GPC grade, 250 ppm BHT) and methanol (VWR, chromanorm) were also employed as received. For UV/Vis measurements methanol (VWR, chromanorm) was used. CDCl_3 was purchased from euriso-top.

9.4. Materials Used in Chapter 7

Methyl methacrylate (MMA, Sigma Aldrich, 99 %, stabilized) was freed from inhibitor by passing through a column of activated basic alumina (VWR). Benzoin (Sigma Aldrich, 98 %) was recrystallized twice in ethanol prior to use. For the SEC/ESI-MS measurements sodium iodide (Fluka, puriss. p.a.), tetrahydrofuran (THF, Scharlau, multisolvent GPC grade, 250 ppm BHT) and methanol (VWR, chromanorm) were employed as received. Pd on activated carbon (Pd/C, Acros Organics, unreduced, 5 % Pd), hydrogen (H_2 , Air Liquide, 99.999 %) and a mixture of ethyl acetate (VWR, p.a.)/ ethanol (technical grade, 95 %) in a ratio of 1:1 were used for the hydrogenation experiments as received. For the post-irradiation PLP-experiments methyl isobutyrate (MIB, Acros Organics, 99 %) was used. Furthermore, hexane (VWR, p.a.) was used for precipitation of the synthesized benzoin-pMMA. Acetonitrile- D_3 and chloroform- D_1 for NMR and CIDNP experiments were purchased from Sigma-Aldrich and used without additional treatment.

10

List of Abbreviations

A	pre-exponential factor
A_i	amplitude
a	hyperfine coupling constant
APCI	atmospheric pressure chemical ionization
BBO crystal	barium borate crystal
Benzoin-pMMA	photo-initiated pMMA initiated by benzoin
BMA	butyl methacrylate
C	transfer constant
c	concentration
CI	chemical ionization
CID	collision-induced decay
CIDEP	chemically induced dynamic electron polarization
CIDNP	chemically induced dynamic nuclear polarization
CLD	chain length distribution
CPA	chirped pulse amplification
Da	dalton
DCM	methylene chloride
Δg	g -factor difference of radicals within a primary radical pair
DFT	density functional theory

10. List of Abbreviations

E	energy
E_a	activation energy
e.g.	exempli gratia (for example)
EI	electron ionization
EMA	ethyl methacrylate
ϵ	type of the exit channel
eq	equivalent
ESI	electrospray ionization
ESI-MS	electrospray ionization-mass spectrometry
ESR	electron spin resonance spectroscopy
eV	electron volt
excimer	excited dimer
f	initiator efficiency
FAB	fast atom bombardment
FI	field ionization
FT-ICR	fourier transform-ion cyclotron resonance
fs	femtosecond
I^{\cdot}	signs of polarizations
HOMO	highest occupied molecular orbital
Hz	hertz
I_2	initiator molecule
IC	internal conversion
ICR	ion-cyclotron resonance
i.e.	id est (that is)
ISC	intersystem crossing
IUPAC	International Union of Pure and Applied Chemistry
k_d	rate coefficient of initiator decomposition
kHz	kilohertz
k_i	rate coefficient of initiation
kJ	kilojoule
k_p	rate coefficient of propagation
$k_{t,c}$	rate coefficient for termination by combination
$k_{t,d}$	rate coefficient for termination by disproportionation
k_{tr}	rate coefficient for transfer
L	liter
LASER	Light Amplification by Stimulated Emission of Radiation
L_i	inflection point
LUMO	lowest unoccupied molecular orbital
M	monomer

MA	methyl acrylate
MALDI	matrix-assisted laser desorption ionization
MALDI-ToF	matrix-assisted laser desorption ionization - time-of-flight
mg	milligram
MHz	megahertz
μ	multiplicity of the precursor
μ s	microseconds
MIB	methyl isobutyrate
mJ	millijoule
mL	milliliter
mm	millimeter
M_a	molecular weight of the ion which is bound to the polymer
M_i	molecular weight at a specific inflection point
M_M	molar mass of one monomer unit
MMA	methyl methacrylate
mol	mole
mmol	millimole
μ M	micromole
MO	molecular orbital
M_r	molecular weight of the unloaded species
MS	mass spectrometry
m/z -ratio	mass-to-charge ratio
n	number of charges per polymer chain
nm	nanometer
NMR	nuclear magnetic resonance
NOPA	noncollinear optical parametric amplifier
ns	nanosecond
ν	laser pulse repetition frequency
OD	optical density
P	polymer
pBMA	poly(butyl methacrylate)
pEMA	poly(ethyl methacrylate)
ps	picosecond
PLP	pulsed laser polymerization
PLP-SEC	pulsed laser polymerization-size-exclusion chromatography
pMMA	poly(methyl methacrylate)
QUIPS	quenched instationary polymerization system
R	gas constant
RAFT	reversible addition-fragmentation chain transfer

10. List of Abbreviations

RAFT-CLD-T	reversible addition-fragmentation chain transfer-chain length distribution-termination
RF	radio frequency
$R_i\cdot$	radical of chain length i
RI	refractive index
r_0	bond distance before radical formation
r_m	bond distance at the S_0 - T_0 mixture point
S	singlet state
SEC	size-exclusion chromatography
SEC/ESI-MS	size-exclusion chromatography-electrospray ionization-mass spectrometry
SOP	single oligomer profile
SP-PLP-ESR	single pulse-pulsed laser polymerization electron spin resonance spectroscopy
SP-PLP-NIR	single pulse-pulsed laser polymerization near-infrared spectroscopy
T	temperature
T	triplet state
τ_i	time constant
TA	transient absorption
TDDFT	time-dependent density functional theory
THF	tetrahydrofuran
ToF	time-of-flight
UV	ultraviolet
UV/Vis	ultraviolet/visible
vs.	versus
X	transfer agent
ZPC	zero point correction

Bibliography

- [1] Barner-Kowollik, C.; Du Prez, F. E.; Espeel, P.; Hawker, C. J.; Junkers, T.; Schlaad, H.; Van Camp, W. *Angew. Chem. Int. Ed.* **2011**, *50*, 60–62.
- [2] Barner-Kowollik, C., Ed. *Handbook of RAFT Polymerization*; Wiley-VCH, Weinheim, **2008**.
- [3] Moad, G.; Rizzardo, E.; Thang, S. H. *Aust. J. Chem.* **2009**, *62*, 1402–1472.
- [4] Matyjaszewski, K.; Xia, J. *Chem. Rev.* **2001**, *101*, 2921–2990.
- [5] Ouchi, M.; Terashima, T.; Sawamoto, M. *Chem. Rev.* **2009**, *109*, 4963–5050.
- [6] Hawker, C. J.; Bosman, A. W.; Harth, E. *Chem. Rev.* **2001**, *101*, 3661–3688.
- [7] Lalevée, J.; Blanchard, N.; Chany, A. C.; El-Roz, M.; Souane, R.; Graff, B.; Allonas, X.; Fouassier, J. P. *Macromolecules* **2009**, *42*, 6031–6037.
- [8] Lalevée, J.; Blanchard, N.; Chany, A.-C.; Tehfe, M.-A.; Allonas, X.; Fouassier, J. P. *J. Phys. Org. Chem.* **2009**, *22*, 986–993.
- [9] Lalevée, J.; Roz, M. E. I.; Tehfe, M. A.; Alaaeddine, M.; Allonas, X.; Fouassier, J. P. *J. Photopolym. Sci. Technol.* **2009**, *22*, 587–590.
- [10] Lalevée, J.; Tehfe, M.-A.; Gimes, D.; Fouassier, J. P. *Macromolecules* **2010**, *43*, 6608–6615.
- [11] Lalevée, J.; Morlet-Savary, F.; Roz, M. E.; Allonas, X.; Fouassier, J. P. *Macromol. Chem. Phys.* **2009**, *210*, 311–319.
- [12] Lalevée, J.; Blanchard, N.; Tehfe, M. A.; Fries, C.; Morlet-Savary, F.; Gimes, D.; Fouassier, J. P. *Polym. Chem.* **2011**, *2*, 1077–1084.
- [13] Lalevée, J.; Fouassier, J. P. *Polym. Chem.* **2011**, *2*, 1107–1113.

- [14] Lalevée, J.; Tehfe, M. A.; Morlet-Savary, F.; Graff, B.; Allonas, X.; Fouassier, J. P. *Prog. Org. Coat.* **2011**, *70*, 83–90.
- [15] Balta, D. K.; Arsu, N.; Yagci, Y.; Sundaresan, A. K.; Jockusch, S.; Turro, N. J. *Macromolecules* **2011**, *44*, 2531–2535.
- [16] Karasu, F.; Arsu, N.; Jockusch, S.; Turro, N. J. *Macromolecules* **2009**, *42*, 7318–7323.
- [17] Keskin, S.; Jockusch, S.; Turro, N. J.; Arsu, N. *Macromolecules* **2008**, *41*, 4631–4634.
- [18] Balta, D. K.; Arsu, N.; Yagci, Y.; Jockusch, S.; Turro, N. J. *Macromolecules* **2007**, *40*, 4138–4141.
- [19] Yagci, Y.; Jockusch, S.; Turro, N. J. *Macromolecules* **2010**, *43*, 6245–6260.
- [20] Yilmaz, G.; Aydogan, B.; Temel, G.; Arsu, N.; Moszner, N.; Yagci, Y. *Macromolecules* **2010**, *43*, 4520–4526.
- [21] Yilmaz, G.; Tuzun, A.; Yagci, Y. *J. Polym. Sci., Part A: Polym. Chem.* **2010**, *48*, 5120–5125.
- [22] Aschenbrücker, J.; Buback, M.; Ernsting, N. P.; Schroeder, J.; Steegmüller, U. *Ber. Bunsen-Ges. Phys. Chem.* **1998**, *102*, 965–971.
- [23] Aschenbrücker, J.; Buback, M.; Ernsting, N. P.; Schroeder, J.; Steegmüller, U. *J. Phys. Chem. B* **1998**, *102*, 5552–5555.
- [24] Yamashita, M.; Fenn, J. B. *J. Phys. Chem.* **1984**, *88*, 4451–4459.
- [25] Yamashita, M.; Fenn, J. B. *J. Phys. Chem.* **1984**, *88*, 4671–4675.
- [26] Aaserud, D. J.; Prokai, L.; Simonsick, W. J. *Anal. Chem.* **1999**, *71*, 4793–4799.
- [27] Gruending, T.; Guilhaus, M.; Barner-Kowollik, C. *Anal. Chem.* **2008**, *80*, 6915–6927.
- [28] Karas, M.; Bachmann, D.; Bahr, U.; Hillenkamp, F. *Int. J. Mass Spectrom. Ion Processes* **1987**, *78*, 53–68.
- [29] Karas, M.; Bachmann, D.; Hillenkamp, F. *Anal. Chem.* **1985**, *57*, 2935–2939.
- [30] Karas, M.; Bahr, U. *TrAC, Trends Anal. Chem.* **1986**, *5*, 90–93.
- [31] Barner-Kowollik, C., Gründling, T., Falkenhagen, J., Weidner, S., Eds. *Mass Spectrometry in Polymer Chemistry*; Wiley-VCH, Weinheim, **2012**.
- [32] Gruending, T.; Weidner, S.; Falkenhagen, J.; Barner-Kowollik, C. *Polym. Chem.* **2010**, *1*, 599–617.

- [33] Zetterlund, P. B.; Busfield, W. K.; Jenkins, I. D. *Macromolecules* **2002**, *35*, 7232–7237.
- [34] Nakamura, T.; Busfield, W. K.; Jenkins, I. D.; Rizzardo, E.; Thang, S. H.; Suyama, S. *J. Am. Chem. Soc.* **1997**, *119*, 10987–10991.
- [35] Buback, M.; Günzler, F.; Russell, G. T.; Vana, P. *Macromolecules* **2009**, *42*, 652–662.
- [36] Hutchinson, R. A.; Richards, J. R.; Aronson, M. T. *Macromolecules* **1994**, *27*, 4530–4537.
- [37] Buback, M.; Gilbert, R. G.; Hutchinson, R. A.; Klumperman, B.; Kuchta, F.-D.; Manders, B. G.; O'Driscoll, K. F.; Russell, G. T.; Schweer, J. *Macromol. Chem. Phys.* **1995**, *196*, 3267–3280.
- [38] Beuermann, S.; Buback, M.; Davis, T. P.; Gilbert, R. G.; Hutchinson, R. A.; Olaj, O. F.; Russell, G. T.; Schweer, J.; van Herk, A. M. *Macromol. Chem. Phys.* **1997**, *198*, 1545–1560.
- [39] Beuermann, S.; Buback, M.; Davis, T. P.; Gilbert, R. G.; Hutchinson, R. A.; Kajiwara, A.; Klumperman, B.; Russell, G. T. *Macromol. Chem. Phys.* **2000**, *201*, 1355–1364.
- [40] Szablan, Z.; Lovestead, T. M.; Davis, T. P.; Stenzel, M. H.; Barner-Kowollik, C. *Macromolecules* **2007**, *40*, 26–39.
- [41] Szablan, Z.; Junkers, T.; Koo, S. P. S.; Lovestead, T. M.; Davis, T. P.; Stenzel, M. H.; Barner-Kowollik, C. *Macromolecules* **2007**, *40*, 6820–6833.
- [42] Günzler, F.; Wong, E. H. H.; Koo, S. P. S.; Junkers, T.; Barner-Kowollik, C. *Macromolecules* **2009**, *42*, 1488–1493.
- [43] Barner-Kowollik, C.; Vana, P.; Davis, T. P. *J. Polym. Sci., Part A: Polym. Chem.* **2002**, *40*, 675–681.
- [44] Zammit, M. D.; Davis, T. P.; Haddleton, D. M. *Macromolecules* **1996**, *29*, 492–494.
- [45] Willemse, R. X. E.; Staal, B. B. P.; van Herk, A. M.; Pierik, S. C. J.; Klumperman, B. *Macromolecules* **2003**, *36*, 9797–9803.
- [46] Gruending, T.; Voll, D.; Guilhaus, M.; Barner-Kowollik, C. *Macromol. Chem. Phys.* **2010**, *211*, 80–90.
- [47] Buback, M.; Frauendorf, H.; Vana, P. *J. Polym. Sci., Part A: Polym. Chem.* **2004**, *42*, 4266–4275.

- [48] Buback, M.; Frauendorf, H.; Günzler, F.; Vana, P. *J. Polym. Sci., Part A: Polym. Chem.* **2007**, *45*, 2453–2467.
- [49] Buback, M.; Frauendorf, H.; Günzler, F.; Vana, P. *Polymer* **2007**, *48*, 5590–5598.
- [50] Buback, M.; Frauendorf, H.; Janssen, O.; Vana, P. *J. Polym. Sci., Part A: Polym. Chem.* **2008**, *46*, 6071–6081.
- [51] Abel, B.; Aßmann, J.; Buback, M.; Kling, M.; Schmatz, S.; Schroeder, J. *Angew. Chem. Int. Ed.* **2003**, *42*, 299–303.
- [52] Abel, B.; Assmann, J.; Buback, M.; Grimm, C.; Kling, M.; Schmatz, S.; Schroeder, J.; Witte, T. *J. Phys. Chem. A* **2003**, *107*, 9499–9510.
- [53] Abel, B.; Buback, M.; Kling, M.; Schmatz, S.; Schroeder, J. *J. Am. Chem. Soc.* **2003**, *125*, 13274–13278.
- [54] Zammit, M. D.; Davis, T. P.; Haddleton, D. M.; Suddaby, K. G. *Macromolecules* **1997**, *30*, 1915–1920.
- [55] Buback, M.; Frauendorf, H.; Günzler, F.; Huff, F.; Vana, P. *Macromol. Chem. Phys.* **2009**, *210*, 1591–1599.
- [56] Kaur, M.; Srivastava, A. K. *J. Macromol. Sci., Polym. Rev.* **2002**, *42*, 481–512.
- [57] *BASF Website*; available at: <http://www.basf.com/group/corporate/en/overview-page:/Brand+Irgacure>.
- [58] Ge, J.; Trujillo, M.; Stansbury, J. *J. Dent. Mat.* **2005**, *21*, 1163–1169.
- [59] Anseth, K.; Newman, S.; Bowman, C. N. In *Biopolymers II*; Peppas, N., Langer, R., Eds.; Advances in Polymer Science; Springer, Berlin / Heidelberg, **1995**; Vol. 122; pp 177–217.
- [60] Fisher, J. P.; Dean, D.; Engel, P. S.; Mikos, A. G. *Annu. Rev. Mater. Sci.* **2001**, *31*, 171–181.
- [61] Anseth, K. S.; Metters, A. T.; Bryant, S. J.; Martens, P. J.; Elisseeff, J. H.; Bowman, C. N. *J. Controlled Release* **2002**, *78*, 199–209.
- [62] Sun, H.-B.; Kawata, S. *NMR, 3D Analysis and Photopolymerization*; Advances in Polymer Science; Springer, Berlin / Heidelberg, **2004**; Vol. 170; pp 169–273.

- [63] Arsu, N.; Reetz, I.; Yagci, Y.; Mishra, M. K. In *Handbook of Vinyl Polymers: Radical Polymerization, Process, and Technology*; Mishra, M. K., Yagci, Y., Eds.; CRC Press: Boca Raton, FL, **2009**; Vol. 20; Chapter Photoinitiated Radical Vinyl Polymerization, pp 141–204.
- [64] Yagci, Y.; Reetz, I. *Prog. Polym. Sci.* **1998**, *23*, 1485–1538.
- [65] Kutal, C.; Grutsch, P. A.; Yang, D. B. *Macromolecules* **1991**, *24*, 6872–6873.
- [66] Balta, D. K.; Cetiner, N.; Temel, G.; Turgut, Z.; Arsu, N. *J. Photochem. Photobiol., A* **2008**, *199*, 316–321.
- [67] Balta, D. K.; Temel, G.; Aydin, M.; Arsu, N. *Eur. Polym. J.* **2010**, *46*, 1374–1379.
- [68] Saraiva, M. F.; Couri, M. R. C.; Le Hyaric, M.; de Almeida, M. V. *Tetrahedron* **2009**, *65*, 3563–3572.
- [69] Dietlin, C.; Allonas, X.; Morlet-Savary, F.; Fouassier, J. P.; Visconti, M.; Norcini, G.; Romagnano, S. *J. Appl. Polym. Sci.* **2008**, *109*, 825–833.
- [70] Gruber, H. F. *Prog. Polym. Sci.* **1992**, *17*, 953–1044.
- [71] Hageman, H. J. *Prog. Org. Coat.* **1985**, *13*, 123–150.
- [72] Arsu, N.; Aydin, M.; Yagci, Y.; Jockusch, S.; Turro, N. J. In *Photochemistry and UV Curing: New Trends*; Fouassier, J. P., Ed.; Research Signpost, Fort P. O.: Trivandrum, **2006**; p 37/661.
- [73] Vana, P.; Davis, T. P.; Barner-Kowollik, C. *Aust. J. Chem.* **2002**, *55*, 315–318.
- [74] Junkers, T.; Wong, E. H. H.; Szablan, Z.; Davis, T. P.; Stenzel, M. H.; Barner-Kowollik, C. *Macromol. Rapid Commun.* **2008**, *29*, 503–510.
- [75] Günzler, F. Ph.D. thesis, University of Göttingen, **2008**.
- [76] Hiemenz, P. C., Lodge, T. P., Eds. *Polymer Chemistry*, 2nd ed.; CRC Press: Boca Raton, FL, **2007**; pp 77–109.
- [77] Matyjaszewski, K., Davis, T. P., Eds. *Handbook of Radical Polymerization*; John Wiley & Sons, Inc., Hoboken, **2002**; pp 187–261.
- [78] Buback, M.; Busch, M.; Kowollik, C. *Macromol. Theory Simul.* **2000**, *9*, 442–452.
- [79] Kuhlmann, R.; Schnabel, W. *Polymer* **1977**, *18*, 1163–1168.
- [80] Hutchison, J.; Lambert, M. C.; Ledwith, A. *Polymer* **1973**, *14*, 250–254.

- [81] Botman, J. I. M.; Derksen, A. T. A. M.; van Herk, A. M.; Jung, M.; Kuchta, F.-D.; Manders, L. G.; Timmermans, C. J.; de Voigt, M. J. A. *Nucl. Instrum. Methods Phys. Res., Sect. B* **1998**, *139*, 490–494.
- [82] Boenig, H. V. In *Encyclopedia of Polymer Science and Engineering*; Mark, H. F., Bikales, N. M., Overberger, C. G., Menges, G., Eds.; Wiley-Interscience, New York, **1988**; Vol. 11; pp 248–261.
- [83] Cantero, I.; Otero, T. F. *Rev. Plast. Mod.* **1996**, *72*, 46–54.
- [84] Bacon, R. G. R. Reduction Activation: A New Polymerisation Technique; *Trans. Faraday Soc.*, **1946**, Vol. 42, pp 140–155.
- [85] Bacon, R. G. R. The Initiation of Polymerisation Processes by Redox Catalysts; *Quarterly Reviews*, **1955**, Vol. 9, pp 287–310.
- [86] Ozturk, T.; Cakmak, I. *Iran. Polym. J.* **2007**, *16*, 561–581.
- [87] Olaj, O. F.; Kauffmann, H. F.; Breitenbach, J. W. *Makromol. Chem.* **1977**, *178*, 2707–2717.
- [88] Kauffmann, H. F.; Olaj, O. F.; Breitenbach, J. W. *Makromol. Chem.* **1976**, *177*, 939–945.
- [89] Olaj, O. F.; Kauffmann, H. F.; Breitenbach, J. W.; Bieringer, H. *J. Polym. Sci., Polym. Lett. Ed.* **1977**, *15*, 229–233.
- [90] Buback, M.; Hinton, C. *Z. Phys. Chem.* **1996**, *193*, 61–85.
- [91] Buback, M.; Lendle, H. *Z. Naturforsch.* **1981**, *36a*, 1371–1377.
- [92] Schnöll-Bitai, I. *Macromol. Rapid Commun.* **1999**, *20*, 162–166.
- [93] Schnöll-Bitai, I. *Macromol. Theory Simul.* **2000**, *9*, 230–241.
- [94] Vana, P.; Yee, L. H.; Davis, T. P. *Macromolecules* **2002**, *35*, 3008–3016.
- [95] Tonge, P., Matthew; Kajiwara, A.; Kamachi, M.; Gilbert, R. G. *Polymer* **1998**, *39*, 2305–2313.
- [96] Buback, M.; Kowollik, C.; Kamachi, M.; Kajiwara, A. *Macromolecules* **1998**, *31*, 7208–7212.
- [97] Van Herk, A. M. *Macromol. Theory Simul.* **2000**, *9*, 433–441.

- [98] Brandrup, A., Immergut, E. H., Grulke, E. A., Eds. *Polymer Handbook*, 4th ed.; John Wiley & Sons, Inc., **1999**; p II/97.
- [99] Mayo, F. R. *J. Am. Chem. Soc.* **1943**, *65*, 2324–2329.
- [100] Christie, D. I.; Gilbert, R. G. *Macromol. Chem. Phys.* **1996**, *197*, 403–412.
- [101] Christie, D. I.; Gilbert, R. G. *Macromol. Chem. Phys.* **1997**, *198*, 663–663.
- [102] Heuts, J. P. A.; Davis, T. P.; Russell, G. T. *Macromolecules* **1999**, *32*, 6019–6030.
- [103] Mahabadi, H. K. *Macromolecules* **1985**, *18*, 1319–1324.
- [104] Moad, G.; Solomon, D. H. In *Azo and Peroxy Initiators*; Moad, G., Solomon, D. H., Eds.; Pergamon Press, London, **1989**; Vol. 3; p 97.
- [105] Moad, G.; Solomon, D. H. In *Chemistry of Bimolecular Termination*; Moad, G., Solomon, D. H., Eds.; Pergamon Press, London, **1989**; Vol. 3; p 147.
- [106] Buback, M.; Hippler, H.; Schweer, J.; Vögele, H.-P. *Makromol. Chem. Rapid Commun.* **1986**, *7*, 261–265.
- [107] Buback, M.; Junkers, T. *Macromol. Chem. Phys.* **2006**, *207*, 1640–1650.
- [108] Buback, M.; Egorov, M.; Junkers, T.; Panchenko, E. *Macromol. Rapid Commun.* **2004**, *25*, 1004–1009.
- [109] Vana, P.; Davis, T. P.; Barner-Kowollik, C. *Macromol. Rapid Commun.* **2002**, *23*, 952–956.
- [110] Johnston-Hall, G.; Theis, A.; Monteiro, M. J.; Davis, T. P.; Stenzel, M. H.; Barner-Kowollik, C. *Macromol. Chem. Phys.* **2005**, *206*, 2047–2053.
- [111] Kneubühl, F. K.; Sigrist, M. W. *Laser*; Vieweg & Teubner, Studium, Wiesbaden, **2008**.
- [112] Birks, J. B. *Rep. Prog. Phys.* **1975**, *38*, 903–974.
- [113] Houtermans, F. G. *Helv. Phys. Acta* **1960**, *33*, 933ff.
- [114] Basov, N. G.; Danilychev, V. A.; Popov, Y. M. *Zh. Eksp. Fiz. i Tekh. Pis'ma. Red.* **1970**, *12*, 473ff.
- [115] Marowsky, G., Basting, D., Eds. *Excimer Laser Technolog*; Springer-Verlag, Berlin, **2005**.

- [116] Genkin, V. N.; Sokolov, V. V. *Doklady Akademii Nauk SSSR* **1977**, *234*, 94–96.
- [117] Aleksandrov, A. P.; Genkin, V. N.; Kitai, M. S.; Smirnova, I. M.; Sokolov, V. V. *Kvantovaya Elektronika (Moscow); J. Quant. Electron.* **1977**, *4*, 976–981.
- [118] Olaj, O. F.; Bitai, I.; Hinkelmann, F. *Makromol. Chem.* **1987**, *188*, 1689–1702.
- [119] Olaj, O. F.; Schnöll-Bitai, I. *Eur. Polym. J.* **1989**, *25*, 635–641.
- [120] Olaj, O. F.; Zifferer, G. *DECHEMA Monographien* **1995**, *131*, 579–598.
- [121] Beuermann, S.; Buback, M. *Prog. Polym. Sci.* **2002**, *27*, 191–254.
- [122] Beuermann, S.; Buback, M.; Davis, T. P.; García, N.; Gilbert, R. G.; Hutchinson, R. A.; Kajiwara, A.; Kamachi, M.; Lacík, I.; Russell, G. T. *Macromol. Chem. Phys.* **2003**, *204*, 1338–1350.
- [123] Asua, J. M.; Beuermann, S.; Buback, M.; Castignolles, P.; Charleux, B.; Gilbert, R. G.; Hutchinson, R. A.; Leiza, J. R.; Nikitin, A. N.; Vairon, J.-P.; van Herk, A. M. *Macromol. Chem. Phys.* **2004**, *205*, 2151–2160.
- [124] Beuermann, S.; Buback, M.; Hesse, P.; Kuchta, F. D.; Lacik, I.; van Herk, A. M. *Pure Appl. Chem.* **2007**, *79*, 1463–1469.
- [125] Barner-Kowollik, C.; Bennet, F.; Schneider-Baumann, M.; Voll, D.; Rölle, T.; Fäcke, T.; Weiser, M.-S.; Bruder, F.-K.; Junkers, T. *Polym. Chem.* **2010**, *1*, 470–479.
- [126] Montaudo, G., Lattimer, R. P., Eds. *Mass Spectroscopy of Polymers*; CRC Press LCC: Boca Raton, FL, **2002**.
- [127] de Koster, C. G.; Duursma, M. C.; van Rooij, G. J.; Heeren, R. M. A.; Boon, J. J. *Rapid Commun. Mass Spectrom.* **1995**, *9*, 957–962.
- [128] Fenn, J. B.; Mann, M.; Meng, C. K.; Wong, S. F.; Whitehouse, C. M. *Science* **1989**, *246*, 64–71.
- [129] Raffaelli, A. *J. Chromatogr.* **2007**, *72*, 11ff.
- [130] Tanaka, K.; Waki, H.; Ido, Y.; Akita, S.; Yoshida, Y.; Yoshida, T.; Matsuo, T. *Rapid Commun. Mass Spectrom.* **1988**, *2*, 151–153.
- [131] Busch, K. L. *J. Mass Spectrom.* **1995**, *30*, 233–240.
- [132] Märk, T. D.; Dunn, G. H. *Electron Impact Ionization*; Springer-Verlag, New-York, **1985**.

- [133] Harrison, A. G. *Chemical Ionization Mass Spectrometry*, 2nd ed.; CRC Press LCC: Boca Raton, **1992**.
- [134] Beckey, H. D. *Principles of Field Ionization and Field Desorption Mass Spectrometry*; Pergamon, Oxford, **1977**.
- [135] Dole, M.; Mack, L. L.; Hines, R. L.; Mobley, R. C.; Ferguson, L. D.; Alice, M. B. *J. Chem. Phys.* **1968**, *49*, 2240–2249.
- [136] Mack, L. L.; Kralik, P.; Rheude, A.; Dole, M. *J. Chem. Phys.* **1970**, *52*, 4977–4986.
- [137] Gaskell, S. J. *J. Mass Spectrom.* **1997**, *32*, 677–688.
- [138] Kebarle, P.; Tang, L. *Anal. Chem.* **1993**, *65*, 972A–986A.
- [139] Lomeli, S. H.; Yin, S.; Ogorzalek, R. R.; Loo, R. R.; Loo, J. A. *J. Am. Soc. Mass Spectrom.* **2009**, *20*, 593–596.
- [140] Ashton, D. S.; Beddell, C. R.; Cooper, D. J.; Green, B. N.; Oliver, R. W. A. *Org. Mass Spectrom.* **1993**, *28*, 721–728.
- [141] Fenn, J. B. *J. Am. Soc. Mass Spectrom.* **1993**, *4*, 524–535.
- [142] Whitehouse, C. M.; Dreyer, R. N.; Yamashita, M.; Fenn, J. B. *Anal. Chem.* **1985**, *57*, 675–679.
- [143] Cole, R. B., Ed. *Electrospray Ionization Mass Spectrometry Fundamentals, Instrumentation and Applications*, 1st ed.; Wiley, New York, **1997**.
- [144] Prokai, L.; Simonsick, W. J. *Rapid Commun. Mass Spectrom.* **1993**, *7*, 853–856.
- [145] Simonsick, W. J.; Prokai, L. In *Chromatographic Characterization of Polymers*; Provder, T., Barth, H. G., Urban, M. W., Eds.; American Chemical Society, **1995**; Chapter 4, pp 41–56.
- [146] Gruendling, T.; Guilhaus, M.; Barner-Kowollik, C. *Macromolecules* **2009**, *42*, 6366–6374.
- [147] Zewail, A. H. *Angew. Chem. Int. Ed.* **2000**, *39*, 2586–2631.
- [148] Kryukov, P. G. *Quantum Electron.* **2001**, *31*, 95–119.
- [149] Dubietis, A.; Butkus, R.; Piskarskas, A. P. *IEEE J. Sel. Top. Quantum Electron.* **2006**, *12*, 163–172.

- [150] Wolf, T. J. A. Photoinduced dynamics of radicals and their precursors in solution on an ultrafast time scale: A femtosecond transient absorption study. Ph.D. thesis, Karlsruhe Institute of Technology (KIT), **2012**.
- [151] Riedle, E.; Beutter, M.; Lochbrunner, S.; Piel, J.; Schenkl, S.; Spörlein, S.; Zinth, W. *Appl. Phys. B: Lasers Opt.* **2000**, *71*, 457–465.
- [152] Bargon, J.; Fischer, H.; Johnsen, U. *Z. Naturforsch., A: Phys. Sci.* **1967**, *22*, 1551–1555.
- [153] Ward, H. R.; Lawler, R. G. *J. Am. Chem. Soc.* **1967**, *89*, 5518–5519.
- [154] Closs, G. L. *J. Am. Chem. Soc.* **1969**, *91*, 4552–4554.
- [155] Closs, G. L.; Closs, L. E. *J. Am. Chem. Soc.* **1969**, *91*, 4550–4552.
- [156] Closs, G. L.; Trifunac, A. D. *J. Am. Chem. Soc.* **1969**, *91*, 4554–4555.
- [157] Closs, G. L.; Trifunac, A. D. *J. Am. Chem. Soc.* **1970**, *92*, 2183–2184.
- [158] Kaptein, R.; Oosterhoff, J. L. *Chem. Phys. Lett.* **1969**, *4*, 195–197.
- [159] Kaptein, R.; Oosterhoff, J. L. *Chem. Phys. Lett.* **1969**, *4*, 214–216.
- [160] Hore, J.; Broadhurst, R. W. *Progr. NMR Spec.* **1993**, *25*, 345–402.
- [161] Goetz, M. *Advances in Photochemistry*; John Wiley & Sons, Inc., **2007**; pp 63–163.
- [162] Yurkovskaya, A.; Morozova, O.; Gescheidt, G. In *Encyclopedia of Radicals in Chemistry, Biology and Materials*; Chatgililoglu, C., Studer, A., Eds.; John Wiley & Sons, Ltd., London, **2012**.
- [163] Hesse, M.; Meier, H.; Zeeh, B. *Spektroskopische Methoden in der organischen Chemie*, 7th ed.; Thieme, Stuttgart, **2005**.
- [164] Seifert, K.-G. *Chem. unserer Zeit* **1976**, *3*, 84–93.
- [165] Barner-Kowollik, C.; Günzler, F.; Junkers, T. *Macromolecules* **2008**, *41*, 8971–8973.
- [166] Junkers, T.; Voll, D.; Barner-Kowollik, C. *e-Polymers* **2009**, 76.
- [167] Spichty, M.; Turro, N. J.; Rist, G.; Birbaum, J.-L.; Dietliker, K.; Wolf, J.-P.; Gescheidt, G. *J. Photochem. Photobiol., A* **2001**, *142*, 209–213.
- [168] Weinstock, H. H.; Fuson, R. C. *J. Am. Chem. Soc.* **1936**, *58*, 1986–1988.
- [169] Fuson, R. C.; Weinstock, H. H.; Ulllyot, G. E. *J. Am. Chem. Soc.* **1935**, *57*, 1803–1804.

- [170] Gray, A. R.; Fuson, R. C. *J. Am. Chem. Soc.* **1934**, *56*, 739–741.
- [171] Gruending, T.; Guilhaus, M.; Barner-Kowollik, C. *Macromol. Rapid Commun.* **2009**, *30*, 589–597.
- [172] Weinstock, H. H.; Fuson, R. C. *J. Am. Chem. Soc.* **1936**, *58*, 1233–1236.
- [173] Colley, C. S.; Grills, D. C.; Besley, N. A.; Jockusch, S.; Matousek, P.; Parker, A. W.; Towrie, M.; Turro, N. J.; Gill, P. M. W.; George, M. W. *J. Am. Chem. Soc.* **2002**, *124*, 14952–14958.
- [174] Voll, D.; Junkers, T.; Barner-Kowollik, C. *Macromolecules* **2011**, *44*, 2542–2551.
- [175] Wolf, T. J. A.; Fischer, J.; Wegener, M.; Unterreiner, A.-N. *Opt. Lett.* **2011**, *36*, 3188–3190.
- [176] Jankowiak, A.; Kaszynski, P. *J. Org. Chem.* **2009**, *74*, 7441–7448.
- [177] Englman, R.; Jortner, J. *Mol. Phys.* **1970**, *18*, 145–164.
- [178] Pawelka, Z.; Kryachko, E. S.; Zeegers-Huyskens, T. *Chem. Phys.* **2003**, *287*, 143–153.
- [179] Lewis, F. D.; Lauterbach, R. T.; Heine, H. G.; Hartmann, W.; Rudolph, H. *J. Am. Chem. Soc.* **1975**, *97*, 1519–1525.
- [180] Lipson, M.; Turro, N. J. *J. Photochem. Photobiol., A* **1996**, *99*, 93–96.
- [181] Shrestha, N. K.; Yagi, E. J.; Takatori, Y.; Kawai, A.; Kajii, Y.; Shibuya, K.; Obi, K. *J. Photochem. Photobiol., A* **1998**, *116*, 179–185.
- [182] Ahlrichs, R.; Bär, M.; Häser, M.; Horn, H.; Kölmel, C. *Chem. Phys. Lett.* **1989**, *162*, 165–169.
- [183] Treutler, O.; Ahlrichs, R. *J. Chem. Phys.* **1995**, *102*, 346–354.
- [184] Eichkorn, K.; Treutler, O.; Öhm, H.; Häser, M.; Ahlrichs, R. *Chem. Phys. Lett.* **1995**, *240*, 283–290.
- [185] Eichkorn, K.; Treutler, O.; Öhm, H.; Häser, M.; Ahlrichs, R. *Chem. Phys. Lett.* **1995**, *242*, 652–660.
- [186] Eichkorn, K.; Weigend, F.; Treutler, O.; Ahlrichs, R. *Theor. Chem. Acc.: Theory, Computation, and Modeling* **1997**, *97*, 119–124.
- [187] Weigend, F. *Phys. Chem. Chem. Phys.* **2006**, *8*, 1057–1065.

- [188] Schäfer, A.; Horn, H.; Ahlrichs, R. *J. Chem. Phys.* **1992**, *97*, 2571–2577.
- [189] Kendall, R. A.; Dunning, T. H.; Harrison, R. J. *J. Chem. Phys.* **1992**, *96*, 6796–6806.
- [190] Furche, F.; Rappoport, D. In *Computational Photochemistry*, theoretical and computational chemistry ed.; Olivucci, M., Ed.; Elsevier: Amsterdam, **2005**; Vol. 16.
- [191] Bauernschmitt, R.; Ahlrichs, R. *Chem. Phys. Lett.* **1996**, *256*, 454–464.
- [192] Bauernschmitt, R.; Ahlrichs, R. *J. Chem. Phys.* **1996**, *104*, 9047–9052.
- [193] Nudelman, N.; Schulz, H. *J. Chem. Res., Synop.* **1999**, 422–423.
- [194] Rathman, T. L.; Woltermann, C. J. *Pharm. Chem. J.* **2003**, *2*, 6–8.
- [195] Fileti, E. E.; Canuto, S. *Int. J. Quantum. Chem.* **2005**, *104*, 808–815.
- [196] Biswas, S. C.; Sen, R. K. *Chem. Phys. Lett.* **1983**, *94*, 415–416.
- [197] Brown, C. J.; Sadanaga, R. *Acta Crystallogr.* **1965**, *18*, 158–164.
- [198] Das, K. K.; Majumdar, D. *THEOCHEM* **1993**, *288*, 55–61.
- [199] El-Sayed, M. A. *J. Chem. Phys.* **1963**, *38*, 2834–2838.
- [200] Seidl, B.; Liska, R.; Grabner, G. *J. Photochem. Photobiol., A* **2006**, *180*, 109–117.
- [201] Jockusch, S.; Koptuyug, I. V.; McGarry, P. F.; Sluggett, G. W.; Turro, N. J.; Watkins, D. M. *J. Am. Chem. Soc.* **1997**, *119*, 11495–11501.
- [202] Jockusch, S.; Landis, M. S.; Freiermuth, B.; Turro, N. J. *Macromolecules* **2001**, *34*, 1619–1626.
- [203] Morales-Cueto, R.; Esquivelzeta-Rabell, M.; Saucedo-Zugazagoitia, J.; Peon, J. *J. Phys. Chem. A* **2007**, *111*, 552–557.
- [204] Turro, N. J.; Ramamurthy, V.; Scaiano, J. C. *Modern Molecular Photochemistry of Organic Molecules*; University Science Books: Sausalito, California, **2010**.
- [205] Ma, C.; Du, Y.; Kwok, W. M.; Phillips, D. L. *Chem. Eur. J.* **2007**, *13*, 2290–2305.
- [206] Singh, A. K.; Palit, D. K.; Mittal, J. P. *Chem. Phys. Lett.* **2002**, *360*, 443–452.
- [207] Lemee, V.; Burget, D.; Jacques, P.; Fouassier, J. P. *J. Polym. Sci., Part A: Polym. Chem.* **2000**, *38*, 1785–1794.
- [208] Kasha, M. *Faraday Discuss.* **1950**, *9*, 14–19.

- [209] Wolf, T. J. A.; Voll, D.; Barner-Kowollik, C.; Unterreiner, A.-N. *Macromolecules* **2012**, *45*, 2257–2266.
- [210] Voll, D.; Hufendiek, A.; Junkers, T.; Barner-Kowollik, C. *Macromol. Rapid Commun.* **2012**, *33*, 47–53.
- [211] Salikhov, K. M.; Molin, Y. N.; Sagdeev, R. Z.; Buchachenko, A. L. *Spin Polarization and Magnetic Effects in Radical Reactions*; Elsevier: Amsterdam, **1984**; p 419.
- [212] AIST, Integrated Spectral Database System of Organic Compounds.
- [213] Nosova, V. M.; Ustynyuk, Y. A.; Bruk, L. G.; Temkin, O. N.; Kisin, A. V.; Storozhenko, P. A. *Inorg. Chem.* **2011**, *50*, 9300–9310.
- [214] Kaiser, T.; Grossi, L.; Fischer, H. *Helv. Chim. Acta* **1978**, *61*, 223–233.
- [215] Wendt, H. R.; Hunziker, H. E. *J. Chem. Phys.* **1984**, *81*, 717–723.
- [216] Gupta, A.; Liang, R.; Tsay, F. D.; Moacanin, J. *Macromolecules* **1980**, *13*, 1696–1700.
- [217] Wöll, D.; Laimgruber, S.; Galetskaya, M.; Smirnova, J.; Pfeleiderer, W.; Heinz, B.; Gilch, P.; Steiner, U. E. *J. Am. Chem. Soc.* **2007**, *129*, 12148–12158.

A

Appendix

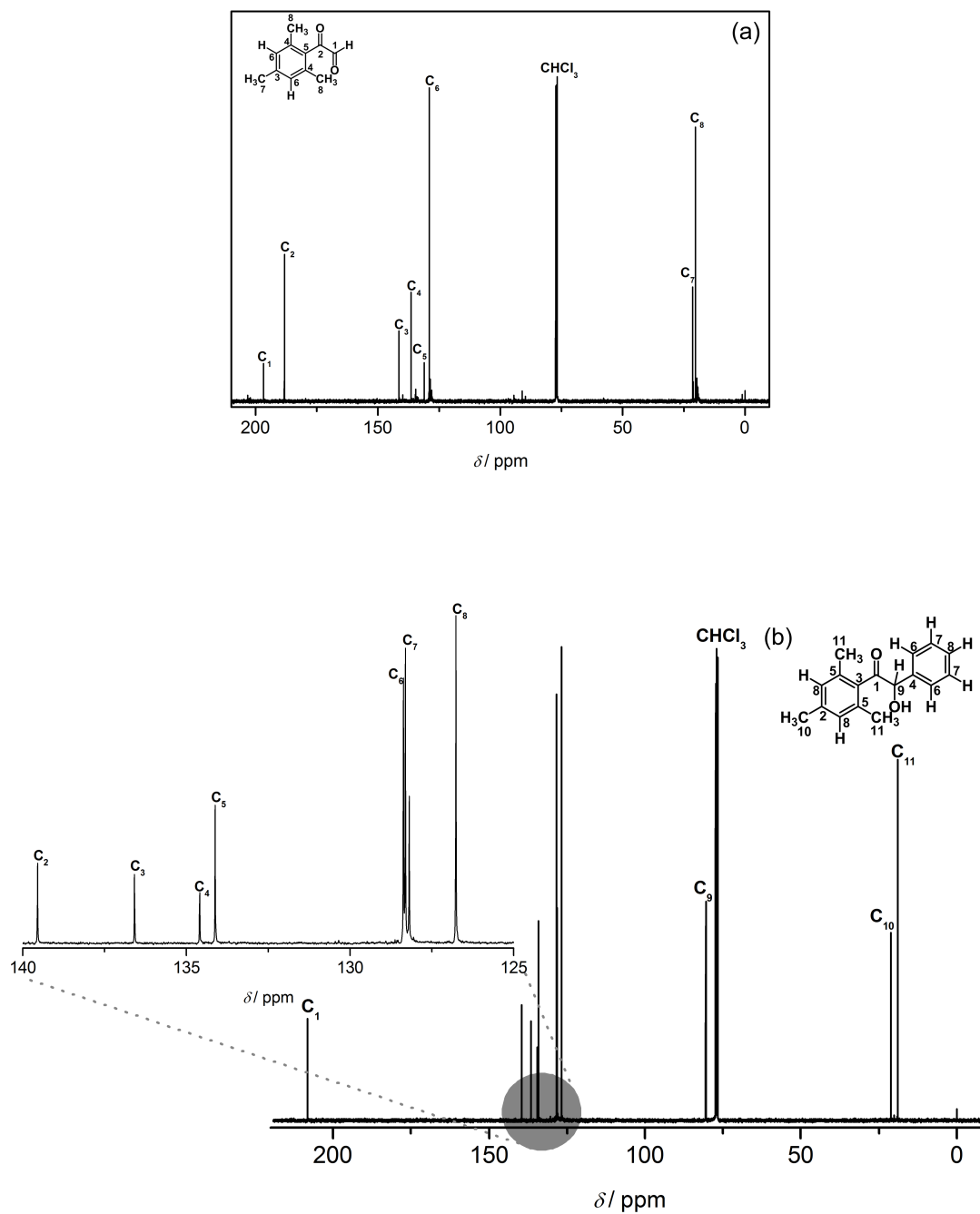
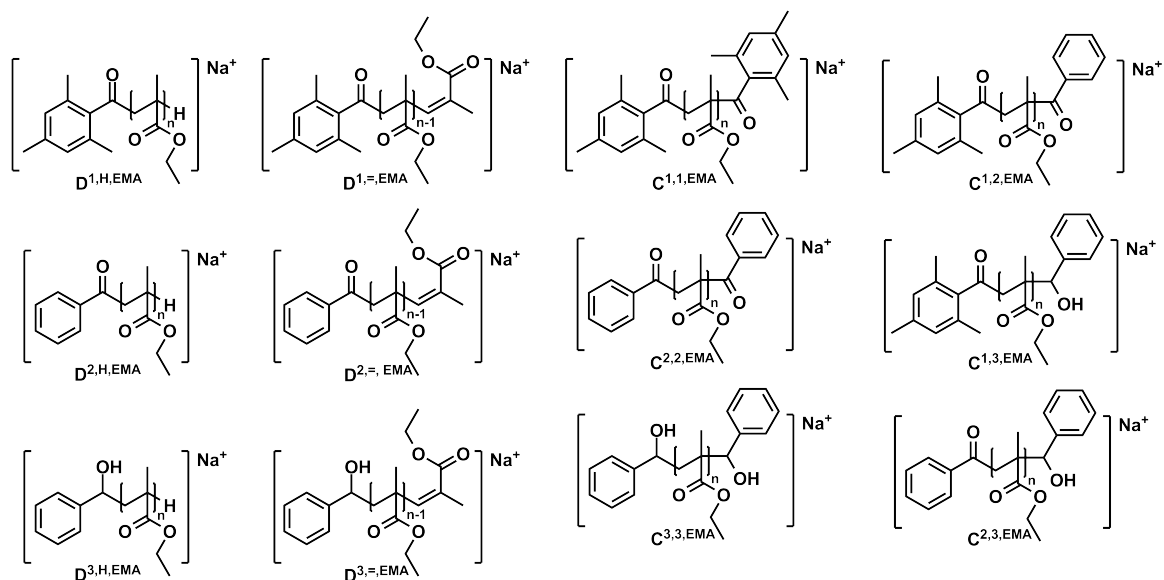
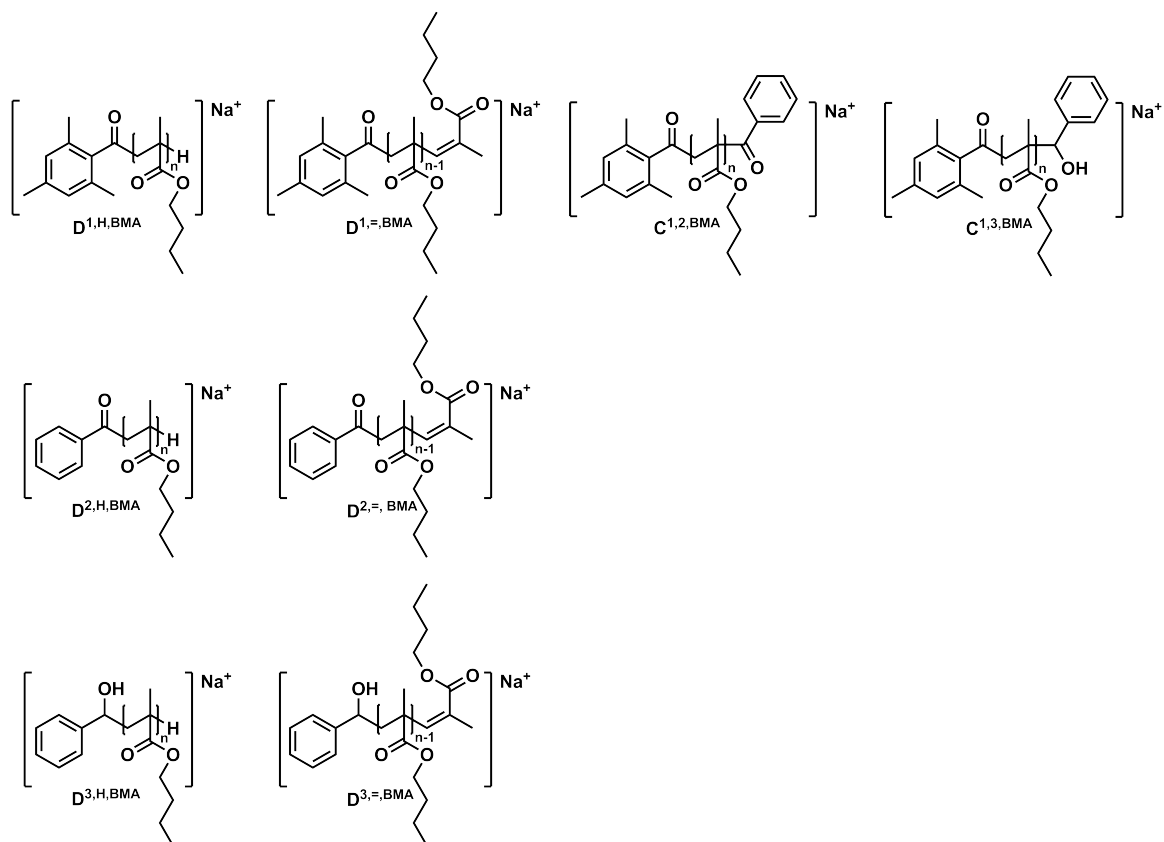


Figure A.1. (a) 100 MHz ^{13}C NMR spectrum of mesitylgyoxal, (b) 100 MHz ^{13}C NMR spectrum of 2,4,6-trimethylbenzoin (A).



Scheme A.1 Expected polymeric disproportionation and combination products in the photochemically-initiated bulk free radical polymerization of EMA in the presence of a mixture of the benzoin (B), and 2,4,6-trimethylbenzoin (A) photoinitiators depicted in Scheme 4.1.



Scheme A.2 Expected polymeric disproportionation and combination products in the photochemically-initiated bulk free radical polymerization of BMA in the presence of a mixture of the benzoin (B), and 2,4,6-trimethylbenzoin (A) photoinitiators depicted in Scheme 4.1.

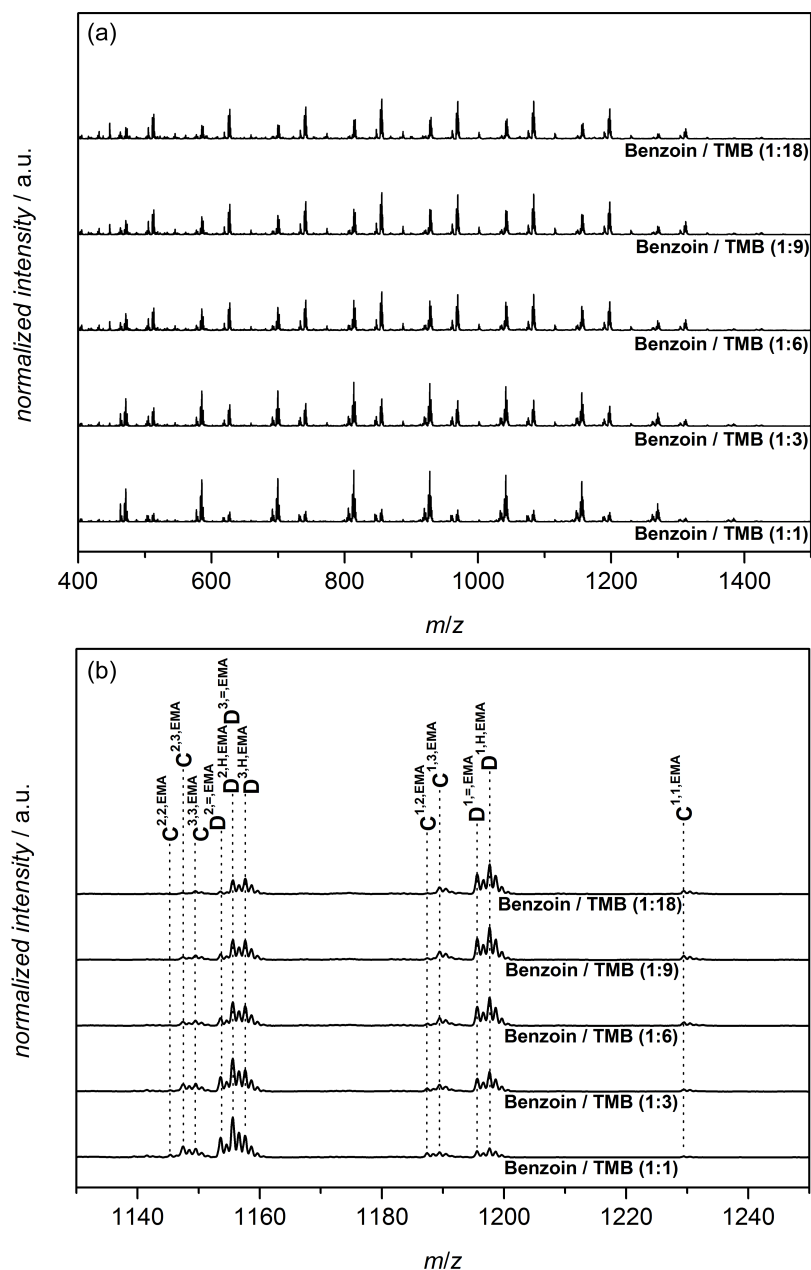


Figure A.2. (a) SEC/ESI-MS overview spectra of polymeric material obtained from five ratios of benzoin/2,4,6-trimethylbenzoin-initiated ($c_{PI} = 5 \times 10^{-3} \text{ mol L}^{-1}$, 1:1, 1:3, 1:6, 1:9, 1:18) PLP of EMA_{bulk} at $\sim 0.35 \text{ mJ/pulse}$ laser energy, 100 Hz, -5°C . The figure shows the singly charged products ionized with sodium iodide at a retention time between 16.86-19.93 min. (b) One repeat unit of the SEC/ESI-MS overview spectra of polymeric material obtained from five ratios of benzoin/2,4,6-trimethylbenzoin-initiated ($c_{PI} = 5 \times 10^{-3} \text{ mol L}^{-1}$, 1:1, 1:3, 1:6, 1:9, 1:18) PLP of EMA_{bulk} at $\sim 0.35 \text{ mJ/pulse}$ laser energy, 100 Hz, -5°C . For the m/z -ratios of the assigned products refer to Table A.1. The nomenclature employed to identify the individual disproportionation and combination products is provided in Scheme A.1.

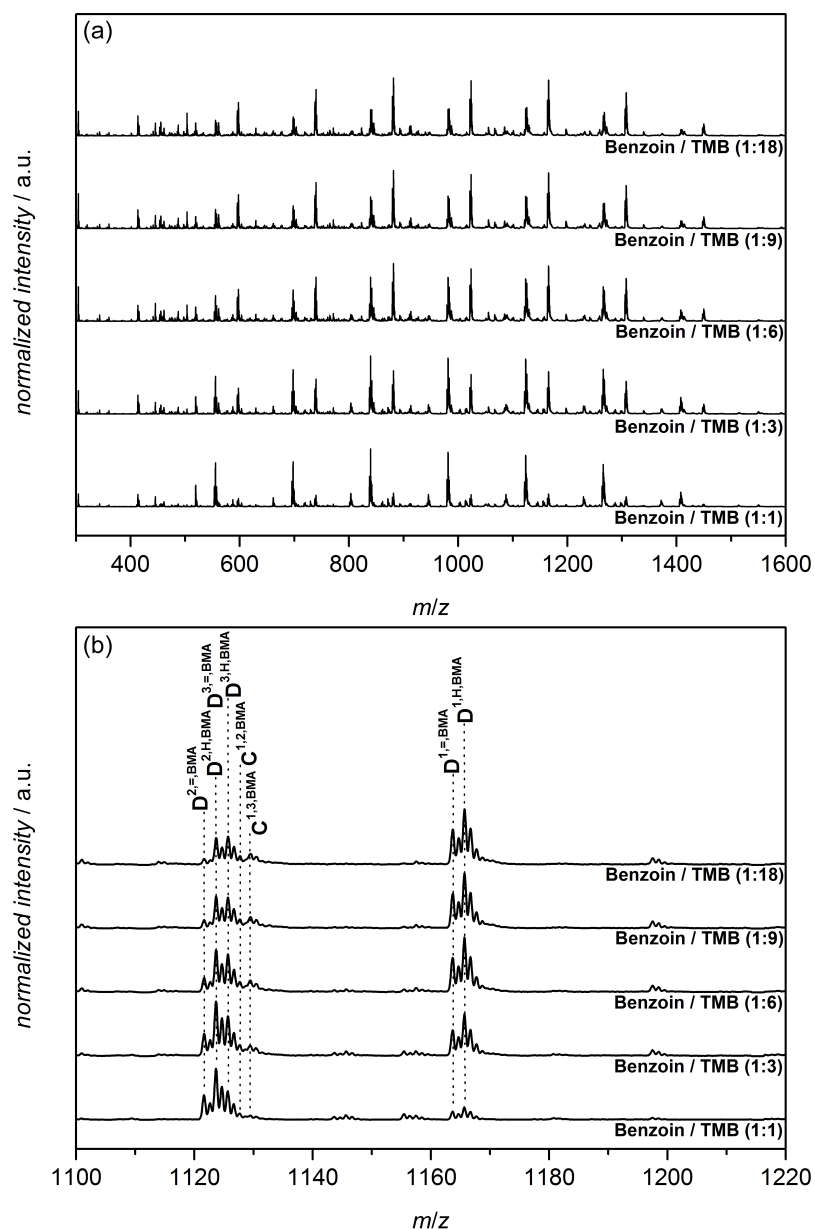


Figure A.3. (a) SEC/ESI-MS overview spectra of polymeric material obtained from five ratios of benzoin/2,4,6-trimethylbenzoin-initiated ($c_{PI} = 5 \times 10^{-3} \text{ mol L}^{-1}$, 1:1, 1:3, 1:6, 1:9, 1:18) PLP of BMA_{bulk} at $\sim 0.35 \text{ mJ/pulse}$ laser energy, 100 Hz, $-5 \text{ }^\circ\text{C}$. The figure shows the singly charged products ionized with sodium iodide at a retention time between 16.86–19.93 min. (b) One repeat unit of the SEC/ESI-MS overview spectra of polymeric material obtained from five ratios of benzoin/2,4,6-trimethylbenzoin-initiated ($c_{PI} = 5 \times 10^{-3} \text{ mol L}^{-1}$, 1:1, 1:3, 1:6, 1:9, 1:18) PLP of BMA_{bulk} at $\sim 0.35 \text{ mJ/pulse}$ laser energy, 100 Hz, $-5 \text{ }^\circ\text{C}$. For the m/z -ratios of the assigned products refer to Table A.2. The nomenclature employed to identify the individual disproportionation and combination products is provided in Scheme A.2.

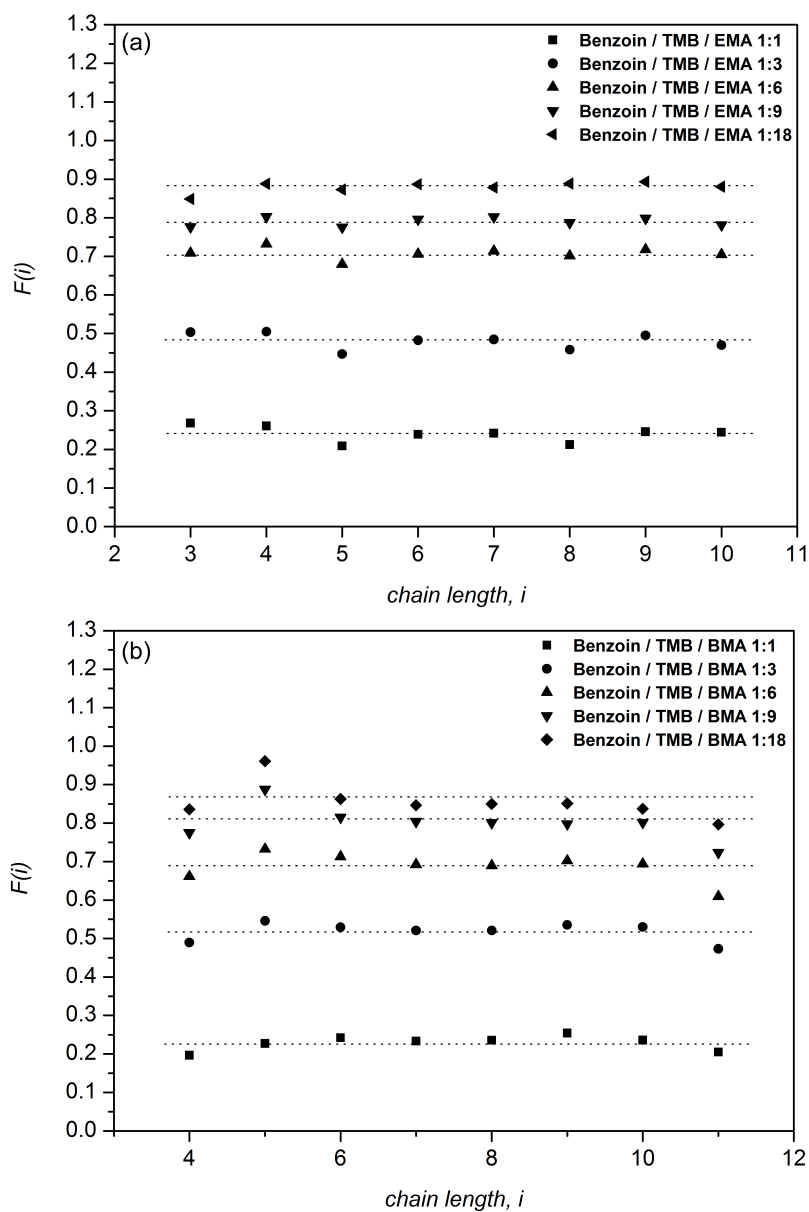


Figure A.4. Intensity-derived mole fractions of polymer chains initiated with mesityl radicals (1). $F(i)$, vs. their chain length, i . The dotted lines give the average of the mole fraction over the entire chain length range of pEMA (a) and pBMA (b) at different photoinitiator ratios.

Table A.1. Collation of the polymeric product signals observed during SEC/ESI-MS of pEMA samples generated during the pulsed laser-initiated bulk free radical polymerization of EMA at 100 Hz and -5 °C. Provided are the experimentally observed as well as theoretically expected m/z -ratios for the found disproportionation (D) and combination (C) products (consisting of 8 or 9 monomer units, n is the number of repeat units). The structures corresponding to the individual peaks are depicted in Scheme A.1. The tabulated values correspond to the peaks displayed in Figure A.2.

Species	Ionization	$(m/z)_{\text{theo.}}$ / Da	$(m/z)_{\text{exp.}}$ / Da	$\Delta(m/z)$ / Da
D ^{1,H,EMA}	Na ⁺	1197.7 ($n = 9$)	1197.7	0
D ^{1,=,EMA}	Na ⁺	1195.7 ($n = 9$)	1195.6	0.1
D ^{2,H,EMA}	Na ⁺	1155.6 ($n = 9$)	1155.6	0
D ^{2,=,EMA}	Na ⁺	1153.6 ($n = 9$)	1153.6	0
D ^{3,H,EMA}	Na ⁺	1157.7 ($n = 9$)	1157.7	0
D ^{3,=,EMA}	Na ⁺	1155.6 ($n = 9$)	1155.6	0
C ^{1,1,EMA}	Na ⁺	1229.7 ($n = 8$)	1229.4	0.3
C ^{2,2,EMA}	Na ⁺	1145.4 ($n = 8$)	1145.6	0.2
C ^{3,3,EMA}	Na ⁺	1149.6 ($n = 8$)	1149.5	0.1
C ^{1,2,EMA}	Na ⁺	1187.6 ($n = 8$)	1187.4	0.2
C ^{1,3,EMA}	Na ⁺	1189.4 ($n = 8$)	1189.7	0.3
C ^{2,3,EMA}	Na ⁺	1147.6 ($n = 8$)	1147.4	0.2

Table A.2. Collation of the polymeric product signals observed during SEC/ESI-MS of pBMA samples generated during the pulsed laser-initiated bulk free radical polymerization of BMA at 100 Hz and -5 °C. Provided are the experimentally observed as well as theoretically expected m/z -ratios for the disproportionation (D) and combination (C) products (consisting of 6 or 7 monomer units, n is the number of repeat units). The structures corresponding to the individual peaks are depicted in Scheme A.2. The tabulated values correspond to the peaks displayed in Figure A.3.

Species	Ionization	$(m/z)_{\text{theo.}}$ / Da	$(m/z)_{\text{exp.}}$ / Da	$\Delta(m/z)$ / Da
D ^{1,H,BMA}	Na ⁺	1165.8 ($n = 7$)	1165.7	0.1
D ^{1,=,BMA}	Na ⁺	1163.8 ($n = 7$)	1163.7	0.1
D ^{2,H,BMA}	Na ⁺	1123.7 ($n = 7$)	1123.7	0
D ^{2,=,BMA}	Na ⁺	1121.7 ($n = 7$)	1121.7	0
D ^{3,H,BMA}	Na ⁺	1125.7 ($n = 7$)	1125.8	0.1
D ^{3,=,BMA}	Na ⁺	1123.7 ($n = 7$)	1123.7	0
C ^{1,2,BMA}	Na ⁺	1127.8 ($n = 6$)	1127.7	0.1
C ^{1,3,BMA}	Na ⁺	1129.5 ($n = 6$)	1129.7	0.2

Table A.3. Minimum energy geometries of benzoin (B) as Cartesian coordinates (x, y, and z) in units of Å optimized with DFT/BP86/def2-SVP. ^[183–188]

Geometry 1	Geometry 2
C -2.9097956 1.3252262 -0.1264521	C 2.6368260 0.8173972 -0.3183687
C -1.9679171 1.0851780 0.8809709	C 1.4385375 0.1462583 0.0293144
C -2.3327736 1.3027020 2.2175136	C 0.9164342 -0.8256845 -0.8564337
C -3.6114225 1.7602067 2.5359998	C 1.5774267 -1.1081712 -2.0624833
C -4.5441504 2.0039555 1.5226982	C 2.7641988 -0.4346466 -2.3973092
C -4.1920484 1.7820727 0.1898696	C 3.2944960 0.5302084 -1.5194179
C -0.5870494 0.5379721 0.5356083	C 0.8076733 0.5435269 1.3322765
O -0.4577053 -0.8093478 0.9487938	O 1.3215065 1.4021006 2.0448688
C 0.5428011 1.3629320 1.1958928	C -0.5557059 -0.0266463 1.8194927
O 1.2165488 0.7989638 2.0584039	O -0.7187646 -1.3943084 1.4691468
C 0.8129148 2.7705224 0.8000565	C -1.6863192 0.8770126 1.3112018
C 0.1189439 3.4143401 -0.2393503	C -1.8265077 2.1842691 1.8253787
C 0.4272846 4.7306709 -0.5820239	C -2.8572874 3.0201402 1.3704232
C 1.4292811 5.4181599 0.1085574	C -3.7646172 2.5612354 0.3978617
C 2.1265707 4.7853583 1.1443014	C -3.6293134 1.2625705 -0.1189139
C 1.8224839 3.4711185 1.4863371	C -2.5928089 0.4260622 0.3319536
H 2.9089532 5.3213027 1.6831659	H 1.1631690 -1.8679691 -2.7461786
H -0.1169790 5.2227959 -1.3888542	H 4.2261083 1.0609382 -1.7783409
H 0.2540749 -0.7822068 1.6327314	H -1.5774210 -1.6905161 1.8442573
H -2.6414884 1.1365118 -1.1690847	H -2.4855336 -0.5907417 -0.0797435
H -4.9187696 1.9558925 -0.6053045	H -4.3338218 0.8952102 -0.8841428
H -5.5444467 2.3598521 1.7733283	H -4.5767232 3.2177245 0.0433795
H -3.8826880 1.9279653 3.5794145	H -2.9558935 4.0387487 1.7815877
H -1.6135684 1.0996924 3.0136817	H -1.1109633 2.5453023 2.5828066
H -0.4551305 0.5934401 -0.5619811	H -0.4952936 0.0871200 2.9274722
H 1.6674849 6.4485153 -0.1600121	H 3.2808985 -0.6625986 -3.3450626
H 2.3559866 2.9578717 2.2863705	H 0.0031807 -1.3706228 -0.5823217
H -0.6706673 2.8923590 -0.7778436	H 3.0271072 1.5717720 0.3832450

Table A.4. Minimum energy geometries of 2,4,6-trimethylbenzoic acid (A) as Cartesian coordinates (x, y, and z) in units of Å optimized with DFT/BP86/def2-SVP.^[183–188]

Geometry 1			Geometry 2				
C	-1.594137	0.944079	3.459516	C	2.902874	0.289756	-0.077877
H	-1.256041	0.336485	2.587634	H	1.828838	0.335235	-0.361039
H	-0.861559	0.774617	4.278203	H	3.429794	-0.278448	-0.880231
H	-2.574952	0.533633	3.782789	H	2.988303	-0.310316	0.854502
C	-1.694512	2.408171	3.094422	C	3.495539	1.671230	0.091315
C	-0.576219	3.256870	3.186584	C	4.611339	1.885114	0.921098
H	0.375174	2.854571	3.577461	H	5.033636	1.035723	1.487257
C	-2.907280	2.962200	2.639809	C	2.958772	2.781088	-0.589953
H	-3.802945	2.319581	2.576155	H	2.074701	2.640963	-1.236969
C	-3.023080	4.314818	2.274032	C	3.501779	4.072211	-0.460451
H	-4.743090	5.618630	2.543537	C	2.857179	5.237403	-1.183322
H	-4.276157	5.378667	0.835881	H	2.415976	5.960919	-0.463857
H	-5.109066	4.056838	1.724910	H	2.051360	4.886030	-1.861798
C	-0.631168	4.613066	2.809988	H	3.590617	5.806574	-1.798347
C	0.612508	5.469597	2.964391	C	5.210149	3.152143	1.060816
H	1.228769	5.483707	2.036005	C	6.417369	3.308438	1.960365
H	1.262344	5.069135	3.771683	H	6.458887	4.306078	2.448695
H	0.376090	6.524038	3.222078	H	7.356017	3.192062	1.374589
C	-1.863550	5.136999	2.337503	H	6.418408	2.539605	2.762891
C	-1.979447	6.583568	1.955476	C	4.649736	4.248855	0.359427
O	-2.703506	7.370100	2.563093	C	5.186770	5.650454	0.531519
C	-1.223277	7.138753	0.713703	O	4.523187	6.528517	1.062324
O	-1.351141	8.533785	0.707633	O	7.169208	4.877341	-0.651296
H	-1.994042	8.721399	1.447467	H	7.977573	5.165789	-1.128706
H	-1.602748	6.706411	-0.104271	C	6.556061	6.034321	-0.111530
C	0.172933	6.760711	0.814613	H	6.409689	6.851311	-0.816529
C	0.612571	5.551959	0.261769	C	7.477797	6.451506	0.927152
H	-0.094054	4.895646	-0.244052	C	8.778538	6.845869	0.591667
C	1.960636	5.186952	0.359199	C	9.668490	7.248668	1.594532
H	2.302612	4.246716	-0.070835	C	9.257701	7.257104	2.932882
C	2.869061	6.030697	1.009474	C	7.956960	6.862740	3.268367
H	3.917663	5.746774	1.085260	C	7.067008	6.459941	2.265502
C	-4.356793	4.867358	1.821124	H	9.098073	6.839307	-0.449379
C	2.413721	7.282619	1.582062	H	10.680281	7.555426	1.333573
C	0.989796	7.430027	1.351390	H	9.949956	7.570424	3.712968
H	3.255154	7.798735	2.041994	H	7.637424	6.869302	4.309412
H	0.647820	8.370263	1.781424	H	6.055217	6.153183	2.526461

Table A.5. Minimum energy geometries of mesitol (C) as Cartesian coordinates (x, y, and z) in units of Å optimized with DFT/BP86/def2-SVP. [183–188]

Geometry 1	Geometry 2
C 1.9375763 -0.2455234 -0.0756153	C 6.1767461 -1.0571073 -0.3649778
C 1.1615670 0.0944634 -1.2305779	H 6.2584657 -2.1419329 -0.6105236
C 1.7880527 0.0984996 -2.5223646	H 6.7437425 -0.5037112 -1.1447372
C 3.1482222 -0.2457709 -2.6188607	H 6.6872442 -0.9035775 0.6100359
C 3.9270112 -0.5771630 -1.4956194	C 4.7296667 -0.6219619 -0.3128637
C 3.2992457 -0.5592121 -0.2373117	C 4.0504560 -0.2207973 -1.4796769
C -0.2712125 0.4970875 -1.1277625	H 4.5974209 -0.1941356 -2.4384278
O -0.8922288 1.0724937 -2.0258247	C 4.0135923 -0.6137983 0.8978154
C 1.0619264 0.4405330 -3.8050844	H 4.5346617 -0.8827904 1.8334616
C 5.3798390 -0.9664669 -1.6404060	C 2.6982259 0.1646836 -1.4658048
C 1.3870168 -0.3047799 1.3358502	C 2.0484437 0.6262472 -2.7547042
C -1.1917616 -0.0278846 -0.0024461	H 1.1142319 0.0660264 -2.9789008
O -1.2336707 -1.2599510 0.0529576	H 1.7685435 1.7001288 -2.7000404
C -2.1313326 0.8726989 0.7278848	H 2.7384834 0.4882954 -3.6134817
C -1.8448281 2.2628490 0.9302708	C 2.6516245 -0.2631095 0.9637925
C -2.7480783 3.0437672 1.6712203	C 1.9708599 -0.2522525 2.3178084
C -3.9407419 2.5196752 2.2052528	H 1.2170362 0.5604416 2.4039543
C -4.2080136 1.1569845 1.9912986	H 1.4459871 -1.2128866 2.5102154
C -3.3328584 0.3157259 1.2781844	H 2.7152254 -0.0999189 3.1285532
H 3.6196466 -0.2498672 -3.6173134	C 1.9827666 0.1097809 -0.2335721
H 1.7169008 0.2331645 -4.6791132	C 0.5350774 0.5272105 -0.2301900
H 0.1200328 -0.1365627 -3.9204837	O 0.1599773 1.6232788 -0.6288901
H 0.7577178 1.5086301 -3.8342491	C -0.5335232 -0.5179151 0.2514655
H 5.9600559 -0.7410069 -0.7196798	O -0.1644522 -1.6165472 0.6476757
H 5.4801203 -2.0611387 -1.8303807	C -1.9820556 -0.0997472 0.2443785
H 5.8620671 -0.4428797 -2.4942539	C -2.7000860 -0.1213442 1.4763321
H 3.8935866 -0.8033900 0.6605529	C -2.0444372 -0.5328100 2.7791026
H 0.8083611 -1.2400466 1.4963696	H -1.1311956 0.0645280 2.9952136
H 2.2179259 -0.2837723 2.0729726	H -1.7291761 -1.5978448 2.7507907
H 0.7036943 0.5350265 1.5827720	H -2.7434394 -0.3981595 3.6311216
H -5.1377238 0.7234856 2.3989022	C -2.6476611 0.2357023 -0.9639820
H -2.5117851 4.1100416 1.8338966	C -1.9576690 0.1994727 -2.3126613
C -0.6206772 2.9697390 0.3811666	H -1.2016972 -0.6134063 -2.3773728
H -0.4552922 3.9271039 0.9204603	H -1.4334854 1.1576285 -2.5197363
H 0.3132148 2.3751954 0.4687509	H -2.6953779 0.0304570 -3.1260759
H -0.7478023 3.2014390 -0.6984240	C -4.0134271 0.5783036 -0.9127176
C -4.8942304 3.4017262 2.9778193	H -4.5323137 0.8206269 -1.8567379

Continuation of Table A.5

Geometry 1			Geometry 2				
H	-5.7632096	2.8284016	3.3650260	C	-4.0546515	0.2527777	1.4750492
H	-4.3878503	3.8831397	3.8449627	H	-4.6034638	0.2523200	2.4333272
H	-5.2880675	4.2250634	2.3387671	C	-4.7341972	0.6120923	0.2935230
C	-3.7320768	-1.1354323	1.1227887	C	-6.1911793	1.0151119	0.3324604
H	-4.7657150	-1.2881416	1.5028369	H	-6.3242220	1.9899423	0.8557562
H	-3.6885256	-1.4718245	0.0652311	H	-6.6145857	1.1222997	-0.6886922
H	-3.0467305	-1.8124494	1.6759390	H	-6.8061830	0.2683979	0.8829339

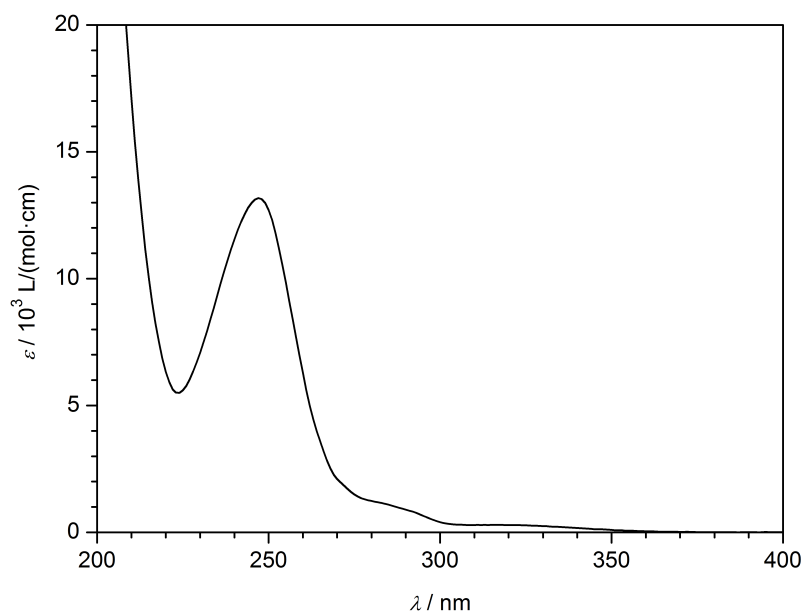


Figure A.5. UV/Vis spectrum of benzoin (B) in methanol solution (200-400 nm) recorded at ambient temperature.

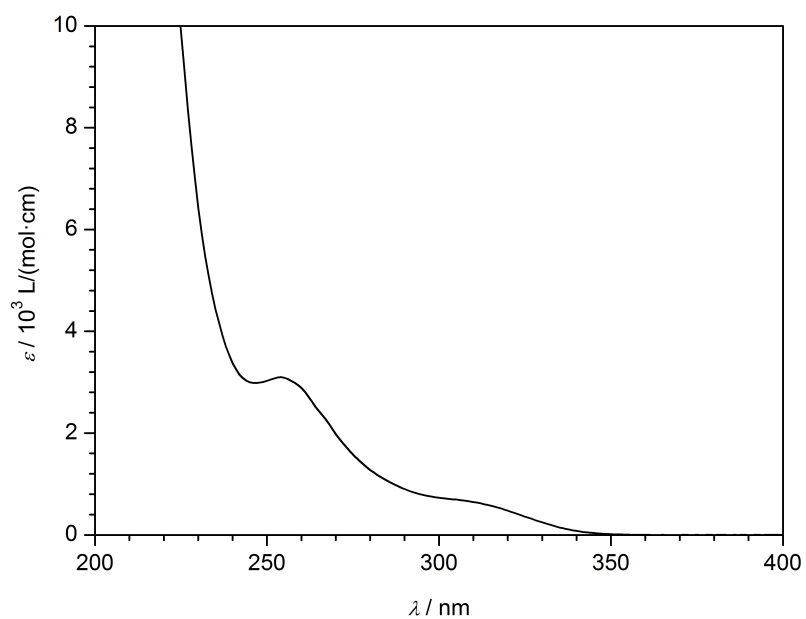


Figure A.6. UV/Vis spectrum of 2,4,6-trimethylbenzoic acid (A) in methanol solution (200-400 nm) recorded at ambient temperature.

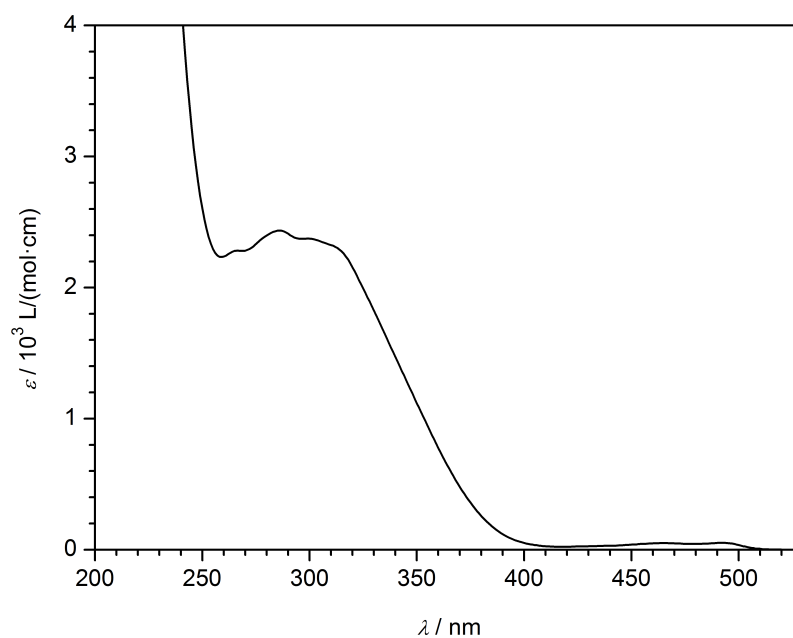
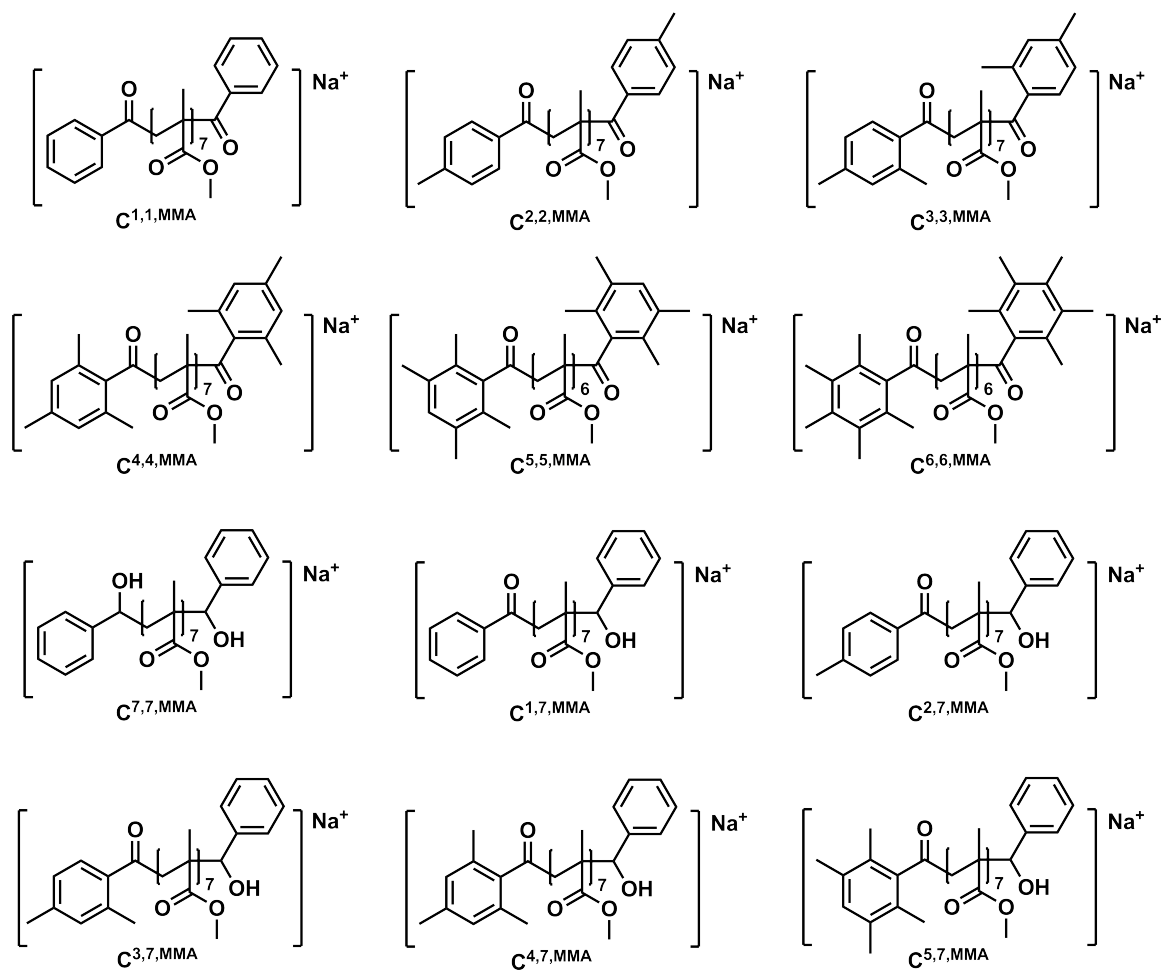
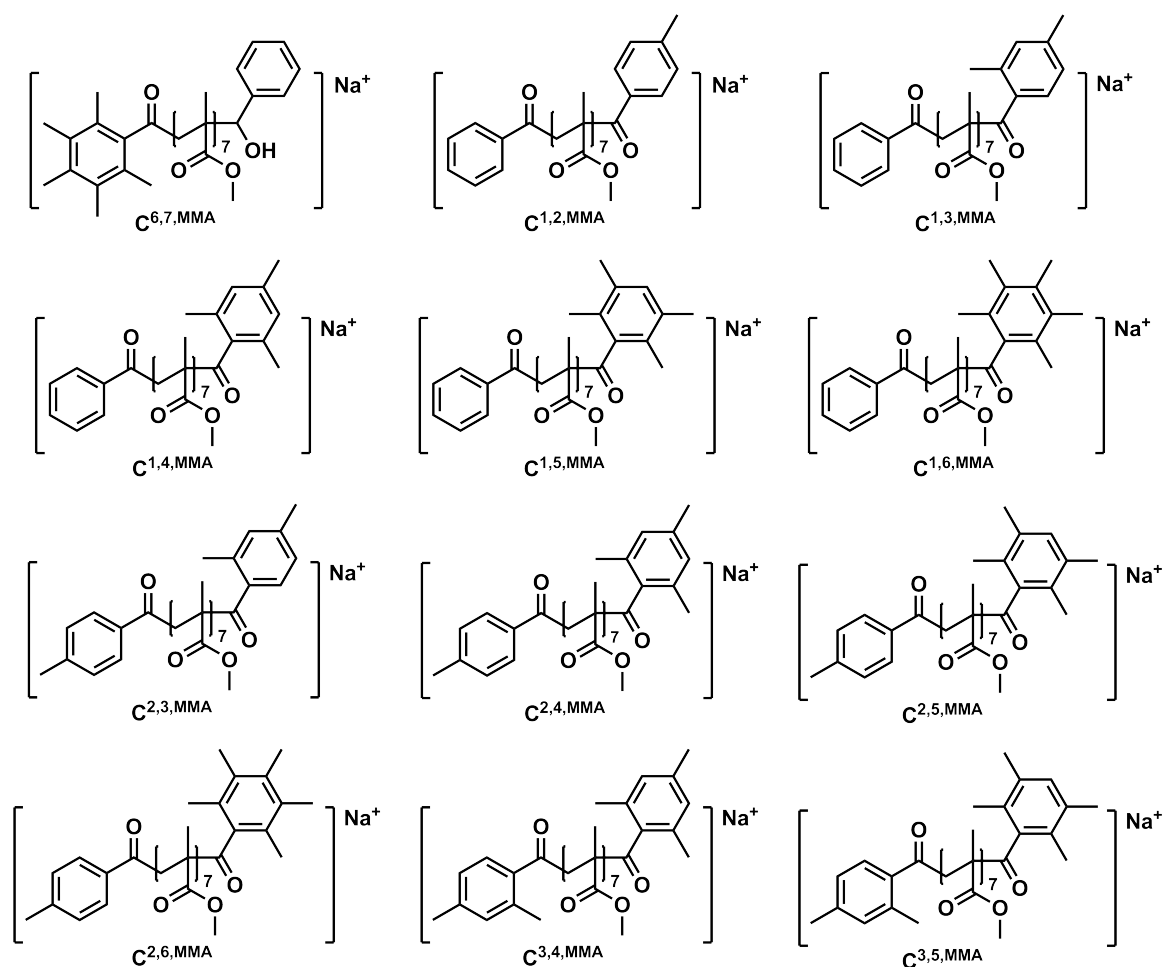


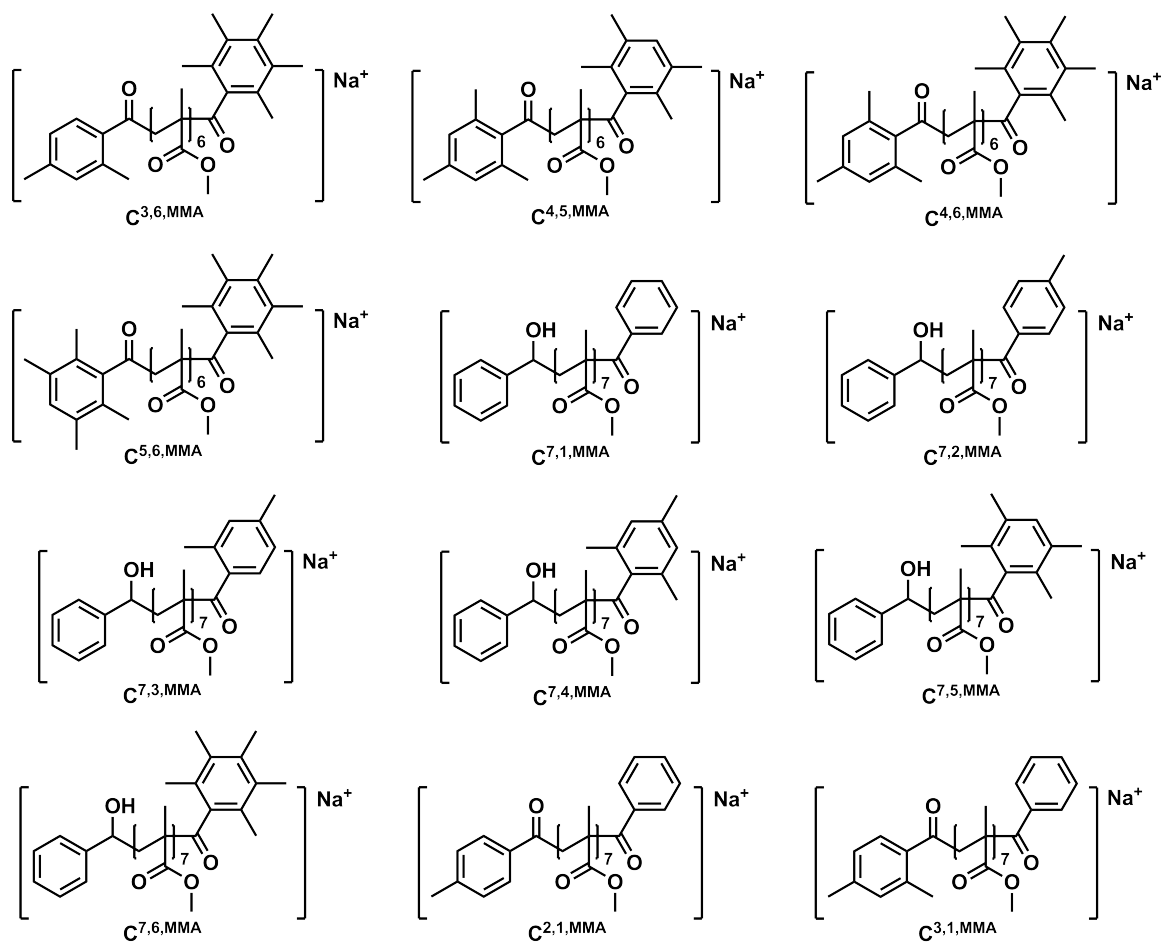
Figure A.7. UV/Vis spectrum of mesityl oxide (C) in methanol solution (200-530 nm) recorded at ambient temperature.



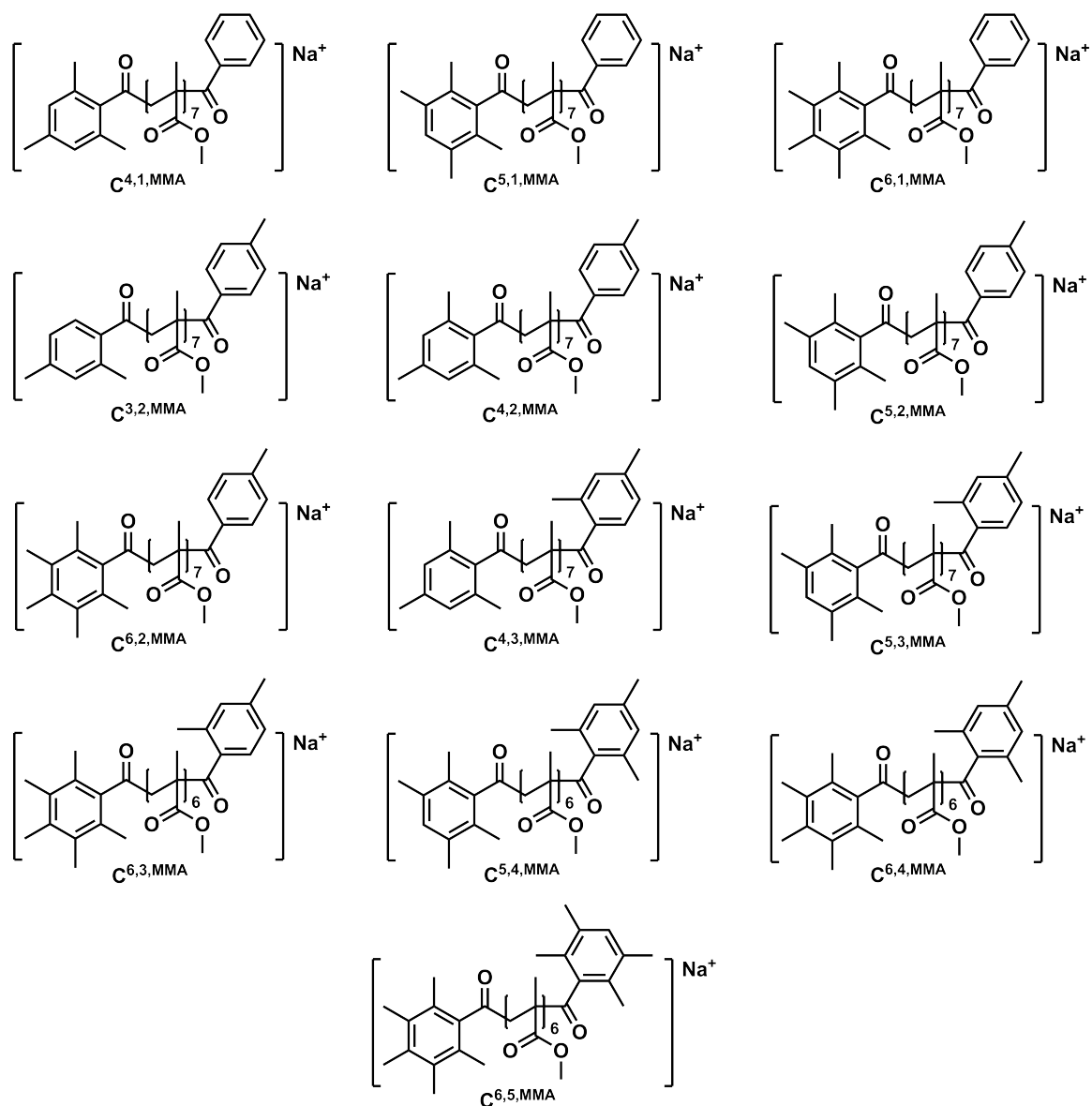
Scheme A.3 Expected polymeric combination products $C^{1,1,MMA}$ - $C^{5,7,MMA}$ in the multi-photo-initiated free radical polymerization of MMA performed in bulk in the presence of a mixture of benzoin (A), 4-methylbenzoin (B), 2,4-dimethylbenzoin (C), 2,4,6-trimethylbenzoin (D), 2,3,5,6-tetramethylbenzoin (E), and 2,3,4,5,6-pentamethylbenzoin (F). See Figure 6.7.



Scheme A.4 Expected polymeric combination products C_{6,7,MMA} - C_{3,5,MMA} in the multi-photo-initiated free radical polymerization of MMA performed in bulk in the presence of a mixture of benzoin (A), 4-methylbenzoin (B), 2,4-dimethylbenzoin (C), 2,4,6-trimethylbenzoin (D), 2,3,5,6-tetramethylbenzoin (E), and 2,3,4,5,6-pentamethylbenzoin (F). See Figure 6.7.



Scheme A.5 Expected polymeric combination products $C^{3,6, MMA} - C^{3,1, MMA}$ in the multi-photo-initiated free radical polymerization of MMA performed in bulk in the presence of a mixture of benzoin (A), 4-methylbenzoin (B), 2,4-dimethylbenzoin (C), 2,4,6-trimethylbenzoin (D), 2,3,5,6-tetramethylbenzoin (E), and 2,3,4,5,6-pentamethylbenzoin (F). See Figure 6.7.



Scheme A.6 Expected polymeric combination products $C^{4,1,MMA}$ - $C^{6,5,MMA}$ in the multi-photo-initiated free radical polymerization of MMA performed in bulk in the presence of a mixture of benzoic (A), 4-methylbenzoic (B), 2,4-dimethylbenzoic (C), 2,4,6-trimethylbenzoic (D), 2,3,5,6-tetramethylbenzoic (E), and 2,3,4,5,6-pentamethylbenzoic (F). See Figure 6.7.

Curriculum Vitae

Date of Birth 1.May 1984
Place of Birth Sinsheim, Germany
Nationality German

Education

11/2009 - Present **Doctoral Studies in Chemistry**
Under the supervision of Prof. Dr. Christopher Barner-Kowollik
Karlsruhe Institute of Technology (KIT), Germany

9/2009 **Diploma in Chemistry**
Living Radical Polymerization of Ferrocene Containing Monomers: Mechanism, Characterization and Blockcopolymers
Under the supervision of Prof. Dr. Christopher Barner-Kowollik
Universität Karlsruhe (TH), Germany

10/2004 - 9/2009 **Studies of Chemistry**
Universität Karlsruhe (TH), Karlsruhe, Germany

7/2003 - 4/2004 **Military Service**
Luftwaffenmusikkorps 2, Karlsruhe, Germany

6/2003 **High School Certificate**
Friedrich-Hecker-Schule, Technisches Gymnasium, Sinsheim, Germany

6/2000 **Middle School Certificate**
Realschule, Eppingen/Elsenz, Germany

Employment History

3/2009 - Present

Institut für Technische Chemie und Polymer Chemie

Karlsruhe Institute of Technology (KIT), Karlsruhe, Germany
Scientific Co-worker

10/2008 - 12/2008

Institut für Technische Chemie und Polymer Chemie

in the group of Prof. Dr. Christopher-Barner-Kowollik, Universität Karlsruhe (TH), Germany
Complementary Scientist (HiWi)

1/2008

Institut für Organische Chemie

in the group of Prof. Dr. Joachim Podlech, Universität Karlsruhe (TH), Germany
Complementary Scientist (HiWi)

Full List of Publications and Conference Contributions

Refereed Journal Publications

- [11] *The Interplay of Different Relaxation Channels in the Excited State Dynamics of Photoinitiators*
Wolf, T. J. A.; Fischer, J.; **Voll, D.**; Wegener, M.; Barner-Kowollik, C.; Unterreiner, A.-N. *Ultrafast Phenomena XVIII* **2012**, in press.
- [10] *UV-Triggered Endgroup Conversion of Photo-Initiated Poly(Methyl Methacrylate)*
Voll, D.; Neshchadin, D.; Hiltebrandt, K.; Gescheidt, G.; Barner-Kowollik, C. *Macromolecules* **2012**, *45*, 5850–5858.
- [9] *A Qualitative and Quantitative Post-Mortem Analysis: Studying Free-Radical Initiation Processes via Soft Ionization Mass Spectrometry*
Voll, D.; Junkers, T.; Barner-Kowollik, C. *J. Polym. Sci., Part A: Polym. Chem.* **2012**, *50*, 2739–2757.
- [8] *Elucidating the Early Steps in Photoinitiated Radical Polymerization via Femtosecond Pump-Probe Experiments and DFT Calculations*
Wolf, T. J. A.; **Voll, D.**; Barner-Kowollik, C.; Unterreiner, A.-N. *Macromolecules* **2012**, *45*, 2257–2266.
- [7] *Quantifying Photoinitiation Efficiencies in a Multi-Photoinitiated Free Radical Polymerization*
Voll, D.; Hufendiek, A.; Junkers, T.; Barner-Kowollik, C. *Macromol. Rapid Commun.* **2012**, *32*, 47–53.

- [6] *Radical Addition Fragmentation Chain Transfer (RAFT) Polymerization of Ferrocenyl(Meth)Acrylates*
Herfurth, C.; **Voll, D.**; Buller, J.; Weiss, J.; Barner-Kowollik, C.; Laschewsky, A. *J. Polym. Sci., Part A: Polym. Chem.* **2012**, *50*, 108–118.
- [5] *Quantitative Comparison of the Mesitoyl vs. the Benzoyl Fragment in Photoinitiation: A Question of Origin*
Voll, D.; Junkers, T.; Barner-Kowollik, C. *Macromolecules* **2011**, *44*, 2542–2551.
- [4] *An Access Route to Poly(ferrocene)s via Modular Conjugation*
Lang, C.; **Voll, D.**; Inglis, A. J.; Dingenouts, N.; Goldmann, A. S.; Barner, L.; Barner-Kowollik, C. *Macromol. Chem. Phys.* **2011**, *212*, 831–839.
- [3] *Detailed Investigation of the Propagation Rate of Urethane Acrylates*
Barner-Kowollik, C.; Bennet, F.; Schneider-Baumann, M.; **Voll, D.**; Rölle, T.; Fäcke, T.; Weiser, M.-S.; Bruder, F.-K.; Junkers, T. *Polym. Chem.* **2010**, *1*, 470–479.
- [2] *A Perfect Couple: Pulsed Laser Polymerization with Online Size Exclusion Chromatography Mass Spectrometry for the Accurate Determination of Propagation Rate Coefficients in Free Radical Polymerization*
Gruending, T.; **Voll, D.**; Guilhaus, M.; Barner-Kowollik, C. *Macromol. Chem. Phys.* **2010**, *211*, 80–90.
- [1] *Determination of Vinyl Acetate Propagation Rate Coefficients via High Frequency Pulsed Laser Polymerization*
Junkers, T.; **Voll, D.**; Barner-Kowollik, C. *e-Polymers* **2009**, 76.

Conference Contributions

- [4] *The Interplay of Different Relaxation Channels in the Excited State Dynamics of Photoinitiators*
Wolf, T. J. A.; Fischer, J.; **Voll, D.**; Wegener, M.; Barner-Kowollik, C.; Unterreiner, A.-N. *Ultrafast Phenomena*, 8th to 13th of July 2012, Lausanne, Switzerland (Poster Presentation).

-
- [3] *Quantifying the Efficiency of Photoinitiation Processes in Free Radical Polymerization of Different Methacrylates via SEC–ESI–MS using Benzoin and 2,4,6–Trimethylbenzoin*
Voll, D.; Junkers, T.; Barner-Kowollik, C. **chemtogether@evonik**, 17th to 19th of November 2010, Marl, Germany (Poster Presentation).
- [2] *RAFT Polymerization of 1–Ferrocenylethyl Acrylate and the Structural Analysis of Poly(vinylferrocene) via ESI–MS*
Voll, D.; Hart-Smith, G.; Barner-Kowollik, C. **CRP meeting**, 17th to 18th of September 2009, Houffalize, Belgium (Poster Presentation).
- [1] *Tuning Radical Reactivity in Polymerizing Systems: Initiation, Control and Synthesis*
Barner-Kowollik, C.; Günzler, F.; Koo, S. P. S.; **Voll, D.**; Zorn, A.-M.; Dietrich, M.; Wong, E. H. H.; Barner, L.; Junkers, T. **EUCHEM Conference on Organic Free Radicals**, 28th of June to 2nd of July 2010, Bologna, Italy (Oral Presentation).

Acknowledgment

(Danksagung)

Mein Dank gilt Prof. Dr. Christopher Barner-Kowollik für die interessante Aufgabenstellung, das stete Interesse am Fortschritt der Arbeit, die vielen Diskussionen und das große Vertrauen das er in mich gesetzt hat.

Prof. Dr. Thomas Junkers danke ich für die Unterstützung zu Beginn der Arbeit.

Prof. Dr. Georg Gescheidt und Dr. Dmytro Neshchadin vom Grazer Institut für Technologie danke ich für den angenehmen Forschungsaufenthalt in Graz (Österreich).

Desweiteren möchte ich mich bei PD Dr. Andreas-Neil Unterreiner und Thomas Wolf für die sehr erfolgreiche Zusammenarbeit auf dem Gebiet der Femtosekunden-Spektroskopie bedanken.

Ich danke auch Volker Winkler, Alexander Quick, Andrea Hufendiek, Kai Hildebrandt und Christiane Lang für die Unterstützung als Vertiefer, HiWi und Diplomand.

Vielen Dank an Gabriele Herrmann und Evelyn Stüring für die organisatorische und administrative Arbeit. Ebenso geht ein großes Dankeschön an Dr. Maria Schneider und Peter Gerstel für stets schnelle Bestellungen, wenn es mal wieder eilig war.

Mein ganz besonderer Dank gilt all denen, die sich in den letzten 4 Jahren das Büro mit mir geteilt haben: Dr. Andrew J. Inglis, Dr. Sandy Koo, Dr. Leena Nebhani, Dr. Christina Schmid, Dr. Mathias Dietrich, Kim Öhlenschläger, Jan Müller, Corinna Preuß, Thomas Paulöhrl, Mathias Glaßner und Elena Frick. Ich werde echt etwas vermissen.

Bedanken möchte ich mich auch bei allen ehemaligen und aktuellen AC-Kollegen. Mein ganz besonderer Dank gilt meinem Labor- und Abzugskollegen Bernhard Schmidt, leider wurde es nichts mehr mit unserem gemeinsamen Paper.

Für die Hilfe mit der SEC/ESI-MS darf ich mich bei Dr. Till Gründling, Michael Kaupp und Kim Öhlenschläger bedanken.

Alexander Hähnel (und seinem Vertiefer) danke ich für die Bilder unseres Excimer-Laser-Systems (PLP).

Danke an Dr. Anna-Marie Zorn und Bernhard Schmidt für die AC-Eis-Pausen.

Für das Korrekturlesen meiner Arbeit danke ich Mathias Glaßner, Jan Müller, Kim Öhlenschläger, Christiane Lang, Alexander Hähnel und Dr. Nathalie Guimard.

Michael Kaupp, Thomas Tischer und Christina Esterle danke ich für die Hilfe beim Schreiben mit \LaTeX .

Abschließend möchte ich mich ganz besonders bei meinen Eltern, meinem Bruder mit Familie, meinen Großeltern und all meinen Freunden für die großartige Unterstützung während der letzten Jahre bedanken.